Titre: Title:	Environmental risks of silver nanoparticles in attached-growth biological wastewater treatment processes: toxicity, persistence and impacts on effluent quality
Auteur: Author:	Sanaz Alizadeh
Date:	2019
Type:	Mémoire ou thèse / Dissertation or Thesis
Référence: Citation:	Alizadeh, S. (2019). Environmental risks of silver nanoparticles in attached-growth biological wastewater treatment processes: toxicity, persistence and impacts on effluent quality [Ph.D. thesis, Polytechnique Montréal]. PolyPublie. https://publications.polymtl.ca/4015/

POLYTECHNIQUE MONTRÉAL

affiliée à l'Université de Montréal

Environmental risks of silver nanoparticles in attached-growth biological wastewater treatment processes: toxicity, persistence and impacts on effluent quality

SANAZ ALIZADEH

DÉPARTEMENT DES GÉNIES CIVIL, GÉOLOGIQUE ET DES MINES

Thèse présentée en vue de l'obtention du diplôme de *Philosophiae Doctor*

Génie civil

Juin 2019

POLYTECHNIQUE MONTRÉAL

affiliée à l'Université de Montréal

Cette thèse intitulée:

Environmental risk of silver nanoparticles in attached-growth biological wastewater treatment processes: toxicity, persistence and impacts on effluent quality

présentée par Sanaz **ALIZADEH**

en vue de l'obtention du diplôme de *Philosophiae Doctor*

a été dûment acceptée par le jury d'examen constitué de :

Michèle PRÉVOST, Ph.D., présidente
Yves COMEAU, Ph.D., membre et directeur de recherche
Subhasis GHOSHAL, Ph.D., membre et codirecteur de recherche
Jason R. TAVARES, Ph.D., membre
Geoffrey I. SUNAHARA, Ph.D., membre externe

DEDICATION

To my parents, my sister Sarah, my brother Ali and my love, Simon

ACKNOWLEDGEMENTS

First and foremost, I express my deep and sincere gratitude to my supervisor, Professor Yves Comeau, for the unique opportunity to work as a member of his team at Polytechnique, for his invaluable contributions, constructive feedback, critical insight and his patience through my research. Thank you for being a role model and such an inspiration, teaching me professionalism and discipline.

I am also sincerely grateful for the tremendous support of my co-supervisor, Professor Subhasis Ghoshal, not only for his guidance into the exotic world of engineered nanoparticles but also for his priceless scientific and technical contributions to this project. Thank you for teaching me to push the limits and target high standards.

I thank Professor Jalal Hawari for all our insightful scientific discussions and valuable guidance.

I am deeply thankful to the members of the jury, Professors Michèle Prévost, Geoffrey I. Sunahara and Jason Tavares.

I give special thanks to the technical staff of the CREDEAU laboratory, for their invaluable professional experience and assistance in the analytical methods and experimental setup implementation: Denis Bouchard, Mélanie Bolduc, Jérôme Leroy and Gabriel St-Jean. Thanks also to my undergraduate interns: Marion Ferret and Simon Amiot, for your support and help in the lab. I also express my heartfelt thanks to my colleagues for their support and help during my Ph.D. studies, especially Kim Lompe, Evelyne Doré, Milad Taghavi, Dominique Claveau-Mallet, Sophie Lévesque, Catherine Brosseau, Jaime Chacana, Dominic Vallerand and Marie Ferland.

I acknowledge the Natural Sciences and Engineering Research Council of Canada, Environment and Climate Change Canada, PerkinElmer Health Sciences Canada, the Fonds de Recherche du Québec Nature et Technologies (FRQNT) and the Canadian Water Network (CWN) for their financial support.

Moreover, I am especially grateful to my partner Simon for his unconditional support and patience and for being part of my life project. I also thank my beloved family for everything they have done in my life and for their support.

RÉSUMÉ

Grâce à leur grande activité antimicrobienne, les nanoparticules d'argent (AgNP) sont les nanoparticules métalliques les plus utilisées de nos jours. Elles sont utilisées dans nombre de secteurs, dont le domaine de la santé, les cosmétiques, les traitements de l'eau et l'industrie alimentaire. Les propriétés « nanospécifiques » de ces nanoparticules pourraient toutefois présenter certains risques écotoxicologiques lors de leur dissémination dans l'environnement. Étant donné leur activité antimicrobienne, les conséquences biologiques que peuvent avoir les AgNP et leur effet inhibiteur potentiel sur les communautés microbiennes présentes dans les procédés biologiques de traitement des eaux usées présentent une préoccupation économique et environnementale.

Des efforts ont été faits pour étudier les impacts des AgNP sur le traitement biologique des eaux usées, mais la controverse persiste. Les AgNP sont reconnues pour nuire à la performance biologique et à l'activité des communautés microbiennes des procédés biologiques de traitement des eaux usées à culture libre à des doses élevées d'AgNP. Cependant, les interactions et les impacts négatifs des AgNP dans les procédés biologiques à culture fixée sont encore mal compris. Les paramètres biologiques ou toxicologiques sont couramment utilisés pour évaluer l'effet inhibiteur des AgNP sur l'efficacité des processus et sur les communautés microbiennes, dans des conditions qui ne sont pas représentatives des conditions typiques des stations de récupération des ressources de l'eau (StaRRE) sans caractérisation quantitative des AgNP.

L'objectif principal de ce projet était de déterminer le devenir, le transport et les impacts chroniques des AgNP dans les procédés biologiques à culture fixée, à des concentrations représentatives des conditions réelles. Les objectifs spécifiques étaient de (1) déterminer le comportement de rétention et de distribution des AgNP dans les procédés biologiques à culture fixée, (2) déterminer les impacts chroniques des AgNP sur les fonctions biologiques primaires et sur la communauté microbienne des biofilms hétérotrophes aérobies permettant l'enlèvement de la matière organique et (3) déterminer les impacts chroniques des AgNP sur les fonctions biologiques primaires et la communauté microbienne des biofilms aérobies autotrophes permettant la nitrification. Les réacteurs biologiques à garnissage en suspension (MBBR), constitue une technologie flexible, simple et robuste qui est utilisée pour mettre à niveau les

procédés biologiques existants afin qu'ils répondent aux exigences actuelles et futures de rejet, tout en minimisant l'empreinte des installations et les coûts d'exploitation. Ainsi, trois différents systèmes communs de MBBR ont été utilisés dans le cadre de cette étude pour évaluer les effets inhibiteurs des AgNP dans les procédés biologiques à culture fixée en combinant les réponses biologiques et les données de distribution et de caractérisation des NP, et de spéciation de l'Ag.

La phase initiale du projet s'est concentrée sur l'évaluation de la sensibilité des procédés biologiques à culture fixée à des concentrations représentatives des conditions réelles. Le devenir et les effets inhibiteurs des AgNP (50 nm) enrobées de polyvinylpyrrolidone (PVP) à des concentrations à l'affluent de 10, 100 et 600 μg/L ont été étudiés pour un MBBR à forte charge, permettant l'enlèvement de la matière organique, avec un court temps de rétention hydraulique (TRH) de 1 heure en tant que traitement secondaire compact. Les AgNP ont démontré un effet inhibiteur dépendant de leur concentration sur la performance du traitement et la viabilité du biofilm à des concentrations d'affluent comprises entre 100 et 600 μg/L de AgNP sur une période de 18 jours. Les conséquences biologiques observées étaient attribuables à la perte de biofilm actif par détachement et à l'accumulation d'AgNP dans le biofilm avec le temps.

Au cours de la deuxième phase, nous avons évalué les impacts chroniques des AgNP (10 et 100 μg/L de AgNP) sur un MBBR à charge moyenne (TRH de 3 h) comme prétraitement d'un système de boues activées et sur une unité de séparation de la matière organique en amont d'un système MBBR nitrifiant. La nitrification joue un rôle essentiel dans les processus d'élimination biologique de l'azote. Ainsi, les réponses et la récupération du biofilm nitrifiant lors d'une exposition chronique à des nanoparticules d'argent ont été évaluées dans un MBBR nitrifiant (TRH de 3 h) à des concentrations d'affluents (10-100 μg/L de AgNP) représentatives des conditions réelles. Les AgNP ont significativement diminué l'efficacité d'enlèvement de la DCO soluble (S_{DCO}) et de l'ammoniaque, causé des dommages à l'intégrité membranaire des bactéries du biofilm, inhibé l'activité enzymatique clé extracellulaire et intracellulaire, causé un stress oxydatif dépendant de la concentration et changé la composition des communautés microbiennes.

La caractérisation quantitative des nanoparticules dans les MBBR, à l'aide de la spectroscopie de masse induite par une seule particule (spICP-MS), a indiqué une adaptation initiale de la biomasse du MBBR suite à l'ajout d'AgNP, avec une augmentation de la libération de l'Ag total avec le temps, principalement sous forme de NP, ainsi qu'une accumulation périodique d'argent dans le

biofilm, associée à un détachement significatif du biofilm de la surface des médias induit par les AgNP. Des formes de nanoparticules d'argent transformées chimiquement et potentiellement moins toxiques (Ag_2S, AgCl) ont été détectées dans l'effluent des MBBR au cours de la période d'exposition. Une fraction significative de la masse cumulée d'Ag (75% à 85%) a été libérée dans l'effluent des réacteurs, indiquant une capacité de rétention limitée du biofilm aérobie hétérotrophe et du biofilm nitrifiant pour les AgNP lors d'une exposition à long terme.

Ce projet de recherche a permis de caractériser les dynamiques d'interaction, la biodisponibilité et les effets inhibiteurs des AgNP dans les systèmes à biofilm de traitement des eaux usées. L'effet des AgNP s'est révélé dépendant de la concentration en nanoparticules, du temps d'exposition et de la configuration du traitement. La caractérisation quantitative des AgNP dans les différents flux des réacteurs (i.e. affluent et effluent) en utilisant la spICP-MS indique que la libération prolongée d'AgNP biodisponible et de biofilm concentré en AgNP dans l'effluent. Ces résultats soulignent la nécessité de stratégies visant à contrôler le rejet de telles nanoparticules par les systèmes des biofilms afin d'atténuer les risques potentiels sur le traitement en aval et sur les écosystèmes recevant les effluents.

Les tests d'exposition à court-terme peuvent ne pas capturer les effets dynamiques des interactions entre le biofilm et les nanoparticules, et les conséquences sur les scénarios d'exposition à long-terme, en particulier pour les procédés de traitement avec de longs temps de rétention des boues. Cette recherche a démontré de l''impact chronique potentiel des nanoparticules à des concentrations représentatives des conditions réelles et qui doit être pris en compte dans les procédés biologiques à culture fixée. La combinaison des méthodologies toxicologiques et de la caractérisation des nanoparticules est essentielle pour développer une compréhension globale du devenir et du comportement des nanoparticules au cours de leur cycle de vie et pour déterminer les risques pour l'environnement. Cette recherche contribue à une meilleure compréhension du devenir et du comportement des AgNP dans les processus de traitement biologiques des eaux usées, en fournissant des informations clés pouvant être utilisées pour prédire les risques environnementaux des nanoparticules (transport, persistance et toxicité) dans les écosystèmes aquatiques et pour guider la réglementation future.

ABSTRACT

Due to their broad-spectrum antimicrobial activities, silver nanoparticles (AgNPs) are the most widely used metal nanoparticles today. They are used in various sectors including health, cosmetics, water treatment and food industry. The 'nano-specific' properties of these nanoparticles, however, can lead to eco-toxicological problems when released into the environment. Given the antimicrobial activity of AgNPs, their biological implications and potential inhibitory effects on the microbial communities of biological wastewater treatment processes have become a significant economic and environmental concern. Much effort has been made to study the effects of AgNPs on biological wastewater treatment, but controversy still exists. AgNPs are observed to negatively affect the biological performance and microbial communities in suspended-growth biological wastewater processes at high AgNP doses (>1 mg/L). Yet, the interaction and adverse impact of AgNPs in attached growth process systems are poorly understood. The biological or toxicological endpoints have been commonly used to evaluate the inhibitory effect of AgNPs on process efficiency and on microbial communities, under conditions that are not representative of typical water resource recovery facility (WRRF) process conditions with no quantitative characterization of AgNPs.

The main objective of this project was to determine the fate, transport and long-term impacts of AgNPs in attached-growth biological wastewater treatment processes at environmentally relevant concentrations. The specific objectives were to determine (1) the retention and distribution behavior of AgNPs in aerobic attached-growth biological processes; (2) the long-tem impacts of AgNPs on primary biological functions and the microbial community of aerobic heterotrophic wastewater biofilms achieving organic matter removal and (3) the long-term impact of AgNPs on primary biological functions and the microbial community of aerobic autotrophic nitrifying wastewater biofilms achieving ammonia removal.

Moving bed biofilm reactors (MBBRs) are commonly used as a simple-yet-robust, flexible and compact technology to retrofit the existing biological processes to meet current and future effluent discharge requirements, while minimizing the plant footprint and operating costs. Thus, three different MBBR systems, representing common MBBR configurations in WRRFs were used in this study

to assess the inhibitory effects of AgNPs in attached-growth biological processes by combining biological responses and the NP distribution, characterization and Ag speciation data.

The initial phase of the project focused on assessing the sensitivity of attached-growth biological wastewater treatment processes at environmentally relevant concentrations of AgNPs. The fate and inhibitory effects of polyvinylpyrrolidone (PVP)-coated AgNPs (50 nm) at influent concentrations of 10, 100 and 600 μg/L were investigated in a high-rate organic matter removing MBBR with a very short hydraulic retention time (HRT) of 1 hour as a compact secondary treatment. AgNPs demonstrated a concentration-dependent inhibitory effect on treatment performance and biofilm viability at influent concentrations of 100 to 600 μg/L AgNPs over an 18 day–exposure. The observed biological implications were due to loss of active biofilm via detachment and the accumulation of AgNPs over time within the biofilm.

In the second phase, we assessed the long-term continuous impact of AgNPs in a medium rate organic matter removal MBBR (HRT of 3 h) as the pre-treatment of an activated sludge system or an organic matter separation unit ahead of a downstream nitrifying MBBR. Nitrification plays a critical role in biological nitrogen removal processes. Thus, in the third phase, the responses and recovery of nitrifying biofilm upon long-term exposure to AgNPs were evaluated in a nitrifying MBBR (HRT of 3 h) at environmentally relevant influent concentrations (10-100 μg/L AgNPs). AgNPs significantly decreased soluble COD (S_{COD}) and ammonia removal efficiency with observed biofilm membrane integrity damage, inhibition of both extracellular and intracellular key enzyme activities, concentration-dependent oxidative stress and the observed shift in microbial community composition.

The quantitative characterization of nanoparticles in MBBRs using single-particle inductively coupled plasma mass spectroscopy (spICP-MS), indicated an initial adaptation of the MBBR biomass to AgNP addition with an increase in total Ag release over time predominantly in NP form, and a periodic silver accumulation in the biofilm coupled with significant AgNP-induced biofilm detachment from the surface of the carriers. Chemically transformed and potentially less toxic forms of silver nanoparticles (Ag_2S, AgCl) were detected in the effluent of the MBBRs over the exposure period. A significant fraction of cumulative mass of Ag (75% to 85%) was released in the effluent of the reactors, indicating a limited retention capacity of aerobic heterotrophic and

nitrifying biofilm for AgNPs over long term exposure, compared to the commonly studied activated sludge.

Overall, this research project demonstrated the distinct interaction dynamics, bioavailability and inhibitory effects of AgNPs in wastewater biofilm systems. It was shown that the effects of AgNPs are highly dependent on nanoparticle concentration, exposure time and treatment configurations. The quantitative characterization of AgNPs in different reactor phases (i.e. influent, bioreactor and effluent) using spICP-MS, suggest the extended release of bioavailable AgNPs and AgNP-rich MBBR biofilm via effluent. These results stress the need for strategies to control the release of such NPs from biofilm systems to attenuate their potential risks for the downstream treatments and effluent receiving ecosystem.

Short-term exposure tests may fail to capture the effects of NP-biofilm interaction dynamics, accumulation and their consequences over long-term exposure scenarios, especially for treatment processes with long sludge retention times. This research demonstrated the potential long-term impact of nanoparticles at environmentally relevant concentrations and highlights the need for distinct consideration of the effects of AgNPs in attached-growth biological processes. A combination of both toxicological methodologies and nanoparticle characterization is critical to develop a comprehensive understanding of the fate and behavior of nanoparticles in their life-cycle. This research contributes to a better understanding of the fate and behavior of AgNPs in biological wastewater processes, providing key information that can be used to predict the environmental risks of nanoparticles (transport, persistence and toxicity) in aquatic ecosystems and to support future regulations.

TABLE OF CONTENTS

LIST OF TABLES

LIST OF FIGURES

LIST OF SYMBOLS AND ABBREVIATIONS

AgNP	Silver nanoparticles
Ag_{bio}	Total silver in bioreactor
$Ag_{carrier}$	Total silver in attached biofilm
Ag_{eff}	Total silver in effluent
Ag_{floc}	Total Silver in biomass flocs
Ag_{inf}	Total silver in influent
Ag_{susp}	Total silver in suspended phase
AMO	Ammonia monooxygenase
AN	Anaerobic
$AgNO_3$	Silver nitrate
ANOVA	Analysis of variance
AOB	Ammonia oxidizing bacteria
AOP	Adverse outcome pathway
AS	Activated sludge
AX	Anoxic
BOD_5	Biochemical oxygen demand after 5 days
CeO_2NP	Cerium oxide nanoparticle
CLSM	Confocal laser scanning microscopy
COD	Chemical oxygen demand
CuONP	Copper oxide nanoparticle
Comammox	Complete ammonia oxidation
DHA	Dehydrogenase
DNA	Deoxyribonucleic acid
DO	Dissolved oxygen
ENP	Engineered nanoparticles
EPS	Extracellular polymeric substances
ERA	Environmental risk assessment
GLU	Glucosidase
HRT	Hydraulic retention time

H_2-DCFDA	Dichlro-dihydrofluorescein diacetate
IC_{50}	The half-maximal inhibitory concentration
ICP-OES	Inductively coupled plasma-optical emission spectrometry
INT	2-(4-iodophenyl)-3-(4-nitrophenyl)-5-phenyl-2H-tetrazolium chloride
MBBR	Moving bed biofilm reactor
$M_{Ag,bio}$	Mass of silver in bioreactor
$M_{Ag,carrier}$	Mass of silver in attached biofilm
$M_{Ag,eff}$	Mass of silver in effluent
$M_{Ag,inf}$	Mass of silver in influent
$M_{Ag,susp}$	Mass of silver in suspended phase of bioreactor
NIST	National Institute of Standards and Technology
NO_2	Nitrate
NO_3	Nitrite
NOB	Nitrite oxidizing bacteria
NOR	Nitrite oxidoreductase
OECD	Organization for economic co-operation and development
OLR	Organic loading rate
OTU	Operational taxonomic unit
OX	Oxic
PCoA	Principal coordinate analysis
PCR	Polymerase chain reaction
POA	Phosphate accumulating organisms
PRO	Protease
PVP	Polyvinylpyrrolidone
ROS	Reactive oxygen species
S_{ALK}	Alkalinity
SBR	Sequencing batch reactors
S_{COD}	Soluble chemical oxygen demand
SpICP-MS	Single-particle inductively coupled plasma–mass spectrometry
SRT	Sludge retention time
SSD	Species sensitivity distribution

TEM-EDS	Transmission electron microscopy-energy dispersive X-ray spectroscopy
TiO_2NP	Titanium oxide nanoparticle
TKN	Total Kjeldahl nitrogen
TP	Total phosphorus
TSS	Total suspended solids
VSS	Volatile suspended solids
WRRF	Water resources recovery facility
ZnONP	Zinc oxide nanoparticle

CHAPTER 1 INTRODUCTION

Nanotechnology, which is one of the fastest developing technologies, empowers us to fabricate and manipulate nano-scale materials that have at least one dimension in the range of 1 to 100 nm. A common nanotechnology product is engineered nanoparticles (ENPs; Auffan et al., 2009). Their physicochemical characteristics include distinct electrical, thermal, mechanical and imaging properties resulting in their wide integration in commercial, medical and environmental applications (Lead et al., 2018). Silver nanoparticles (AgNPs) are one of the ENPs at the forefront over the last decade due to their broad-spectrum antimicrobial activity (McGillicuddy et al., 2017). AgNPs are extensively used in healthcare and hygiene products, the textile and food industries, paints, cosmetics, medical devices, sunscreen, bio-sensors, clothing and electronics (Lead et al., 2018; Singh et al., 2019). Despite their industrial and economic merits, dynamic growing applications of AgNPs would inevitably lead to their release into the environment during their production, transport, circulation and disposal processes (Tolaymat et al., 2017). Discharged AgNP-containing wastes deliver a significant fraction of released AgNPs into municipal wastewater resource recovery facilities (WRRFs) at an estimated influent concentration ranging from 10 ng/L to 150 μg/L (Gottschalk et al., 2013; Keller and Lazareva, 2013; Li et al., 2013)

WRRFs are of vital significance for urban systems with a central role in achieving water security. Biological wastewater treatment plays a central part of WRRFs. Given the antimicrobial activity of AgNPs, concerns regarding the potential negative impacts of released AgNPs on biological wastewater processes have received greater attention in recent years. The inhibitory effect of AgNPs (0.1 to 50 mg/L) was extensively studied in suspended-growth biological systems, achieving biological organic matter, nitrogen and phosphorus removal, over various exposure durations (7 to 150 days). These studies indicated that the effects of AgNPs are highly dependent the property of the AgNPs (e.g. size, shape and coating) and their concentrations, exposure time, and treatment configurations.

Attached growth biological processes, such as moving bed bioreactors (MBBRs) processes, are compact technologies with relatively low capital costs that can achieve similar treatment targets as suspended growth systems while requiring a smaller carbon and ecological footprint due to higher biomass surface area/volume ratio (Ødegaard, 2016). Such processes are commonly used to upgrade or replace existing biological processes to meet current and new effluent discharge

requirements. However, there are gaps in knowledge on the environmental fate and inhibitory effects of AgNPs in attached-growth biological treatment systems. Therefore, systematic research, using a combination of both physical and chemical characterization of AgNPs (e.g. size, composition, and dissolution) and toxicological endpoints are required. This will allow first, to understand the interaction mechanisms between AgNPs and mature, mixed culture wastewater biofilms and second, to investigate the corresponding AgNP-induced inhibitory effects at environmentally representative NP concentrations under typical WRRF process conditions. The main research questions that were addressed in this thesis are:

(a) Is long-term exposure to AgNPs a concern for attached-growth biological process suitability at environmentally relevant concentrations?

(b) How does long-term exposure to AgNPs affect the microbial communities in wastewater biofilm processes?

(c) What is the main mechanism of toxicity of AgNPs in biofilm processes?

(d) What is the critical role of attached growth biofilm processes on the environmental fate of AgNPs?

This research is part of a project entitled «Environmental risks of engineered nanoparticles in municipal wastewater treatment plants, toxicity, persistence and impacts on effluent quality» in collaboration with Natural Sciences and Engineering Research Council of Canada, Environment and Climate Change Canada, PerkinElmer Health Sciences Canada, the Fonds de Recherche du Québec Nature et Technologies (FRQNT), the Canadian Water Network (CWN), SNC Lavalin Environment, the City of Calgary and the City of Saint-Hyacinthe.

This thesis is structured in eight chapters. Chapter 1 is for this Introduction. Chapter 2 presents a critical review on environmental exposure of AgNPs in WRRFs, their implications for biological wastewater treatment processes and characterization, and quantification of AgNPs in WRRFs. Chapter 3 summarizes the objectives, hypotheses and methodologies. Chapters 4, 5 and 6 present published, submitted and in preparation manuscripts, respectively. The first article (Chapter 4), presents the results on vulnerability assessment of attached-growth biological wastewater treatment processes upon exposure to environmentally relevant concentrations of AgNPs in high rate MBBRs. The second article (Chapter 5) presents the biological implications of the continuous inflow of low concentrations

of silver nanoparticles on the biological performance and microbial communities of aerobic heterotrophic wastewater biofilm. The third article (Chapter 6) demonstrates the responses and recovery of nitrifying MBBRs upon chronic exposure to silver nanoparticles in terms of biological performance and microbial community. Finally, Chapters 7 and 8 provide a general discussion followed by Conclusions and Recommendations, respectively. Supplemental information for articles 1, 2 and 3 is presented in Appendices A, B and C, respectively.

CHAPTER 2 CRITICAL LITERATURE REVIEW

2.1 Engineered nanoparticles, an emerging class of environmental contaminants

Nanotechnology is a fast-developing field with advanced research in drug delivery and tissue engineering (Singh et al., 2019; Singla et al., 2019), communication technology and smart materials (Garg, 2019; Lou et al., 2019), water and wastewater treatment technologies (Hasbullah et al., 2019) and new sustainable food production (Cerqueira and Pastrana, 2019) with a predicted $3 trillion market by 2020 (McGillicuddy et al., 2017; Roco, 2011). Engineered nanoparticles (ENPs) are defined as any intentionally produced particles with a characteristic dimension in the range of 1 to 100 nm (Auffan et al., 2009a). While sharing the same chemical composition as their bulk materials, ENPs inherit distinct physicochemical properties (e.g. reactivity, electrical, optical and magnetic properties) as compared to their bulk-sized particles. Nearly all sectors of the global economy, including energy, health, cosmetics and agriculture, take advantage of the promising and desirable merits of ENPs.

ENPs can be classified into different groups based on their composition (Figure 2.1). The distinctive surface properties, crystalline structure and reactivity of ENPs are a function of their nanoscale size. The high percentage of atoms located at the particle surface leads to stresses and strains on the lattice structure of the particles resulting in a larger proportion of surface edges with higher reactive facets per mass relative to bulk materials of the same composition (Auffan et al., 2010). As a result, their physicochemical behaviors, thermodynamics and toxicology cannot be extrapolated directly from their bulk material and therefore, this new class of emerging contaminants constitutes one of the most critical environmental challenges.

Nanotechnology was already undergoing rapid growth before 2000, but it was only after 2006 that concerns about the potential risks of ENPs in relation to human health and the environment began to arise. The path initiated by the World Economic Forum when the specific topic “nanoparticle toxicity” was included in its Global Risks reports (Laborda et al., 2016; Maynard et al., 2006; Wiesner et al., 2006). Recently, the Organization for Economic Co-operation and Development (OECD) classified metal nanoparticles, including silver nanoaprticles (AgNPs), as the most environmentally relevant ENPs with a significant priority to address their adverse

biological impact and potential toxicity in nano-environmental health and safety research (Neale et al., 2013).

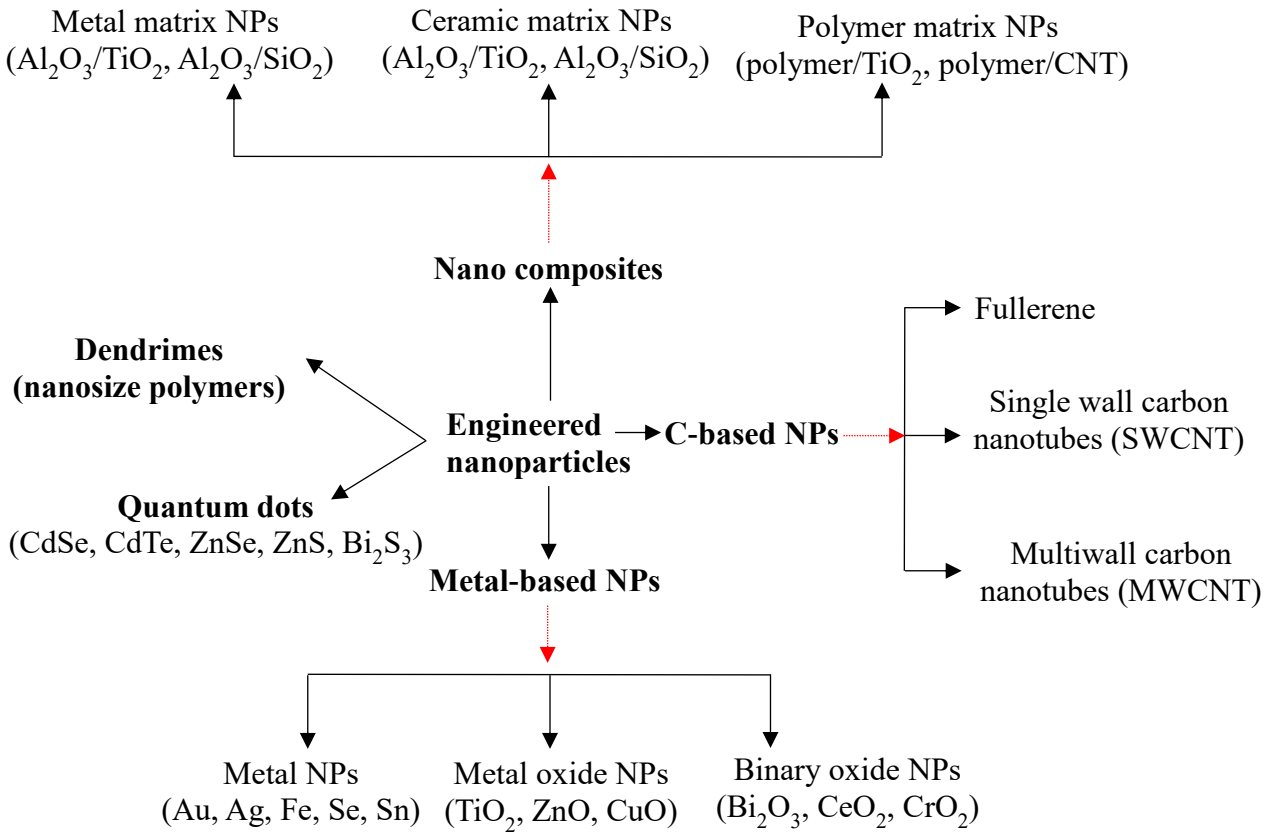

Figure 2.1 : Classification of ENPs based on their composition

2.2 Silver nanoparticles: background, inventory and current applications

Silver has been widely used for centuries due to its antibacterial properties (Nowack et al., 2011). Persian kings, such as Cyrus the Great, used silver-based water containers to prevent contamination and to preserve water quality during war (McGillicuddy et al., 2017). The Macedonians and Hippocrates used silver for such medical purposes as wound healing and treatment of ulcers (Alexander, 2009). Colloidal silver was registered as a biocidal material in 1954 and has been used in medications for nearly one hundred years in the United States (Nowack et al., 2011; Reidy et al., 2013). The application of silver as an anti-bacterial agent has a

long history, but the production of engineered AgNPs has enabled various technologies and fields to take advantage of their promising merits.

AgNPs are one of the most widely used metal nanoparticles in various consumer products such as clothing and footwear as odor-reducing agent or wet wipes, cosmetics, as well as food processing, pharmaceutical and healthcare products and also as an alternative disinfectant and anti-biofouling agent in industrial pipelines (e.g. in the food, fermentation, water treatment industries) due to their effective antimicrobial properties (Huang et al., 2016; Mohanta et al., 2017; Patlolla et al., 2012). AgNPs are increasingly applied in the areas of microelectronics and medical imaging due to their high electrical and thermal conductivity, and unique optical properties (McGillicuddy et al., 2017; Zhang et al., 2016a). With an initial estimated AgNP production rate of 500 million of tonnes per year in 2009 (Mueller and Nowack, 2008), an approximate production rate of 800 million of tonnes per year AgNPs is expected by 2025 with greater marketing value than other ENPs (Pulit-Prociak and Banach, 2016). According to data from the Woodrow Wilson Center's Project on Emerging Nanotechnologies, 24% of nanomaterial-based consumer products currently contain AgNPs (Vance et al., 2015).

2.3 Production and application

AgNPs can be synthesized using either a top-down or a bottom-up approach. In the top-down techniques, bulk silver is used as the initial structure and is mechanically reduced to nano size Ag using techniques such as lithography or laser ablation with limited control over such important physical parameters as the size and shape of the particles (Fabrega et al., 2011a; Tolaymat et al., 2010). The bottom-up approach involves an initial dissolution of silver salts (e.g. silver nitrate) into a solvent, followed by the addition of a reducing agent (e.g. $NaBH_4$), with the supplementary application of a stabilizing agent (e.g. citrate) to prevent NP agglomeration (Reidy et al., 2013). Biological reduction, or green synthesis methods, using microorganisms and plant extracts, is of increased interest as a cost-effective and less toxic technique when compared to physical and chemical methods (El Badawy et al., 2010). Various coating agents (e.g. polymers and surfactants) are used in the synthesis of AgNPs to prevent their agglomeration through electrostatic repulsion, steric repulsion or both. The most prevalent coating agents are citrate, sodium borohydride ($NaBH_4$), and polyvinylpyrrolidone (PVP) (Badawy et al., 2010).

2.4 Why are silver nanoparticles important for the environment?

The increasing use of AgNPs, primarily due to their antimicrobial properties, inevitably leads to their release and accumulation in the environment. AgNPs can enter the environment over several phases of their life-cycle via three release scenarios including (i) release during production of raw materials and nano-enabled products (e.g. textiles and fabrics); (ii) release during application and consumption (e.g. cosmetics, water filters, alternative health supplements) and (iii) resale by discharge of AgNP-containing wastes (Gottschalk et al., 2013; Tolaymat et al., 2017). Material flow analyses demonstrated the potential release of AgNPs into different environmental compartments (i.e. soil, water, air, landfills). Nevertheless, their potential implications for the environment and human health are not yet well understood (Gottschalk et al., 2009; Keller and Lazareva, 2013; Keller et al., 2013; Mueller and Nowack, 2008). Uncertainties about the 'nano-specific' novel properties of these nanoparticles and their potential biological impact have raised new concerns over the fate, transport and long-lasting adverse effects of AgNPs in the environment (Bundschuh et al., 2018; Wimmer et al., 2019). Consequently, a fundamental understanding of their environmental behavior, interactions and transformations is crucial for identifying the potential risks associated with their release (Sharma et al., 2019; Zhang et al., 2018a).

2.4.1 Mechanisms of the potential AgNP toxic action

Once the NPs interact with a physiologically active site on the cell surface, they can affect cell metabolism and disrupt cellular homeostasis by overwhelming stress response, resulting in a toxic outcome (Schirmer, 2014; Wu et al., 2012). Previous studies have shown the negative impacts of AgNPs on such organisms as bacteria, algae, fungi, invertebrates, plants and fishes (Bondarenko et al., 2013; Lead et al., 2018; Navarro et al., 2008). The exact mechanisms of the potential toxic actions of AgNPs are not clearly known and remain a debated topic. The possible antibacterial mechanisms (Figure 2.2) of silver nanoparticles include:

(1) Adhesion of AgNPs to bacterial surfaces and cell membrane integrity damage:
    - The large surface/volume ratio and special binding sites of AgNPs enhance the particle/cell surface contacts (Auffan et al., 2009b). The electrostatic interaction between AgNPs and negatively charged lipopolysaccharide and teichoic acid of Gram-negative and Gram-positive bacterial cell walls, respectively, facilitate the AgNPs attachment onto cell membranes (Ahmad et al., 2017; Durán et al., 2016) which may

possibly alter membrane properties and directly damage the cell membrane (Prabhu and Poulose, 2012).

(2) Transport through the cell membrane and intracellular direct interactions with DNA and proteins:
    - The interaction of AgNPs with the sulfur and phosphorus of the DNA can lead to problems in DNA replication and modulate signal transduction by dephosphorylating the peptide substrates on tyrosine residues, leading to the termination of cell growth (Prabhu and Poulose, 2012).

(3) Oxidative dissolution of AgNPs and release of antimicrobial Ag^+ ions via three major pathways of (a) extracellular dissolution of AgNPs in media, (b) interfacial dissolution of the surface-bound AgNPs and (c) intracellular dissolution AgNPs via a "Trojan-horse" type of mechanism:
    - The bioavailable dissolved Ag interacts with thiol-containing proteins in the cell wall and affects their functions and destabilizes the outer membrane of cells by an accumulation of immature membrane precursor proteins (Mirzajani et al., 2011).
    - The dissolved Ag interacts with the thiol group of vital enzymes, sulphur-containing proteins in the bacterial cell wall cytoplasmic proteins leading to the disruption of respiration and the establishment of a proton motive force (Sedlak et al., 2012).
    - The intracellular dissolved Ag interferes with critical biomolecules within the cell and disrupts ATP production and DNA replication (Durán et al., 2016)

(4) Extracellular and intracellular reactive oxygen species (ROS) generation:
    - Oxidation of AgNPs can form extracellular the superoxide radical ($O_2^{\bullet-}$) or hydroxyl radicals via a mechanism similar to Fenton reaction (He et al., 2012). The interaction between AgNPs and Ag^+ and functional groups of proteins, involved in cell respiratory chain, can also lead to intracellular ROS production (Liu and Hurt, 2010). ROS generation can result in the disruption of the cell membrane integrity and cause protein decomposition and DNA damage (Durán et al., 2016).

The toxic effect of AgNPs is ascribed to both nanoparticles and dissolved ions released from AgNPs, however, which fraction dominates the toxicity appears inconclusive (Beer et al., 2012; Kawata et al., 2009; Navarro et al., 2008). Recent toxicological studies concluded that oxidative AgNP dissolution and release of Ag^+ and/or subsequent reactive oxygen species (ROS) generation may explain most of the overall toxicity of AgNPs towards bacteria with a greater toxicity of AgNPs as compared to Ag^+ ions at the same Ag concentration (Ivask et al., 2014; Kubo et al., 2018; Seitz et al., 2015; Zhang et al., 2016a). Nevertheless, contradictory evidence has indicated that Ag^+ ions have a comparable or even higher toxicity and antimicrobial activities

than AgNPs (Pokhrel et al., 2012; Silva et al., 2014; Su et al., 2011). Most previous studies, reporting the Ag^+-mediated toxicity of AgNPs, used silver nitrate ($AgNO_3$) as a source of bioavailable free Ag^+ ions at a concentration of 0.05 to 10 mg/L in simple growth media, which is not considered as an 'environmentally relevant' condition (Beer et al., 2012; Choi et al., 2018). The transformation of AgNPs in a biochemically rich environmental medium, such as wastewater, will alter the bioavailability of AgNPs and/or released dissolved Ag and change the total dynamics of NP-cell interactions (Azimzada et al., 2017). The uncertainty regarding which silver species (i.e., silver ions or silver nanoparticles) is more toxic has to be investigated further with careful experimental design under conditions that are representative of corresponding environmental conditions.

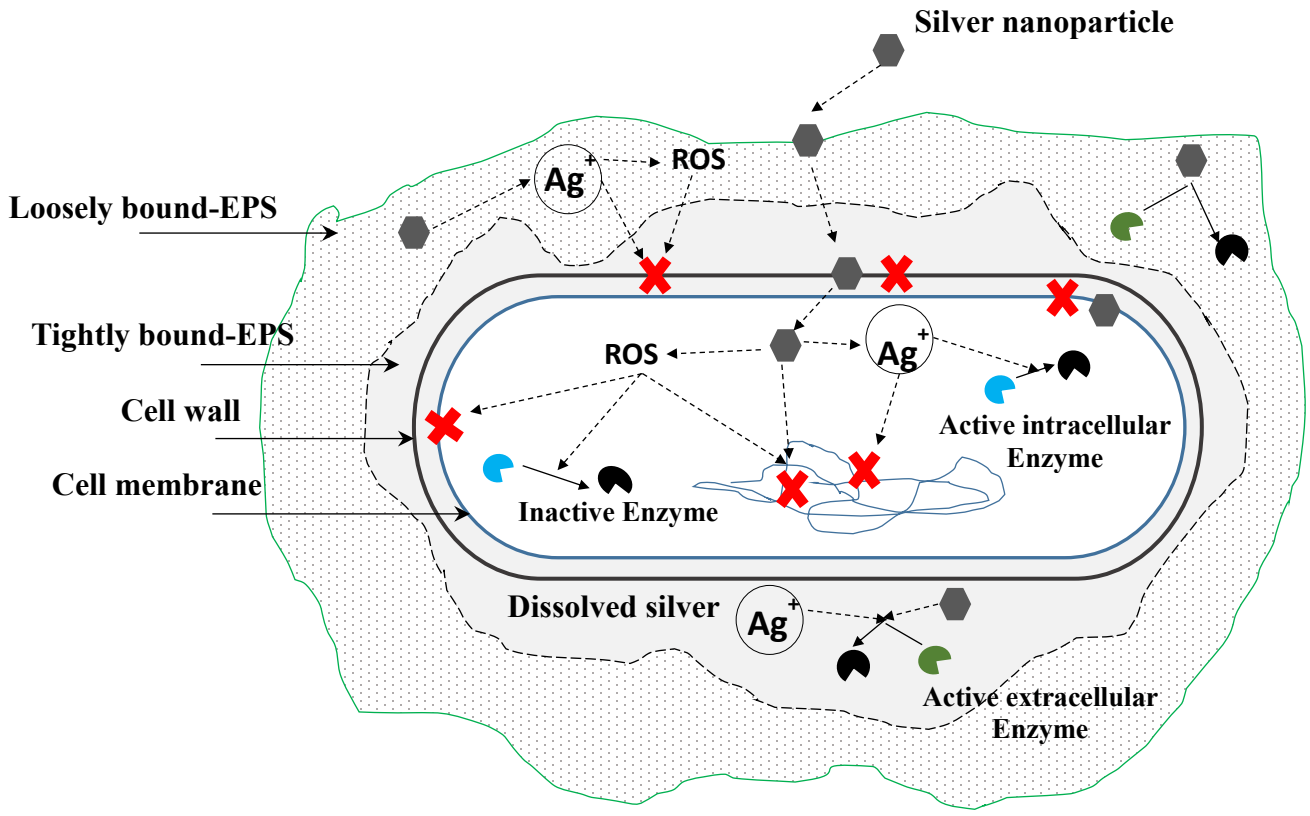

Figure 2.2 : Proposed toxicity mechanisms of silver nanoparticles

2.5 Environmental exposure of AgNPs in water resource recovery facilities (WRRFs)

2.5.1 An overview of wastewater treatment processes

Continuous population growth, urbanization and industrialization as well as unsustainable water use practices have led to a major water quality crisis with extensive stress on water resource supplies and the environment (Buonocore et al., 2018; van der Hoek et al., 2016). In this context, wastewater and WRRFs are of vital significance for urban systems with a central role in achieving future water security. Wastewater treatment plants are now renamed as WRRFs to reflect the demand for new processes not only to meet current and future effluent discharge requirements but also to achieve nutrient removal/recovery, energy efficiency and reuse of wastewater-derived resources (e.g. water, nutrients, energy, biosolids, cellulose fibers, biopolymers, bioplastics) with an emphasis on sustainability (Brosseau et al., 2016; van der Hoek et al., 2016). WRRFs use a combination of physical, chemical, and biological processes to achieve the principal treatment goals of removing solid, organic and microbiological components to improve effluent quality. Treatment efficiency is adapted according to initial wastewater characteristics and the environmental discharge standards, mainly in terms of biological oxygen demand (BOD_5), suspended solids and nutrients (e.g. ammonia, nitrate, phosphorus). A typical treatment of wastewater entails step-wise processes, including preliminary, primary, secondary, tertiary and advanced stages (Figure 2.3).

Preliminary treatment removes coarse solids and other large materials (e.g. pieces of wood, cloth, paper, plastics, garbage) using basic screening and filtration processes. Primary treatment is designed to remove organic and inorganic solids by sedimentation or flotation. Secondary treatment uses biological processes to remove readily biodegradable organics up to 90% removal of BOD_5 and total suspended solids by utilizing many different types of microorganisms in a controlled environment. Primary and secondary treatment removes the majority of BOD_5 and suspended solids. Nevertheless, the wastewater may still contain high percentages of P, N and emerging contaminants such as endocrine-disrupting chemicals and pharmaceutically active compounds including antibiotics. Therefore, the quality of water after this level of treatment is still insufficient to efficiently protect the receiving waters or to provide reusable water for

industrial and/or domestic recycling. Tertiary treatment and advanced treatments use a series of specialized chemical and physical processes such nanofiltration, ozonation or activated carbon, to remove remaining specific pollutants (Giebner et al., 2018; Watkinson et al., 2007). The primary sludge, produced from primary sedimentation, and secondary sludge from biological treatment are further treated by a number of different processes such as anaerobic digestion (Metcalf and Eddy-AECOM, 2014). The remaining solid fractions, recovered throughout the liquid processing chain, require further processing for thickening, stabilizing, dewatering, drying, valorization and disposal.

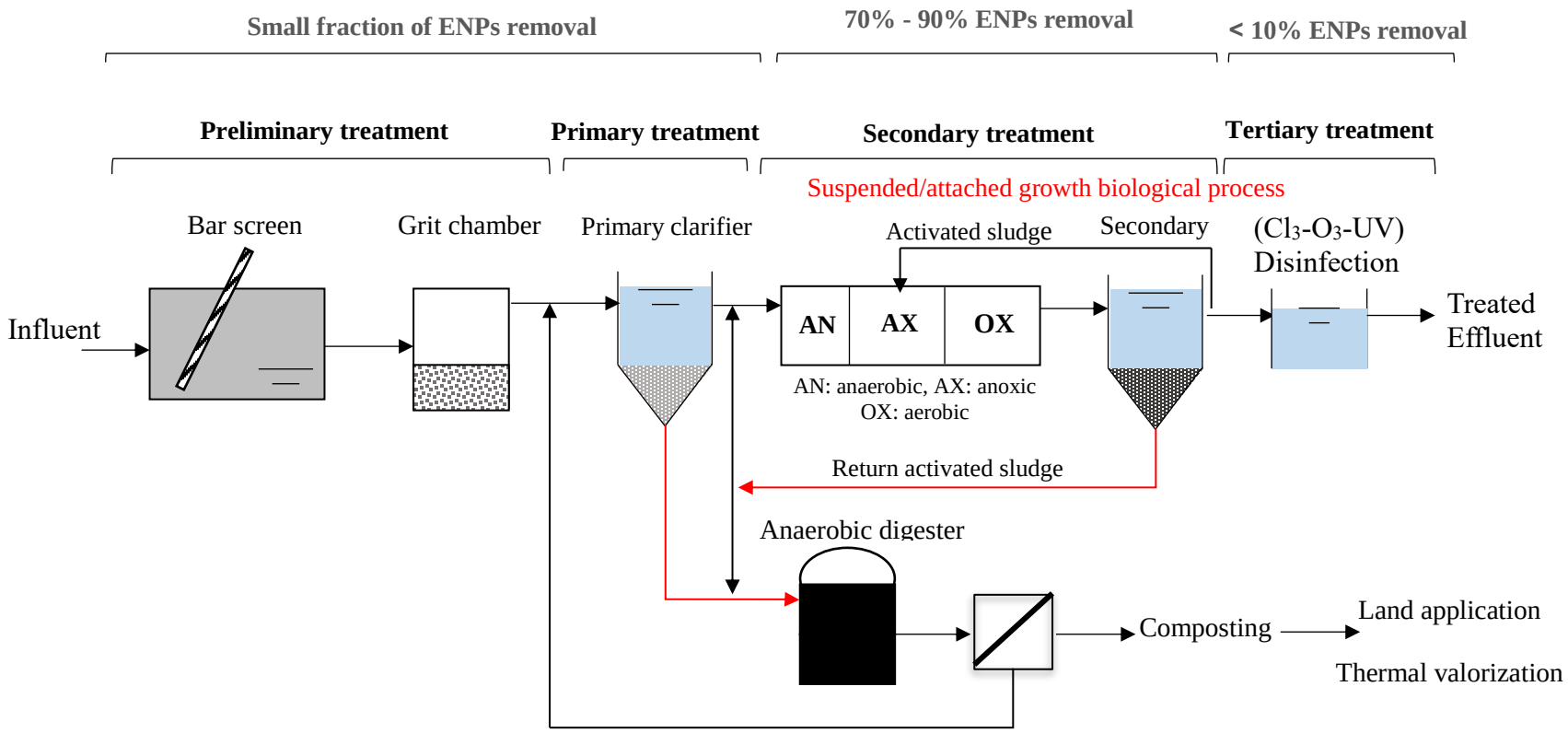

Predominant microbial groups

AN: heterotrophic fermenters, phosphate accumulating organisms (PAOs)
AX : heterotrophic denitrifiers
OX: aerobic heterotrophs, PAOs, nitrifiers
AD: fermenters, sulphate-reducers, methanogens

Figure 2.3 : Typical wastewater treatment system and the possible distributions of ENPs (adapted from Wu et al. (2018)).

Materials flow analyses of released AgNPs from personal care products, various household and industrial products suggest that a significant fraction of the AgNP-laden domestic and industrial waste enters WRRFs with an estimated influent concentration ranging from 10 ng/L to 150 μg/L (Table 2.1; Gottschalk et al., 2009; Li et al., 2013). Thus, WRRFs serve as a key interface between ENPs release and their environmental distribution into downstream ecosystems by their liquid or biosolids discharges. Generally, a small fraction of influent AgNPs would be removed during the pretreatment stage (e.g. bar screens and grit removal) and primary treatment (Brar et al., 2010; Hou et al., 2012; Kaegi et al., 2013). AgNPs entering the secondary treatment processes, comprised of suspended or attached growth biological treatments, can adhere to the microbial cell surfaces or extracellular polymeric substances (EPS). Both laboratory and full-scale studies demonstrated relatively high removal of AgNPs (70% to 90%) by biomass in biological treatment and biosolids treatment trains (Figure 2.3; Kaegi et al., 2013; Li et al., 2013; Neale et al., 2013; Park et al., 2013). AgNPs associated with biomass can be transformed through dissolution–complexation/precipitation reactions, which greatly influence their antimicrobima activites. Yet, the fraction of nanoparticles that is not captured during biological processes will potentially reach aquatic organisms via effluent discharge into surface water posing an ecotoxicological risk (Table 2.1). Given the antimicrobial activity of AgNPs, their potential inhibitory effects on sensitive microbial communities responsible for important environmental biogeochemical cycling cannot be overlooked. Of particular concern is the potential deleterious effect of AgNPs on the microbial community involved in biological wastewater treatment processes and the resulting treatment efficiency (Hou et al., 2012; Sheng et al., 2015). The fate and transport of AgNPs in WRRFs and their potential risks in the biological wastewater processes, however, are poorly understood.

2.5.2 Transformations of AgNPs and their implication for toxicity

Upon release into wastewater systems, AgNPs will be subject to physical and chemical transformations which can significantly change their physicochemical properties (e.g. size, surface charge, solubility), distribution, bioavailability and toxicity in WRRFs. AgNPs either agglomerate together (i.e., homo-agglomeration) or aggregate with other organic or inorganic particles (i.e., hetero-aggregation) depending on their colloidal stability (Badawy et al., 2010).

Table 2.1: Measured or predicted silver concentrations in full-scale WRRFs (Wang and Chen, 2016; Zhang et al., 2016a).

Wastewater component	Location measured silver concentrations	Concentration	Silver species	References
Influent	Nine full-scale WRRFs (Germany)	0.32 -3.05 μg/L 0.06 - 1.50 μg/L	Total Ag AgNPs	Li et al.,2013a
	Nine full-scale WRRFs (UK)	12.0 ng/L	Total Ag	Johnson et al., 2014
	One full WRRF (Ontario, Canada)	1.90- 2.16 μg/L	AgNPs	Hoque et al., 2012
	A full-scale WRRF (Colorado, USA)	0.52 μg/L, 0.20 μg/L	AgNPs, Dissolved Ag	Mitrano et al., 2012
	One WWTP influent (Germany)	371 ng/L	Total Ag	Hartmann & Schuster, 2013
Effluent	Nine full-scale WRRFs (Germany)	1.0–9.4 ng/L	AgNPs	Li et al., 2013a
	Nine full-scale WRRFs in the UK	0.084 μg/L	Total Ag	Johnson et al., 2011
	A full-scale WRRF (Colorado, USA)	0.10 μg/L, 0.060 μg/L	AgNPs, Dissolved Ag	Mitrano et al., 2012
	A full-scale WRRF (Beijing, China)	2.49 μg/L	Total Ag	Liu et al.,2009
	Two full-scale WRRFs with industrial contributions (Colorado, USA)	0.340 - 0.537 μg/L	Total Ag	Wen et al.,2002
	Predicted silver concentrations			
Influent	Europe	2-18 μg/ L 0.0425 μg/L	Total Ag AgNPs	Blaser et al., 2008 Gottschalk et al.,2009
Effluent	Europe	0.012 - 2.73 μg/L	Total Ag	Blaser et al., 2008
	New York, USA	0.004 - 0.26 μg/L	AgNPs	Lazareva and Keller, 2014
	Shanghai, China	0.008 - 0.13 μg/L		
	Switzerland	0.0298 - 0.127 μg/L	AgNPs	Gottschalket al.,2010
	USA	0.0164 - 0.0747 μg/L		
Sludge	USA	0.27 - 13 mg/ kg	AgNPs	Hendren et al.,2013
	USA	1.29 - 5.86 mg/kg		
	Europe	1.31 - 4.44 mg/kg		
	London, UK	0.58 -1.37 mg/kg	Total Ag	Lazareva and Keller, 2014
	Shanghai, China	0.18 - 0.54 mg/kg		

Considering the effect of coating agents on the colloidal stability of AgNPs against homo-agglomeration (El Badawy et al., 2010), hetero-aggregation of AgNPs is more likely in a biochemically rich wastewater medium in the presence of various ligands and biological macromolecules (Badawy et al., 2010; Huynh and Chen, 2011; Li et al., 2011). Hetero aggregation can modify the particle surface chemistry, particle size and the dissolution of NPs as well as preventing close proximity between AgNPs and bacteria (Badawy et al., 2010; Li et al., 2011)

Generally, NPs are unstable under oxygen-rich aqueous conditions as an oxide layer (Ag_2O) can be formed around the particle and Ag^+ is released in the presence of an oxidizing agent such as dissolved oxygen and protons (Liu et al., 2012). AgNPs and dissolved Ag^+ usually coexist under aerobic conditions and contribute to inhibitory effects of AgNPs (Zhang et al., 2018a). The dynamics of dissolution and the complex nature of Ag^+ release are governed by both particles chemical and surface properties (e.g. surface coating, size, shape) and external environmental parameters (e.g. pH, dissolved organic carbon, inorganic/organic ligands, temperature) (Azodi et al., 2016; Liu et al., 2018; Molleman and Hiemstra, 2017; Zhang et al., 2018a). Oxidative dissolution strongly mediates the toxicity of AgNPs in wastewater as a primary transformation process (Zhang et al., 2018a). A fraction of the released Ag^+ ions may interact with ligands, such as S^{2-} or Cl^- or functional groups of bio-macromolecules in wastewater to form AgCl, Ag_2S, AgNPs and silver complexes in different treatment steps in WRRFs (Azodi et al., 2016; Kaegi et al., 2013; Reidy et al., 2013).

Sulfidation is considered as one of the most important processes that govern the fate and toxicity of AgNPs in WRRFs. Sulfidation of AgNPs, may lead to the formation of partly sulfidated ($Ag(0)/Ag_2S$) or fully sulfidated (Ag_2S) particles, with the latter being formed in high sulfide concentrations which exist in anaerobic environments (Figure 2.4) (Zhang et al., 2018a). The extent of NP sulfidation is highly influenced by particle size and coating, dissolved organic matter concentration, the presence of available reactive sulfide species (H_2S, HS^-) and the HS^-/Ag ratio, among other factors (Azimzada et al., 2017; Kent et al., 2014; Zhang et al., 2018a). Sulfidation of AgNPs was shown to hinder AgNP dissolution partly or completely, due to the formation of Ag_2S and organosulfur complexes which limit the toxicity of AgNPs (Azodi et al., 2016; Levard et al., 2011). Sulfidation of AgNPs, even in the presence of a strong coating agent such as PVP, is proposed as the final thermodynamic fate of AgNPs, which can minimize the

concentration of dissolved Ag (Levard et al., 2013; Liu et al., 2011). Several studies have reported the sulfidation of AgNPs in wastewater streams (Azimzada et al., 2017; Georgantzopoulou et al., 2018; Kaegi et al., 2013) and during sludge treatment (Kampe et al., 2018; Kim et al., 2016; Meier et al., 2016). The non-uniform sulfidation of the AgNP surface contributes to NP dissolution (Kent et al., 2014). Recent studies have reported the bioavalibility and toxicity of sulfidized AgNPs through wastewater treatment processes to different organisms (Kampe et al., 2018; Kraas et al., 2017).

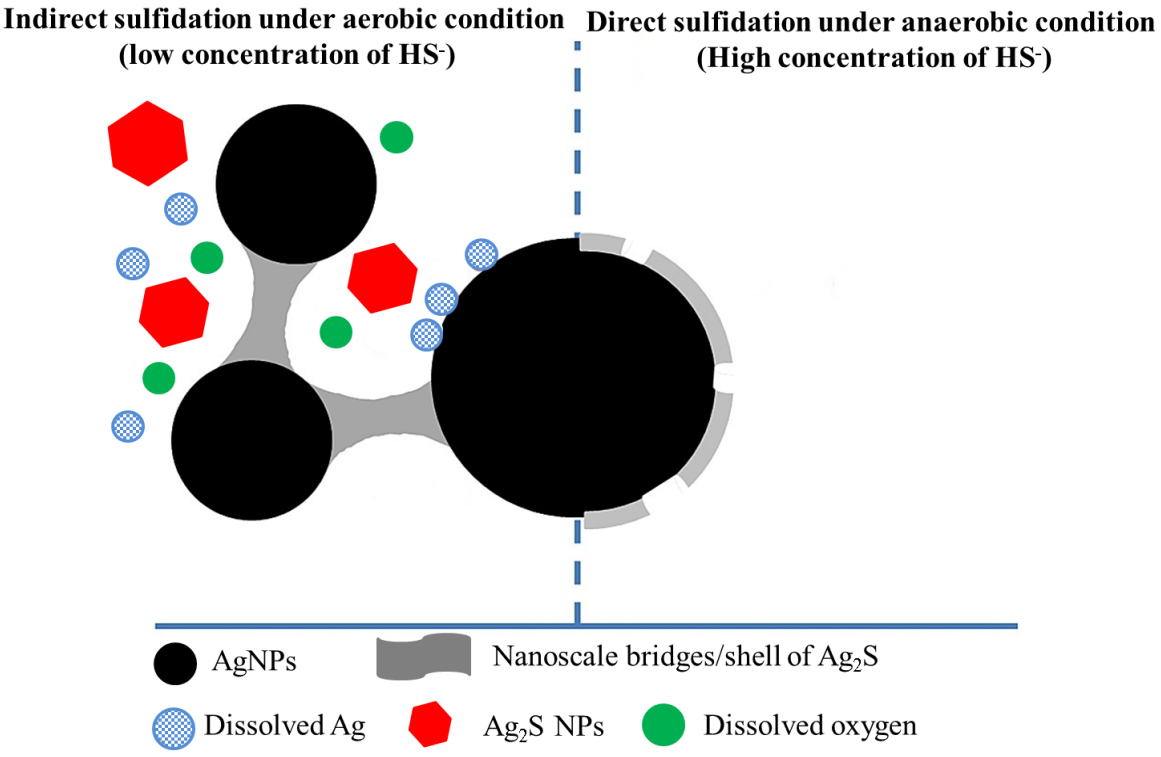

Figure 2.4 : Proposed sulfidation mechanisms of AgNPs (adapted from Zhang et al., (2018a).

Chloride can also act as a sink for Ag^{+} ions released from the oxidative AgNP dissolution by forming insoluble $AgCl_{(s)}$ species at low Cl^{-} concentrations and soluble chloro-silver complexes (i.e., $AgCl_2^{-}$, $AgCl_3^{2-}$, $AgCl_4^{3-}$) at high Cl^{-} concentrations (Figure 2.5) (Azodi et al., 2016; Zhang et al., 2018a). The formation of a nanoscale AgCl layer on the AgNPs with a core (Ag NPs)-shell (AgCl NPs)-type structure at a low Cl/Ag ratio can hinder further dissolution of AgNPs and

decrease their toxic effect (Ho et al., 2010; Levard et al., 2013; Li et al., 2010), but the conversion of the AgCl shell to soluble species of $AgCl_X^{(X-1)-}$ at a high Cl/Ag ratio, can enhance the dissolution of AgNPs and Ag^+-mediated toxicity (Zhang et al., 2018a). Despite the mitigation role of sulfidation and chlorination on the toxicity of AgNPs, recent studies have demonstrated that the transformation products (Ag_2S and AgCl or $AgCl_X^{(X-1)-}$) inherit different morphologies, sizes and various toxicological responses compared to the initial AgNPs, which can still remain bioavailable with inhibitory effects on microorganism (e.g. plants, soil, freshwater biofilm bacteria) (da Silva et al., 2011; Hassellöv et al., 2008; Wu et al., 2018). These transformation pathways are strongly correlated. Oxidative dissolution of AgNPs is considered as the primary step for other processes, except for the direct sulfidation pathway under anaerobic conditions (Zhang et al., 2018a). Thus, transformation pathways and their correlations cannot be overlooked in performing a full risk assessment of AgNPs in WRFFs.

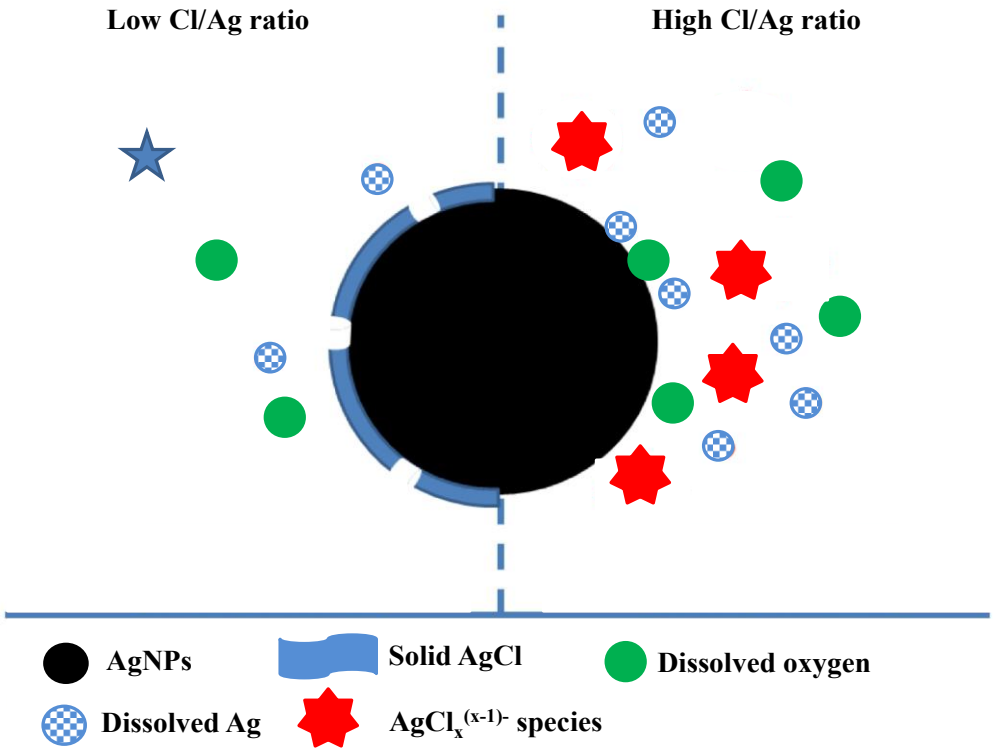

Figure 2.5 : Proposed interactions of AgNPs and chloride (adapted from Zhang et al., (2018a).

2.5.3 Characterization and quantification of AgNPs in WRRFs

Characterization (e.g. size, shape, composition) and quantification of ENPs are critical for government agencies and researchers to develop a comprehensive understanding of the fate and behavior of ENPs in their lifecycle, environmental risks and adaptation of future regulations (Merrifield et al., 2017; Nowack, 2017). Initially, material flow analysis tools have been developed to estimate the environmental concentration of ENPs at the global (Giese et al., 2018; Keller et al., 2013; Song et al., 2017), regional and local levels (Gottschalk et al., 2009; Gottschalk et al., 2013; Keller and Lazareva, 2013). These estimations, however, are based on a number of uncertain assumptions and generalizations (Nowack, 2017). Accurate quantitative characterization of ENPs is mandatory for their environmental risk assessments. To date, a wide range of analytical techniques have been applied for ENP characterization and quantification in simple matrices (Table 2.2). Their application is not feasible in most cases (e.g. biological systems) due to the key limitations of these techniques, such as the inability to perform measurements at low and environmentally relevant concentrations in complex matrices and due to issues with instrumentation capabilities (e.g. detection limits) (Merrifield et al., 2017).

Electron microscopy-based imaging and spectroscopy techniques (e.g. X-ray absorption spectroscopy) have been used recently for NP characterization in complex media, but it did not address pertinent limitations such as detection limits, matrix interferences and speciation (Cervantes-Avilés et al., 2019; Laborda et al., 2016). Scanning and transmission electron microscopy (SEM and TEM, respectively) are widely used for the detection and morphological characterization of AgNPs in WRRFs and in environmental samples, but image acquisition of NPs in such complex matrices is labor intense and can be biased at environmentally-relevant concentrations (Cervantes-Avilés et al., 2019; Doolette et al., 2013). The combination of element-specific techniques, such as inductively coupled plasma mass spectrometry (ICP-MS), ICP-optical emission spectrometry (ICP-OES) with SEM or TEM are the most commonly employed techniques for elemental quantification of ANPs in various complex matrices such as wastewater (Choi et al., 2017; Kaegi et al., 2013; Sheng et al., 2018), effluent from washing machines (Farkas et al., 2011), commercial AgNP-plastic food containers (Echegoyen and Nerín, 2013),

paints (Kaegi et al., 2010; Kumar et al., 2008) or natural surface water (Furtado et al., 2016; Li and Lenhart, 2012).

Using ICP-MS and OES for the chemical quantification of AgNPs is beneficial, but the information is limited to only total Ag concentrations which is not a sufficient predictor of AgNPs fate in environmental matrices (Azimzada et al., 2017). The biological implications of AgNPs are ascribed to both concentrations of NPs and dissolved Ag, yet an open question remains as which fraction dominates the toxicity, particularly in biochemically rich wastewater matrices (Azimzada et al., 2017). Therefore, quantification of Ag in both NP and dissolved forms in the compartments of interest, are necessary for the validation and comprehensive understanding of the fate of AgNPs in complex environmental conditions.

Table 2.2: Analytical techniques for ENP characterization.

Analytical technique	Instrument	Measured parameter
Separation	CFUF/Ultrafiltration	Size
	Sed-FFF	Buoyant mass, equivalent spherical volume diameter
	Flow-FFF	Hydrodynamic diameter, diffusion coefficient
	Centrifugation	Sedimentation coefficient
Microscopy	EM	Shape, size, aggregation state, crystal structure
	AFM	Shape, size, aggregation state
Spectroscopy	ICP-MS	Total elemental composition in bulk
	ICP-OES	Total elemental composition in bulk
	EDX	Semi-quantitative elemental composition for single particles
Light scattering	EELS	Elemental and chemical information
	DLS	Hydrodynamic diameter
	NTA	Size distribution
	XRD	Crystal structure and crystallite size

Note: CFUC: cross-flow ultrafiltration, Sed-FFF: sedimentation field-flow fractionation, Flow-FFF: flow field-flow fractionation, EM: electron microscopy, AFM: atomic force microscopy, ICP-MS: inductively coupled plasma mass spectrometry, ICP-OES: inductively couple plasma optical emission spectrometry, EDX: energy-dispersive X-ray spectroscopy, EELS: electron energy-loss spectroscopy, DLS: dynamic light scattering, NTA: nanoparticle tracking analysis, XRD: X ray diffraction (da Silva et al., 2011; Hassellöv et al., 2008).

The combination of ICP-MS with separation techniques such as ultracentrifugation (Unrine et al., 2012), ultrafiltration (Furtado et al., 2016), cloud point extraction (CPE) (Choi et al., 2017; Liu et

al., 2009) or ionic exchange resins (Hadioui et al., 2015) as a pre-treatment, have been used to obtain additional information on NP concentrations by removing dissolved metal. NP recovery efficiency is highly dependent on the NP and water characteristics with the associated risk of irreversible NP agglomeration/aggregation leading to low efficiency in tracking the original morphology of NPs in environmental samples (Abad-Alvaro et al., 2017; Li et al., 2012).

ICP-MS can be used as an element-specific detector, when coupled on-line with continuous separation techniques such as hydrodynamic chromatography (HDC) or field flow fractionation (FFF), to obtain additional quantitative information regarding the NP size (Abad-Alvaro et al., 2017; Gray et al., 2012; Tiede et al., 2010). Interaction between ENPs and the column in HDC could retain the NPs and lead to poor size resolution (Gray et al., 2012). Relatively low recovery (< 80%) of NPs from the channel membrane in FFF techniques is reported due to unknown nonspecific interactions between particles and channel membranes (Gschwind et al., 2013), making them inadequate techniques for the study of ENPs in complex systems.

Single-particle inductively coupled plasma–mass spectrometry (spICP-MS) is an emerging and powerful technique for simultaneous quantitative characterization of metal NP size distributions, particle number concentrations, dissolved metal concentrations at low NPs concentrations in complex, organic matter-rich, environmental matrices with minimal sample perturbation (Azodi et al., 2016; Merrifield et al., 2017). In standard ICP-MS analysis, metal ions are detected based on their mass to charge ratio and their corresponding intensity readings are integrated over long dwell times (0.3 – 1 s) to determine the metal concentration in the samples (Pace et al., 2012). In contrast, the spICP-MS technique is based on the generation of discrete pulses of clusters of ions that arise from each single particle, when operated at a very low number concentration (10^8 particles/L or lower) and very high data acquisition frequencies (10^2 – 10^5 Hz) (Laborda et al., 2016). The signal is monitored at a higher time resolution than standard ICP-MS, with a very short dwell time (e.g. 100 μs) which results in a signal greater than the constant dissolved background, which is related to the mass of metal in the NP (Pace et al., 2012).

SpICP-MS has been successfully used for the analysis of sizes and concentrations of ENPs, and to quantify and characterize TiO_2NPs, AuNPs and AgNPs in cosmetics and antimicrobial

products (Cascio et al., 2015; De la Calle et al., 2017; Rujido-Santos et al., 2019), CuNPs, ZnONPs, TiO_2 and AgNPs in biological tissues and plants (Keller et al., 2018; Nath et al., 2018; Yamashita et al., 2019) and soil (del Real et al., 2018; González-Fuenzalida et al., 2018; Mahdi et al., 2017; Navratilova et al., 2015; Schwertfeger et al., 2017). Recently, spICPMS were used for the detection, characterization of AgNPs in natural water and lake samples (Jiménez-Lamana and Slaveykova, 2016; Wimmer et al., 2019), seawater (Toncelli et al., 2017) and drinking water (Donovan et al., 2018, 2016; Venkatesan et al., 2018).

Challenges for AgNPs characterization in various wastewaters include not only the need for advanced detection, identification and quantification of AgNPs in wastewater treatment systems, but also the inherent characteristics and preparation of the samples due to the variable composition of different wastewater, inorganic components (e.g. S^{2-}, Cl^{-}) and organic ligands (e.g. poly-alcohols, amines, carboxylic acids) (Merrifield et al., 2017). The key advantages of spICP-MS include elemental selectivity and low detection limits, direct and simultaneous characterization of AgNPs and their ionic compartments make it a suitable method for AgNPs analysis in different processes of WRRFs (Cervantes-Avilés et al., 2019). SpICP-MS have been used for the detection, tracking the dissolution and transformation of spiked AgNPs in wastewater influent and effluent at environmentally relevant AgNP concentrations (0.10 to 500 μg/L) (Azimzada et al., 2017; Azodi et al., 2016; Mitrano et al., 2014; Théoret and Wilkinson, 2017; Tuoriniemi et al., 2017). The information regarding the realistic influent and effluent concentrations of AgNPs in different treatment chains in WRRFs, as well as their size distribution and persistence in these complex media is scarce. The AgNP incidental mass concentrations and removal at various stages of wastewater treatment processes, and their corresponding mass balance in such complex matrix are still missing.

2.6 Implications of AgNPs for biological wastewater treatment processes

Biological treatment is an important and integral part of WRRFs with a significant economic advantage, both in terms of capital investment and operating costs, and the flexibility to handle a wide range of wastewater characteristics and flows. Biological treatment uses a variety of microorganisms, principally bacteria, to (a) convert the biodegradable dissolved, colloidal and particulate organic matters into simple end-products (e.g. CO_2, H_2O, N_2 or HNO_3) and additional

biomass, (b) capture and incorporate the suspended and non-settable colloidal solids into biological flocs and (c) transform or remove nutrients (N and P) (Metcalf and Eddy-AECOM, 2014). The simplified aerobic biological oxidation of organic matter by *ordinary heterotrophic organisms* (X_{OHO}) is presented by equation 2.1.

$$\underbrace{C_6H_{12}O_6}_{\textit{Organic matter}} + O_2 + NH_3 + PO_4^{3-} \xrightarrow{\textit{Microorganisms}} \underbrace{C_5H_7O_2N}_{\textit{New biomass}} + CO_2 + H_2O \qquad \textbf{2.1}$$

Biological treatment processes can be classified by their mechanisms of microbial growth either as aerobic/anaerobic suspended growth, attached growth processes or various combinations of both. In suspended growth processes, the microorganisms, involved in the treatment, are maintained in suspension by mixing or aeration. Activated sludge (AS), lagoons and anaerobic digesters are among the most frequently used suspended growth processes for wastewater treatment. In attached growth systems, the microorganisms are attached to a support medium in the form of an assemblage of microbial cells enclosed in a matrix of bacterial EPS, known as biofilm (Loupasaki and Diamadopoulos, 2013). Natural (e.g. rocks, stones, gravels, sand) or artificial (e.g. plastic) supporting materials can be used for biofilm development which can be either fixed or suspended in the reactor. In fixed-medium systems, such as trickling filters or biological aerated filters, the biological reactions occur in the biofilm developed in the static media. Alternatively, biofilm media are kept continuously moving, either by mechanical, hydraulic or air forces in moving-medium systems, such as rotating biological contactors or fluidized bed biofilm reactors. Considerable attention has been paid to the potential adverse effects on biological wastewater treatment systems due to the antimicrobial properties of ANPs as discussed in the following section.

2.6.1 Fate and inhibitory effects of AgNPs in suspended-growth biological wastewater treatments

The potential toxicity of AgNPs on biological wastewater treatment was initially studied using batch tests with active biomass obtained from bench-scale or full-scale activated sludge systems, mainly exposed to a single dose of 0.5 to 50 mg/L AgNPs over a period of 1 to 24 h (Choi et al.,

2008; Giao et al., 2012; Lara et al., 2011; Sun et al., 2013). These studies concluded that there was a selective bacterial inhibition at sufficiently high AgNP doses (> 1 mg/L). Yet, this conclusion was driven under a high-concentration short-term exposure scenario that was not representative of typical WRRF process conditions (Colman et al., 2018; Zhang et al., 2016a). Thus, more recent studies have tended to investigate the chronic AgNP-induced inhibitory effects at environmentally representative NP concentrations under more realistic scenarios.

The inhibitory effect of AgNPs (0.1 to 50 mg/L) was extensively studied in suspended-growth systems, achieving biological organic matter, nitrogen and phosphorus removal, over various exposure durations (7 to 150 days) (Table 2.3,4). Chronic exposure to AgNPs demonstrated the minimal impact on the removal of organic matter by heterotrophic microorganisms. For example, the concentration of 100 μg/L AgNPs had no adverse effect on organic matter removal and bacterial activities of activated sludge over a 50-day exposure in a sequencing batch reactor (SBR) (Zhang et al., 2016b) and over a 65-day exposure in a membrane bioreactor (Zhang et al., 2014). Only high AgNPs concentrations (up to 10 mg/L) slightly reduced organic matter removal efficiency (Table 2.3). Thus, the majority of recent studies focused primarily on the inhibitory effect of AgNPs on biological nutrient removal (Table 2.4). These studies demonstrated a dose-dependent impact of AgNPs on the biological nitrogen removal and nitrifying biomass activity caused by oxidative stress, cell membrane damage and inactivation of key enzymes at sufficient AgNP doses (up to 1 mg/L). Wastewater microbial species/groups demonstrated a species-specific susceptibility upon exposure to AgNPs (Qiu et al., 2016; Quan et al., 2015; Xu et al., 2017; Zheng et al., 2017). Ammonia oxidizing bacteria (AOB) demonstrated higher vulnerability towards AgNPs treatment, as compared to nitrite oxidizing bacteria (NOB) and organic matter consuming heterotrophs (Alito and Gunsch, 2014; Liang et al., 2010; Zhang et al., 2016b). No significant inhibitory effects of AgNPs is reported on phosphorus removal efficiency below 5 mg/L AgNPs in enhanced biological phosphorus removal systems either with short-term or long-term exposure (Xu et al., 2017; Zhang et al., 2014; Zhang et al., 2016b; Zhang et al., 2018b). Chronic exposure to AgNPs was reported to demonstrate an initial impact of AgNPs on the biological performance of activated sludge systems. A fast recovery of the treatment efficiency, however, was reported due to the relatively high functional redundancy of wastewater microbial communities (Alito and Gunsch, 2014; Quan et al., 2015; Tan et al., 2015).

Process configuration governs biomass growth processes and determines the stability and transformation of AgNPs in the process and their bioavailability and the consequent impact on wastewater microbial communities (Zhang et al., 2016a). The main process configurations that were tested were limited to SBRs and in a few cases, to membrane bioreactors (Table 2.3). SBRs have a unique reactor configuration where aerobic and anaerobic/anoxic conditions occur sequentially. Anaerobic/anoxic conditions with considerable loading of organic matter on the AgNP surface makes the AgNPs susceptible to changes in the aggregation state, oxidation state, precipitation of secondary phases and sorption of (in)organic species on the NP surface, reducing their bioavailability before reaching the aerobic period of the SBRs. The lack of dissolved oxygen and the abundance of organic matter bound to the AgNPs in the anoxic state would also decrease the subsequent dissolution of AgNPs in both the anoxic and aerobic zone. Transformation of AgNPs into Ag–sulfhydryl complexes and Ag_2S during short anoxic/aerobic phases can also reduce their toxicity (Doolette et al., 2013; Yuan et al., 2015). High concentrations of dissolved oxygen and relevant pH (7.7 to 7.8) in other aerobic biological wastewater treatment processes provide thermodynamically favorable conditions for the oxidation and dissolution of AgNPs, influencing their dynamics, especially at low NP concentrations (Azodi et al., 2016; Merrifield et al., 2017). The previous research covers only the tip of the iceberg for all possible combinations of scenarios in real WRRFs. Process configurations, such as completely mixed versus plug flow systems with different oxygen demand, sludge retention time, hydraulic retention time (HRT), biomass characteristics and the size and coating of the AgNPs used under distinct experimental conditions may result in different biological responses to the presence of AgNPs (Quan et al., 2015; Yazdanbakhsh et al., 2019; Zheng et al., 2017).

Table 2.3 : Effect of AgNPs on the organic matter removal in suspended-growth biological wastewater processes.

Treatment System	Effective volume (L)	SRT (d)	HRT (h)	AgNP diameter (nm)	AgNP conc. (mg/L)	Exposure time (d)	Exposure scenario	Impacts	Ref.
Organic matter removal									
SBR	0.9	NA	12	23	0.1 - 0.5	15	Daily spike per cycle	No significant effect on COD removal efficiency	Hou et al., 2012
	7.7	20	8	30	2 - 30	290		Stable COD removal efficiency (92%) < 2 mg/L AgNPs Moderate inhibitory effect @ 2 - 30 mg/L AgNPs	Xu et al, 2017
	1	NA	12	30	0.1 - 0.5	0.5		No significant effect on COD removal efficiency	Chen et al., 2014
	5	15	10	20	0.1 - 10	50	Continuous feeding	No significant effect on COD removal efficiency	Zhang et al.,2016a
	2.2	20	12	119	1 - 5	68	Continuous feeding 1 mg/L for 28 d, increased to 5 mg/L AgNPs for another 40 d	No significant effect on COD removal efficiency Significant impact on EPS composition and activated sludge stability Significant shift in bacterial community structure	Qiu et al., 2016
	2	13	5.3	32	0.2 - 2	122	Spike and continuous feeding	Initial moderate decrease in COD removal efficiency with treatment recovery within 7 days following the pulse or continuous additions of AgNPs Significant change of microbial diversity structure	Alito and Gunsch,2014

Table 2.4: Effect of AgNPs on nitrogen and phosphorus removal in suspended growth biological wastewater process (cont'd).

Treatment System	Effective volume (L)	SRT (d)	HRT (h)	AgNP diameter (nm)	AgNP Con. (mg/L)	Exposure time (d)	Exposure scenario	Impacts	Ref.
Nitrogen/ Phosphorus removal									
SBR	1.5	NA	6	20	5 - 50	22	Two SBRs with flocculent sludge and another two with granular sludge	No inhibitory effect on NH_4 oxidation rate, denitrification efficiency and SOUR of granular activated sludge	Gu et al.,2014
							Daily spike each cycle	Significant inhibition of the NH_4 oxidation rate denitrification efficiency, and SOUR of flocculated activated sludge at both influent AgNP concentrations	
	5	NA	15	10	2.5	10	Daily spike per cycle	No inhibitory effect on nitrification	Doolette et al., 2013
	4	10	NA	20 - 40	1 - 5	130	One-time addition	No inhibitory effect on phosphorus removal efficiency	Chen et al., 2013
							Spike of 3 mg/L AgNPs on day 50	No inhibitory effect on exopoly-phosphatase and polyphosphate kinase enzymatic activities	
							One-time addition of 5 mg/L AgNPs on day 80	Stable microbial community structure with altered the microstructure of EPS	

Table 2.4: Effect of AgNPs on nitrogen and phosphorus removal in suspended growth biological wastewater process (end).

Treatment System	Effective volume (L)	SRT (d)	HRT (h)	AgNP diameter (nm)	AgNP Con. (mg/L)	Exposure time (d)	Exposure scenario	Impacts	Ref.
Nitrogen/ Phosphorus removal									
SBR	2	23	48	52	0.1 - 20	42	Continuous feeding with a sequential weekly increase from 0.1 to 20 mg/L	No inhibitory effect on nitrification below 10 mg/L AgNPs Significant decrease of the functional gene for NH_4 and NO_3 oxidation and microbial community diversity at 10 and 20 mg/L AgNPs	Ma et al.,2015
MBR	7.2	140	12	10	0.1	60	Continuous feedingp	No significant effect on total nitrogen removal	Zhang et al., 2014

2.7 Fate and inhibitory effect of AgNPs in attached-growth biological wastewater treatments

2.7.1 Overview of attached–growth biological wastewater processes

Increasingly stringent discharge limits with a demand for self-sustainable processes with respect to energy, carbon, nutrients and resource recovery, make it imperative to find ways to upgrade existing WRRFs while maintaining low emission standards (Bertanza et al., 2018; Ødegaard, 2016). Attached growth processes are commonly used as an upgrade or a replacement for existing conventional cost-intensive suspended growth systems, (e.g. activated sludge) to meet current and future effluent discharge standards while minimizing plant footprint and operating costs (Falletti and Conte, 2007; Walden and Zhang, 2018). Attached growth processes provide advantages to suspended growth systems in terms of higher biomass concentrations (with larger specific surface areas) in smaller reactor volumes, shorter HRT, operational flexibility and greater resilience under unfavourable environments (Leyva-Díaz et al., 2017; Ødegaard, 2006). Biofilm processes are more compact, with lower treatment capital costs, which can achieve similar treatment targets to suspended growth systems while requiring smaller carbon and ecological footprints due to their higher biomass density in the reactor (Ødegaard, 2006).

Hybrid systems processes offer an alternative which is based on the coexistence of both suspended and attached biomass (Jiang et al., 2018; Silva-Teira et al., 2018). Various types of biofilm processes, such as trickling filters, rotating biological contactors, fixed media submerged or granular media biofilters and fluidised bed reactors have been used extensively for both municipal and industrial wastewater treatment (Aslam et al., 2017; Hassard et al., 2015; Oyarzun et al., 2019; Sonwani et al., 2019). Despite their advantages, these processes have some drawbacks such as mechanical failures, hydraulic instability and back washing demand (Leyva-Díaz et al., 2017; Safwat, 2018).

Moving bed biofilm reactors (MBBRs) were developed in 1989 to overcome these drawbacks and still take advantage of their benefits (Ødegaard, 2006). MBBRs have found a niche in the treatment of municipal and industrial wastewaters as a compact technology for biological wastewater treatment due to its advantages of compactness, simplicity, stability and increased reaction rates (Ødegaard, 2016). The basic principle of the MBBR process is that the biomass

growth attached to the submerged plastic carriers is suspended in continuous motion throughout the entire volume of the reactor by aeration under aerobic conditions or by mechanical mixing under anoxic/anaerobic conditions with no sludge recycling and a relatively high sludge age (Kermani et al., 2008; Leyva-Díaz et al., 2017). The movement of the carriers regulates an efficient substrate mass transfer to the attached biofilm and maintains the thin biofilm layer via hydrodynamic shear forces as a self-cleaning mechanism for the carriers and controlling clogging biomass (Young et al., 2016). The filling ratio (the ratio between the apparent carrier volume and the operation volume of the bioreactor) is kept below 70%, a lower value than for other biofilm systems (Rusten et al., 2006). AnoxKaldnes carriers are the most widely used carrier brand for wastewater treatment, as biofilms primarily develop on the protected surface inside the plastic carrier.

MBBRs can be used for primary, secondary or tertiary treatment, under aerobic, anoxic and anaerobic conditions as a single reactor or configured as several reactors-in-series. Process flow sheets and bioreactor configurations are chosen according to the wastewater characteristics, specific treatment objectives, site layout, existing basin configuration, system hydraulics and existing treatment scheme (Kermani et al., 2008). MBBRs achieving organic matter removal can be operated as low, medium, or high-rate processes. Low-rate MBBRs, receiving an organic loading rate smaller than range 5 g BOD_5 m^{-2} d^{-1}, promote nitrification. Medium-rate MBBRs typically are designed for an organic loading in the range 5 to 10 g BOD_5 m^{-2} d^{-1}. High-rate MBBR systems, are used as a compact secondary treatment, when only BOD removal is required, with a typical organic loading rate of 15 to 20 g BOD_5 m^{-2} d^{-1} and very short bioreactor HRTs (30 to 90 min) with the necessity of chemically enhanced liquid–solids separation and/or flotation (Kermani et al., 2008; Ødegaard, 2000). Biomass grown in high-rate MBBRs can maximize the bio-transformation the rapidly biodegradable chemical oxygen demand (COD) that is soluble (S_B) and colloidal (C_B) into stored particular matters (X_{STO}) and heterotrophic biomass (X_{OHO}), while minimizing the oxidation of colloidal and particulate COD to enhance maximum biogas production achieved by anaerobic sludge digestion (Brosseau et al., 2016).

For conventional mainstream ammonia removal, a nitrifying biomass should be enriched. Nitrification operates in two-steps, first with the biological oxidation of ammonia to nitrite by chemolithotrophic ammonia oxidizing bacteria (AOB), such as *Nitrosomonas*, *Nitrosospira* and

Nitrosococcus, followed by the biologically oxidation of nitrite to nitrate by nitrite oxidizing bacteria (NOB) such as *Nitrobacter* and *Nitrospira* (Young et al., 2017). Nitrifying bacteria in wastewater biofilms proliferate at BOD_5/TKN (BOD/N) smaller than 1.0, whereas an heterotrophic outer layer may hinder nitrifiers for oxygen and nutrients, alter the activity of the nitrifying communities and the ability of the system to remove ammonia at higher C/N ratios (Young et al., 2016). Nitrifier growth proliferation, a stable nitrifying biofilm growth and the best nitrification rates (0.7 to 1.2 g NH_4-N m^{-2} d^{-1}) can be achieved in low carbon environments with a C/N ratio below 1.0 (Hoang et al., 2014; Young et al., 2017). Thus, nitrifying MBBRs are conventionally separated from carbon removal MBBRs and are located downstream of such processes in municipal WRRFs as tertiary nitrification to minimize the adverse effects of carbon-removing heterotrophs overgrowing and smothering the nitrifying autotrophs (Nogueira et al., 2002; ter Haseborg et al., 2010). Nitrogen removal using the MBBR process can also be achieved as pre- or post-denitrification.

MBBRs have been successfully used for municipal and industrial wastewater, including pulp and paper and poultry processing wastewater, pharmaceutical, dairy and aquaculture wastewater and wastewater containing emerging contaminants such as petroleum hydrocarbons (Demeter et al., 2017; Kragelund et al., 2018; Qaderi et al., 2018; Safwat, 2018). MBBRs can be easily combined with other pre- or post- treatment technologies such as settling and membrane separation or used in a series of aerobic and anaerobic MBBRs, thus, increasing the likelihood of achieving a 'zero discharge' goal (Bakar et al., 2018). Nitrifying MBBR has been used recently to provide cost effective, efficient, post carbon removal upgrade systems to current passive lagoon treatment systems at temperatures as low as 1 ^{0}C (Young et al., 2016; Young et al., 2017). In 2014, more than 1,200 wastewater treatment plants in at least 50 countries utilized MBBR technology in both the municipal and industrial sectors with over 36 in North America (Borkar et al., 2013). However, there is a gap in knowledge regarding the environmental fate and inhibitory effects of AgNPs in such treatment chains.

2.7.2 AgNP-biofilm interactions and their implications on attached growth process

Biofilm structures include an outer region of loosely bound EPSs (LB-EPSs), an inner region of tightly bound EPSs (TB-EPSs) and the core bacterial cells (Miao et al., 2017; Wang et al., 2018). EPSs provide architecture, stability and protection for biofilms (Flemming and Wingender, 2010; Sheng and Liu, 2011). Biofilms are comprised of different phenotypes and genotypes, compared to planktonic cells, which impart specific biological activities, metabolic pathways and stress responses (Stewart and Franklin, 2008). Thus, distinct responses of biofilms can be expected upon NP-exposure, however, the information regarding the distribution, interactions and biological implications of AgNPs in attached growth biological processes have not been reported in the literature.

AgNPs initially attach to the heterogeneously amphiphilic surface of the biofilm by electrostatic interactions which subsequently diffuse deeper into the EPS matrix (Peulen and Wilkinson, 2011; Song et al., 2011). AgNP-biofilm interactions, their mobility in the biofilm matrix and their bioavailability depend highly upon their diffusion coefficients, which will be related to their size and physicochemical characteristics of AgNPs as well as the nature of the biofilm and environmental parameters such as water chemistry (Fabrega et al., 2011b; Ikuma et al., 2015; Mitzel and Tufenkji, 2014). A high retention of AgNPs is reported in short term exposure to a single dose of AgNPs (1 to 200 mg/L) with a sequential dose-dependent inhibition of biofilm formation, biofilm structural alteration, inactivation of metabolic activity, and reduction of the biofilm volume (Fabrega et al., 2009; Mallevre et al., 2016; Sheng et al., 2015; Walden and Zhang, 2018). Findings have shown the higher potential of biofilm bacteria than planktonic bacteria to withstand the toxic effects of AgNPs, primarily due to the presence of extracellular polymeric substances (EPS) which act to reduce AgNP diffusion in biofilms over short term exposure conditions (Peulen and Wilkinson, 2011; Walden and Zhang, 2016). However, these studies used mono-species, particularly *P. putida*-based biofilms at different maturity stages in simplified biological media with a short exposure (24 to 96 h) at relatively high concentrations of AgNPs which are not representative of typical WRRF process conditions.

Environmental biofilms consist of consortia of species which highly influence each other in a synergistic and antagonistic manner (Burmølle et al., 2014). Interspecies interactions in mature multispecies biofilms such as wastewater ones, result in emergent functions and capabilities which play an important role in its resistance and adaptation to AgNPs (Røder et al., 2016). The silver resistance gene, located on plasmids, can be transferred between bacterial strains (Joo and Aggarwal, 2018). Thus, the understanding of NP-biofilm interactions, obtained from previous studies using model mono-species biofilms is not fully representative of the behavior of complex microbial communities upon AgNP exposure (Barker et al., 2018; Walden and Zhang, 2016).

A limited number of studies have been conducted to investigate the potential impact of AgNPs, ZnONPs, CuNPs and CeO_2NPs on wastewater biofilm, obtained from sequencing batch biofilm reactors, rotating biological contactors or granular sludge (Hou et al., 2015a; Hou et al., 2014; Hou et al., 2015b; Miao et al., 2017; Sheng and Liu, 2011; Sheng et al., 2015; Wang et al., 2018; Zheng et al., 2017). Findings have indicated a high bacterial tolerance of mature wastewater biofilms to metal oxide nanoparticles (> 50 mg/L) without significant effect on the biofilm microbial community and function over short-term exposure (8 to 24 h). Wastewater biofilms demonstrated a similar high tolerance upon 24 h exposure to 200 mg/L AgNP treatment (Sheng and Liu, 2011; Sheng et al., 2015).

Single high dose of NPs over short-term exposure is relevant for examining the short-term impact and mechanisms in wastewater biofilm, but such approaches may fail to capture the effects of the expected accumulation and higher mass transport of AgNPs by diffusion into deeper layers of the biofilm over extended time intervals. Thus, they underestimate the potential toxicity of AgNPs over long-term exposure scenarios (Colman et al., 2018). Further research is required to understand the interaction mechanisms between AgNPs and mature, mixed culture wastewater biofilms and to investigate the corresponding AgNP-induced inhibitory effects at environmentally representative NP concentrations under conditions that are representative of typical WRRF processes. Previous studies have used biological or toxicological endpoints to evaluate the inhibitory effect of AgNPs on process efficiency and on microbial communities. The quantitative characterization of AgNPs, however is missing in these studies. Consequently, they fail to validate and understand the fate of AgNPs and their mechanisms of toxicity in such complex environmental conditions.

CHAPTER 3 RESEARCH OBJECTIVES, HYPOTHESES AND METHODOLOGY

3.1 Critical assessment of past research findings

Much effort has been made to study the potential risks of AgNPs in biological wastewater processes, but controversy remains about their specific effects. Available data implies that the inhibitory effects of AgNPs in suspended-growth biological wastewater treatment depends largely on the process configuration, redox conditions, the concentration of AgNPs and dissolved silver, their transformation as well as exposure time. The majority of previous studies have used the biological or toxicological endpoints to evaluate the inhibitory effect of AgNPs on suspended-growth treatment efficiency and their microbial communities using some reactor configurations (e.g, SBR, MBR) under distinct experimental conditions. A rigorous physical and chemical characterization of AgNPs (e.g. size, composition, dissolution) is missing in most studies. Thus, current research still fails to provide a fundamental understanding of the environmental behavior, interactions and transformations of AgNPs for the possible combinations of scenarios in real WRRFs.

Suspended growth biological processes are extensively used to elucidate the fate and biological implications of AgNPs in wastewater biological treatment processes. Attached-growth biological processes are rarely investigated, however, for the environmental fate and inhibitory effects of AgNPs. A few studies demonstrated a high tolerance of wastewater biofilm upon exposure to a single high dose of AgNPs over short-term exposure which is not representative of typical WRRF process conditions. Such approaches may underestimate the potential toxicity of AgNPs in attached-growth systems over long-term exposure. Thus, further research is required to understand the interaction mechanisms between AgNPs and mature, mixed culture wastewater biofilms and to investigate the corresponding AgNP-induced inhibitory effects at environmental NP concentrations under conditions that are representative of typical WRRF processes.

3.2 Research objectives

The general objective of this research project is to determine the fate, transport and chronic impact of environmental concentrations of AgNPs in attached growth wastewater treatment processes.

The specific objectives are to:

(1) Determine the retention and distribution behavior of AgNPs in aerobic attached-growth biological processes;
(2) Determine the impact of long-term continuous release of AgNPs on primary biological functions and the microbial community of aerobic heterotrophic wastewater biofilms, achieving organic matter removal and
(3) Determine the impact of AgNPs long term continuous release on primary biological functions and the microbial community of aerobic autotrophic nitrifying wastewater biofilms, achieving ammonia removal.

Research questions arise concerning the interaction dynamics, bioavailability and chronic inhibitory effects of AgNPs in engineered biofilm processes.

(1) Is long-term exposure to AgNPs a concern for attached-growth biological process suitability at their environmental concentrations?
(2) How does long-term exposure to AgNPs impact the microbial communities in wastewater biofilm processes?
(3) What is the main mechanism of toxicity of AgNPs in biofilm processes?
(4) What is the critical role of attached growth biofilm processes on the environmental release of bioavailable AgNPs via effluent as well as the potential biological implications for treatment chain efficiency of downstream processes?
(5) What are the strategies to control the release of such AgNPs from biofilm systems?

3.3 Original scientific hypotheses

The objectives of the project are derived from the following hypotheses:

(1) Aerobic heterotrophic and nitrifying wastewater biofilm retains a large fraction of AgNPs (> 90%) in an attached–growth MBBR process, receiving a continuous inflow of low concentrations of AgNPs up to a saturation level.

Originality: A quantitative Ag fractionation in terms of nanoparticle, dissolved Ag and total Ag are determined in influent, bioreactor, biofilm and effluent of an attached-growth MBBR process

as well as NP mean diameters and transformed species is undertaken for the first time in this study which allows us to assess the AgNPs aggregation state, dissolution and distribution between different phases of the MBBR.

The higher biomass surface area/volume ratio in the MBBR process enhances the deposition rate of AgNPs to the attached biomass leading to a higher Ag retention per unit weight of biomass in the reactor, compared to activate sludge systems. The hypothesis will be rejected if aerobic wastewater biofilm demonstrates a limited retention capacity for AgNPs with extensive AgNPs washout via the effluent.

(2) Long-term continuous exposure to environmental concentrations of AgNPs (< 100 μg/L) does not influence significantly the COD removal efficiency, which is primary biological activity of the aerobic heterotrophic biofilm and the biofilm microbial communities in an attached–growth MBBR process achieving organic matter removal.

Originality: This is the first study evaluating the fate and chronic impact of AgNPs at environmentally-relevant concentrations in an attached–growth MBBR system achieving organic matter by combining the biological response and NP characterization.

Biofilm bacteria have a higher potential to withstand the toxic effects of AgNPs than planktonic bacteria, primarily due to the presence of extracellular polymeric substances (EPS) which reduce AgNP diffusion in biofilms. The hypothesis will be refused if the COD removal efficiency, primary biological activities of the microbial communities (diversity and composition) of the aerobic heterotrophic wastewater biofilm are significantly decreased (>5%) by chronic exposure to environmental concentrations of AgNPs (<100 μg/L).

(3) Long-term continuous exposure to environmental concentrations of AgNPs (< 100 μg/L) does not significantly influence the nitrification, primary biological activities of aerobic nitrifying biofilm (e.g. viability, key enzymatic activities) and the biofilm microbial communities in an attached–growth nitrifying MBBR.

Originality: To the best of our knowledge, this is the first study evaluating the fate and chronic impact of AgNPs at environmentally-relevant concentrations of AgNPs in an attached–growth nitrifying MBBR system, by combining the biological response and NP characterization.

Autotrophic nitrifying bacteria are slow growing organisms with a limited ability to produce EPS. The hypothesis will be refused if the nitrification, primary biological activities of ammonia oxidizing bacteria (AOB) and nitrite oxidizing bacteria (NOB) and microbial communities of aerobic nitrifying wastewater biofilm are significantly decreased (>5%) by chronic exposure to environmental concentrations of AgNPs (< 100 μg/L).

3.4 Research strategy and methodology

Attached growth processes, such as MBBRs are commonly used as an upgrade or replacement for existing biological processes to meet current and future effluent discharge requirements. Therefore, a MBBR system was chosen in this study to investigate the inhibitory effects of AgNPs in attached-growth biological processes. The MBBR can be used as a primary, secondary or tertiary treatment as a single reactor or configured as several reactors-in-series. Three different MBBR systems, representing the common MBBR configurations in WRRFs, achieving organic matter removal and nitrification were used. Total biofilm surface area and HRT are the main scaling parameters in such processes. A high-rate organic matter-removal MBBR with a very short hydraulic retention time (HRT of 1h) was used as a compact secondary treatment for BOD removal (Figure 3.1a). A medium-rate organic matter-removal MBBR (HRT of 3 h) was used to represent two different scenarios, including (a) COD-removal MBBR as the pre-treatment of an activated sludge (AS) system to upgrade an existing WRRF (Figure 3.1b) and (b) COD-removal MBBR for separation of BOD ahead of the biological N-removing step, in a serial MBBR configuration (Figure 3.1c). The nitrifying MBBR (HRT of 3 h) was used to represent a post carbon removal nitrifying biofilm system or a tertiary nitrification system after a convention AS system with stringent effluent standards (Figure 3.1d). The chronic impact of AgNPs in an attached growth wastewater treatment process was studied at nominal influent concentrations of 10, 100 and 600 μg/L AgNPs. Although these concentrations would be at the higher end of the estimated concentration for WRRFs, they would mimic a worst-case scenario, such as flooding events or production plant outfalls.

Nanoparticle surface coating characteristics highly influence their surface chemistry, dissolution and transformation in complex environmental media with consequent changes in their bioavailability and toxicity (Tejamaya et al., 2012). Polyvinylpyrrolidone (PVP) is one the most commonly used stabilizer for AgNPs, preventing their aggregation via inter-particle steric stabilization (Levard et al., 2011; Mitzel and Tufenkji, 2014; Song et al., 2011). PVP is a non-toxic and homogeneous amphiphilic polymer containing both a hydrophilic component (the pyrrolidone moiety) and a hydrophobic group (the alkyl group with six carbons per monomer unit)(Koczkur et al., 2015; Ziaei-Azad and Semagina, 2014). PVP is a very stable polymer, with inert physicochemical properties over a range of pH values and ionic strength (Kedia and Kumar, 2012; Tejamaya et al., 2012). 40 kDa PVP-stabilized AgNPs were commonly used in eco-toxicological exposure studies due to their high stability under different environmental conditions (Ahlberg et al., 2014; Cervantes-Avilés et al., 2019; Doolette et al., 2013; King et al., 2015; Mitzel and Tufenkji, 2014; Sheng et al., 2018; Song et al., 2011; Tejamaya et al., 2012). Thus, the research conducted in this thesis used 50-nm AgNPs, capped with 40 kDa PVP polymers, purchased from Nanocomposix (Econix silver), for better comparison and validation of our experimental data with previous literature.

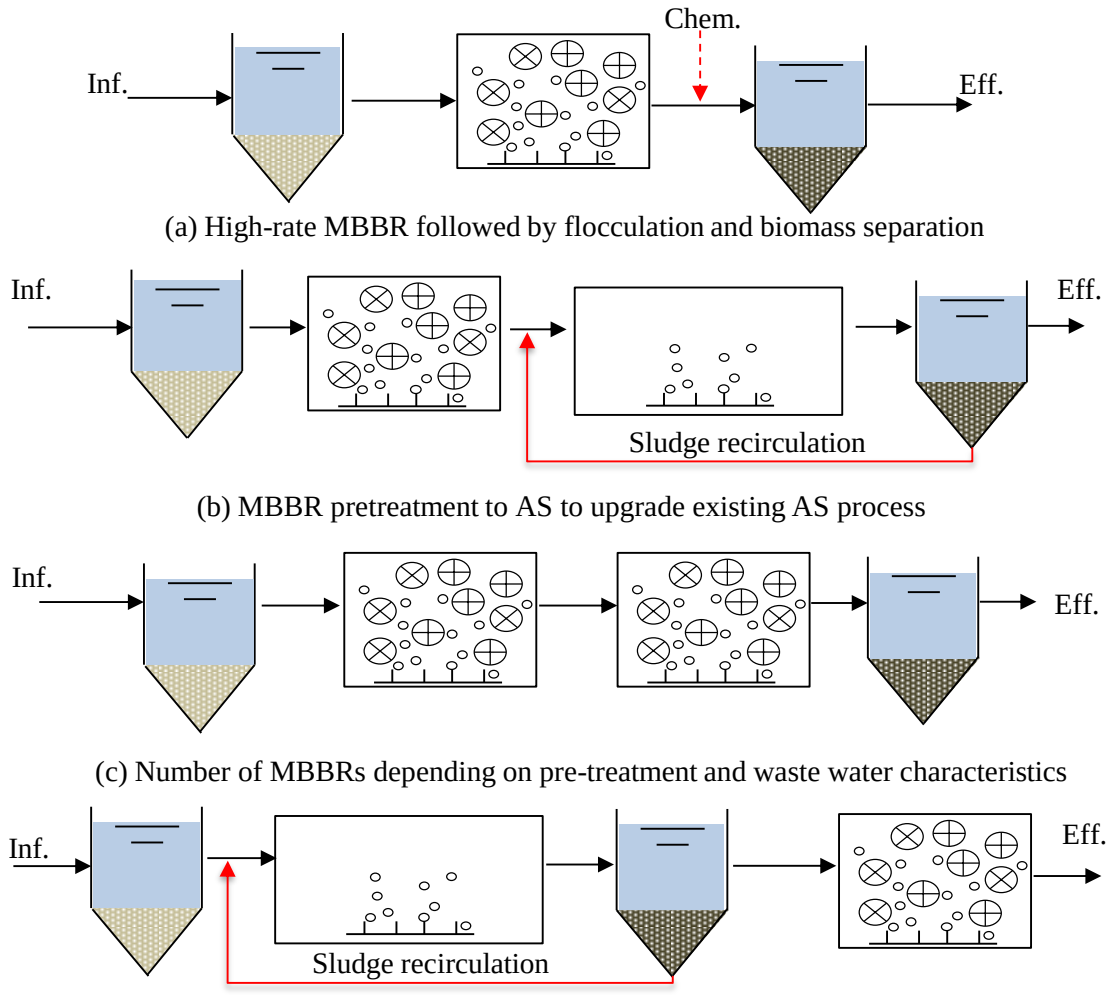

(a) High-rate MBBR followed by flocculation and biomass separation

(b) MBBR pretreatment to AS to upgrade existing AS process

(c) Number of MBBRs depending on pre-treatment and waste water characteristics

(d) Tertiary nitrification. MBBR placed after a conventional AS

Figure 3.1: Typical process flow sheet for COD removal, nitrification and a combined C/N removal MBBR system (adapted from McQuarrie and Boltz, 2011).

Rigorous physical and chemical characterization of AgNPs combined with extensive biological and toxicological evaluations in WRRFs are critical in laying the ground for a better understanding of their environmental fate and the inhibitory effects of AgNP in WRRFs. Cell membranes and enzymes are significantly involved in the toxicity mechanisms of AgNPs. They might be the main biological targets of the interactions of AgNPs with the surface of bacteria cells. Thus, AgNPs would significantly alter the cell structures (e.g. cell membranes) and damage its components (such as nucleic acids, lipids, proteins, enzyme conformational changes) and lead to paralyzed important cellular functions (e.g. metabolic activities) (Grün et al., 2018).

Both intracellular dehydrogenase (DHA) enzymes and extracellular hydrolactic enzymes, such as α-glucosidase (α-Glu) and protease (PRO), play critical roles in wastewater biological processes. The DHA specific activity is directly related to the oxidative organic substrate transformation rate and in turn, can be correlated to viable biomass fractions (Goel et al., 1998). The extracellular α-Glu and PRO, released by heterotrophic biofilm bacteria, are responsible for the degradation of carbohydrates and proteins in wastewater influencing the removal of organic matter and biofilm microbial metabolism. Performance of nitrifying biofilm is directly related to the activities of membrane-bound ammonia monooxygenase (AMO) and nitrite oxidoreductase (NOR) (Barker et al., 2018). Autotrophic AOB uses the AMO to catalyze ammonia oxidation; NOB subsequently oxidizes nitrite to nitrate using NOR (Spieck et al., 1998). Oxidative stress as the consequence of intracellular ROS generation and its impact on membrane integrity has been reported as an alternative, major AgNP-specific mechanism toxicity (Choi et al., 2008).

The experimental approach, therefore, was organized in 5 main parts to validate or invalidate the research hypotheses.

1) Characterize AgNPs and dissolved Ag mass concentrations, nanoparticle mean diameters, total Ag and a cumulative Ag mass distribution in different phases of the MBBR.
2) Determine the impact of AgNPs on the performance of the MBBRs in terms of soluble COD (S_{COD}) and ammonia removal efficiency and effluent quality.
3) Characterize the biological response in terms of biofilm viability intracellular and extracellular specific enzymatic activities involved in organic matter removal and nitrification.
4) Determine the oxidative stress induced by AgNPs via measurement of intracellular reactive oxygen species (ROS).
5) Determine the impact of AgNPs on the microbial community structure and composition.

To avoid repetition with the upcoming chapters, a summary of the methods is presented in Table 3.1. Details on reactor configurations and operations, biofilm biological response characterization and AgNPs analysis are presented in Chapters 4, 5 and 6. A summary of the experimental approach for each hypothesis along with expected results and the corresponding chapters of the thesis are presented in Table 3.2.

Table 3.1: Experimental methodology

1.Experimental setup	**Moving bed biofilm reactors** 1 L MBBRs, fed with a synthetic soluble influent HRT of 1 to 3 hours 60% volumetric filling ratio with AnoxKaldnes K5 carrier
2.Characterization of biofilm biological response to long-term AgNPs exposure	**Biological treatment performance:** S_{COD} /Ammonia removal efficiency Effluent quality **Viability assay:** Live/dead Baclight bacterial viability kit (Molecular Probes, Invitrogen, Kit L13152) and the microplate reader (BioTek, USA) Confocal scanning Laser microscopy **Enzymatic activity:** **α-Glycosidase** = colorimetric method with 1% p-nitrophenyl-d-glucopyranoside as a substrate **Dehydrogenase** = colorimetric method with 2-(4-Iodophenyl)-3-(4-nitrophenyl)-5-phenyl-2H-tetrazolium chloride as substrate **AMO** = Analytical method with 2 mM $(NH4)_2SO_4$ in 0.01M PBS solution (pH 7.4) as a substrate **NOR** = Analytical method with 1 mM $NaNO_2$ in 0.01M PBS solution (pH 7.4) as a substrate
3.Toxicological impact of AgNPs on biofilm microorganism	**Reactive oxygen species assay (ROS)** 20 min incubation of control and treated biofilm with 10 μM dichlorofluorescein diacetate (H_2DCF-DA), at 37 °C. Determination of the generated DCF at Ex/Em of 488 nm /525 nm
4. Effects AgNPs on bacterial community compositions	**DNA extraction- MiSeq (Illumina) next generation sequencing** FastDNA®spin kit (MP Biomedicals, Santa Ana, CA)-Universal Primers :16S V_4 Forward and Reverse Primers
5.Fate and transformation of AgNPs	**SpICP-MS/ICP-MS:** Influent, effluent and bioreactor samples were analyzed the first 7 days and every 4 days after **TEM-EDS**

Table 3.2 : Experimental approach to validate (or invalidate) the research hypothesis and corresponding chapters of the thesis (cont'd).

	Specific Objective	Hypothesis	Experimental approach	Expected result	Chapter
1	Determine the retention and distribution behavior of AgNPs in aerobic attached-growth biological processes	Aerobic wastewater biofilm retains a significant fraction of AgNPs (>90%) in an attached –growth MBBR process.	AgNPs, dissolved Ag and total Ag analysis in influent, effluent and bioreactor samples over the exposure period using spICP-MS/ICP-MS and TEM-EDS Calculation of cumulative Ag mass distribution in different reactor phases	High retention capacity of attached biofilm for AgNPs without extensive AgNPs washout via effluent.	4, 5, 6
2	Determine the chronic impact of AgNPs on primary biological functions and the microbial community of aerobic heterotrophic wastewater biofilms, achieving organic matter removal	Chronic exposure to environmental concentrations of AgNPs (<100 μg/L) will not significantly influence the COD removal efficiency, primary biological activities and microbial communities of aerobic heterotrophic biofilm in an attached growth MBBR process achieving organic matter removal.	Monitoring performance indicators including S_{COD} removal efficiency, effluent quality Characterize the biofilm cell membrane integrity using DNA-binding stains Determine the AgNP-mediated oxidative stress via intracellular ROS measurement Characterize microbial metabolic functions by intracellular DHA and extracellular α-Glu and PRO specific enzymatic activities using colorimetric assays Characterize the microbial community compositions using high-throughput sequencing	Significant inhibition of S_{COD} removal efficiency Significant inhibition of biofilm cell membrane integrity damage Significant inhibition of specific activities of both intracellular DHA and extracellular α-Glu and PRO enzymes Significant generation of intracellular ROS Shift in biofilm microbial community composition	4, 5

Table 3.2: Experimental approach to validate (or invalidate) the research hypothesis and corresponding chapters of the thesis (end).

	Specific Objective	Hypothesis	Experimental approach	Expected result	Chapter
3	Determine the chronic impact of AgNPs on primary biological functions and on the microbial community of aerobic autotrophic nitrifying wastewater biofilms, achieving ammonia removal.	Chronic exposure to environmental concentrations of AgNPs (<100 μg/L) will not significantly influence the nitrification, primary biological activities of aerobic nitrifying biofilms (e.g, viability and key enzymatic activities) and the biofilm microbial communities in an attached–growth nitrifying MBBR	Monitoring ammonia removal efficiency and effluent quality Characterize the biofilm cell membrane integrity using DNA-binding stains Determine the AgNP-mediated oxidative stress via intracellular ROS measurement Characterize microbial metabolic functions by membrane bound AMO and NOR specific enzymatic activities using analytical technique Characterize the microbial community compositions before and after exposure to AgNPs using high-throughput sequencing	Significant inhibition of ammonia removal efficiency Significant inhibition of biofilm cell membrane integrity damage Significant inhibition of specific activities of both AMO and NOR specific enzymatic activities Significant generation of dose-dependent intracellular ROS Shift in biofilm microbial community composition	6

CHAPTER 4 ARTICLE 1: FATE AND INHIBITORY EFFECT OF SILVER NANOPARTICLES IN HIGH RATE MOVING BED BIOFILM REACTORS

Our objective was to assess the vulnerability of attached-growth biological wastewater treatment processes, receiving continuous inflow of environmental relevant concentrations of AgNPs. The fate and inhibitory effects of polyvinylpyrrolidone (PVP)-coated AgNPs (50 nm) at nominal concentrations of 10, 10 and 600 μg/L were determined for the first, using a high rate moving bed biofilm reactor (MBBR). Single particle inductively coupled plasma mass spectrometry (spICP-MS) was used to quantitatively characterize the aggregation state, dissolution and distribution of AgNPs between different reactor phases (i.e. influent, bioreactor and effluent). Our results suggest that the inhibitory effects of AgNPs can be a concern even at concentrations as low as 100 to 600 μg/L Ag in biological attached growth wastewater treatments, with a limited retention capacity of biofilms for AgNPs compared to the commonly used activated sludge systems. This chapter was published as a research paper in the journal of *Science of the Total Environment* in 2018. Supplementary information is presented in Appendix A.

Alizadeh, S., Ghoshal, S., & Comeau, Y. (2019). Fate and inhibitory effect of silver nanoparticles in high rate moving bed biofilm reactors. *Science of the Total Environment, 647,* 1199-

FATE AND INHIBITORY EFFECT OF SILVER NANOPARTICLES IN HIGH RATE MOVING BED BIOFILM REACTORS

Sanaz Alizadeh[1*], Subhasis Ghoshal[2], Yves Comeau[1]

[1]Department of Civil, Geological and Mining Engineering, Polytechnique Montreal, 2500 Polytechnique road, Montreal (Quebec) Canada H3T 1J4

[2] Department of Civil Engineering and Applied Mechanics, McGill University, 817 Sherbrooke Street West, Montreal (Quebec) Canada H3A 0C3

[*]Corresponding author: sanaz.alizadeh@polymtl.ca

ABSTRACT

Municipal water resource recovery facilities are the primary recipients of a significant fraction of discharged silver nanoparticle (AgNP)-containing wastes, yet the fate and potential risks of AgNPs in attached-growth biological wastewater treatment processes are poorly understood. The fate and inhibitory effects of polyvinylpyrrolidone (PVP)-coated AgNPs at environmentally relevant nominal concentrations (10, 100, 600 μg/L) were investigated, for the first time, in high rate moving bed biofilm reactors (MBBRs) for soluble organic matter removal. The behavior and removal of continuously added AgNPs were characterized using single-particle inductively coupled plasma mass spectrometry (spICP-MS). While no inhibitory effect at average influent concentration of 10.8 μg/L Ag was observed, soluble COD removal efficiency was significantly decreased at 131 μg/L Ag in 18 days and 631 μg/L Ag in 5 days with suppressed biofilm viability. The inhibitory effect of AgNPs on treatment efficiency was highly correlated to the retained mass of total Ag in attached biofilm on the carriers. Biofilm demonstrated limited retention capacity for AgNPs over 18 days. Considerable mass of Ag (38% to 75%) was released via effluent, predominantly as NPs. We detected some chemically transformed and potentially less toxic forms of silver nanoparticles (Ag_2S, AgCl), over the exposure period. This study demonstrated the distinct interaction dynamics, bioavailability and inhibitory effects of AgNPs in a biofilm system. Release of bioavailable AgNPs via effluent and AgNP-rich biofilm, sloughing off the carriers, can affect the treatment chain efficiency of downstream processes. Thus, the inhibitory effects of AgNPs can be a concern even at concentrations as low as 100 to 600 μg/L Ag in biological attached growth wastewater treatments.

Keywords: Silver nanoparticles, moving bed biofilm reactor, toxicity, single particle ICP-MS, dissolution.

4.1 Introduction

Silver nanoparticles (AgNPs) are the most widely used metal nanoparticles in various commercial products, cosmetics, food processing and also as an alternative disinfectant and anti-biofouling agent in various products and in industrial pipelines (e.g. in the food, fermentation and water treatment industries), due to their effective antimicrobial properties (Huang et al., 2016; Liu et al., 2014; Patlolla et al.; 2012, Mohanta et al., 2017). Materials flow analyses of released AgNPs from personal care products, various household and industrial products suggest that a significant fraction of discharged AgNP-containing wastes enter municipal water resource recovery facilities (WRRFs) with an estimated influent concentration of AgNPs around 1.5 μg/L (Gottschalk et al., 2009; Li et al., 2010). Thus, WRRFs play an important role in controlling the release of such engineered nanoparticles (ENPs) into the environment by their liquid or biosolids discharges.

The toxicity of AgNPs to bacteria is caused by cell membrane damage, inactivation of key enzymes and DNA, and oxidative stress via the generation of reactive oxygen species (Durán et al., 2016). Given the antimicrobial activity of AgNPs, their potential inhibitory effects on microbial communities involved in biological wastewater treatment processes and the implications for treatment efficiencies cannot be overlooked. The inhibitory effect of AgNPs (0.1 to 20 mg/L) was extensively studied in suspended-growth systems over various exposure scenarios (20 to 70 days) (Alito and Gunsch, 2014; Yang et al., 2014; Zhang et al., 2016c). Attached-growth biological processes (e.g. moving bed biofilm bioreactors), however, are rarely investigated for the environmental fate and inhibitory effects of AgNPs.

Biofilm is comprised of different phenotypes and genotypes which impart specific biological activities, metabolic pathways, and stress responses (Stewart and Franklin, 2008). The extracellular polymeric substances (EPS), primary components of the biofilm, play a crucial role in both AgNP-biofilm interactions, subsequent diffusion of NPs into the biofilm and their toxicity (Fabrega et al., 2009; Peulen and Wilkinson, 2011). A few recent studies have reported the high retention of AgNPs by biofilm, inhibition of biofilm formation, biofilm structural alteration, inactivation of metabolic activity, and reduction of the biofilm volume (Fabrega et al., 2009; Mallevre et al., 2016; Park et al., 2013). These studies used mono-species biofilms at different

maturity stages with exposure time between 24 h to 96 h over a range of AgNPs concentrations (1 to 100 mg/L). These toxicity experiments were conducted in simplified biological media, under conditions that are not representative of typical WRRF process conditions.

Various studies, including those discussed above, have used biological or toxicological endpoints to evaluate the inhibitory effect of AgNPs on process efficiency and on microbial communities but did not evaluate changes in AgNP characteristics such as size and composition, or their dissolution. High concentration of dissolved oxygen and relevant pH (7.7 to 7.8) in aerobic biological wastewater treatment processes provide thermodynamically favorable conditions for oxidation and dissolution of AgNPs, influencing their dynamics, especially at low NP concentrations (Azodi et al., 2016; Merrifield et al., 2017). Neither total Ag nor Ag^{+} concentrations are sufficient predictors of AgNPs inhibitory effects (Azimzada et al., 2017). Therefore, quantification of Ag in its NP and dissolved forms, in the compartments of interest, are necessary for the validation and comprehensive understanding of the fate of AgNPs and their mechanisms of toxicity in such complex environmental conditions.

Studies of the fate of AgNPs at environmentally relevant concentrations in complex environmental matrices are scarce, due to the challenges of analytical methods. Single-particle inductively coupled plasma mass spectrometry (spICP-MS) is an emerging analytical technique that is able to simultaneously characterize metal NP size distributions, particle number concentrations and dissolved metal concentrations at low NPs concentrations in complex, organic matter-rich, environmental matrices (Azodi et al., 2016; Mitrano et al., 2012; Pace et al., 2012).

The specific objectives of this study were to (1) characterize the retention and distribution behavior of AgNPs in aerobic attached-growth biological wastewater treatment process and to (2) determine the inhibitory effect of AgNPs on the COD removal efficiency and biofilm viability of a continuous exposure at nominal influent concentrations of 10 to 600 μg/L AgNPs. A lab-scale high-rate moving bed biofilm reactor (MBBR), for organic matter removal, was used in this study and fed with a synthetic soluble influent. The impact of AgNPs on the performance of the MBBRs was characterized in terms of soluble COD (S_{COD}) removal efficiency, effluent quality and biofilm viability over a period of 18 days. The biofilm membrane integrity was evaluated using a fluorescent microscopy technique with two DNA-binding stains (SYTO-9 and propidium iodide). The nanoparticle mean diameters, AgNP and dissolved Ag mass concentrations were

simultaneously quantified in influent, bioreactor and effluent samples using spICP-MS to assess aggregation state, dissolution and distribution between different reactor phases. The retention capacity of the attached biofilm for Ag was estimated based on the cumulative total Ag mass balance. To the best of our knowledge, this is the first study evaluating the fate and toxicity of PVP-AgNPs at environmentally relevant concentrations in attached-growth MBBR systems.

4.2 Materials and Methods

4.2.1 Reactor configuration

Three 1 L lab-scale MBBR reactors, operated in parallel under identical conditions, were fed with synthetic soluble influent (Figure 4.1). Synthetic wastewater was used throughout the experimental phase to ensure constant influent characteristics and well-controlled conditions to identify the inhibitory effects of the PVP-AgNPs. The concentrated solution (2.5 g S_{COD}/L) was based on a recipe adapted from OECD (1976) to obtain a typical C/N/P ratio of 100/12/2 for a medium to high strength domestic wastewater (Metcalf & Eddy-AECOM, 2014) (Table 4.1). Sodium acetate, soy protein and peptone were used to mimic the readily-degradable carbonaceous content of wastewater (Table 4.1). The synthetic influent provided C, N, P and minerals to favor biofilm growth. The concentrated feed was pumped and diluted with tap water before entering the reactors to obtain a COD concentration of 250 mg S_{COD}/L at organic loading rate of 11.2 g COD m^{-2} d^{-1} of active surface area (Table 4.1) to be representative of the soluble fraction (without TSS) of a medium strength wastewater (Metcalf & Eddy-AECOM, 2014). Tap water was used as dilution water to provide additional minerals (Mg, Ca, etc.). The characteristics of the synthetic influent, after dilution of the concentrated solution, are presented in Table 4.2.

The reactors operated at a hydraulic retention time (HRT) of 1 hour, pH of 7.4 ± 0.1, a dissolved oxygen concentration (DO) of 6.5 ± 0.9 mg/L and 60% volumetric fill ratio with AnoxKaldnes K5 carriers (Veolia Water Technologies Canada Inc.) with a specific active surface area of 800 m^2/m^3. The carriers were kept in suspension by aeration. The air was humidified to compensate for evaporation from the reactors. In the preliminary start-up phase, all reactors were inoculated with K3 carriers, collected from the full-scale MBBR at the Mascouche Terrebonne WRRF (Quebec, Canada) for a period of five days to favor biofilm growth and to ensure the

development of a representative microbial community of a WRRF (Brosseau et al., 2016). Subsequently, the K3 carriers were removed from the reactors. The temperature was controlled at 21 ± 0.2 °C in the double-jacketed MBBRs by a circulator (Programmable Circulator 9712, PolyScience, USA).

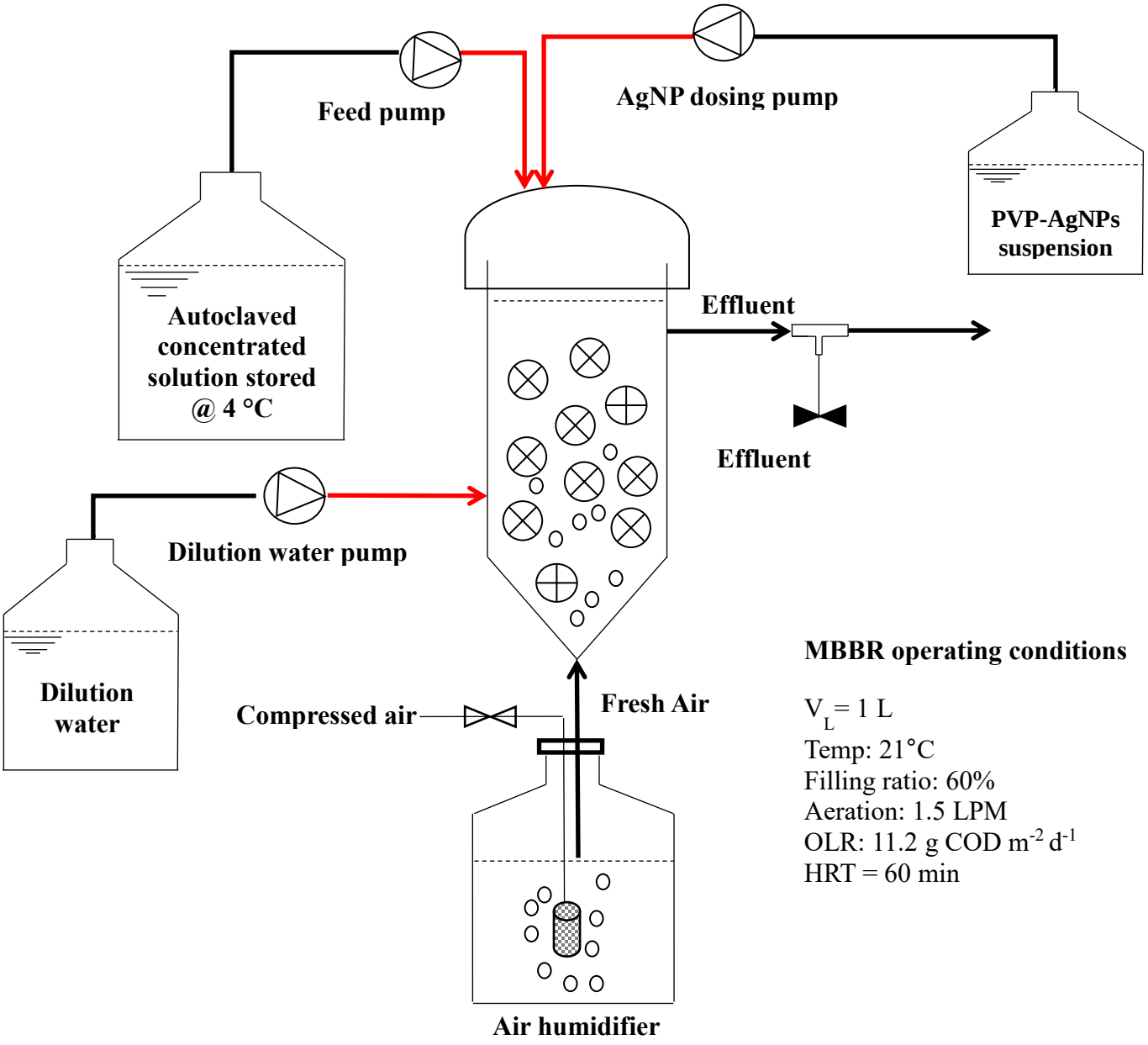

Figure 4.1: Schematic of the experimental setup.

Table 4.1: Concentrated feed composition of the synthetic wastewater

Compounds	**Chemical formula**	**Concentration**	
Sodium acetate trihydrate	$CH_3COONa \cdot 3H_2O$	933	mg COD/L
Sodium propionate	CH_3CH_2COONa	400	mg COD/L
Soy peptone	–	1393	mg COD/L
Nutrient broth	–	305	mg COD/L
Dipotassium phosphate	K_2HPO_4	265	mg/L
Ammonium chloride	NH_4Cl	533	mg/L
Sodium chloride	NaCl	63	mg/L
Calcium chloride	$CaCl_2$	100	mg/L
Ferric chloride	$FeCl_3$	5	mg/L
Magnesium chloride hexahydrate	$MgCl_2.7H_2O$	4	mg/L

Table 4.2 : Average characteristics of the MBBR synthetic influent after dilution with tap water

Parameters	**Symbol**	**Units**	**Value**
Total COD	COD	mg/L	261 ± 10
Soluble COD	S_{COD}	mg/L	247 ± 6
Total 5-day carbonaceous BOD	$CBOD_5$	mg/L	119 ± 5
Biodegradability COD/BOD ratio	f_{COD_BOD}	g/g	2.2
Total Kjeldahl nitrogen	TKN	mg N/L	28 ± 3
Total ammonia (NH_3+NH_4^+)	S_{NH4}	mg N/L	14.6 ± 0.8
Oxidized nitrogen (nitrite plus nitrate)	S_{NOx}	mg N/L	0.05 ± 0.01
S_{NH4}/TKN ratio	f_{SNH4_TKN}	g N/g N	0.56 ± 0.04
Total phosphorus	TP	mg P/L	5.9 ± 0.9
Soluble phosphate	S_{PO4}	mg P/L	3.8 ± 0.6
S_{PO4}/TP ratio	f_{SPO4_TP}	g P/g P	0.64 ± 0.04

4.2.2 PVP-AgNPs exposure to MBBRs

AgNPs (nanoparticles of Ag(0)), capped with 40 kDa PVP polymer, were purchased from Nanocomposix (Econix silver) in aqueous suspension with a stock concentration of 5.35 mg/mL and nominal diameter of 50 nm. SpICP-MS (PerkinElmer NexION 300X) analyses provided a mean diameter of 52 ± 0.5 nm. According to the AgNP product description, the zeta potential and surface area of AgNPs were -55 mV (at pH 4.6) and 10.7 m^2/g, respectively. The spherical shape of AgNPs was observed by transmission electron microscopy (TEM). All three reactors reached quasi steady-state conditions after about 30 days as indicated by a stable S_{COD} removal efficiency. Afterwards, the reactors were monitored for 45 days as a control period. Influent AgNP suspensions were prepared by dilution of PVP-AgNPs stock suspension in Milli-Q water and sonicated for 10 min at 35 kHz to ensure that the NPs were dispersed. The AgNP influent suspensions were pumped to each reactor from day 76 at a constant flow rate (1.65 ± 0.03 mL/min), resulting in an average influent total Ag concentration of 10.8 ± 0.3 μg/L Ag ($MBBR_1$), 131 ± 7 μg/L Ag ($MBBR_2$) and 631 ± 27 μg/L Ag ($MBBR_3$) after dilution. The influent nanoparticle suspensions were replenished regularly. Characterization of particle size and concentration of influent AgNPs suspensions indicated the stability of NP in influent stock over every 72 h period. The average characteristics of influent in each MBBR (Table A.1) were used for mass balance analysis.

The AgNP exposure experiment lasted 18 days in the MBBRs, during which the effluent water quality, attached biofilm viability and Ag distribution were monitored. Chemical oxygen demand (COD), total suspended solids (TSS) and volatile suspended solids (VSS) were measured according to Standard Methods (APHA et al., 2012). Glass microfiber 1.2 μm filters (Whatman® 934-AH™, GE Healthcare Life Sciences, USA) and 0.45 μm cellulose membrane filters (MF-Millipore™, EMD Millipore, USA) were used for suspended solids and soluble COD analyses, respectively.

4.2.3 Biofilm total biological viability

The inhibitory effect of AgNPs on biofilm membrane integrity was evaluated using the Live/Dead *Baclight* bacterial viability kit (Molecular Probes, Invitrogen, Kit L13152) and confocal laser scanning microscopy (CLSM) using the modified protocol of Young et al. (2016).

Three K5 carriers were randomly chosen in each reactor before and after exposure to AgNPs. The carriers were cut to expose the inner surfaces and were kept in 2 mL of bioreactor suspension that also contained suspended biomass, and placed in the special container for CLSM imaging. The biofilm and suspended-biomass containing samples were stained with two DNA-binding stains (SYTO-9 and propidium iodide). A minimum of 5 randomly-chosen microscopic fields were scanned for CLSM. All fluorescence images of biofilm were obtained using a LSM 510 META Axioplan 2 confocal laser scanning microscope with 40X objective (Carl Zeiss; Jena, Germany), equipped with 488 nm argon laser and 543 and 633 nm helium–neon lasers (Blanc et al., 2005).

4.3 Silver analyses

4.3.1 Total metal analysis

The influent, bioreactor and effluent were sampled on days 76, 78, 81, 84, 89 and 94. Bioreactor and effluent samples contained suspended flocs (50 to 150 mg TSS/L) but no K5 carriers. All samples were homogenized for 30 s with a vortex mixer prior to total Ag analysis. Samples were digested, in duplicate, using 65% nitric acid (HNO_3) and 30% hydrogen peroxide (H_2O_2) (ratio of 5:1) on a hot digestion block at 95 ^oC for 30 minutes (Yuan et al., 2015). The total Ag concentration was determined using a PerkinElmer NexION 300x ICP-MS in standard mode. Calibration solutions were prepared fresh prior to each analysis from a dissolved Ag standard of 1000 mg/L in 4% HNO_3 (PlasmaCAL). Each sample was measured in triplicate. Quality control (QC) samples (0.1 μg Ag/L in 2% HNO_3) were analyzed after every 10 samples. Ag recovery in the QC samples was between 99% to 105%.

4.3.2 AgNP characterization

AgNP concentration and size as well as dissolved Ag were determined simultaneously in aqueous samples (Figure 4.2) by spICP-MS and data analyses was performed by the Syngistix nano application module (version 1.1) as described by Azodi et al. (2016). The homogenized samples were allowed to settle for about 30 to 45 s and the aqueous supernatant was collected thereafter for analysis. A dwell time of 100 μs and sampling time of 100 to 150 s were used. Instrumental and data acquisition parameters of the analysis are indicated in Appendix A (Table A.1). The

minimum detectable AgNP concentration in deionized water was 10 ng/L (14200 particle/mL) for 50 nm AgNPs (95% recovery) and detection limit of dissolved Ag was about 30 ng/L in single particle mode. The detection limit for AgNP size was ~10 nm in deionized water by spICP-MS as determined in our prior study (Azodi et al., 2016).

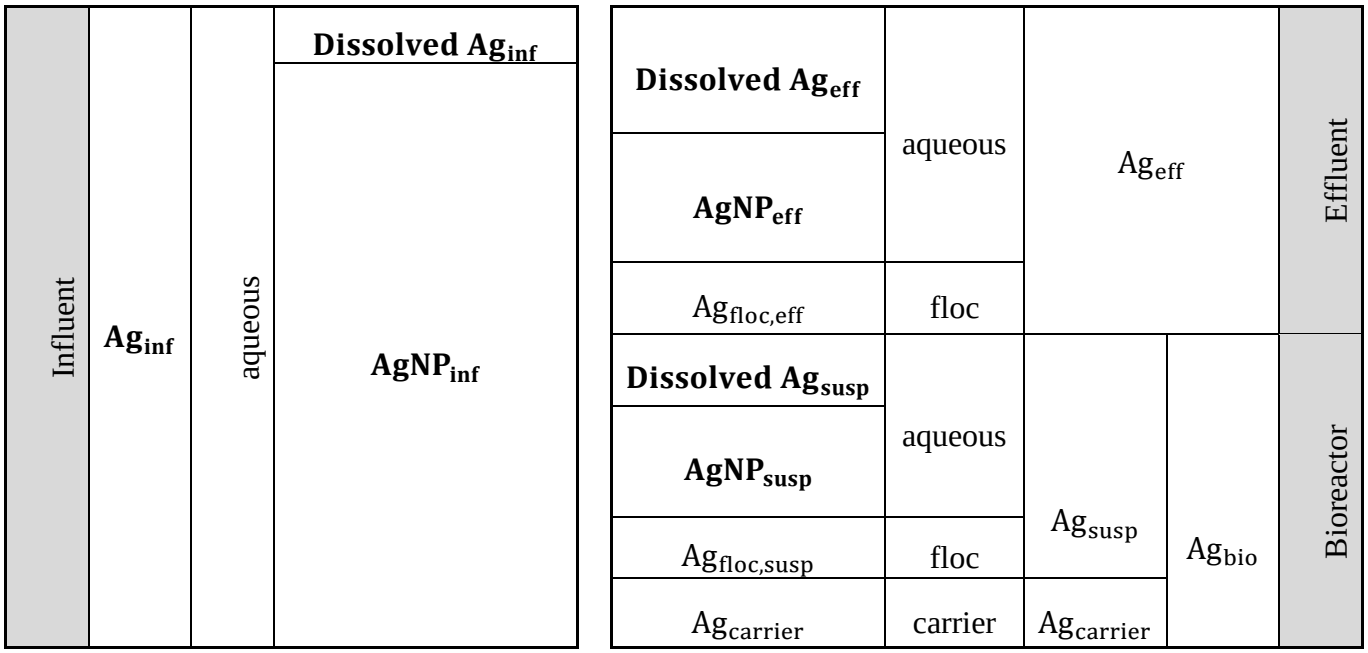

Note: Bold characters refer to analytically determined parameters; susp: suspended phase in MBBR

Figure 4.2 : Fractionation of Ag in influent, bioreactor and effluent of MBBRs.

4.3.3 Cumulative Ag mass balance

Ag mass balance was performed based on the total Ag in the influent, bioreactor and effluent (Figure 4.2). No direct measurements were done on solid fractions of samples. The amount of total Ag associated with biomass, including the flocs (Ag_{floc}) and attached biomass ($Ag_{carrier}$), were calculated using the measured fractions of Ag in influent (Ag_{inf}), bioreactor (Ag_{bio}) and effluent (Ag_{eff}) (Figure 4.2). The concentration of Ag associated with suspended floc (Ag_{floc}), for both the effluent and bioreactor, was calculated using the aqueous phase Ag (i.e. AgNPs + dissolved Ag) obtained from spICP-MS analysis of the supernatant of the samples after settling and Ag from the total metal analyses of the homogenized samples (Eq.1).

$$[Ag_{floc}]_{ti} = [Ag]_{ti} - ([AgNPs]+[\text{ dissolved Ag}])_{ti} \quad (1)$$

Where $[Ag]_{ti}$ represents $[Ag_{eff}]_{ti}$ for effluent and $[Ag_{susp}]_{ti}$ for the bioreactor. The mass of Ag in influent ($M_{Ag,inf}$), bioreactor ($M_{Ag,bio}$) and effluent ($M_{Ag,eff}$) of each MBBR, for each time interval (Δt) were calculated from Equations 2 to 5. The mass of Ag in bioreactor consisted of the mass of Ag in the suspended phase of the bioreactor ($M_{Ag,susp}$) and the retained mass of Ag by attached biofilm on the carrier ($M_{Ag,carrier}$). As shown in Figure 4.2, the suspended phase of bioreactor included both concentrations of Ag in aqueous phase and suspended flocs (Ag_{floc}).

$$(M_{Ag,inf})_{ti} = (Q_{inf})_{ti} * [Ag_{inf}]_{ti} * (t_i - t_{i-1}) \quad (2)$$

$$(M_{Ag,eff})_{ti} = (Q_{eff})_{ti} * [Ag_{eff}]_{ti} * (t_i - t_{i-1}) \quad (3)$$

$$(M_{Ag,susp})_{ti} = V_{bio} * [Ag_{susp}]_{ti} \quad (4)$$

$$(M_{Ag,bio})_{ti} = (M_{Ag,inf})_{ti} - (M_{Ag,eff})_{ti} \quad (5)$$

Where Q_{inf} (L/day), Q_{eff} (L/day) and V_{bio} (L) are the flow rate of influent and effluent and volume of the bioreactor, respectively. In the final step, the retained mass of Ag by attached biofilm on the carrier ($M_{Ag,carrier}$) was estimated (Equation 6).

$$(M_{Ag,carrier})_{ti} = (M_{Ag,bio})_{ti} - (M_{Ag,susp})_{ti} \quad (6)$$

4.3.4 Statistical analysis

The statistical significance of differences between treatments ($p < 0.05$), before and after exposure to AgNPs, was evaluated using one-way repeated measures ANOVA in Statistica version 12 (StatSoft Inc., USA).

4.4 Results

4.4.1 Effects of AgNPs on treatment efficiency

The S_{COD} removal efficiency was determined in three MBBRs, in response to the continuous exposure to three nominal doses of 10, 100 and 600 μg/L AgNPs. Prior to exposure to AgNPs,

each MBBR was monitored for 30 days (day 45 to 75) under quasi steady state conditions as a control period (Figure 4.3). Effluent nitrate concentration remained around 0.4 mg N/L, showing no significant nitrification occurring in the MBBRs as expected at such high rate conditions (results not shown). Specific S_{COD} removal rate stabilized at 10.7 ± 0.2 g S_{COD} m^{-2} d^{-1}, 10.5 ± 0.3 g S_{COD} m^{-2} d^{-1} and 9.9 ± 0.5 g S_{COD} m^{-2} d^{-1}, corresponding to a S_{COD} removal efficiency of 89% ± 0.5%, 89 % ± 0.3% and 89% ± 1.4% in $MBBR_1$, $MBBR_2$ and $MBBR_3$, respectively, over the control period. After the start of AgNP addition, at average measured concentration of 10.8 ± 0.38 μg/L Ag in its influent, $MBBR_1$ maintained an average S_{COD} removal efficiency of 89% ± 1.5% over the 18-day exposure period. Therefore, S_{COD} removal efficiency was not significantly affected ($p > 0.05$) over an 18-day continuous exposure to influent concentration of 10.8 μg/L Ag in the influent (Figure 4.3A_1).

At higher influent concentrations of AgNPs (100 and 600 μg/L), two phases were observed for MBBR response to AgNP exposure. An unperturbed phase comprised the time interval after injection of AgNPs, in which the biological activity of biofilm bacteria remained stable with no significant impact of AgNPs. A second phase corresponded to the period during which the biomass was significantly inhibited. Unperturbed phases of 96 h and 48 h were observed in $MBBR_2$ (131 ± 7 μg/L Ag) and $MBBR_3$ (631 ± 27 μg/L Ag), respectively. The second phase started thereafter (Figure 4.3A_2-A_3) where the effluent S_{COD} gradually increased, decreasing the S_{COD} removal efficiency significantly ($p < 0.05$) by about 22% over 12 days in $MBBR_2$ and 25% after 3 days in $MBBR_3$ (Figure 4.3B). Therefore, soluble COD removal efficiency was significantly decreased to 66% ± 0.7% in 18 days in $MBBR_2$ (131 ± 7 μg/L Ag) and to 64% ± 2.8% in 5 days in $MBBR_3$ (631 μg/L Ag). The significant increase of TSS concentration in effluent, in both systems receiving 131 and 631 μg/L Ag (Figure 4.3C) indicated significant detachment of biofilm which was likely due to the antibacterial properties of AgNPs and/or dissolved Ag.

4.4.2 Effect of AgNPs on biofilm total biological viability

The potential bactericidal effect upon introduction of AgNPs in the MBBRs on biofilm bacteria was characterized in terms of cell membrane integrity using CLSM. The CLSM images of stained biofilm, exposed to different dosages of AgNPs, demonstrated the concentration-

dependent inactivation of biofilm total biological viability (Figure 4.4). The extent of viability inhibition was from no significant detectable membrane integrity damage at the lowest concentration (10.8 μg/L Ag) (Figure 4.4A_2) to a noticeable increase in the number of dead cells in the presence of 131 μg/L Ag and 631 μg/L Ag during the exposure period (Figure 4.4B_2-C_2).

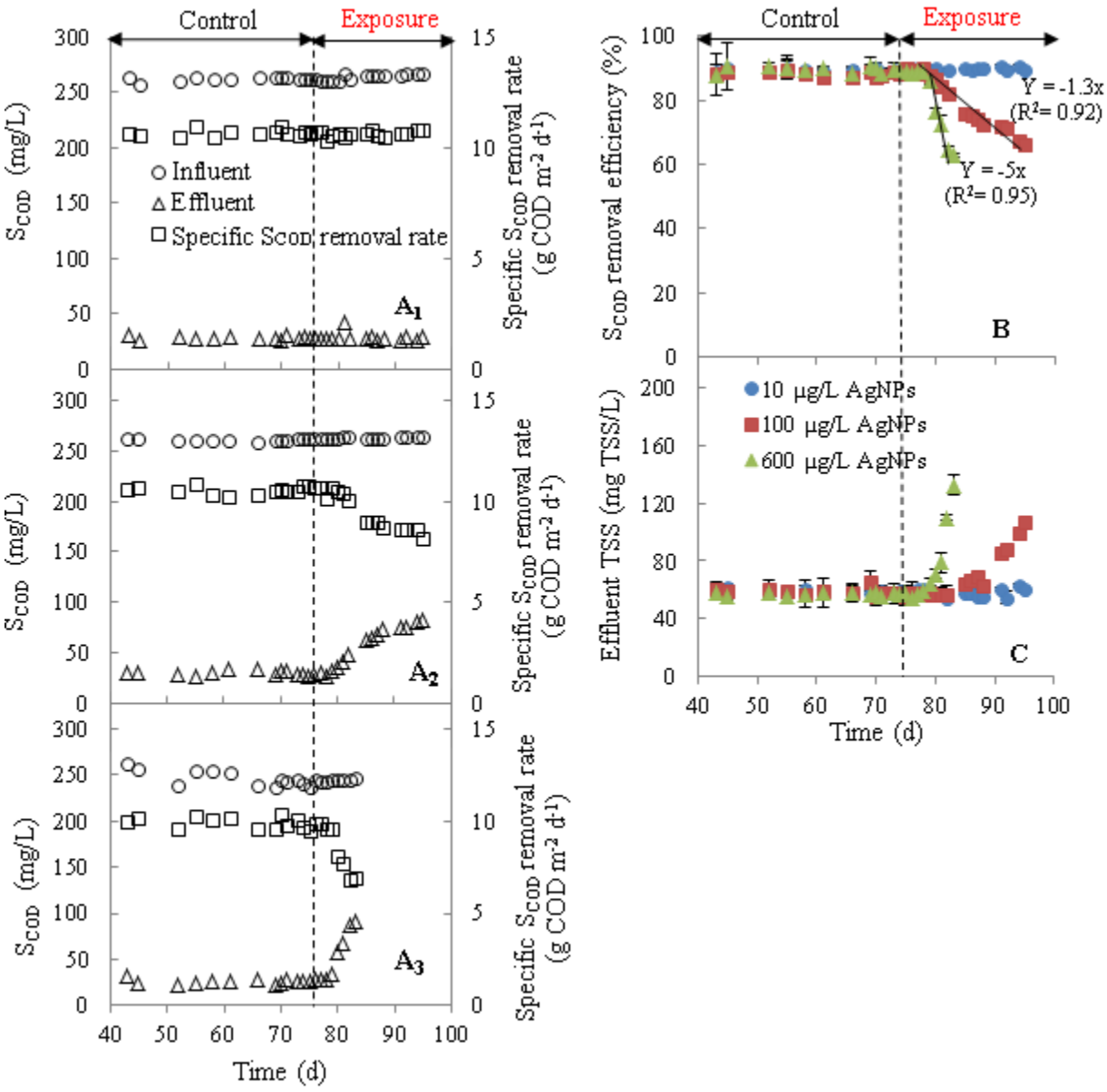

Figure 4.3 : Effect of PVP-AgNP addition on MBBR performance at (A_1) 10 μg/L AgNPs (A_2) 100 μg/L AgNPs, (A_3) 600 μg/L AgNPs, (B) S_{COD} removal efficiency and (C) Effect of AgNP addition on MBBR TSS_{eff} (error bars are only shown when larger than symbol size).

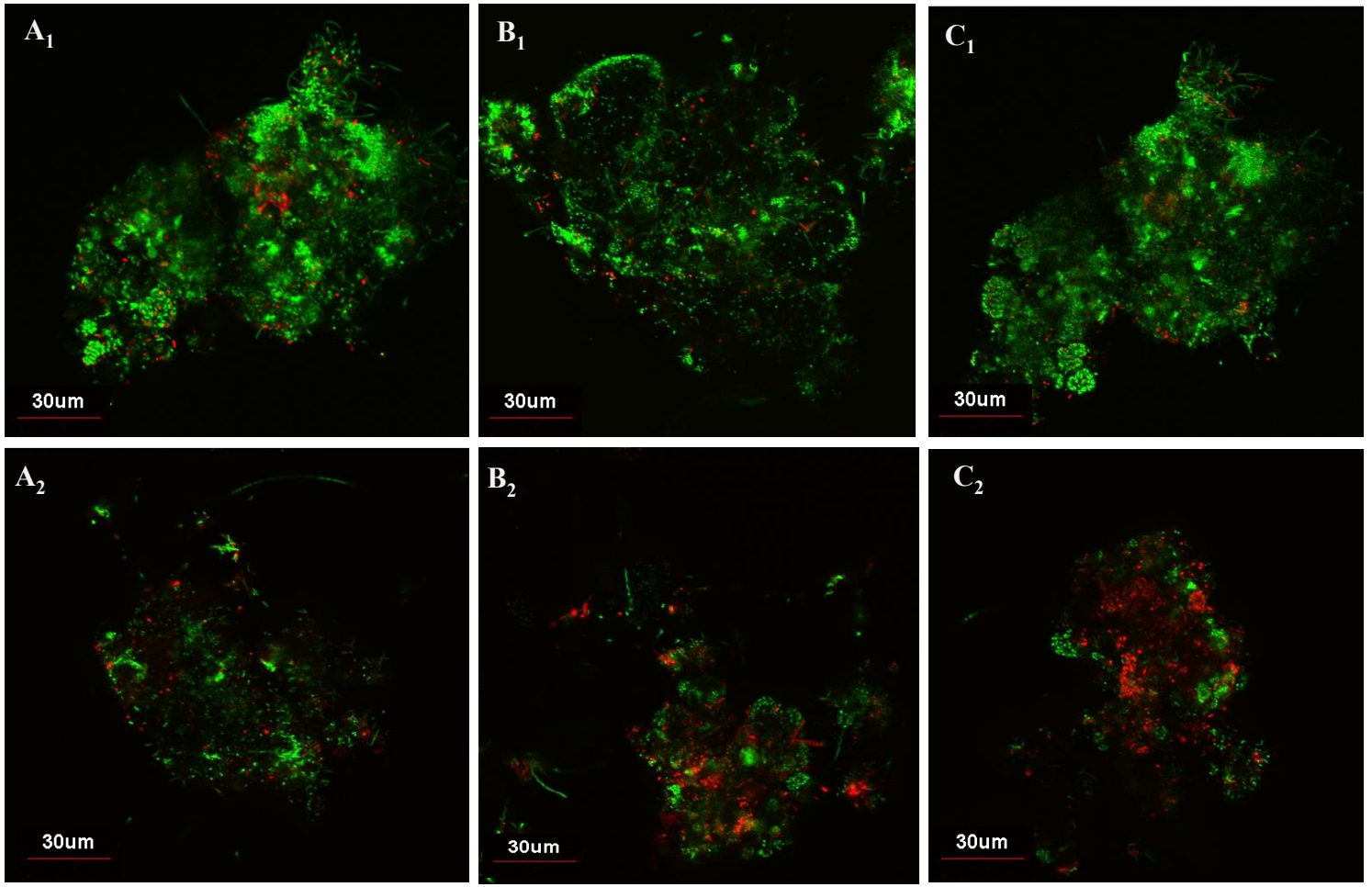

Figure 4.4 : CLSM image of stained biofilm in the absence of AgNPs (A_1-C_1) and following addition of 10 μg/L (A_2) and 100 μg/L of AgNPs (B_2) after 18 days exposure and 600 μg/L AgNPs (C_2) after 5 days of exposure.

4.4.3 Fate and transport of AgNPs

4.4.3.1 Total silver

Ag retention efficiency was determined using the total silver concentration in the influent and effluent of MBBRs and is shown in Figure 4.5. With an average influent total Ag concentration ($[Ag_{inf}]$) of 10.8 ± 0.3 μg/L, $MBBR_1$ retained about 21% of $[Ag_{inf}]$ on day 76 which increased to 65% of $[Ag_{inf}]$ in bioreactor by day 81 (Figure 4.5A). Afterwards, the Ag retention efficiency stabilized at 52% ± 5% by day 94. $MBBR_2$, receiving Ag_{inf} concentration of 131 ± 7 μg/L, demonstrated higher retention efficiency of Ag over the first 5 days (Figure 4.5B). More than 30% of $[Ag_{inf}]$ were retained in $MBBR_2$ on day 76, which reached up to 85% of $[Ag_{inf}]$ on day 81. The retention efficiency subsequently decreased to 54% from day 81 to day 84, likely due to saturation of biofilm outer layers by AgNPs and/or biofilm sloughing off from the surface of the carriers. Thereafter $MBBR_2$ recovered its capacity to retain about 55% ± 9% of $[Ag_{inf}]$ from day 84 to day 94. A higher concentration of AgNPs affected the biomass in $MBBR_3$ receiving Ag_{inf} concentration of 631 ± 27 μg/L, differently (Figure 4.5C). The highest retention efficiency of 47% was attained after 1-hour exposure (one HRT) on day 76. Afterwards, the retention capacity of biofilms dramatically declined resulting in retention efficiency as low as 5% in 48 hours (day 78), but the system was able to recover its ability to retain AgNPs up to 35% by day 79 but fluctuated, changing to 20% over 24 hours by day 80.

The cumulative mass of total Ag, loading in the influent ($M_{Ag_{inf}}$), effluent ($M_{Ag_{eff}}$) and attached biofilm ($M_{Ag_{carrier}}$) are shown in Figure 4.6 A. Cumulative Ag mass balance was about 98% in all three reactors with negligible mass of Ag in the suspended phase of MBBRs. Attached biofilm retained 62% of $M_{Ag_{inf}}$ (0.79 mg) in $MBBR_1$ and 78% of $M_{Ag_{inf}}$ (12.14 mg) in $MBBR_2$ by day 81, which slightly decreased afterward. Retention of 54% of cumulative $M_{Ag_{inf}}$ (4.6 mg $Ag/m^2_{active\ surface}$) and 61% of cumulative $M_{Ag_{inf}}$(65 mg $Ag/m^2_{active\ surface}$) were observed by attached biofilm ($Ag_{carrier}$) in $MBBR_1$ and $MBBR_2$, respectively, by day 94. In $MBBR_3$, the mass balance suggests that more than 75% of cumulative $M_{Ag_{inf}}$ (43 mg) was released via the effluent over 5-day exposure indicating poor retention capacity of biofilm at higher AgNP concentrations (Figure 4.6 A).

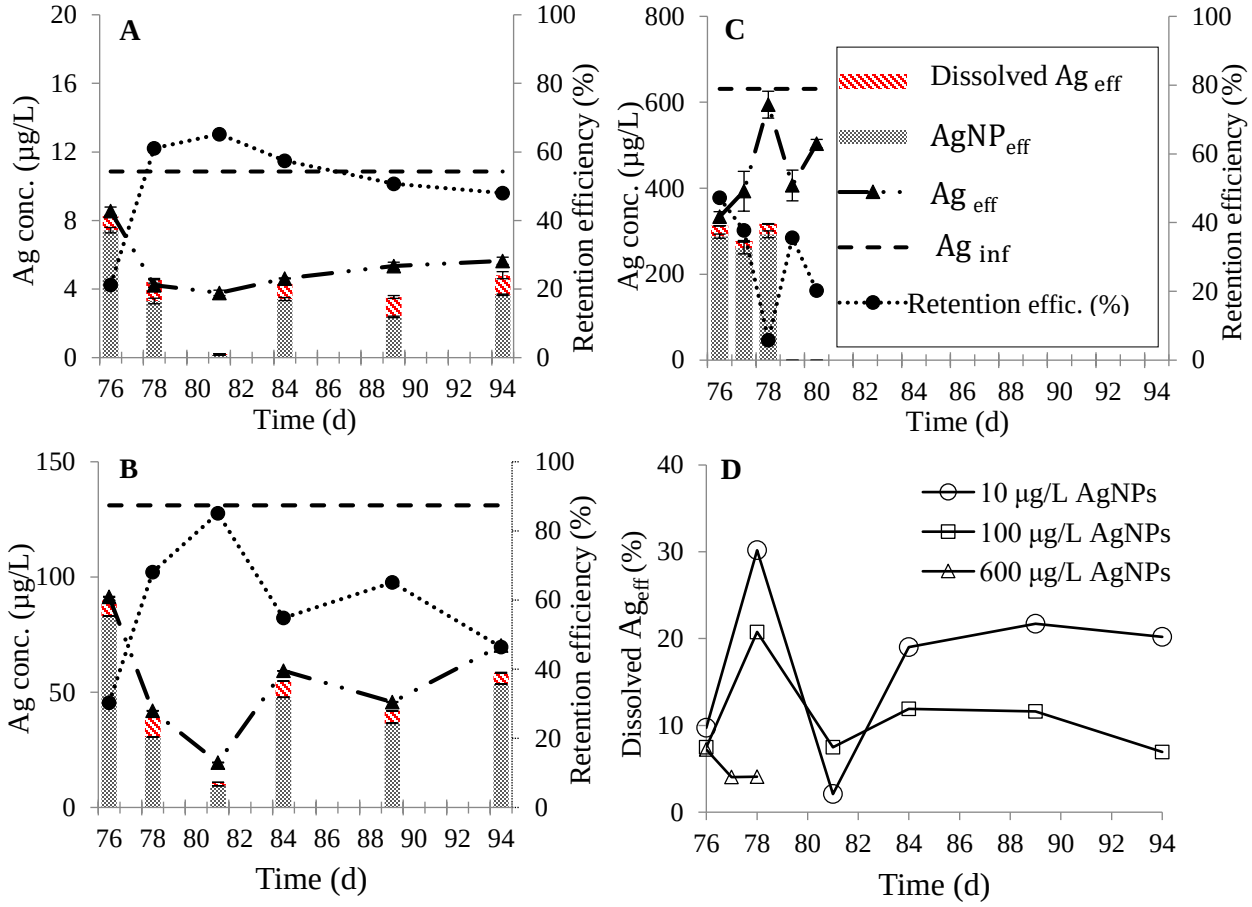

Figure 4.5 : Fate and retention of Ag in MBBRs receiving influent concentration of (A)10 μg/L, (B)100 μg/L, (C) 600 μg/L AgNPs and (D) dissolution of $AgNP_{eff}$ (error bars are only shown when larger than symbol size).

4.4.3.2 AgNPs

Concentrations of AgNPs, and dissolved Ag were measured simultaneously in influent suspensions (Table A.1) and the aqueous phase of samples collected from the MBBR bioreactors (Figure A.1A-C) and the effluents (Figure 4.5), using spICP-MS. For $MBBR_1$ (Figure 4.5A, bar graphs), receiving an average influent concentration of 8.1 ± 2.3 μg/L AgNPs ($[AgNP_{inf}]$) and mean diameter of 48 ± 3 nm, its effluent contained 7.4 ± 0.2 μg/L and 3.3 ± 0.2 μg/L AgNPs on days 76 and 78, respectively (Figure 4.5A). Over the first 48 hours of exposure, a larger cumulative fraction of $[Ag_{eff}]$ (78% to 87%) was detected in NP form in the aqueous phase of the effluent ($AgNP_{eff}$) with mean diameter in the range of 49 ± 0.4 to 52 ± 0.6 nm (Figure A.1D).

Concentrations of $AgNP_{eff}$ were depleted afterwards. On day 81, [$AgNP_{eff}$] (0.15 ± 0.01 μg/L), with mean diameter of 40 ± 0.5 nm, represented less than 4% of [Ag_{eff}] indicating significant association of AgNPs to TSS_{eff}. Thereafter [$AgNP_{eff}$] concentration increased and represented an average 61% of [Ag_{eff}] (3.2 ± 0.7 μg/L AgNPs), with mean diameter from 35 ± 1 to 48 ± 0.2 nm, between day 89 and day 94.For $MBBR_2$, receiving an average $AgNP_{inf}$ concentration of 75 ± 7 μg/L of a mean diameter of 47 ± 2 nm, a similar evolution in the distribution of AgNPs was observed in the effluent (Figure 4.5B). A concentration of 83 ± 2 μg/L $AgNP_{eff}$ was measured after one-hour continuous exposure to AgNPs (one HRT), constituting 91% of detected [Ag_{eff}] with mean diameter of 53 ± 0.1 nm (Figure A.1D). Following a decrease in [Ag_{eff}], 19.5 ± 0.2 μg/L Ag_{eff} was released on day 81 where [$AgNP_{eff}$] (9.4 ± 0.1 μg/L with mean diameter of 46 ± 0.1 nm) accounted for 48% of [Ag_{eff}] and remaining 43% of [Ag_{eff}] (8.6 μg/L) was associated with the effluent suspended solids, with a relatively small mass fraction accounted for by the dissolved concentration of Ag_{eff}. As the [Ag_{eff}] increased thereafter, the major fraction of released silver was in the form of AgNPs (79% ± 2% of [Ag_{eff}]) with mean diameter of 47 ± 6 nm (Figure A.1D). For $MBBR_3$ (Figure 4.5C), receiving an average $AgNP_{inf}$ concentration of 442 ± 26 μg/L of mean diameter of 49 ± 1 nm, more than 85% of released [Ag_{eff}] (289 ± 5 μg/L) was detected as $AgNP_{eff}$ over the first hour exposure. Along with the significant increase in [Ag_{eff}] concentration by day 78 (48 h), likely due to significant increase of TSS_{eff}, [$AgNP_{eff}$] (293 ± 8 μg/L) represented about 50% of the [Ag_{eff}]. No significant change was observed in mean diameter (Figure A.1D). For later sampling times, such as day 81, spICP-MS analysis was not feasible due interferences from the high concentration of suspended solids.

4.4.3.3 Dissolved Ag

Average dissolved Ag_{inf} concentrations of 2.5 ± 0.6 μg/L, 14.4 ± 6.0 μg/L and 39 ± 19 μg/L were measured in influent of $MBBR_1$, $MBBR_2$ and $MBBR_3$, respectively, indicating AgNP dissolution of 23%, 11% and 6% in influent NP stock solution (Table A.1). SpICP-MS analyses showed variations in dissolved Ag concentrations over time in the effluent of both $MBBR_1$ and $MBBR_2$, whereas less than 7% of [Ag_{eff}] were measured in dissolved form in $MBBR_3$ over the short exposure time (Figure 4.5 D). The maximum dissolved Ag concentration of 1.30 ± 0.04 μg/L

(30% of [Ag_{eff}]) and 8.7 ± 1.0 μg/L (21% of [Ag_{eff}]) were measured in the effluent of $MBBR_1$ and $MBBR_2$, respectively, over the first 48 h (Figure 4.5 A, B, D). Afterwards, dissolved Ag concentration decreased and stabilized at about 20% of [Ag_{eff}] in $MBBR_1$ and 10% of [Ag_{eff}] in $MBBR_2$ by day 94 (Figure 4.5 D). Measured dissolved Ag in influent NP suspensions, entering reactors via separate constant flow, is likely in form of Ag^+ as AgNPs suspensions were prepared in pure water. However, the detected dissolved Ag in bioreactor and effluent samples are likely partially or completely complexed via interaction with suspended biomass.

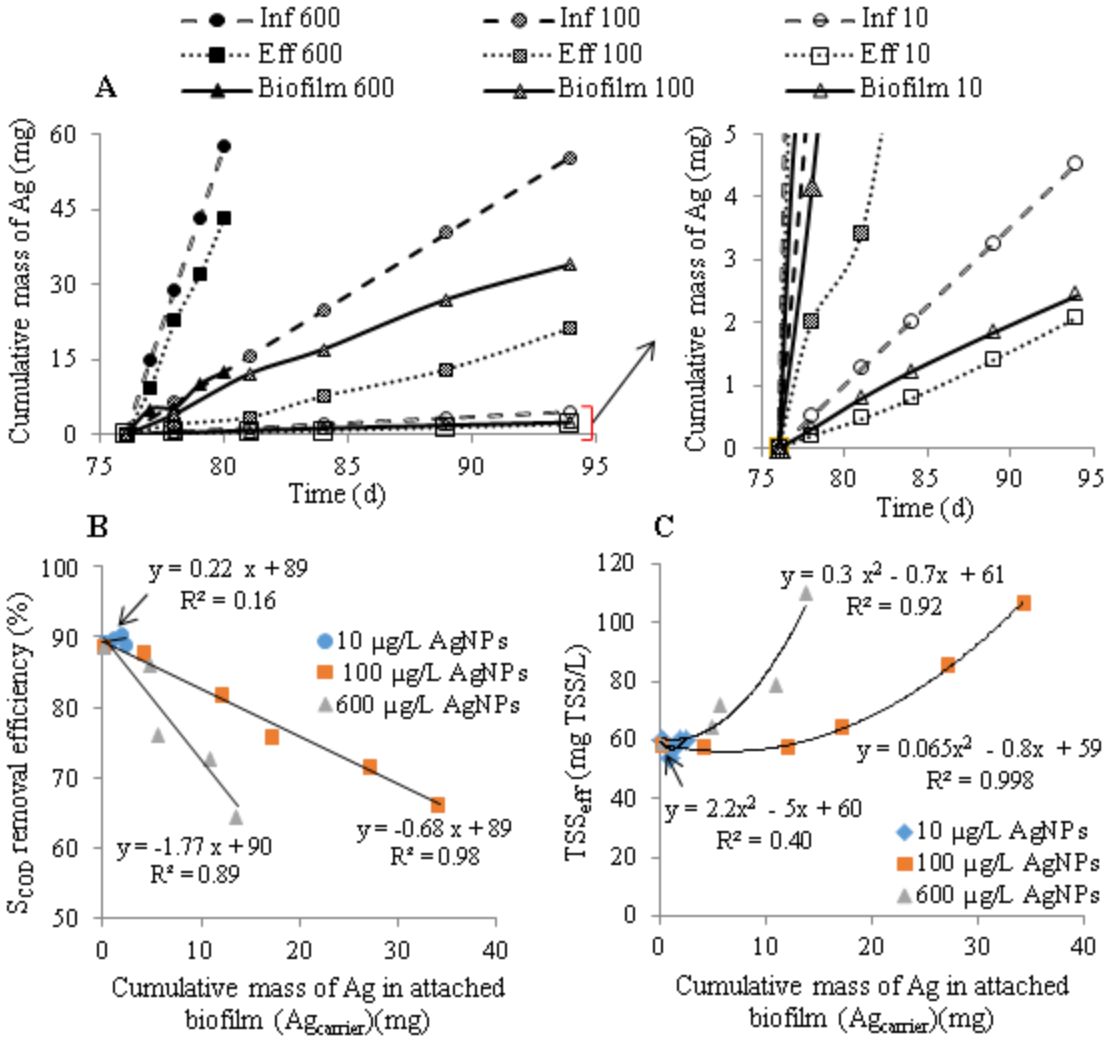

Figure 4.6 : Cumulative Ag mass balance in influent (Inf) effluent (Eff) and attached biofilm (Biofilm), (B) correlation between $Ag_{carrier}$ and SCOD removal efficiency and (C) correlation between Agcarrier and TSS_{eff} (Note: negligible Ag_{susp}).

4.5 Discussion

4.5.1 Inhibitory effect of AgNPs on S_{COD} removal efficiency and biofilm viability

The concentration-dependent inhibitory effect of AgNPs on S_{COD} removal efficiency was observed at nominal influent concentrations of 100 and 600 μg/L AgNPs in high rate MBBRs. These results are in contrast with recent studies. It is reported that the environmentally relevant concentration of 100 μg/L AgNPs had no adverse effects on carbon removal and bacterial activities of activated sludge over a 50-day exposure in a sequencing batch reactor process (Zhang et al., 2016c) and over a 65-day exposure in a membrane bioreactor (Zhang et al., 2014). These contrasting results could be due to differences between the process configurations, such as completely mixed versus batch system with different oxygen demand, sludge retention time, HRT, biomass characteristics and the size and coating of the AgNPs used under distinct experimental conditions. The process configuration governs biomass growth processes and determines the stability and transformation of AgNPs in the process and the bioavailability of Ag and their consequent impact on the wastewater microbial communities (Zhang et al., 2016a).

Attached growth processes such as in an MBBR, provide higher biomass concentrations (with larger specific surface area) in smaller reactor volumes as compared to suspended growth process such as activated sludge (Barwal and Chaudhary 2014). Therefore, higher biomass surface area/volume ratio in MBBR enhances the deposition rate and the mass transport of AgNPs to attached biomass, leading to enhanced Ag retention per unit weight of biomass in the reactor, compared to activate sludge systems. This results in relatively high toxicity even at lower influent concentrations. Our mass balance analysis indicated the accumulation of 3.2 mg Ag/g$VSS_{biofilm}$ in 5 days in $MBBR_3$ (631 μg/L Ag influent) and 4.9 mg Ag/g$VSS_{biofilm}$ in $MBBR_2$ (131 μg/L Ag influent) over 18 days. In contrast, Zhang et al. (2016c) reported the accumulated concentration of 0.47 mg Ag/gVSS in activated sludge, collected from a sequencing batch reactor (100 μg/L AgNPs influent) over 50 days. The significant accumulation and associated mass transport of Ag through the protective biofilm EPS into deeper layers of biofilm can result in toxicity to the biofilm biomass. The AgNPs transported into the biofilm can undergo dissolution delivering toxic Ag^+ directly to adherent cells. The inhibitory effect of AgNPs at doses of both 131 μg/L and

631 μg/L Ag was correlated also to the loss of active biofilm via detachment due to metabolic stress and the accumulation of AgNPs over time within the biofilm.

The observed variation in inhibition effects of AgNPs at similar nominal influent AgNP concentrations can also be correlated to the differences in specific exposure conditions of activated sludge systems reported elsewhere (Zhang et al., 2014; Zhang et al., 2016c). In these studies, AgNPs suspensions were injected into the anoxic chamber with the mixed liquor recirculation between the aerobic chamber and the anoxic chamber. This resulted in AgNPs first being exposed to a 2 h anoxic stage where there would have been considerable loading of organic matter on the AgNP surface which would have made AgNP susceptible to changes in aggregation state, oxidation state, precipitation of secondary phases and sorption of (in)organic species before reaching the aerobic zone. Wastewater ligands and ions (e.g. HS^-, Cl^-, SO_4^{2-}, HPO_4^{2-}) would react with injected AgNPs and dissolved Ag and form the silver complexes/precipitates**,** leading to reduced bioavailability (Behra et al., 2013). Simultaneously, AgNPs in the activated sludge could be transformed into Ag–sulfhydryl complexes and Ag_2S during the short anoxic phase, and therefore, reduce their toxicity (Doolette et al., 2013; Yuan et al., 2015). The lack of dissolved oxygen, and the abundance of organic matter bound to the AgNPs in the anoxic state would also decrease the subsequent dissolution of Ag in both the anoxic and aerobic zone. In our study the AgNPs stock suspensions were pumped directly to each reactor (aerobic zone), enabling dissolution at all times, and thus distinct inhibitory level would be expected. Furthermore, Barker et al. (2018) suggested that the expected toxicity of AgNPs should not be based solely on the AgNP concentration in the wastewater influent or even the total mass load but rather on a more complex combination of factors including the influent AgNP concentration, total mass loading and the exposure time.

The inhibitory effect of AgNPs on treatment efficiency was highly correlated ($0.89 < R^2 < 0.98$) to the retained mass of Ag in the carriers ($Ag_{carrier}$) (Figure 4.6 B). The bioavailability and toxicity of retained AgNPs in the porous structure of biofilm are highly rface of bacteria (Peulen and Wilkinson, 2011). The lack of significant adverse effects on treatment efficiency of $MBBR_1$ at low concentrations of AgNPs, is likely due to the lower than threshold concentration for toxicity of AgNPs and Ag^+, or due to the complexation of Ag^+ to biological macromolecules and the sorption of those macromolecules to AgNPs in the biofilm EPS, reducing the diffusive flux of

AgNPs and Ag^+ within the biofilm layers and reduce their toxicity (Kroll et al., 2014). Hindered nanoparticle diffusion in biofilms was demonstrated by Peulen and Wilkinson (2011). The interaction between EPS molecules and AgNPs results in the formation of stable complexes on the surface of AgNPs (e.g. corona effect) which could reduce the bioavailability and toxicity of AgNPs (Wirth et al., 2012). As in the case of $MBBR_2$ and $MBBR_3$, exposure to higher concentrations of AgNPs can lead to significant accumulation and mass transfer of AgNPs into deeper layers of biofilm.

Significant increase of TSS concentration in effluent of $MBBR_2$ and $MBBR_3$, due to the detachment of biofilm from the carriers, was highly correlated ($0.92 < R^2 < 0.99$) to the retained mass of Ag in the carriers ($Ag_{carrier}$) (The thinning effect of AgNPs on the biofilm (i.e., detachment and release of outer layers was reported at AgNPs concentrations higher than 200 μg/L (Fabrega et al., 2009), but was achieved at 131 μg/L Ag in this study. The interaction of AgNPs with an EPS matrix can potentially interfere with the cell to cell adhesion to the surface due to its cell wall destabilizing properties as an antimicrobial agent (Goswami et al., 2015). Grün et al. (2016) suggested that the complexation of Ag^+ and binding to AgNP surfaces by carboxyl, hydroxyl and amine macromolecules in EPS can impair interactions which mediate adhesion of the biofilm to surfaces, leading to diminished cohesive forces within the biofilm matrix. Thus, the biofilm detachment not only can inversely affect the treatment efficiency but also it can increase the risk of environmental exposure of AgNPs via the release of retained nanoparticles by detached biomass in the treated effluent.

Membrane integrity of the intact cells defines their potential metabolic activity whereas the cells with damaged membranes can be classified as permeabilized/dead cells (Foladori et al., 2010). The concentration-dependent alteration of membrane permeability and inactivation of attached biofilm were observed in MBBRs. Both AgNPs and the bioavailable dissolved Ag, released from the oxidative dissolution of AgNPs, and could have damaged the membrane integrity of attached biofilm at influent concentrations of 131 and 631 μg/L Ag which was consistent with S_{COD} removal efficiency loss in corresponding reactors. AgNPs up to 80 nm have demonstrated the ability to penetrate the outer membrane of bacteria (Morones et al., 2005). The large surface/volume ratio and special binding sites of AgNPs enhance the particle/cell surface contacts (Auffan et al., 2009). Upon attachement of AgNPs on to cell membrane, (a) released Ag^+ from

oxidative disslution, can interact with thiol-containing proteins in the cell wall and destabilize the outer membrane of cells by an accumulation of immature membrane precursor proteins (Mirzajani et al., 2011) and (b) AgNP-induced oxidative stress can damage the cell membrane by the generation of reactive oxygen species (ROS), leading to cell membrane integrity disruption and decomposition (Durán et al., 2016).

Contradictory results have been reported recently regarding the AgNP-induced membrane integrity damage and inhibition of viable biofilm. The inhibitory effect of AgNPs, with mean particle size of 50 nm, is reported at concentration as low as 5 μg/L towards *P. aeruginosa* biofilms over 24 h exposure (Kalishwaralal et al., 2010) whereas a number of studies reported considerably higher concentrations for inhibition or deactivation of biofilms. Fabrega et al. (2009) reported no significant effect of AgNPs (mean diameter of 65 nm) on *P. aeruginosa* biofilm viability at concentrations between 20 to 2000 μg/L of AgNPs over 24 h exposure time. Similarly, Sheng and Liu (2011) suggested the high tolerance of attached biofilms in wastewater over 24 h exposure to 200 mg/L AgNPs. This observed difference is likely due to disparity between the biological and structural properties of biofilm and the nature of the AgNPs used under distinct experimental conditions, particularly the exposure time. The physicochemical characteristics of NPs (size and coating) and the nature and age of the biofilm highly influence their diffusion coefficient. Peulen and Wilkinson (2011) suggested that as the density of biofilm increases with age, the pore size distribution shifts to smaller pore sizes altering deposition and bioavailability of AgNPs in denser, more developed biofilm.

4.5.2 Behavior of PVP-AgNPs in biofilm-laden media

The bioavailability of AgNPs is highly dependent on their chemical speciation, size-dependent diffusive fluxes and their particle coatings (Azimzada et al., 2017; Azodi et al., 2016). No evidence of aggregation was observed in the effluent of the three reactors, with no significant change in particle size (Figure A.1D). Mitzel and Tufenkji (2014) also reported a high stability of PVP-AgNPs in suspension and little change in their size or electrophoretic mobility with changing ionic strength. The steric stabilization of AgNPs by PVP polymers typically prevents the particle aggregation over a range of pH values and ionic strength (Song et al., 2011).

Despite the initial high retention capacity of biofilm for AgNPs, $MBBR_1$, $MBBR_2$ and $MBBR_3$ released 38%, 46% and 75% of the cumulative mass of Ag via their effluent over long-term exposure scenarios (at effluent concentration of 0.05 to 0.5 mg/L, Figure 4.5). The cumulative mass released from the reactors was calculated from the measured effluent concentrations and the flow rates. Approximately 55% to 79% of concentration of released total silver in the effluent of the reactors ($[Ag_{eff}]$) was in the form of NPs and about 7% to 31% of $[Ag_{eff}]$ (1.14 to 24.5 μg/L) as dissolved Ag. Herrling et al. (2016) also reported high retention capacity of heterotrophic biofilms only at short exposure times (up to 3 h) over 27-day exposure in MBBR before release of silica-coated iron oxide nanoparticles by the detachment of loaded biofilms. It is likely that association with biomass is the main retention pathway of AgNPs in reactors receiving lower concentrations of AgNPs (10 to 100 μg/L AgNPs). At higher concentrations (600 μg/L AgNPs), however, other mechanisms affect the attachment efficiency of AgNPs to the biofilm surface (Mitzel and Tufenkji, 2014). The initial high retention of PVP-AgNPs by the attached biofilm (Fig. 5) suggests a high affinity of PVP-AgNPs for uncoated surfaces of biofilm via hydrophobic interactions between hydrophobic PVP coatings of AgNPs and heterogeneously amphiphilic surface of biofilm (Song et al., 2011). In longer-term exposure scenarios, however, as the concentration increases in the bioreactor, the saturation of biofilm outer layers by local accumulation of the nanoparticles and biofilm sloughing off from the surface of the carriers can reduce the retention capacity of biofilm.

The inhibitory effect of AgNPs is ascribed to both nanoparticle and dissolved ions released from AgNPs; however which fraction dominates toxicity appears inconclusive (Beer et al., 2012; Navarro et al., 2008; Kawata et al., 2009). Most previous studies, reporting the Ag^+-mediated toxicity of AgNPs, used silver nitrate ($AgNO_3$) as a source of bioavailable free Ag^+ ions at concentration of 0.05 to10 mg/L in simple growth media (Beer et al., 2012; Choi et al., 2017). In our study, the inhibitory effect of AgNPs was observed in $MBBR_2$ (131 μg/L Ag) and $MBBR_3$ (630 μg/L Ag) with an average influent dissolved Ag concentrations of 14.4 ± 6.0 μg/L (11% $[Ag_{inf}]$) and 39 ± 19 μg/L (6% $[Ag_{inf}]$) respectively which were lower than the reported inhibitory dissolved Ag concentrations (Beer et al., 2012; Choi et al., 2017). The detected dissolved Ag in bioreactors, $MBBR_2$ (5 to 11 μg/L) and $MBBR_3$ (24 to 56 μg/L) (Figure A.1) were likely partially or completely complexed via interaction with suspend biomass. Although

significant accumulation and mass transfer of AgNPs into deeper layers of biofilm would deliver toxic Ag^+ directly to adherent cells via the (interfacial) dissolution of the surface-bound NPs in biofilm matrix. Therefore, the measured dissolved Ag content in each reactor could not be fully be attributed to the observed toxicity, and the presence of AgNP accounts for some part of the toxicity of AgNPs and is consistent with previously reported studies (Navarro et al., 2008; Kawata et al., 2009). Apart from extracellular dissolution in media, diffused AgNPs in biofilm EPS can partly follow a "Trojan-horse" type of mechanism (Hsiao et al., 2015). Cell surface-associated AgNPs serve as carriers that penetrate cell membranes and dissolve to release a large amount of bioavailable Ag^+ intracellularly, able to interact with cell molecules and damage cell functions (Park et al., 2010; You et al., 2018); however the current knowledge on the mechanism by which AgNPs interact with the cytosol environment and the dissolution properties of intracellular AgNPs remains limited (You et al., 2018).

Our results suggest a concentration-dependent dissolution regime where the higher dissolution, in terms of the fraction of Ag dissolved relative to total Ag added, is higher at lower concentration of AgNPs (10 and 100 μg/L) in the effluent of reactors which is consistent with previous studies (Azodi et al., 2016; Hadioui et al., 2013; Zhang et al., 2016b). The lower percentage of dissolved Ag at higher influent concentration is likely due to high proton depletion (Liu and Hurt, 2010). The observed dissolution pattern in MBBR effluent (Figure 4.5D) was consistent with the proposed two-phase dissolution kinetics, including a short, initial phase with a high release rate, and a longer, second phase with more gradual release (Mitrano et al., 2014). The dissolution behavior of AgNPs depends on the chemistry of the aqueous medium (e.g. ionic strength, pH), the characteristics of NPs (e.g. size, particle concentration) as well as the nature of the surface capping agents (Azodi et al., 2016). PVP-coated AgNPs comprise an inner hard sphere of AgNPs covered with a relatively thick coating of high molecular weight PVP polymer which is uncharged with an amide group that also favors dissolution (Song et al., 2011). Azodi et al. (2016) attributed the decrease in dissolved Ag concentrations in the wastewater effluent samples to the reformation of the secondary NPs from dissolved Ag. We detected changes in chemistry of the particles (Ag_2S, AgCl) in the effluent of all MBBRs using TEM-EDS analysis (Figure A.2).

Sulfidation of AgNPs, may lead to the formation of partly sulfidated ($Ag(0)/Ag_2S$) or fully sulfidated (Ag_2S) particles, with the latter being formed at high sulfide concentrations existing in

anaerobic environments. For partially sulfidated AgNPs, dissolution of Ag (0) with release of Ag^+ can occur (Zhang et al., 2018). In our reactors, the influent sulfate (SO_4^{2-}, 16.3 μM, in concentrated feed), as the only source of sulfur, needs to be reduced to bisulfide (HS^-) by sulfate-reducing bacteria as an essential step for the sulfidation of AgNP. Only anoxic/anaerobic zones, within the lower layers of biofilm, could favor the growth of sulfate-reducing bacteria (Auvinen et al., 2017). Due to high concentration of dissolved oxygen (6.5 mg O_2/L) and lack of enough electron donors (low concentration of organic compounds), an incomplete sulfate reduction is expected. Therefore, considering the low ratio of S/Ag (0.037 to 0.25, based on 10% influent sulfate reduction) in our reactors, and the presence of dissolved Ag at concentrations ranging from 1.14 to 56 μg/L (bioreactor) it may be concluded that although sulfidation of AgNPs occurred, it did not cause Ag to be unavailable to bacteria and did not prevent toxicity.

The sulfidation of AgNPs, even in the presence of strong capping agents such as PVP, is proposed as the final thermodynamic fate of AgNPs, which can minimize the concentration of dissolved Ag (Levard et al., 2011; Liu and Hurt, 2010). The non-uniform sulfidation of AgNP surface, however, may still contribute to NP dissolution (Kent et al., 2014). In parallel, the influent chloride (12.5 mM in concentrated feed, Table 4.1) can act as a sink for Ag^+ ions released from oxidative dissolution of PVP-AgNPs by forming insoluble AgCl(s) species at low Cl^- concentrations and soluble chloro-silver complexes (i.e., $AgCl_2^-$, $AgCl_3^{2-}$, $AgCl_4^{3-}$) at high Cl^- concentrations (Azodi et al., 2016; Zhang et al., 2018) leading to a high Ag^+ gradient between the surface of AgNPs and a bulk solution that further favor the dissolution of AgNPs. It should be noted that AgNP bioavailability in biological matrices can be highly influenced by the complexation/competition with components in the wastewater effluent. The release of AgNP-rich biofilm sloughed of the carrier surface can adversely affect the efficiency of downstream treatment chains such as nitrifying MBBRs. Thus, the potential impact of AgNPs in the receiving environment would still be a concern even at proposed environmental concentrations.

The risks associated with exposure to AgNPs during wastewater treatment, can be attenuated by possible changes in their aggregation state, surface composition, their reactivity. Coagulation-flocculation process and chemical precipitation for treatment of the AgNP-containing stream can likely increase their hetero-aggregation, leading to lower Ag bioavailability prior the biological treatment in WRRFs. Folens et al. (2017) reported the high efficiency of a poly aluminum

chloride coagulant in combination with a pH-correction and an anionic polyelectrolyte as flocculant as an effective combination for Ag removal in wastewater matrix. Downstream of biological process, incorporation of reactive media such as slag filters (Claveau-Mallet et al., 2013) can potentially reduce the Ag via complexation/precipitation reactions with the widely present inorganic and organic substances. There is a need to evaluate the efficacy of such approaches and to understand how NPs behave under such conditions.

4.6 Conclusion

This study was focused on assessing the sensitivity of attached-growth biological wastewater treatment processes at environmental relevant concentrations of AgNPs. This is the first study that investigated the fate and inhibitory effect of PVP-AgNPs in high rate carbon removal MBBRs, at nominal concentrations of 10 to 600 μg/L AgNPs. Although previous studies suggested no lethal impact of certain nanoparticles (e.g. CeO_2, TiO_2, CuO and AgNPs) on biofilm system, our results indicated the adverse effect of PVP-AgNPs on structural and functional response of the biofilm in MBRR which was dependent on the exposure time and influent Ag concentration. Suppressed soluble COD removal efficiency and biofilm membrane integrity damage in reactors could affect the stability of such high-rate treatments. The observed significant biofilm detachment from the surface of the carriers could affect the sludge retention time of the reactors and the biomass specialization. The quantitative characterization of nanoparticles in MBBRs, using spICP-MS, and Ag mass balance indicated the limited retention capacity of aerobic heterotrophic biofilm for AgNPs over long term exposure. Our findings imply lower efficiency of MBBRs to retain AgNPs compared to the commonly used activated sludge systems. The release of AgNP-rich biofilm, sloughed off the carriers, could affect the treatment chain efficiency of a downstream nitrifying MBBR or the effluent receiving stream. Our results stress the need for strategies to control the release of such NPs from biofilm systems. This study contributes to a better understanding of the fate and behavior of AgNPs in biological wastewater processes, providing key information that can be used to predict the environmental risks of ENPs (transport, persistence and toxicity) in aquatic ecosystems.

Acknowledgements

The authors thank the Natural Sciences and Engineering Research Council of Canada (Grant no. STPGP 430659–12), Environment and Climate Change Canada, PerkinElmer Health Sciences Canada, the Fonds de Recherche du Québec Nature et Technologies (FRQNT), the Canadian Water Network (CWN), SNC Lavalin Environnment, the City of Calgary and the City of Saint-Hyacinthe for their financial support. The authors thank Jean-Philippe Massé, Le Centre de Caractérisation Microscopique des Matériaux of Polytechnique Montreal for TEM/EDS analysis, Nicolas Tran-Khanh of Polytechnique Montreal for CLSM analyses, the Terrebonne/Mascouche WRRF for assistance with wastewater sampling and Dr. Flavio Piccapietra of McGill for assistance with spICP-MS analyses and data interpretation.

CHAPTER 5 ARTICLE 2: IMPACTS OF CONTINUOUS INFLOW OF LOW CONCENTRATIONS OF SILVER NANOPARTICLES ON BIOLOGICAL PERFORMANCE AND MICROBIAL COMMUNITIES OF AEROBIC HETEROTROPHIC WASTEWATER BIOFILM

The long-term impact of AgNPs was reported for the first time in this study, using aerobic heterotrophic wastewater biofilms, in moving bed biofilm reactors (MBBRs) at nominal influent concentrations of 10.9 and 109 μg/L AgNPs to approximate environmentally relevant concentrations of AgNPs. Sixty four days exposure to both influent AgNP concentrations significantly inhibited the biological performances of heterotrophic biofilms in MBBRs. Heterotrophic biofilm contributed to AgNPs removal efficiency at an initially high level (60 to 71%) which gradually decreased to 25% in MBBRs by end of the exposure period. The results signify that short-term exposure studies, using a single high-dose of nanoparticles in biofilm systems can underestimate the NP-mediated susceptibility of biofilms by exluding the cumulative effect of NP-biofilm interaction dynamics over long-term exposures. This chapter was published as a research paper in the journal of *Environmental Science and Technology* on July 11th, 2019. Supplementary information is presented in Appendix B.

Alizadeh, S., Abdul Rahim, A., Guo, B., Hawari, J., Ghoshal, S. and Comeau, Y.(2019). Impacts of continuous inflow of low concentrations of silver nanoparticles on biological performance and microbial communities of aerobic heterotrophic wastewater biofilm. *Environmental science & technology. 53,15, 9148-9159*

IMPACTS OF CONTINUOUS INFLOW OF LOW CONCENTRATONS OF SILVER NANOPARTICLES ON BIOLOGICAL PERFORMACE AND MICROBIAL COMMUNITIES OF AEROBIC HETEROTROPHIC WASTEWATER BIOFILM

Sanaz Alizadeh[1*], Arshath Abdul Rahim[2], Bing Guo[2], Jalal Hawari[1], Subhasis Ghoshal[2], Yves Comeau[1]

[1]Department of Civil, Geological and Mining Engineering, Polytechnique Montreal, 2500 Polytechnique road, Montreal (Quebec) Canada H3T 1J4

[2]Department of Civil Engineering and Applied Mechanics, McGill University, 817 Sherbrooke Street West, Montreal (Quebec) Canada H3A 0C3

[*]Corresponding author: sanaz.alizadeh@polymtl.ca

ABSTRACT

Attached-growth wastewater processes are currently used in water resource recovery facilities (WRRFs) for upgrades required due to an increase in influent loading or to reach more stringent discharge criteria. Yet, the distribution and long-term inhibitory effects of silver nanoparticles (AgNPs) in attached growth biological wastewater processes and their impact on involved microbial communities are poorly understood at relevant, low concentrations. Retention, distribution and long-term inhibitory effect of polyvinylpyrrolidone (PVP)-coated AgNPs were evaluated in bench-scale moving bed biofilm reactors (MBBRs), achieving soluble organic matter removal, over a 64 day exposure to nominal concentrations of 10 and 100 μg/L. Distributions of continuously added AgNPs were characterized in the influent, bioreactor and effluent of MBBRs using single particle inductively-coupled plasma mass spectroscopy (spICP-MS). Aerobic heterotrophic biofilms in MBBRs demonstrated limited retention capacity for AgNPs over long-term exposure, with release of AgNPs, and Ag-rich biofilm sloughed from the carriers. Continuous exposure to both influent AgNP concentrations significantly decreased soluble chemical oxygen demand (S_{COD}) removal efficiency (11% to 31%) and reduced biofilm viability (8% to 30%). Specific activities of both intracellular dehydrogenase (DHA) and extracellular α-glucosidase (α-Glu) and protease (PRO) enzymes were significantly inhibited (8% to 39%) with an observed NP dose-dependent intracellular reactive oxygen species (ROS) production and shift in biofilm microbial community composition by day 64. Our results indicated that long-term exposure to AgNPs in biofilm processes at environmentally relevant concentrations can impact the treatment process stability and the quality of the discharged effluent.

5.1 Introduction

Engineered nanoparticles (ENPs) are manufactured at an estimated rate of 11.5 million tons per year for various industrial and commercial applications (Vance et al., 2015). Silver nanoparticles (AgNPs) are predominantly used as antimicrobial agents in commercial products, cosmetics, food processing and water industries (Vance et al., 2015). This rapidly developing nanotechnology market, however, is leading to their environmental exposure, with a significant fraction of the AgNP-laden domestic and industrial waste streams being released in municipal water resource recovery facilities (WRRFs) at an estimated influent concentration ranging from 10 ng/L to 105 μg/L (Gottschalk et al., 2009; Keller and Lazareva, 2013; Li et al., 2013). Thus, WRRFs serve as a key interface between ENPs releases and their environmental distribution into downstream ecosystems.

Suspended growth biological processes have been extensively used to elucidate the fate and potential impacts of AgNPs in wastewater biological treatment processes. Previous studies on the inhibitory effects of AgNPs (0.1 to 50 mg/L) in suspended-growth systems showed adverse effects on the biological performance and biomass activity caused by oxidative stress, cell membrane damage and inactivation of key enzymes at sufficient AgNP doses (>1 mg/L) (Alito and Gunsch, 2014; Liang et al., 2010; Sheng et al., 2018; Yuan et al., 2015; Zhang et al., 2014; Zhang et al., 2016c). Yet, the information regarding distribution, accumulation and biological implications of AgNPs in attached growth biological processes over long-term exposures have not been reported in the literature.

Attached growth processes, such as moving bed biofilm reactors (MBBRs), are commonly used as an upgrade or replacement for existing biological processes to meet current and new effluent discharge requirements, while minimizing plant footprint and operating costs (Falletti and Conte, 2007; Walden and Zhang, 2018). In 2014, more than 1200 WRRFs in at least 50 countries utilize the MBBR technology in both the municipal and industrial sectors with over 36 in North America (Biswas et al., 2014; Borkar et al., 2013). A limited number of studies investigated the impact of a single dose of AgNPs (1 to 200 mg/L) over 24 to 96 h, using mono-species biofilms, particularly *P. putida* based biofilms or wastewater biofilms in simplified biological media (Fabrega et al., 2009; Fabrega et al., 2011; Mallevre et al., 2016; Walden and Zhang, 2018).

Their findings indicated higher potential of biofilm bacteria than planktonic bacteria to withstand the toxic effects of AgNPs, primarily due to the presence of extracellular polymeric substances (EPS), the primary components of biofilm (Fabrega et al., 2011), which act to reduce AgNP diffusion in biofilms (Peulen and Wilkinson, 2011) over short term exposure conditions. Yet, the results of short-term exposure studies may fail to capture the effects of the expected accumulation of AgNPs and higher mass transport of AgNPs by diffusion into deeper layers of the biofilm over extended time intervals, thus underestimating the potential toxicity of AgNPs over long-term exposure scenarios (Alizadeh et al., 2019; Barker et al., 2018). Further research is thus required first, to understand the interaction mechanisms between ENPs and mature, mixed culture wastewater biofilms and second, to investigate the corresponding AgNP-induced inhibitory effects at environmentally representative NP concentrations under conditions that are representative of typical WRRF processes.

Rigorous physical and chemical characterization of AgNPs combined with extensive biological and toxicological evaluations in WRRFs are critical in laying the grounds for a better understanding of their environmental fate and for the design of better alternative treatment strategies and future regulations (Walden and Zhang, 2016). The current understanding of the environmental fate and transformation of ENPs is limited due to the limitations of ENP characterization techniques in complex environmental matrices containing ENPs at very low, environmentally relevant concentrations (Merrifield et al., 2017; Vidmar et al., 2018). Single-particle inductively coupled plasma–mass spectrometry (spICP-MS) is an emerging powerful technique with the potential to address such limitations, providing quantitative characterization of metal NP size distributions, particle number concentrations and dissolved metal concentrations at low NPs concentrations in complex, organic matter-rich, environmental matrices such as wastewaters (Azodi et al., 2016; Mitrano et al., 2012; Pace et al., 2012).

In this study, we investigated the impact of continuous injection of low concentrations of AgNPs in an attached growth wastewater treatment process using aerobic heterotrophic wastewater biofilms at nominal influent AgNP concentrations of 10.9 and 109 μg/L. These concentrations are low but would still be at the higher end of the estimated concentrations in wastewater influents, and they could also reflect release from biosolid-treated soil or landfills by flooding events or production plant or waste management site discharges (Giese et al., 2018). The specific

objectives of this study were (1) to characterize the retention and transport of Ag (AgNPs, dissolved Ag and total Ag) in the bioreactor and effluent in an attached-growth wastewater MBBR and (2) to determine the long-term impact of AgNPs on soluble COD (S_{COD}) removal efficiency, biofilm cell membrane integrity, extracellular and intracellular enzyme activities, and microbial community of wastewater biofilms. Two bench-scale MBBRs were operated for organic matter removal and were fed with a synthetic soluble influent representative of a municipal wastewater. The impacts of AgNPs on the performance of the MBBRs were characterized by monitoring several performance indicators including S_{COD} removal efficiency, effluent quality and enzymatic activity over a 9-week (64 d) exposure period. The biological responses of aerobic heterotrophic biofilm were characterized in terms of (i) biofilm cell membrane integrity using DNA-binding stains, (ii) AgNP-mediated oxidative stress via intracellular ROS measurement and (iii) microbial metabolic functions by intracellular DHA and extracellular α-Glu and PRO specific enzymatic activities using colorimetric assays. The biofilm microbial community compositions, at both influent AgNPs concentrations, were characterized through high-throughput sequencing. The aggregation state, dissolution and distribution of AgNPs were determined between different reactor components (i.e. influent, bioreactor and effluent) using spICP-MS techniques and transmission electron microscopy with energy dispersive X-ray spectroscopy (TEM EDS). To the best of our knowledge, this is the first study evaluating the long-term inhibitory effect of AgNPs on attached-growth wastewater process efficiency and its microbial communities at environmentally relevant AgNP concentrations (< 100 μg/L AgNPs) by combining biological responses and the NP distribution, characterization and Ag speciation data .

5.2 Materials and Methods

5.2.1 Reactor configuration and AgNPs exposure

Two 1 L bench-scale MBBRs (Figure B.1: Schematic of the experimental MBBR), achieving organic matter removal at a hydraulic retention time (HRT) of 3 hours, operated in parallel under identical conditions, were fed a synthetic soluble influent (Table B.1) to ensure constant influent characteristics and well-controlled conditions to characterize the inhibitory effects of the PVP-

AgNPs. The concentrated synthetic wastewater (1.3 ± 0.2 g S_{COD}/L) was pumped and diluted with tap water before entering the reactors to obtain an influent COD concentration of 655 ± 6 mg S_{COD}/L at an organic loading rate of 11 ± 0.2 g COD m^{-2} d^{-1} of active surface area, to be representative of the soluble fraction of a medium to high strength domestic wastewater with typical COD/TKN/TP ratio of 100/12.0/2.0. The characteristics of the synthetic influent (Table B.2) and detailed reactor operation conditions are presented as supplementary information (SI). The characteristics of the synthetic influent (Table B.2) and detailed reactor operation conditions are presented as Appendix B. MBBRs were operated at a hydraulic retention time (HRT) of 3 hours, pH of 7.2 ± 0.1, a dissolved oxygen concentration (DO) of 6 ± 0.2 mg/L and maintained at 21 ± 1 °C. Each MBBR was filled with high-density polyethylene Anoxkaldnes K5 carrier (d: 26 mm; h: 4 mm, Veolia Water Technologies Canada Inc.) with specific active surface area of 800 m^2/m^3 at filling ratio of 60 % using 198 carriers (0.65 L of K5 carriers), corresponding to a total active surface area of 0.52 m^2 in each reactor. The actual volume of plastic at a 100% filling ratio of K5 carrier was determined experimentally (fp = 0.110 $L_{plastic}/L_{carrier}$). K5 carriers at 60% filling ratio corresponded to 0.060 $L_{plastic}/L_{reactor}$ in each MBBR. A control (0 Ag) MBBR was operated in parallel with two AgNP-fed MBBRs, under identical conditions, as a nursery reactor to obtain biofilm for calibration of the biological tests (e.g. *Bac*light viability test) and to replace the removed carriers after each sampling, to keep the constant number of the carriers in tested MBBR. The experimental design accounted for a comparison of treatment efficiency and biofilm biological responses in control period (day 90-124, no AgNP) and during the exposure period (day 125-189) in same reactor.

Two MBBR reactors were operated without any AgNP addition for 124 days. Quasi steady-state for S_{COD} removal efficiency was reached after 43 days. The last 34 days of the 124 day period served as a control period to observe the reactor and biofilm response without AgNP addition. Influent AgNP suspensions were prepared by dilution of 50 nm (nominal diameter) PVP-coated AgNPs stock suspension (4.73 mg/mL, Nanocomposix Inc., San Diego, US) in Milli-Q water. The zeta potential and surface area of AgNPs were -37.8 mV (at pH 4) and 9.8 m^2/g (as stated by the manufacturer), with a mean diameter of 48 ± 2 nm (SpICP-MS, PerkinElmer NexION 300X). The AgNP influent suspensions were pumped to each reactor from day 125 at a constant flow rate (2.7 ± 0.1 mL/min). The influent nanoparticle suspensions were replenished every 24 h.

The effluent quality was analyzed three times per week over the control period, every day over the first week of AgNP exposure and every 3 to 4 days by the end of exposure period (64 days). Composite samples were collected for both influent and effluent characterization (350 - 500 mL) at each sampling point and were analyzed in triplicates. Chemical oxygen demand (COD), measured according to Standard Methods (APHA et al., 2012) . The concentration of suspended biomass was measured in the effluent of the reactors in terms of total suspended solids (TSS) and volatile suspended solids (VSS) concentrations according to standard method 2450D-E (APHA et al., 2012). The catalytic activity and the microbial community of the suspended biomass were not analyzed.

5.2.2 Silver analyses

Composite sample (150 to 300 mL) for each influent, bioreactor and effluent of MBBRs were collected everyday over the first 5 days of AgNP exposure (day 125-130) and every 3 to 7 days (day 133-189) afterwards, corresponding to a total of 20 sampling points in a 64-day exposure period. Bioreactor and effluent samples contained suspended flocs (145 to 380 mg TSS/L) but no K5 carriers. AgNP concentration and size as well as dissolved Ag were determined simultaneously using spICP-MS, supported by Syngistix nano application module (version 1.1) as described by Azodi et al. (2016). For spICP-MS analysis, homogenized bioreactor, influent and effluent samples were allowed to settle for about 30 to 45 s and the aqueous supernatant was collected. Thus, the AgNP in the supernatant analyzed by spICP-MS were unattached to any biomass present in the sample, and can be assumed to be freely suspended AgNPs or AgNPs easily detached from biomass. Total Ag concentration was independently measured in acid-digested homogenized samples using a PerkinElmer NexION 300x ICP-MS in standard mode as described in our previous study (Alizadeh et al., 2019). Instrumental and data acquisition parameters of the analysis are indicated in Appendix B (Table B.3). A cumulative Ag mass distribution in influent ($M_{Ag,inf}$), bioreactor ($M_{Ag,bio}$) and effluent ($M_{Ag,eff}$) of each MBBR was calculated based on the corresponding total Ag concentrations, obtained from ICP-MS analysis, influent and effluent flow rates, and volume of the bioreactor for each time interval (Δt) as described in our previous study (Alizadeh et al., 2019). Ag fractionation and the detailed equations and Ag mass calculations are presented in Appendix B.

5.2.3 Biofilm cell membrane integrity and key enzymatic activities of attached biofilm

Biofilm biological responses were characterized, in triplicates, every seven days over the control (day 90-124) and AgNP exposure periods (day 125-189). Five carriers were chosen randomly at each sampling time. The attached biofilm was recovered from the surface of carriers, as described in Appendix B. The inhibitory effect of AgNPs on the biofilm cell membrane integrity was evaluated using the Live/Dead Baclight bacterial viability kit (Molecular Probes, Invitrogen, Kit L13152) and a micro plate reader (Synergy-HT, BioTek, USA) as described by Chen et al. (2012). In this technique, the live and dead cells are differentiated on the basis of membrane integrity. The green fluorescent stain, SYTO-9 stains all bacteria and red fluorescent stain, propidium iodide (PI) stains the cells with damaged membranes (Asadishad et al., 2011).

The specific activities of DHA, α-Glu and PRO enzymes were measured by a colorimetric method using 0.5% 2-(4-iodophenyl)-3-(4-nitrophenyl)-5-phenyl-2H-tetrazolium chloride (INT), 1% p-nitrophenyl α-D-glucopyranoside and 0.5% azocasein, respectively, as a substrate for the reactions (Goel et al., 1998; Von Mersi and Schinner, 1991). The intracellular ROS production, as an indicator of oxidative stress, was determined using dichlorodihydrofluorescein diacetate (H_2DCF-DA, Molecular Probes, Invitrogen) (Gu et al., 2014). H_2-DCFDA was used as a cell-permeant reagent that measures hydroxyl, peroxyl and other reactive oxygen species activity in cells. The quenching effects of AgNPs on absorbance or fluorescence intensity in corresponding assays were tested at different Ag concentration (0.0, 0.1, 0.5, 1.0 and 5.0 mg/L). No interference of AgNPs was detected with absorbance or fluorescence intensity in the proposed range of AgNP concentrations in these assays (Figure B.3-4). Details regarding all enzyme activity and ROS assays are provided in Appendix B.

5.2.4 DNA Extraction, sequencing and microbial community analysis

Biofilm samples were collected from $MBBR_1$ and $MBBR_2$ at the end of the control period ($MBBR_{10}^{124}$, $MBBR_{100}^{124}$) and after exposure to AgNPs for 64 days (day 189) ($MBBR_{10}^{189}$, $MBBR_{100}^{189}$). For each set of the microbial community data, 10 carriers were selected randomly from each reactor; the retained biofilm was homogenized and used for DNA extraction. One

biofilm sample per reactor was used for DNA extraction at each sampling point. Genomic DNA was extracted from the biofilm samples using FastDNA®spin kit (MP Biomedicals, Santa Ana, CA) following the manufacturer's instructions, and sent for library preparation and sequencing on the Illumina Miseq PE250 platform at McGill University and Génome Québec Innovation Centre (Montréal, Québec). Bacterial universal primers 515F (5′-GTGCCAGCMGCCGCGGTAA-3′) and 806R (5′-GGACTACHVGGGTWTCTAAT-3′) were used to amplify the V4 variable region of the 16S rDNA. Bioinformatics analysis was performed using QIIME2 pipelines. The de-multiplexed forward and reverse sequences were quality-filtered using DADA2 at 100% sequence similarity (Callahan et al., 2016b). Taxonomy was assigned using the 99% operational taxonomic unit (OTU) similarity in the Green Genes reference database.

5.2.5 Statistical Analysis

The statistical significance of differences between treatments ($p < 0.05$), before and after exposure to AgNPs, was evaluated with one-way repeated measures ANOVA using Statistica version 12 (StatSoft Inc., USA). Alpha-diversity, beta-diversity and their statistical tests were analyzed in QIIME2. The data from each reactor at end of the control and exposure periods were pooled together as two replicates (n = 2) and differences, as proposed by Kroll, et al.(2016), to test the effect of AgNP on alpha diversity indices. Principal coordinates analysis (PCoA) was constructed using weighted UniFrac distance matrix. A heatmap was generated in R using the "gplots" package.

5.3 Results and discussion

5.3.1 Fate of AgNPs in MBBRs over 64 days

The influent of $MBBR_1$ and $MBBR_2$ contained an average concentration of 10.9 ± 1.6 μg/L AgNP ($[AgNP_{inf}]$) and 109.3 ± 10 μg/L $AgNP_{inf}$, with mean diameter (d_{mean}) of 49 ± 7 nm and 48 ± 2 nm, respectively (Figure B.5A,B). The fractionation of Ag as NP, dissolved or total, in each component of the reactor is provided in Figure B.2. The corresponding total Ag concentration in the influent ($[Ag_{inf}]$) was 14 ± 2 μg Ag /L and 130 ± 14 μg Ag /L due to the presence of some Ag^+ (Figure 5.1 A, B). SpICP-MS analyses showed less than 10% variation in

dissolved Ag concentrations ([dissolved Ag_{inf}]), in influent NP stock solutions of both reactors over time (Figure 5.1 A, B).

Three distinct trends (phases) were observed for Ag concentration profiles in both reactors over the 64-day Ag loading (Figure 5.1 A, B). Phase I corresponded to the first 15 days of AgNP loading (day 125-140) during which both reactors accumulated Ag in response to the AgNP addition and reached a relatively stable Ag retention efficiency (61% to 72% of [Ag_{inf}]). A major fraction of the effluent total silver ([Ag_{eff}]) (40% to 63%) was associated with total suspended solids in effluent (TSS_{eff}) in MBBRs. Effluent AgNP concentration ($AgNP_{eff}$) in $MBBR_1$ (0.2 to 1.4 μg/L) and $MBBR_2$ (2.9 to 5.5 μg/L) corresponded to approximately 10% ± 3% of [Ag_{eff}] and 16% ± 4% of [Ag_{eff}] , respectively, over Phase I. Based on the SpICP-MS analyses in phase 1 (day 125-140), the concentration of dissolved Ag in the effluent supernatant of $MBBR_1$ and $MBBR_2$ varied between 0.20 ± 0.01 to 3.6 ± 0.04 μg/L and 4.7 ± 0.5 to 11.9 ± 0.7 μg/L respectively, representing about 16% to 49% of [Ag_{eff}] in $MBBR_1$ and 18% to 30% of [Ag_{eff}] in $MBBR_2$ (Figure 5.1 A, B). The measured dissolved Ag in bioreactor and effluent were likely partially or completely complexed to dissolved organic carbon excreted by bacteria or thiol-containing organic ligands in biofilm EPS (Azimzada et al., 2017; Azodi et al., 2016; Levard et al., 2012). A high concentration of dissolved oxygen (6 ± 0.2 mg/L) and pH of 7.2 to 7.5 in the MBBRs, over the exposure time, provided thermodynamically favorable conditions for oxidation driven dissolution of AgNPs. The attached biofilm retained about 60% to 71% of cumulative mass of total Ag loading in the influent ($M_{Ag_{inf}}$) in $MBBR_1$ (1.6 mg Ag/m^2 of carrier active surface) and $MBBR_2$ (20.1 mg Ag/m^2 of carrier active surface) by the end of Phase 1 (day 140), indicating an initial high Ag biofilm retention capacity (Figure 5.1 D, E). The carrier active surface area represents the biofilm covered surface area.

Phase II started with a gradual increase of [Ag_{eff}] which reached a maximum concentration of 8.9 ± 1.7 μg/L Ag in $MBBR_1$ and 118.6 ± 1.5 μg/L Ag in $MBBR_2$ over 10 days (day 140 - 150) decreasing the Ag retention efficiency significantly ($p < 0.05$) compared to Phase I due to biofilm detachment (Figure B.8). A larger fraction of [Ag_{eff}] (20% to 37%) was detected as NPs in the effluent supernatant of $MBBR_1$ (2.1± 0.1 to 3.3 ± 0.1 μg/L) and $MBBR_2$ (9.0 ± 0.4 to 26.5 ± 0.3 μg/L). The [dissolved Ag_{eff}] in $MBBR_1$ and $MBBR_2$ represented about 22% ± 3% of [Ag_{eff}] (1.3

± 0.6 to 3.0 ± 0.7 μg/L) and 25% ± 8% of [Ag_{eff}] (11.9 ± 1.5 to 25.3 ± 3.9 μg/L) respectively, in this phase (Figure 5.1 A, B). By the end of the second phase (day150), the attached biofilm retained about 44% of cumulative $M_{Ag_{inf}}$ in $MBBR_1$ and about 54% of cumulative $M_{Ag_{inf}}$ in $MBBR_2$ (Figure 5.1 D, E), followed by a continuous decrease in retention efficiency (Figure 5.1 A, B).

The higher Ag retention efficiency by uncoated surfaces of biofilm in phase I was due to the hydrophobic interaction between the heterogeneous amphiphilic moieties of biofilm and hydrophobic PVP coatings of AgNPs (Lin et al., 2012). As the concentration of AgNPs increased inside the reactors during Phase II, the accumulation of the PVP-AgNPs on the outer layer of biofilms over time could cause steric repulsion of the PVP- and EPS-coated AgNPs in suspension and reduce further deposition on the collector surface (Jian-Zhou et al., 2015; Lin et al., 2012). Mitzel and Tufenkji (2014) indicated the decreased retention of PVP-AgNPs in biofilm-coated sand due to repulsive electrostatic forces between the PVP coatings and the biofilm EPS.

Phase III corresponded to the period with Ag release and retention recovery events in both reactors (day 154 - 189). The Ag distribution profile in $MBBR_1$ consisted of two Ag release events on day 154 (week 4) and day 164 (week 6) with the [$AgNP_{eff}$] (9.9 ± 1.7 μg/L to 14.0 ± 0.7 μg/L) constituting 61% to 87% of detected [Ag_{eff}] (Figure 1A, C). Despite a slight Ag recovery in retention by biofilm by day 175 (week 7), significantly higher [Ag_{eff}] were released over the last two weeks of exposure, predominantly in the form of AgNPs (81% to 96% of [Ag_{eff}]). The Ag release events could be attributed to the processes described above for Phase II, as well as detachment of the biofilm outer layer, and release of easily detachable AgNPs from the biomass. Effluent samples showed higher TSS during Phase III (Figure B.8) indicating increases in effluent biomass concentrations. Although some fluctuations in TSS values were observed, especially for $MBBR_2$, the changes in TSS did not coincide with the Ag release events. This underscores the likelihood that Ag release events were not solely attributable to biomass sloughing but rather a number of processes as stated above.

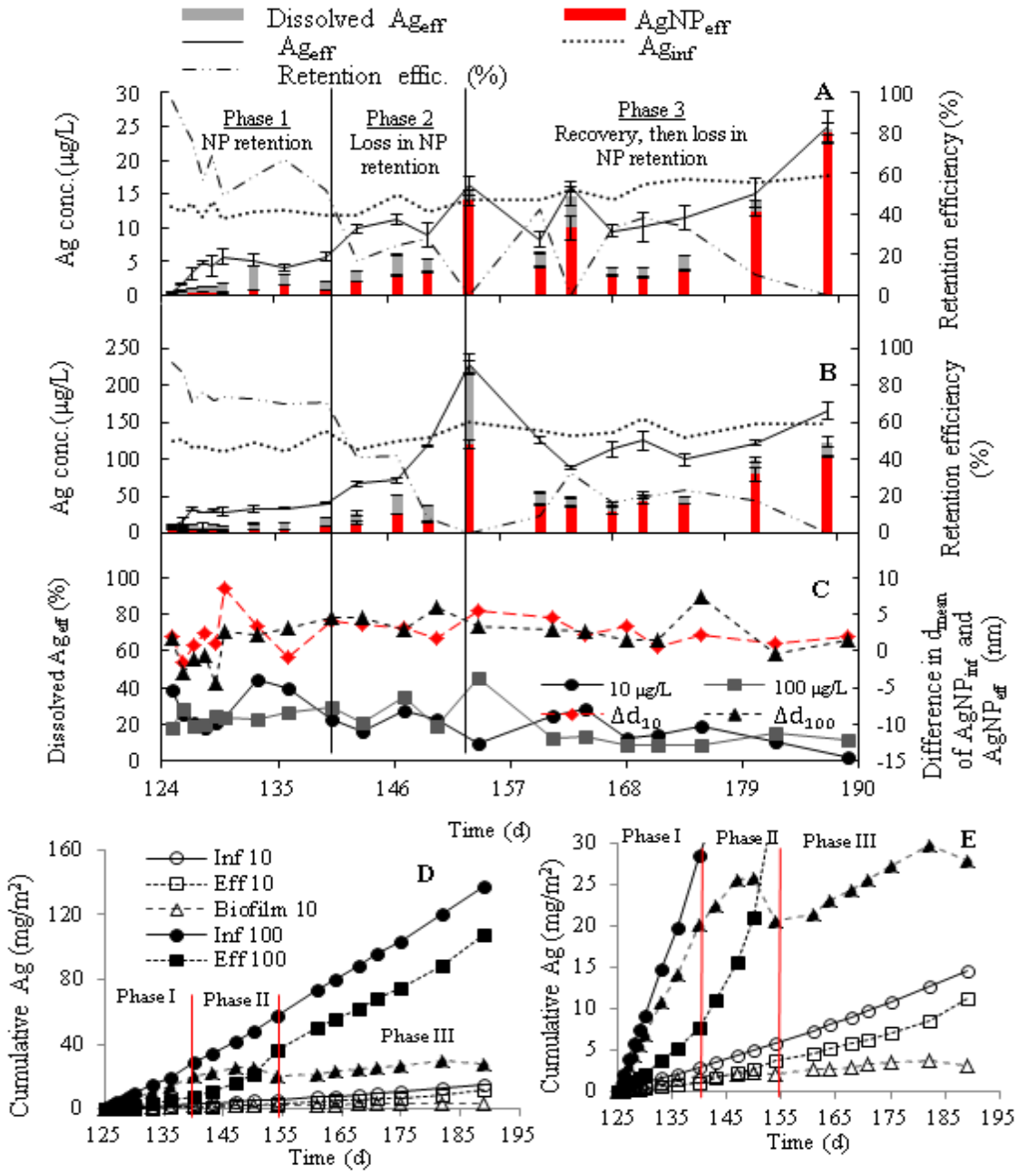

Figure 5.1: Fate and retention of Ag in MBBR receiving influent concentration of (A) 10 μg/L AgNPs and (B) 100 μg/L AgNPs, (C) dissolution of $AgNP_{eff}$ (%) and difference in mead diameter (d_{mean}) of $AgNP_{inf}$ and $AgNP_{eff}$, (D) cumulative Ag mass distribution in influent (Inf), attached biofilm (Biofilm) and effluent (Eff) and (E) enlarged Y-scale of panel D.

$MBBR_2$ demonstrated a lower recovery for Ag retention over a longer time interval as compared to $MBBR_1$ during the Phase III. The maximum Ag release of 229 μg/L Ag_{eff} was observed at the beginning of Phase III (day 154) in $MBBR_2$, and this value of $[Ag_{eff}]$ was almost entirely comprised of $AgNP_{eff}$ (52% of $[Ag_{eff}]$) and dissolved Ag_{eff} (45% of $[Ag_{eff}]$) in the aqueous phase of the effluent (Figure 5.1B). Thus only 3% of the Ag_{eff} was associated with the suspended effluent biomass (TSS_{eff}), as observed in $MBBR_1$. Thereafter, $[AgNP_{eff}]$ (40 to 104 μg/L) represented an average 40% to 65% of $[Ag_{eff}]$ between day 161 and day 189 (Figure 5.1 B). A relatively smaller mass fraction of $[Ag_{eff}]$ was accounted for dissolved Ag_{eff} (11% to 15%) in both reactors in Phase III compared to Phases I and II (Figure 5.1 C). Attached biofilm retained less than 20% of cumulative $M_{Ag_{inf}}$ in $MBBR_1$ (2.9 mg Ag/m^2 of carrier active surface) and $MBBR_2$ (27.7 mg Ag/m^2 of carrier active surface), respectively, and significant fraction of cumulative $M_{Ag_{inf}}$ (> 78%) was released via the effluent of the both reactors by the end of Phase III (day 189; Figure 5.1 D, E), indicating poor retention capacity of the biofilm over long term exposure. An initial high retention of AgNPs and silica-coated iron oxide in wastewater biofilms were reported at low NP concentrations over exposure (1 to 3 h) but there was an increase in NP concentrations and detachment of NP-rich biofilms over longer exposure time (e.g., 27 d) (Azimzada et al., 2017; Herrling et al., 2016).

The mean diameter of $AgNP_{eff}$ was smaller than $AgNP_{inf}$ by 1.5 to 7 nm in $MBBR_1$ and by 1 to 8.5 nm in $MBBR_2$ at different time points during the exposure period, despite the minor aggregation over initial days in phase I (Figure 5.1 C). The magnitude of change in the diameters was small because of the short average residence time (3 h) of the AgNPs in the reactor. The limited dissolution of PVP-AgNPs was demonstrated in deionized water or wastewater effluent over short retention time (3 to 5 h) in batch systems with similar small change in particle mean diameter (<10%) (Azodi et al., 2016; Mitrano et al., 2014). The particle size distribution of $AgNP_{eff}$ had slightly higher concentrations of smaller particles compared to $AgNP_{inf}$ (Figure B.6). The relatively high amount of dissolved Ag_{eff} on certain days (e.g., day 133 in $MBBR_1$ and day 154 in $MBBR_2$) cannot be accounted for the changes in particle diameters in the effluent. It is likely that detachment and release of soluble complexes Ag from the biofilm/EPS matrix resulted in relatively high fraction of [dissolved Ag_{eff}] relative to$[Ag_{eff}]$.

A general conclusion from previous studies conducted in batch experiments, sequencing batch reactors, membrane bioreactors and municipal WRRFs indicated an efficient AgNP removal (72% to 95%) via accumulation in suspended growth activated sludge processes with no extensive AgNP release as compared to MBBRs (Kaegi et al., 2013; Li et al., 2013; Zhang et al., 2014; Zhang et al., 2016c). The quantitative characterization of nanoparticles in MBBRs, using spICP-MS, indicated an initial adaptation of MBBR to silver addition. The higher SRT/HRT and biomass surface area/volume ratios in MBBRs, as compared to activated sludge process, favors Ag retention per unit weight of biomass in the reactor, resulting in an initial higher accumulation of Ag in attached biomass over short exposure time. Over longer exposure time, the local accumulation of nanoparticles on the biofilm outer layers and biofilm sloughing off the carriers reduce the retention capacity of biofilm, with a periodic silver retention in MBBRs and with an increase in total Ag release, predominantly in NP form.

The observed decrease in fraction of dissolved Ag ($[\text{dissolved Ag}_{\text{eff}}]$) relative to $[\text{Ag}_{\text{eff}}]$ over time in both MBBRs can be attributed to the removal of Ag^+ via their interaction with functional groups of macromolecules such as cysteine and methionine in the biofilm EPS matrix and their organic ligands, such as thiols (Azimzada et al., 2017; Gondikas et al., 2018; Ho et al., 2010). Complete inhibition or significant decrease of AgNPs dissolution was reported in the presence of Cl^- ions at low Cl/Ag ratios (Ho et al., 2010). We observed AgNPs associated with biomass in TEM images and the colocation of Cl and Ag in the effluent of the MBBRs using TEM-EDS analysis (Figure B.7). Complexation of dissolved silver in wastewater effluents and their significantly reduced bioavailability were reported for a 7 day-experiment (Azimzada et al., 2017). Azodi et al. (2016) attributed the decrease in dissolved Ag concentrations in the wastewater effluent to the reformation of the secondary NPs from dissolved Ag, which could also lead to reduced dissolved Ag.

5.3.2 Effects of AgNPs on the biological performance of a heterotrophic aerobic biofilm

The biofilm-mediated S_{COD} removal efficiency was determined in the two MBBRs in response to the 64-day continuous exposure to $[\text{AgNP}_{\text{inf}}]$ of 10.9 and 109 μg/L (Figure 5.2A, B). Prior to exposure to the AgNPs, both reactors consisted of 98% ± 0.2% viable biofilm over the control

period (day 90-124) (Figure 5.3A) which stabilized the S_{COD} removal efficiency at 93% under quasi steady state conditions (Figure 5.2 A-C). The biodegradation of S_{COD} remained stable, after injection of AgNPs, with an average S_{COD} removal efficiency of 92% ± 0.7% over the first 35 days (day 125-161) in $MBBR_1$ ($0.19 < p < 0.99$) and 91% ± 2% over 23 days (day 125-147) in MBBR2 ($0.21 < p < 0.99$) indicating an unperturbed primary phase (Figure 5.2 C) with relatively stable biofilm viability (94% to 96%, $0.15 < p < 0.99$) (Figure 5.3 A). Measured AgNP concentrations in $MBBR_1$ (0.16 to 0.60 μg/L $AgNP_{bio}$) and $MBBR_2$ (0.7 to 5.02 μg/L $AgNP_{bio}$) and their corresponding dissolved Ag_{bio} of 0.3 to 1.2 μg/L and 1.5 to 8.4 μg/L, respectively, over Phase I (Figure B.5 C,D) were much lower than previously reported threshold inhibitory concentrations for toxicity of AgNPs and dissolved Ag for biofilms ($IC_{50,\ PVP\text{-}AgNP@48h}$ = 114 μg/L and $IC_{50,Ag^+@48h}$ = 44 μg/L; Yang and Alvarez, 2015).

As AgNP concentration increased in reactors (Figure B.5 C,D), a secondary phase was observed with higher numbers of inactivated cells, resulting in significant biofilm cell membrane integrity damage ($p < 0.05$) in $MBBR_1$ (8% ± 0.6%) and $MBBR_2$ (31% ± 1.3%) by day 189 (Figure 5.3A). The S_{COD} removal efficiency significantly decreased ($p < 0.05$) by about 11% ± 1% over 29 days (day 160-189) in $MBBR_1$, and by 31% ± 2% after 41 days (day 147-189) in $MBBR_2$ (Figure 5.2C), corresponding to the observed patterns in Ag_{bio} and Ag_{eff} time profiles. Exposure to both $AgNP_{inf}$ concentrations also induced biofilm detachment from the surface of the carriers, corresponding to the significant increase of TSS_{eff} (Figure B.8). Significant detachment of wastewater biofilm and concurrent release of accumulated AgNPs were similarly reported at environmentally relevant AgNPs concentrations (22 and 105 μg/L AgNPs) (Walden and Zhang, 2018).

The inhibitory effect of AgNPs on both the S_{COD} removal efficiency (Figure 5.2D) and the membrane integrity damage (Figure 5.3B) were highly correlated ($0.80 < R^2 < 0.94$) to the accumulated mass of Ag in attached biomass. High biomass surface area/volume ratio in attached growth processes (e.g. MBBR) enhances the deposition rate of AgNPs to attached biomass over time, leading to enhanced Ag retention per unit weight of biomass in MBBR. Thus, significant accumulation and associated mass transport of AgNPs into deeper layers of the biofilm can lead to extensive spatial distribution of AgNPs in the biofilm cells, delivering toxic Ag^+ directly to

adherent cells via interfacial dissolution of the surface-bound AgNPs and/or partly via direct uptake, leading to an enhanced time exposure and greater toxicity (Hsiao et al., 2015).

Intracellular ROS did not significantly change in $MBBR_1$ (10.9 μg/L $AgNP_{inf}$), whereas its concentration increased significantly (1.78-fold, $p < 0.05$) in $MBBR_2$ (109 μg/L $AgNP_{inf}$) over 64 days (Figure 5.2C), consistent with reported concentration-dependent ROS production in activated sludge (Gu et al., 2014). No correlation between biofilm membrane integrity damage and ROS production was observed in $MBBR_1$ whereas it was highly correlated to increased ROS generation in $MBBR_2$ ($R^2 = 0.97$) (Figure 5.3D), indicating both ROS-mediated and ROS-independent effects of AgNPs on cell membrane integrity (Gu et al., 2014). The interaction between AgNPs/Ag^+ and the functional groups of proteins, involved in the cell respiratory chain, can lead to intracellular ROS production. Biofilm was able to regulate the ROS production at lower AgNP concentrations (1.4 to 9.04 μg/L $AgNP_{bio}$), likely via ROS scavenging enzymes (e.g. superoxide dismutase), higher concentrations of AgNPs in $MBBR_2$ (10.3 to 46.2 μg/L $AgNP_{bio}$), however, caused significant overproduction of ROS which can overwhelm the antioxidant systems and induce oxidative damage to cell membranes by for example modification of the unsaturated fatty acids of the membrane phospholipids (Abdal Dayem et al., 2017; Birben et al., 2012).

5.3.3 Inhibitory effect of AgNPs on key enzymatic activities of aerobic heterotrophic biofilm

Average DHA specific activity was inhibited by about 11% ± 2% and 27% ± 2% in $MBBR_1$ and $MBBR_2$, respectively, after 64 days (Figure 5.4A_1). The specific activity of α-Glu and PRO were reduced by 16% ± 2% and 8% ± 1%, respectively, in $MBBR_1$. Higher enzyme activity inhibitions, up to 39% ± 2% (α-Glu) and 18% ± 2% (PRO), were observed at higher [$AgNP_{inf}$] in $MBBR_2$ (Figure 5.4 B_1, C_1), indicating a dose-dependent effect of AgNPs on specific enzymatic activities of biofilms (Asadishad et al., 2018; Xu et al., 2017a).

The deleterious effect of AgNPs on the intracellular DHA activity displayed an initial lag phase whereas both extracellular enzymes α-Glu and PRO reacted to the presence of AgNPs in the early stage of exposure in both reactors, indicating a distinct inhibitory profile of enzymes. α-Glu had the highest inhibition rate constant and the shortest half-life (p<0.05) among the three enzymes

(Table B.4), indicating high susceptibility of this enzyme to AgNPs. Significantly different inhibition rates and half-lives of all three enzymes upon exposure to AgNPs (Table B.4) indicated the distinct sensitivity of these enzymes to AgNPs due to their different properties and location patterns in the biofilm matrix (Schug et al., 2014).

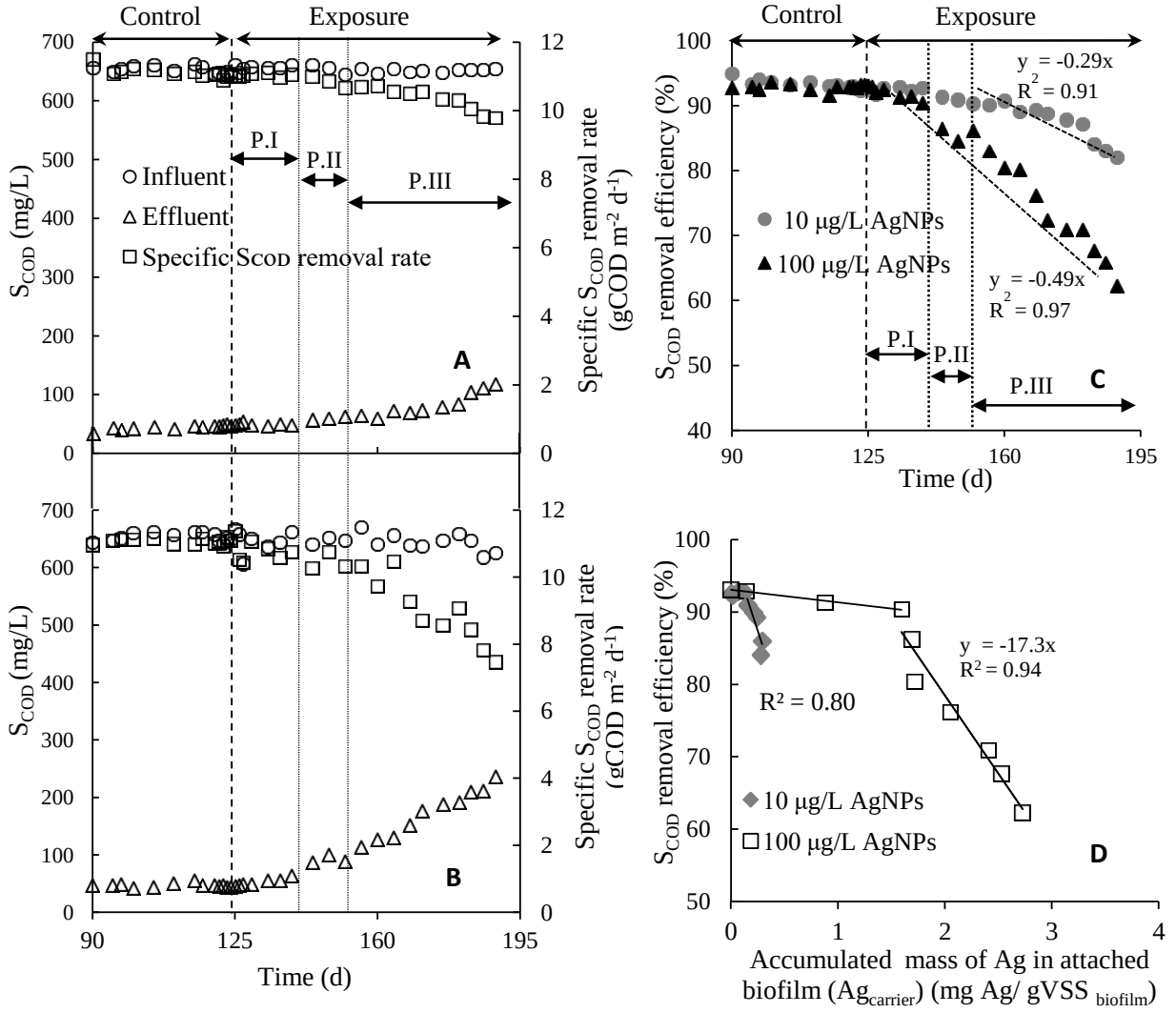

Figure 5.2 : Effect of PVP-AgNPs addition on MBBR performance at (A) 10 μg/L AgNPs (B) 100 μg/L AgNPs, (C) S_{COD} removal efficiency and (D) correlation between $Ag_{carrier}$ and S_{COD} removal efficiency (error bars are only shown when larger than symbol size). Note: P.I-III refers to three observed phases in Ag distribution profile.

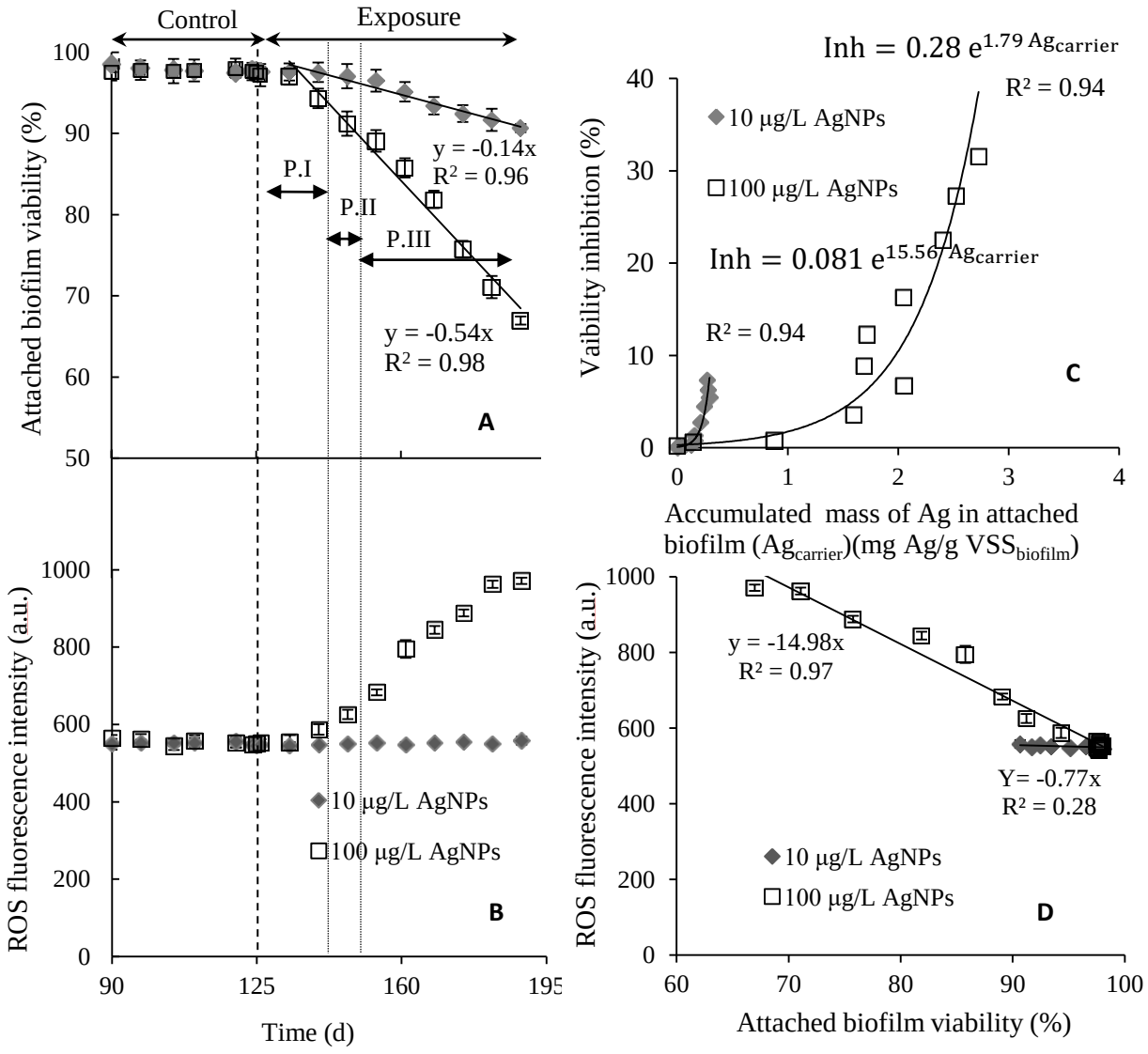

Figure 5.3: Effect of continuous PVP-AgNP injection on (A) attached cell viability, (B) intracellular ROS generation. (C) Correlation between $Ag_{carrier}$ and attached biofilm viability inhibition and (D) correlation between viability inhibition and intracellular ROS generation (error bars are only shown when larger than symbol size). Note: P.I-III refers to three observed phases in Ag distribution profile.

The intact biofilm matrix confines the enzymes which can be freely diluted in the matrix, confined in the EPS network or localized intracellularly. Major PRO activities are associated with tightly bounded-EPS and pellets of aerobic wastewater biomass, whereas α-Glu activities are

largely bound with loosely bounded-EPS (Yu et al., 2007). Therefore α-Glu would be more accessible for AgNPs as compared to PRO or DHA. The extracellular α-Glu is directly involved in the degradation of carbohydrates in wastewater, influencing the removal of organic matter and microbial metabolism. The higher sensitivity of this enzyme upon direct contact with AgNPs and dissolved Ag can adversely affect the organic matter removal efficiency, the chemical structure of EPS and the stability of biofilm structure (Hassard et al., 2018; Wang et al., 2013).

The inhibitory effects of AgNPs on specific enzymatic activities of biofilm was highly correlated ($0.80 < R^2 < 0.96$) to the accumulated mass of Ag in attached biomass (Figure 5.4A_2-C_2). The observed pattern highlights the major role of diffusion of retained AgNPs in the biofilm-laden system upon the targeted delivery of both AgNPs and dissolved Ag in close proximity of enzymes and possibly inside the cell in order to reach the Ag concentration needed to exceed inhibitory limits. Upon the initial contact with enzymes in the biological media, nanoparticles acquire a protein corona leading to substantial structural changes of the enzyme (Ahlberg et al., 2014). Extracellular enzymes (e.g. α-Glu) interact initially via their functional groups (e.g. carboxyl, hydroxyl, amine, amido, keto) with both the ring and polyvinyl domain of PVP coating and the oxygen atom involved in PVP-nanoparticle complex form.

The strong bonding of AgNPs and dissolved Ag with electron donors containing sulfur, oxygen, or nitrogen (e.g. thiols, carboxylates, phosphates, hydroxyl, amines, imidazoles, indoles) across the enzymes can form silver complexes which shield the active sites and alter the enzyme's conformation or distort its 3D structure so it no longer retains its full enzymatic activity (Wigginton et al., 2010). Breaking through the barrier of outer membrane permeability, AgNPs and dissolved Ag can strongly associate with specific sequences of amino acids on the DHA active site and thiol (–SH) group of cysteine, by replacing the hydrogen atom to form –S–Ag, and irreversibly inactivate dehydrogenase enzymatic functions leading to cellular respiration inhibition (Kim et al., 2008; Wigginton et al., 2010). Moreover, the ROS-mediated protein oxidation and microbial community composition alteration can result in loss of function for enzymes associated with biofilms and in a cutback in their production and secretion (Schug et al., 2014).

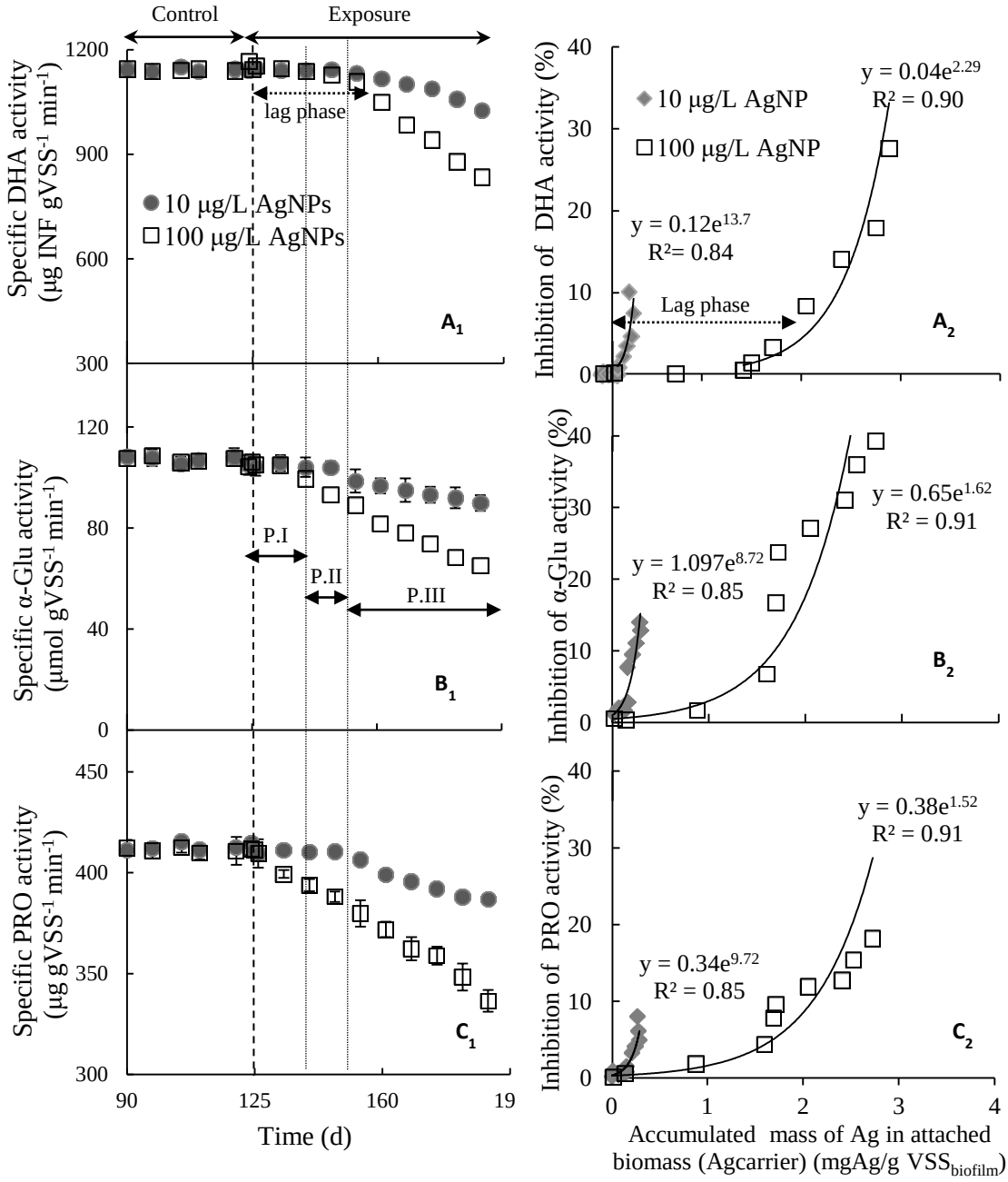

Figure 5.4: Effect of continuous PVP-AgNP injection on specific activity of (A_1) DHA (B_1) α-Glu and (C1) PRO, (A_2-C_2) correlation between $Ag_{carrier}$ and enzyme activity inhibition (Error bars are only shown when larger than symbol size).

5.3.4 Effects of AgNPs on the microbial community of the heterotrophic wastewater biofilm

Seven major phyla *(Proteobacteria, Bacteroidetes, Verrucomicrobia, Gemmatimonadetes Planctomycetes, Actinobacteria*) were identified (abundance > 1%) at the end of the control period in both reactors ($MBBR_{10}^{124}$, $MBBR_{100}^{124}$) (Figure 5.5A), as previously reported in microbial composition wastewater biofilm studies (Miao et al., 2017; Wang et al., 2018). *Proteobacteria* was the most abundant phylum majorly comprised of *Alphaproteobacteria*, *Betaproteobacteria* and *Gammaproteobacteria*. Certain phyla demonstrated a distinct pattern at two [$AgNP_{inf}$] after 64 days of exposure (day 189). AgNPs influenced biofilm microbial phylum abundance in a dose-dependent manner, which was confirmed by the principal coordinate analysis (PCoA) based on the weighted UniFrac distance matrix with 75% of total variance on PCoA1 axis (Figure B.9). The observed pattern indicated various responses among taxa, including a range from susceptibility towards silver (*e.g. Bacteroidetes* and *Gemmatimonadetes)* to tolerance against silver (*e.g.Planctomycetes),* as reported in previous studies (Cao et al., 2018; Grün et al., 2018).

The heatmap of genera, with total sequence reads higher than 150 in selected phyla, showed the distinct sensitivity of certain genera at both [$AgNP_{inf}$] (Figure 5.5B). The relative abundance of *Rhodobacter*, identified as the most abundant OTU at the genus level (*Rhodobacteraceae, α-proteobacteria*) decreased in both reactors. Higher abundance of *Paracoccus* other dominant genera from the *Rhodobacteraceae* family and *Zooglea* (*ß-proteobacteria*) at higher [$AgNP_{inf}$], is likely associated with their heavy metal resistance to enhance their survival in metal-contaminated environments (Zheng et al., 2017a). The abundance of *Sphingomonas* genus (*Sphingomonadaceae)* decreased in $MBBR_{10}^{189}$ whereas its abundance increased in $MBBR_{100}^{189}$, possibly due to the presence of signaling molecules (e.g. sphingolipids) in their outer membrane maintaining community diversity at higher silver concentrations (Yang et al., 2014b). The genera affiliated with *Xanthomonadaceae* family such as *Stenotrophomona* (*ɣ-proteobacteria*) are reported as N-acyl-homoserine-lactone (AHL) producers in aerobic granular sludge and biofilm, contributing to AHL-mediated quorum sensing signaling, integrity and biofilm stability (Tan et

al., 2014). Thus, the reduction in their relative abundance at both [$AgNP_{inf}$] affected both COD removal efficiency and integrity of biofilm structures.

Chronic exposure to both [$AgNP_{inf}$] greatly decreased the relative abundance of genera affiliated to three dominant orders in the *Bacteroidetes* phylum (*Sphingobacteriales*, *Flavobacteriales*, *Cytophagales*) known as the core members of microbial communities in WRRFs degrading complex organic materials resulting in reduced abundance of *Bacteroidetes* and a correlated lower COD removal efficiency in both reactors (Chen et al., 2016). Similar differential susceptibilities to AgNPs were observed in other identified phyla with a shift towards silver-tolerant genera (e.g. *Gemmata*) or more sensitive genera (e.g *Gemmatimonas)*. The alpha diversity of the microbial community was not significantly impacted (Table B.5) and the microbial community composition was slightly changed, as shown in Figure 5.5. The observed shift in the microbial community composition can trigger a potential impairment of the biofilm biological functions pertaining to organic matter biodegradation, enzymatic activities and biofilm structural properties.

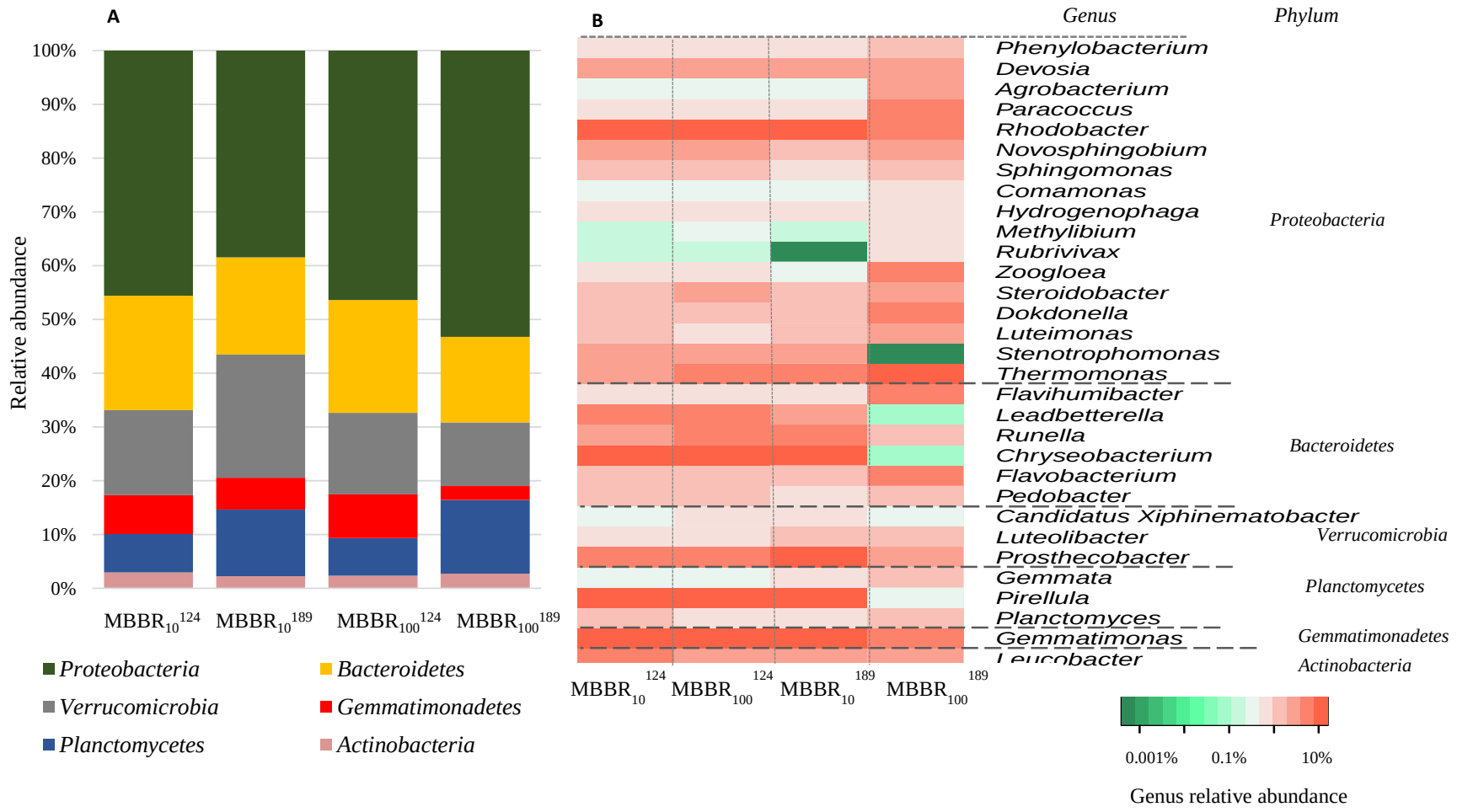

Figure 5.5: (A) Taxonomic classification of 16S rDNA paired-end sequencing from the biofilm samples at different AgNP concentrations at phylum level and (B) heatmap of genera with total sequence reads higher than 150 in selected phyla. Note: Superscripts 124 and 189 represent the biofilms collected at the end of control period (day 124) and after 64 days of AgNPs exposure (day 189) in MBBRs, respectively.

5.4 Environmental implications

The MBBR technology has been successfully used for the treatment of many types of wastewaters from municipalities, paper mills, pharmaceutical industries and fish farms (Revilla et al., 2016). MBBRs can be easily combined with other pre- or post- treatment technologies such as settling and membrane separation or used in a series of aerobic and anaerobic MBBRs, thus increasing the likelihood of achieving a 'zero discharge' goal (Bakar et al., 2018). Our findings indicate that the extended release of AgNPs and Ag-rich biomass via effluent of a MBBR can exert adverse effects on downstream treatments that may lead to membrane fouling due to higher effluent TSS concentration, for example, or pose a potential risks in effluent receiving streams. Our results show that long-term continuous exposure to AgNPs can result in a cumulative effect on NP-biofilm interaction dynamics leading to NP-mediated susceptibility in the biofilm and signify that short-term exposure tests may underestimate the inhibitory effects of AgNPs in biofilm-laden environments, especially for treatment processes with long sludge retention times. However, there was no sulfidation of AgNPs in these MBBRs deployed here, due to lack of sulfur in the synthetic wastewater. Sulfidation of AgNPs has been shown to retard dissolution of AgNP due to formation of Ag_2S and organosulfur complexes and could have resulted in lower toxicity to the heterotrophic biofilm (Azodi et al., 2016; Levard et al., 2011).

Acknowledgements

The authors thank the Natural Sciences and Engineering Research Council of Canada (Grant no. STPGP 430659–12), Environment and Climate Change Canada, PerkinElmer, Health Sciences Canada, the Fonds de Recherche du Québec Nature et Technologies (FRQNT), the Canadian Water Network (CWN), SNC Lavalin Environment, the City of Calgary and the City of Saint-Hyacinthe for their financial support. The authors thank Mr.Arshath Abdul Rahim of McGill for assistance with spICP-MS analyses and data interpretation, Bing Guo for bioinformatics analyses and data interpretation, Jean-Philippe Massé, Le Centre de Caractérisation Microscopique des Matériaux of Polytechnique Montreal for TEM/EDS analysis, and Jean-Baptiste Burnet for DNA extraction and the Terrebonne/Mascouche WRRF for assistance with wastewater sampling.

CHAPTER 6 RESPONSE AND RECOVERY OF NITRIFYING MBBR BIOMASS UPON LONG-TERM CONTINUOUS EXPOSURE TO SILVER NANOPARTICLES

6.1 Introduction

Silver nanoparticles (AgNPs) have been increasingly used over the last decade in biomedical, cosmetics and food production, notably, due to their broad-spectrum antimicrobial activity (Hasbullah et al., 2019; Huang et al., 2016). The increasing application of AgNPs leads to their release and accumulation in the surrounding environment (Zhang et al., 2019). A significant fraction of the AgNP-laden domestic and industrial waste streams, released during production of nano-enabled products (e.g. textiles and fabrics), application and consumption (e.g. cosmetics or water filters) enter municipal water resource recovery facilities (WRRFs) at an estimated influent concentration ranging from 0.01 to 105 μg/L (Gottschalk et al., 2013; Shafer et al., 1998; Tolaymat et al., 2017). Biological wastewater treatment is the central part of WRRFs with significant capital and operating costs. Therefore, the potential adverse effect of AgNPs on such processes, particularly the biological nutrient removal processes, is a significant economic and environmental concern (Sheng et al., 2018; Zhang et al., 2016).

The inhibitory effects of AgNPs (0.1 to 50 mg/L) in a pure nitrifying culture (e.g. *Nitrosomonas europaea*), nitrifying bacteria isolated from WRRFs and suspended growth biological nutrient removal processes, including nitrification, have been characterized over short term (1 to 24 h) and long-term (20 to 70 days) exposure scenarios (Alito and Gunsch, 2014; Arnon et al., 2008; Xu et al., 2017a; Yang et al., 2014a; Yuan et al., 2013; Zhang et al., 2016c). Ammonia oxidizing bacteria (AOB) were reported to be more vulnerable to AgNP treatment than nitrite oxidizing bacteria (NOB) and heterotrophs (Jeong et al., 2014; Liang et al., 2010; Yang et al., 2014a). Oxidative stress, outer-membrane destabilization and inactivation of key enzymes, including ammonia monooxygenase (AMO) and nitrite oxidoreductase (NOR) have been reported as the main toxicity mechanisms for AgNPs in such processes (Barker et al., 2018; Gwin et al., 2018; Xu et al., 2017a). Yet, the interactions and biological impact of AgNPs in wastewater nitrifying biofilms are poorly understood.

Contrary to conventional suspended growth processes, attached growth processes, specifically moving bed biofilm reactors (MBBRs), have shown great potential as an upgrade or replacement technology for nitrification even at low temperatures, while minimizing the plant footprint and operating costs (Barwal and Chaudhary, 2014; Biswas et al., 2014; Ødegaard, 2016; Young et al., 2017). Mono-species biofilms (e.g. *Nitrosomonas europaea*) and wastewater biofilms (mixed culture), have demonstrated higher capacity to cope with the inhibitory effects of AgNPs than planktonic bacteria, when receiving a single high-dose of AgNPs over short-term exposure, primarily due to interactions of AgNPs and extracellular polymeric substances (EPS) (Barker et al., 2018; Choi et al., 2010; Sheng and Liu, 2011; Sheng et al., 2015; Walden and Zhang, 2018).

Short-term exposures, however, may fail to include the cumulative effect of NP-biofilm interaction dynamics over long-term exposures, therefore underestimating the NP-mediated susceptibility in biofilm-laden environments (Alizadeh et al., 2019; Barker et al., 2018). Thus, the interaction and biological implication of AgNPs in wastewater biofilm-laden processes need to be investigated at environmentally representative NP concentrations under conditions that are representative of typical WRRF processes (Barker et al., 2018; Colman et al., 2018). A rigorous physical and chemical characterization of AgNPs (e.g. size, composition, dissolution) has been absent from most ecotoxicological studies (Cervantes-Avilés et al., 2019). Single-particle inductively coupled plasma–mass spectrometry (spICP-MS) allows simultaneous and sensitive characterization of AgNPs and dissolved Ag, which makes it a suitable method for identifying AgNPs in different processes of WRRFs (Cervantes-Avilés et al., 2019).

The specific objectives of this study were to determine (1) the fate and behavior of AgNPs in an aerobic attached-growth nitrifying process, (2) the impact of long term exposure of AgNPs on primary biological functions and the microbial community of aerobic autotrophic nitrifying wastewater biofilms, achieving ammonia removal and (3) the recovery potential of the nitrifying biofilm after long-term AgNP-stress at both the physiological and metabolic levels. Three bench-scale nitrifying MBBRs were fed with a synthetic influent. The nitrifying MBBR were used to represent a post carbon removal nitrifying biofilm system or a tertiary nitrification system after a conventional activated sludge system with stringent effluent standards. The impact of AgNPs on the performance of the nitrifying MBBRs, receiving influent concentrations of 15 ± 2 and 121 ± 9 μg/L Ag, were characterized by monitoring the main performance indicators including ammonia

removal efficiency, effluent quality (e.g. total suspended solids (TSS), nitrite and nitrate) and key enzymatic activity over a 60-day exposure period. The biological responses of aerobic nitrifying biofilms were characterized in terms of (i) biofilm cell membrane integrity using DNA-binding stains, (ii) AgNP-mediated oxidative stress via intracellular ROS measurement and (iii) microbial metabolic functions of AMO and NOR specific enzymatic activities using analytical assays. The biofilm microbial community compositions, in control and tested MBBRs, were characterized through high-throughput sequencing. The distribution and dissolution of AgNPs were determined between different reactor components (i.e. influent, bioreactor and effluent) using spICP-MS techniques and transmission electron microscopy with energy dispersive X-ray spectroscopy (TEM-EDS). To the best of our knowledge, this is the first study to evaluate the fate and biological implications of AgNPs in an attached-growth nitrification process and to determine the impact on its microbial communities at environmentally relevant AgNP concentrations (< 100 μg/L AgNPs).

6.2 Materials and methods

6.2.1 Reactor configuration and AgNPs exposure

Three 1 L bench-scale nitrifying moving bed biofilm reactors (MBBRs), achieving ammonia removal were operated in parallel, under the same loading and operational conditions throughout the study. The nitrifying MBBRs were fed with a synthetic influent (Table 6.1; adapted from Young et al., 2016) with an influent ammonia concentration of 70 mg NH_4-N/L. Each MBBR operated at a hydraulic retention time (HRT) of 3 hours, pH of 8.1 ± 0.1, dissolved oxygen concertation (DO) of 8.0 ± 0.5 mg/L, and a 60% volumetric filling ratio with AnoxKaldnes K5 carriers (Veolia Water Technologies Canada Inc.) with a specific active surface area of 800 m^2/m^3. Synthetic wastewater was used throughout the experimental phase to provide stable loading rates with limited variations. The temperature was controlled at 21 ± 0.2 °C in the double-jacketed MBBRs by a circulator (Programmable Circulator 9712, PolyScience, USA). The MBBRs were initially inoculated with colonized K3 carriers, collected from a full-scale MBBR at the Mascouche Terrebonne WRRF (Quebec, Canada) for a period of 10 days to favor biofilm growth and to ensure the development of a representative microbial community of a WRRF. Subsequently, the K3 carriers were removed from the reactors. The concentrated synthetic

wastewater (226 ± 5 mg NH_4-N/L) was pumped and diluted with tap water before entering the reactors to obtain an influent ammonia concentration of 69 ± 3 mg NH_4-N/L at a loading rate of 1.2 ± 0.2 g NH_4-N m^{-2} d^{-1} of active surface. The characteristics of the synthetic influent, after dilution of the concentrated solution are presented in Table 6.2.

Table 6.1 : Concentrated feed composition for the synthetic wastewater

Compound	**Chemical formula**	**Concentration**	
Ammonium sulfate	$(NH_4)_2SO_4$	630	mg /L
Ammonium chloride	NH_4Cl	365	mg/L
Potassium dihydrogen phosphate	K_2HPO_4	200	mg/L
Calcium chloride	$CaCl_2$	104	mg/L
Magnesium chloride	$MgCl_2$	243	mg/L
Sodium bicarbonate	$NaHCO_3$	910	mg/L
Ferric chloride	$FeCl_3$	5	mg/L

Table 6.2 : Average characteristics of the MBBR synthetic influent after dilution with tap water

Parameters	**Symbol**	**Units**	**Value**
Total ammonia (NH_3 + NH_4^+)	S_{NH4}	mg N/L	69 ± 3
Oxidized nitrogen (nitrite plus nitrate)	S_{NOx}	mg N/L	0.14 ± 0.02
Total phosphorus	TP	mg P/L	23.3 ± 0.7
Soluble phosphate	S_{PO4}	mg P/L	15.3 ± 0.5
S_{PO4}/TP ratio	f_{SPO4_TP}	g P/g P	0.64 ± 0.02
Alkalinity	S_{ALK}	mg $CaCO_3$/L	488 ± 5

Quasi steady-state for ammonia removal efficiency was reached in each MBBR after 53 days. The reactors were monitored afterwards to ensure the development of mature biofilm. The reactor and biofilm responses were determined over the last 60 days of the 292 day operation period as a control period day without AgNP addition. $MBBR_1$ was assigned as the control reactor and $MBBR_2$ and $MBBR_3$ received AgNPs. Influent AgNP suspensions were prepared by dilution of PVP-coated AgNPs stock suspension (4.73 mg/mL, 99% purity, Nanocomposix Inc., San Diego,

CA) in Milli-Q water. The zeta potential and surface area of AgNPs were -37.8 mV (at pH 4) and 9.8 m^2/g, respectively, based on the AgNP product description, with a mean diameter of 48 ± 2 nm (spICP-MS, PerkinElmer NexION 300X). The AgNP influent suspensions were pumped to $MBBR_2$ and $MBBR_3$ from day 293 at a constant flow rate (2.7 ± 0.1 mL/min), resulting in an average influent total Ag concentration of 15 ± 2 and 121 ± 9 μg/L Ag, respectively, after dilution. The influent nanoparticle suspensions were changed regularly every 24 h. The effluent water quality, biofilm biological responses (e.g. viability or enzyme activity) and the Ag distribution were monitored over 60 days of Exposure and a 35-day Recovery period. In the recovery period AgNP addition was ceased. Ammonia (NH_4), nitrite (NO_2) and nitrate (NO_3) concentrations were quantified in filtered samples (0.45 μm) by an ion chromatograph (ICS 5000 AS-DP DIONEX) equipped with an AS18 column according to method MA 300 Ions 1.3. Total suspended solids (TSS) and volatile suspended solids (VSS) were measured according to Standard Methods (APHA et al., 2012).

6.2.2 Silver analyses

The influent, bioreactor and effluent were sampled every 24 h over the first week of exposure (days 293 - 297) and every 3 to 5 days afterwards (days 297 - 353) for a total period of 60 days. Total Ag concentrations in those samples were measured in acid-digested homogenized samples using a PerkinElmer NexION 300x ICP-MS in standard mode as described in our previous study (Alizadeh et al., 2019). The concentration and size of the AgNP as well as dissolved Ag, in the influent, bioreactor and effluent samples, were determined simultaneously using spICP-MS, supported by Syngistix nano application module (version 1.1) as described by Azodi et al. (2016). Ultra-uniform gold nanoparticle (Nanocomposix, 55.5 nm) at a concentration of 9.84 x 10^4 particles/mL, diluted in MBBR effluent, was used to determine the transport efficiency (5.5 to 7.5 %) for spICP-MS analysis. The dwell time of 100 μs with a sampling time of 100 s was used for the analyses and all instrumental and data acquisition parameters of the analysis are indicated in Table C.1 in Appendix C. The collected wastewater samples were vortexed for 1 min. The homogenized samples were allowed to settle for about 30 to 45 s and the aqueous supernatant samples were analyzed in triplicates using appropriate dilutions. Each set of analysis included the blanks and National Institute of Standards and Technology (NIST) standard reference AgNPs to

ensure the reliability of the measurement. The set of analysis also included spiked silver nanoparticles in MBBR effluent (100 ng/L) and dissolved Ag (50 ng/L) as quality control, resulting in 96% recovery for both elements. The total Ag concentrations, obtained from ICP-MS analysis, influent and effluent flow rates, and volume of the bioreactor for each time interval (Δt) were used to calculate a cumulative Ag mass distribution in influent ($M_{Ag,inf}$), bioreactor ($M_{Ag,bio}$) and effluent ($M_{Ag,eff}$) in each MBBR as described in our previous study (Alizadeh et al., 2019).

6.2.3 Characterization of biofilm biological response to long-term AgNPs exposure

The attached biofilm was recovered from the surface of carriers according to a standardized procedure (Reboleiro-Rivas et al., 2013). Carriers (n = 7) were chosen randomly at each sampling time. These carriers were cut and vortexed for 1 min and the resultant biofilm suspensions were collected by centrifuging for 5 min at 3000 x *g*. This process was repeated twice. The biofilm pellet obtained after the last centrifugation was re-suspended in 5 - 8 mL of sterile buffer solution (0.5% NaCl or 0.01 M phosphate buffer) used for viability assessment, enzymatic activity and ROS assays. All assays included triplicate samples, a blank and a positive control (70% propanol-treated inactivated biofilm) where five reads per replicate at the corresponding setting were obtained by a microplate reader. Bacterial viability of the attached biofilms was evaluated using the Live/Dead *Baclight* bacterial viability kit (Molecular Probes, Invitrogen, Kit L13152) and a micro plate reader (Synergy-HT, BioTek, USA) as described by Chen et al. (2012). Briefly, triplicates of the biofilm samples (100 μL) were mixed with 100 μL of DNA-binding stains (SYTO-9 and propidium iodide, PI) in each well of a 96-well microplate and incubated at room temperature in the dark for 15 min. The fluorescence intensity of the stained bacterial suspensions (F_{cell}) was determined at excitation at 488 nm and detection at 635 nm (red) and 530 nm (green), for PI and SYTO 9, respectively. The green/red fluorescence ratios ($R_{G/R}$) were used to compare the bacterial inactivation triggered by AgNPs.

The enzymatic activity of ammonia monooxygenase (AMO) and nitrite oxidoreductase (NOR) were determined according the method proposed by Zheng et al. (2011). Briefly, the biofilm samples were washed 3 times with 0.01 M phosphate buffer (pH 7.4) and the re-suspended pellets

were sonicated at 20 kHz and 4 °C for 5 min. The resulting homogenate was centrifuged at 12 000 *g* and 4 °C for 10 min to remove cell debris and the crude extracts in the supernatant were obtained for the measurement of enzyme activity. The crude extract (100 μL) was mixed with 1.9 mL of 0.01 M phosphate buffer containing 2 mM $(NH_4)_2SO_4$ (pH 7.4) and 0.01 M phosphate buffer containing 1 mM $NaNO_2$ (pH 7.4) for AMO and NOR assays, respectively. The vials were then incubated in a water bath at 30 ^oC for 30 min and then centrifuged immediately, followed by measuring the produced nitrite in the AMO activity assay or the reduced nitrite in NOR activity assay in supernatant (Ensign et al., 1993; Meincke et al., 1992). Key enzyme activities were based on the protein content as determined by the bicinchoninic acid (BAC) method (Pierce© BCA Protein Assay Kit, Thermo Scientific, USA) with bovine serum albumin (BSA) as the standard as described by Chacana et al. (2017). The specific activities of AMO or NOR were presented as the produced μmol NO_2-N mg protein^{-1} min^{-1} or the reduced μmol NO_2-N mg protein^{-1} min^{-1}.

Dichlorodihydrofluorescein diacetate (H_2DCF-DA, Molecular Probes, Invitrogen) was used as a cell-permeant detector for the intracellular ROS hydroxyl, peroxyl and other reactive oxygen species in cells, as an indicator of oxidative stress (Mu and Chen, 2011). The biofilm suspension was washed three times with a phosphate buffer (0.01 M, pH 7.5)**.** The pellets were re-suspended in 0.01 M phosphate buffer containing 50 μM H_2DCF-DA. The resulting mixture was incubated at 21 ± 1 °C in the dark for 30 min. The phosphate buffer containing H_2DCF-DA was removed by centrifugation and then suspended in a phosphate buffer. The biofilm suspension was transferred into 96-well plates (Molecular Devices, San Jose, CA) and the generated fluorescent fluorescein dichlorofluorescein (DCF) was measured at excitation/emission wavelengths of 495/525 nm. A standard curve was generated with hydrogen peroxide to ensure the performance of the instrument. Control wells included Ag-NPs with (H_2-DCFDA) to consider any quenching effects on the dye fluorescence emission.

6.2.4 DNA Extraction, sequencing and microbial community analysis

Biofilm samples were collected from all three MBBRs at 6 distinct sampling times, including the midpoint of the Acclimation phase (day 150), beginning and end points of the control period (days 232 and 292), in the middle (day 323) and end of Ag Exposure period (day 353) and end of

Recovery period (day 388). For each set of the microbial community data, 5 carriers were selected randomly from each reactor. The retained biofilm was homogenized and immediately stored at −20 °C until DNA extraction. DNA was extracted in duplicate for each sample. Genomic DNA was extracted from the biofilm samples using the DNeasy PowerSoil Kit (QIAGEN, Toronto, Ontario) following the manufacturer's instructions. The 16S rRNA genes were amplified using previously described primers 515F and 806R (Apprill et al., 2015; Parada et al., 2016) and barcoded for library construction (Table 6.3). The pooled library was sent for sequencing on the Illumina Miseq PE250 platform at McGill University and Génome Québec Innovation Centre (Montréal, Québec). Bioinformatics analysis was performed using Qiime2 (Caporaso et al., 2010) pipelines. The de-multiplexed forward and reverse sequences were paired, quality-filtered and chimera removed using DADA2 (Callahan et al., 2016) in Qiime2. Taxonomy was assigned using 99% clustering for the operational taxonomic unit (OTU) with references in the Silva (version 132) database (Quast et al., 2013). Alpha-diversity and beta-diversity were analyzed using R "vegan" package (Oksanen et al., 2017). Principal coordinates analysis (PCoA) was constructed using the Bray-Curtis distance matrix. The significance level of community distance was tested using permutational multivariate analysis of variance, using the function Adonis from the R "vegan" package. The statistical significance of differences between treatments ($p < 0.05$), before and after exposure to AgNPs, was evaluated with one-way repeated measures ANOVA using Statistica version 12 (StatSoft Inc., Palo Alto, CA).

Table 6.3 : PCR primers and conditions for Illumina sequencing.

	Primer Pair (5'-3') [a]	Conditions[b]	Cycle no.
Illumina PCR1	515F (47 nt) CTT TCC CTA CAC GAC GCT CTT CCG ATC TGT GYC AGC MGC CGC GGT AA 806R (54 nt) GTG ACT GGA GTT CAG ACG TGT GCT CTT CCG ATC TGG ACT ACN VGG GTW TCT AAT	Initial denaturation: 94 °C, 3 min Denaturation: 94 °C, 30 s Annealing: 62 °C, 45 s Elongation: 72 °C, 1 min Final elongation: 72 °C, 10 min	25
Barcode PCR2	Uniprimer1 (45 nt) AAT GAT ACG GCG ACC ACC GAG ATC TAC ACT CTT TCC CTA CAC GAC Uniprimer2 (45 nt) CAA GCA GAA GAC GGC ATA CGA GAT-variable index (8 nt)-GTG ACT GGA GTT C	Initial denaturation: 94 °C, 3 min Denaturation: 94 °C, 30 s Annealing: 59 °C, 20 s Elongation: 72 °C, 45 s Final elongation: 72 °C, 5 min	15

[a]Primers from IDT, Coralville, IA
[b]Reagents from New England Biolabs Ltd, Whitby, ON: Taq DNA polymerase with standard Taq buffer, deoxynucleotide (dNTP) solution mix.

6.3 Results and discussion

6.3.1 Fate of AgNPs in MBBRs in Exposure and Recovery periods

The influent of $MBBR_2$ and $MBBR_3$ contained an average concentration of 9.6 ± 2.4 μg/L AgNP ([$AgNP_{inf}$]) and 91 ± 19 μg/L $AgNP_{inf}$, with mean diameter (d_{mean})) of 41 ± 2 nm and 40 ± 2 nm, respectively (Figure C.1), corresponding to a total Ag concentrations ([Ag_{inf}]) of 15 ± 2 Ag and 121 ± 9 μg/L Ag in $MBBR_2$ and $MBBR_3$, respectively (Figure 6.1A, B). SpICP-MS analyses showed about 17% variation in dissolved Ag concentrations ([dissolved Ag_{inf}]), in the influent NP stock solutions of both reactors over time (Figure C.1). Ag retention efficiency was determined using the total silver concentration in the influent and effluent of MBBRs (Figure 6.1). Ag concentration profiles in both MBBRs consisted of two phases over the 60-day Ag loading (Figure 6.1A, B). In Phase I, an average Ag retention efficiency of 70% ± 9% to 74% ± 8% was observed in $MBBR_2$ and $MBBR_3$ respectively, over the first 11 to 15 days of AgNP loading (Figure 6.1A,B). The effluent Ag concentrations in $MBBR_2$ (4.8 ± 1.6 μg/L Ag_{eff}) and $MBBR_3$ (34.1 ± 6.1 μg/L Ag_{eff}) were mainly comprised of nanoparticles ($AgNP_{eff}$) at an

average concentration of 3.3 ± 1.1 μg/L (70% [Ag_{eff}]) and 23.8 ± 6.3 μg/L (62% [Ag_{eff}]), respectively. SpICP-MS analyses showed variations in dissolved Ag concenrtation in the effluent supernatant of $MBBR_2$ (0.2 to 2.4 μg/L) and $MBBR_3$ (2.1 to 8.2 μg/L) representing about 6% to 35% of effluent Ag concentration in this period (Figure 6.1B, C).

In Phase II, the evolutions in the Ag distributions of $MBBR_2$ and $MBBR_3$ were different. In $MBBR_2$, two Ag release events were observed on days 307 and 353 with the effluent AgNP concentrations (26.1 ± 0.1 μg/L to 29.4 ± 0.3 μg/L) constituting 74% to 96% of effluent total Ag detected (Figure 6.1A, C). The Ag retention efficiency varied about 28% to 41% between the two release events with a higher effluent Ag concentration release (10.4 to 15.8 μg/L Ag) predominantly in the form of AgNPs (4.5 to 8.9 μg/L, 66% to 85% of [Ag_{eff}]). The observed pattern was likely due to saturation of the outer layers of the biofilm by AgNPs. A relatively smaller mass fraction of effluent Ag concentrations was accounted for the dissolved Ag_{eff} (5% to 15%) between the two releases (day 310 to 346) (Figure 6.1C). The relatively high fraction of effluent dissolved Ag relative to effluent total Ag concentrations (51%), observed on day 329, with no significant change in particle mean diameters in the effluent, is likely due to the detachment and release of soluble complexes of Ag from the biofilm/EPS matrix.

In $MBBR_3$, over the second phase, total Ag concentration gradually increased in the effluent, reaching a maximum of 184 ± 3 μg/L Ag in 11 days (day 310 to 321), decreasing the Ag retention efficiency, due to the significant detachment of the biofilm, in contrast to the observed pattern in $MBBR_2$ during the same time period (Figure 6.1B). Ag release and retention recovery events were observed subsequently (day 321 to 353). Significantly higher concentrations of Ag (81 ± 1 to 172 ± 8 μg/L Ag) was released via effluent between day 329 to day 353, with the effluent AgNP concentrations (28.5 ± 2.1 to 69 ± 3 μg/L) constituting 19% to 40% of detected effluent Ag concentration (Figure 6.1B, C). A major fraction of the released total silver ([Ag_{eff}]) (40% to 71%) was associated with total suspended solids in effluent (TSS_{eff}) in $MBBR_3$ (49 to 117 μg/L Ag) in this interval, due to the detachment of the biofilm, sloughing off from the surface of the carriers. The reactor did not retain any Ag by day 353.

In the Recovery phase (day 353-388), the Ag_{eff} concentration decreased over the first 20 days and stabilized afterward at 7.8 ± 1.3 μg/L Ag and 20.3 ± 3.3 μg/L Ag, in $MBBR_2$ and $MBBR_3$ respectively, by day 388. Based on spICP-MS data, $AgNP_{eff}$, concentrations in $MBBR_2$ (0.51 to 0.95 μg/L) and $MBBR_3$ (1.3 to 1.7 μg/L) with mean diameter between 28 and 31 nm and their corresponding dissolved concentrations, 1.1 to 4.2 and 2.2 to 5.2 μg/L, in the effluent supernatant of both reactors represented about 7% to 9% and 20% to 32% of effluent Ag concentrations in this period (Figure 6.1A, B). The released total silver ($[Ag_{eff}]$) (57% to 72%) was mainly associated with effluent solids during this period.

The attached biofilm ($Ag_{carrier}$) retained about 1.6 and 21.5 mg Ag/m^2 of carrier active surface in $MBBR_2$ and $MBBR_3$ (Figure 6.1D, E) corresponding to 63% to 73% of cumulative mass of total Ag loading in the influent ($M_{Ag_{inf}}$) during phase I, indicating an initial high Ag biofilm retention capacity. The cumulative mass balance, however, suggested that a significant fraction of cumulative $M_{Ag_{inf}}$ (> 89%) was released via the effluent MBBRs by day 353. Similar limited retention capacity of wastewater biofilm for NPs over long-term exposure and release of NPs by detachment of NP-rich biofilms were reported (Alizadeh et al., 2019; Herrling et al., 2016; Walden and Zhang, 2018).

The decrease in dissolved Ag_{eff} concentration in both MBBRs over time is likely due to the complexation of the Ag^+ ions released from the oxidative dissolution of PVP-AgNPs with influent chloride (3.98 mM) and the association of the dissolved Ag with reduced sulfur moieties of organic ligands, mainly thiol (SH^-) in biofilm EPS (e.g. cysteine and methionine), forming chloro-silver complexes, Ag_2S NPs or core-shell Ag-Ag_2S NP, respectively (Zhang et al., 2018). Similar complexation of dissolved silver in wastewater effluents and their significantly reduced bioavailability were reported in a 7 day experiment (Azimzada et al., 2017). The reformation of the secondary NPs may also be attributed to the decrease in dissolved Ag concentrations in the effluent samples (Azodi et al., 2016; Meier et al., 2016). Similarly, secondary particles (Ag_2S, AgCl) were detected in the effluent of all MBBRs using TEM-EDS analysis (Figure C. 2).

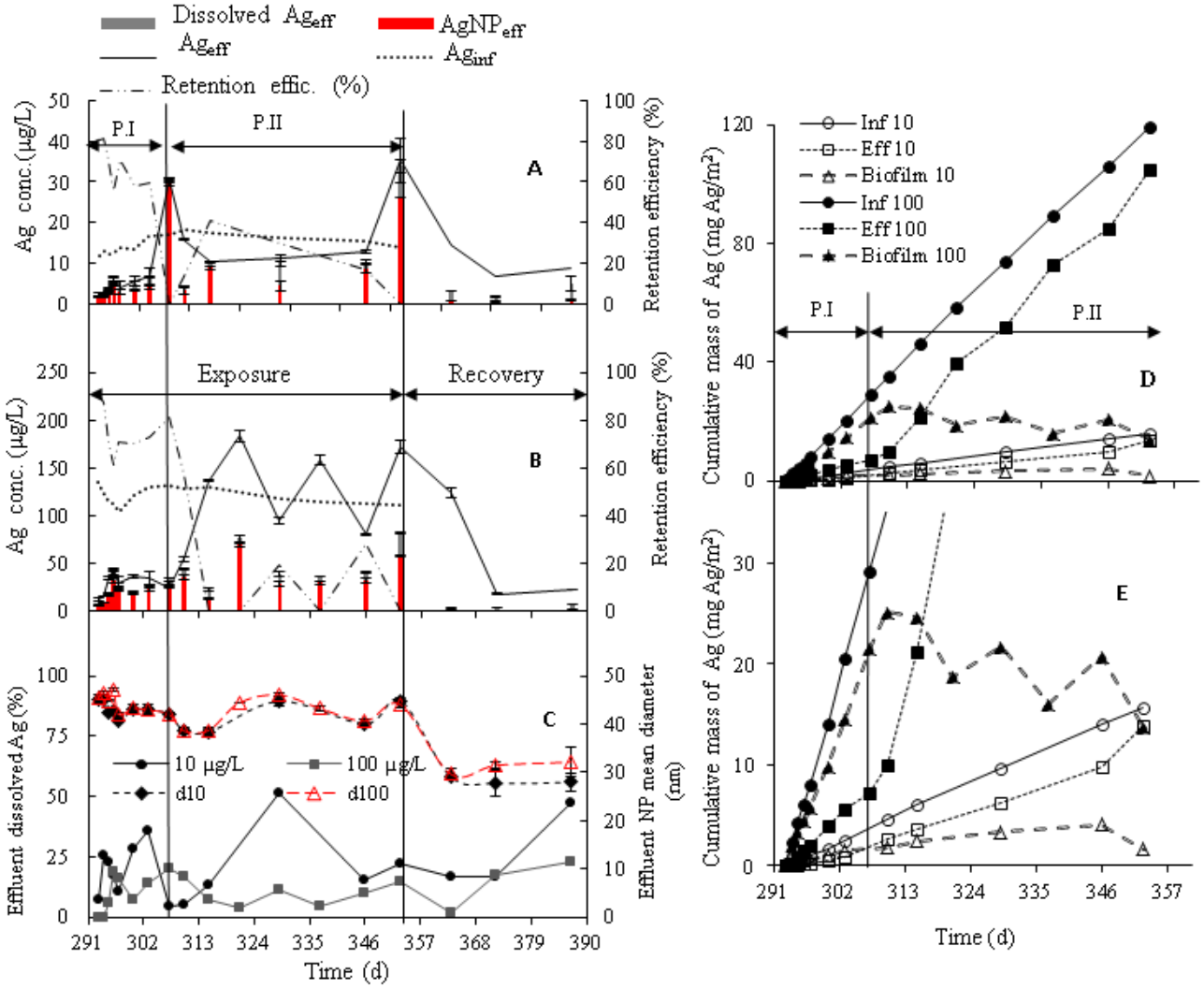

Figure 6.1: Fate and retention of Ag in MBBR receiving nominal AgNP influent concentration of (A) 10 μg/L ($MBBR_2$) and (B) 100 μg/L AgNPs ($MBBR_3$); (C) $AgNP_{eff}$ mean diameter and dissolution of $AgNP_{eff}$ (%); (D) cumulative Ag mass distribution in influent (Inf), effluent (Eff) and attached biofilm (Biofilm), (E) enlarged Y-scale of panel D. Note: P.I-II refers to two observed phases in Ag distribution profile.

6.3.2 Effects of AgNPs on the biological performance of a nitrifying aerobic biofilm

Biofilm-mediated nitrification activity was determined in the MBBRs in response to the 60-day continuous exposure to 15 ± 2 and 121 ± 9 μg/L Ag_{inf} and a 35-day post-Exposure Recovery

period (Figure 6.2). Prior to AgNP injection, each MBBR was monitored for 60 days (day 232 to 292) under quasi steady state conditions as a control period. The specific NH_4 removal rate stabilized at 1.15 ± 0.06, 1.17 ± 0.03 and 1.18 ± 0.03 g NH_4-N $m^{-2}\,d^{-1}$ (Figure 6.2A-C), corresponding to a NH_4 removal efficiency of 95 ± 1.6%, 95 ± 1.1% and 95 ± 0.7 % in $MBBR_1$, $MBBR_2$ and $MBBR_3$, respectively, over the control period (Figure 6.2D). The nitrifying biofilm was constituted of an average of 97.5% ± 0.5% viable biofilm during this period (Figure 6.3 A). The MBBR effluents contained about 0.4 ± 0.1 mg NO_2-N/L with less than 10% mass balance error for removed NH_4-N and produced NO_2-N and NO_3-N over the control period (Figure 6.2), which is consistent with previous studies (Hoang et al., 2014; Young et al., 2016; Young et al., 2017).

$MBBR_1$ (control) maintained a stable NH_4 removal efficiency of 94% ± 1% over both the Exposure and Recovery periods. In $MBBR_2$ (15 μg/L Ag_{inf}) and $MBBR_3$ (121 μg/L Ag_{inf}), after the addition of AgNP, a first unperturbed phase of 47 days (day 293-340) and 33 days (day 293-326) was observed, respectively, with an average NH_4 removal efficiency of 95 ± 2% (Figure 6.2D) and a relatively stable biofilm viability (> 95%; Figure 6.3 A) in both MBBRs which was comparable to the control MBBR. A second phase was observed afterwards with significant inhibition of the biological activity of nitrifying biofilm with an increase of Ag concertation in both MBBRs. The NH_4 removal efficiency decreased significantly ($p < 0.05$) down to 81% over 13 days in $MBBR_2$ and down to 64% after 27 days in $MBBR_3$ (Figure 6.2D) over 60 days. Similarly, a significant inhibition of viable attached biofilm (10% to 25%) was observed in $MBBR_2$ and $MBBR_3$ by day 353 (Figure 6.4 A). The increase in effluent TSS concentration in both MBBRs indicated a significant detachment of the biofilm (Figure 6.2E).

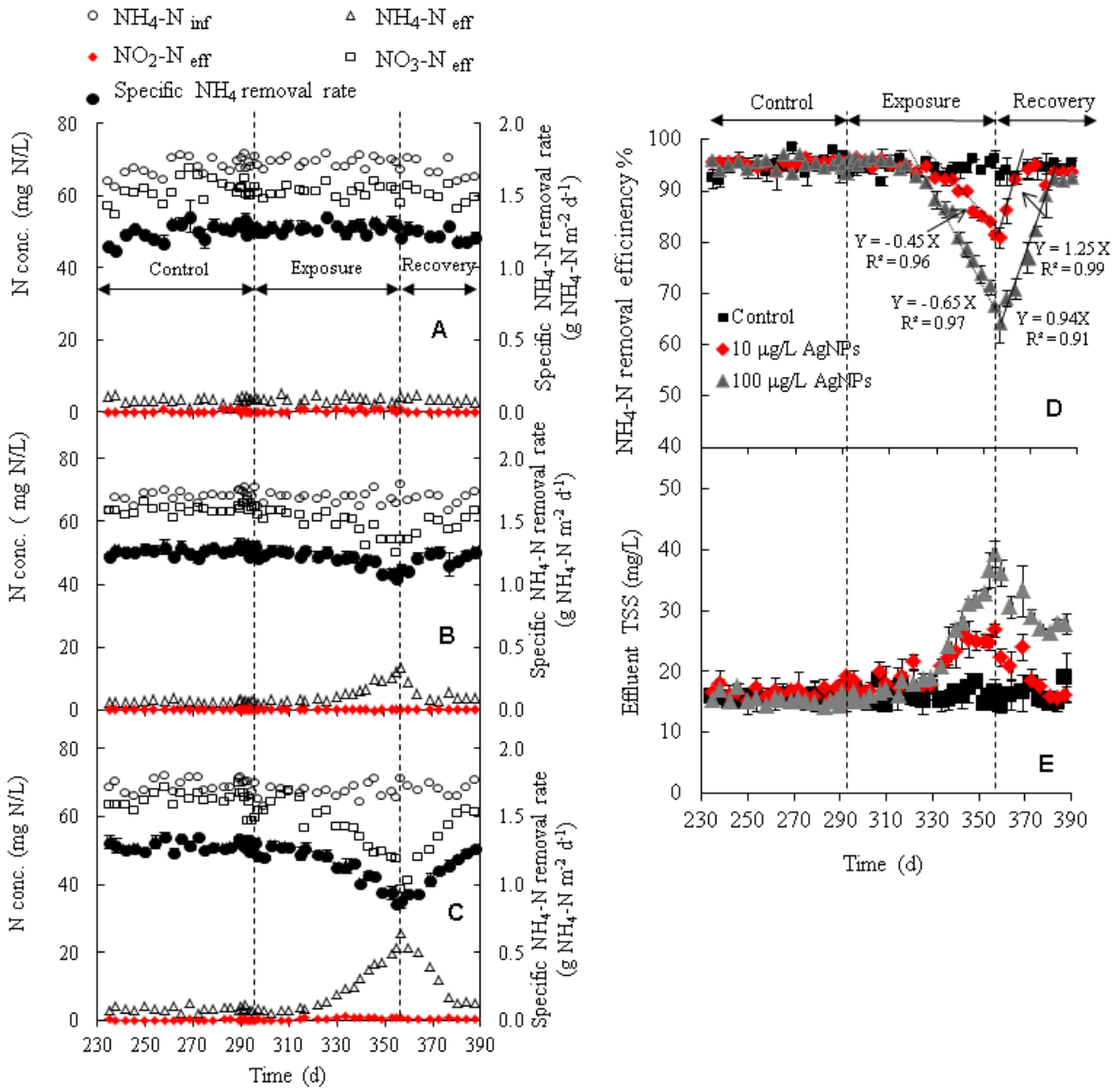

Figure 6.2 : Effect of PVP-AgNPs on nitrifying MBBR performance at (A) control, (B) 10 μg/L AgNPs, (C) 100 μg/L AgNP and (D) ammonia removal efficiency; (E) effect of AgNP addition on MBBR TSS_{eff} (error bars are only shown when larger than symbol size).

The effluent NO_2 concentration, over the AgNPs Exposure period (0.4 to 1.1 μg/L NO_2-N/L), was comparable to the control period in all MBBRs with no statistical difference between each unit (Figure 6.2A-C). The effluent NO_3 concentration, however, was gradually reduced with a

simultaneous increase of AgNP concentration in the second phase in Ag-treated MBBRs (Figure C.1). The concentration of NO_3 in $MBBR_2$ and $MBBR_3$ was lower than in the control reactor ($p < 0.05$), indicating an inhibition of ammonia oxidation by AOB, rather than a nitrite transformation by NOBs. The observed higher sensitivity of AOBs to AgNPs, than to NOBs is consistent with results from previous studies indicating a higher sensitivity of AgNPs, TiO_2 and CeO_2 to AOBs than NOBs (Alito and Gunsch, 2014; Jeong et al., 2012; Sheng et al., 2015; Wang et al., 2018; Xu et al., 2017b; Yang et al., 2014a; Zheng et al., 2011). The AgNP continuous inflow was ceased after 60 days and the recovery capacity of the AgNP-impaired nitrifying biofilms was assessed over a 35-day post-Exposure Recovery period. $MBBR_2$ recovered to a steady state NH_4 removal efficiency of 94% ± 2% with more than 95 ± 2% viable biofilm after 7 d. Nitrifying biofilm, exposed to higher AgNP influent concentration in $MBBR_3$, however, recovered only after 24 days in terms of NH_4 removal efficiency (92 ± 1%) and biofilm viability (89 ± 1%).

The observed long-term concentration-dependent inhibitory effect of AgNPs on nitrification at both influent AgNP concentrations (15 and 121 μg/L Ag) in nitrifying MBBRs is in contrast with recent studies. Nitrification inhibition of pure culture (e.g. *Nitrosomonas europaea*) and enriched nitrifying bacteria isolated from wastewater treatment plants, are reported upon short exposure (1 to 24 h) to 100 μg/L to 1000 μg/L of various types of AgNPs (Arnaout and Gunsch, 2012; Choi and Hu, 2009; Choi and Hu, 2008; Radniecki et al., 2011). The extent of reported nitrification inhibition by AgNPs, however, are not consistent between lab-scale studies. The inhibitory effects of AgNPs on nitrification of activated sludge was reported in a Modified Ludzack–Ettinger activated sludge system after a 12-h period of AgNP shock loading at 750 μg/L AgNPs (Liang et al., 2010). No adverse effect of AgNPs, however, were reported on nitrification and bacterial activities of activated sludge over 15 to 65 days of exposure to 100 to 500 μg/L AgNPs in sequencing batch reactor (SBR) or membrane bioreactor processes (Chen et al., 2014; Hou et al., 2012; Zhang et al., 2014; Zhang et al., 2016). A temporary decrease in nitrification efficiency was observed in SBRs receiving pulse or continuous loading of 200 μg/L AgNPs but the functional biological activities recovered in 24 h (Alito and Gunsch, 2014). These contradictory results are likely due to differences between AgNP characteristics (e.g. size and coating), biomass physical structure, surface properties, microbial population dynamics, functional stability and reactor configurations used under distinct experimental conditions.

Higher biomass concentrations (with a larger specific surface area) in smaller reactor volumes and a relatively high SRT to HRT ratio in attached growth (e.g. MBBR) versus suspended growth processes (e.g. activated sludge), enhance the accumulation and associated mass transport of AgNPs into deeper layers of the biofilm over time, leading to greater toxicity (Barker et al., 2018; Binh et al., 2016).

6.3.3 Key microbial enzymatic activity and toxicity impact after long-term exposure

Two metabolic enzymes of AMO and NOR play critical roles in catalyzing nitrification. Thus, the inhibitory effect of AgNPs on the specific activity of these two enzymes and their post-Exposure recoverability were assessed at both $AgNP_{inf}$ concentrations (Figure 6.4). During the Control period, the specific activities of AMO (0.076 ± 0.002 μmol NO_2-N mg protein^{-1} min^{-1}) and NOR (0.16 ± 0.006 μmol NO_2-N mg protein^{-1} min^{-1}) in $MBBR_2$ and $MBBR_3$, respectively, were comparable to the control reactor ($MBBR_1$) over the control period. During the Exposure period, specific AMO activity was inhibited by $12 \pm 2\%$ and $24 \pm 0.9\%$ in $MBBR_2$ and $MBBR_3$, respectively, after 60 days of AgNP addition, consistently with an observed decrease in effluent NO_3 and reduction in NH_4 removal efficiency in corresponding MBBRs. At the end of the Recovery period, the nitrifying biofilm in AgNP-treated MBBRs had recovered their AMO enzymatic activity.

Nitrification inhibition (25%) is reported after exposure to 500 μg/L of 30 nm AgNPs for 12 hours where the expression of the active and catalytic subunits of the ammonia monooxygenase genes (*amoA* and *amoB*) were significantly down regulated, resulting in AMO activity inhibition (Zheng et al., 2017b). Ag^+ and AgNPs can inhibit the AMO enzyme by replacing the redox active Cu/Fe core of the enzyme and the association of Ag^+ with cysteine containing residues within the AMO enzyme (Barker et al., 2018; Radniecki et al., 2011). The NOR specific activity, in both Ag-treated MBBRs (0.158 ± 0.002 μmol NO_2-N mg protein^{-1} min^{-1}) showed no significant differences from the control (0.159 ± 0.004 μmol NO_2-N mg protein^{-1} min^{-1}) after 60 days of exposure (Figure 6.4), which was consistent with the reported absence of inhibitory effect of AgNPs, CeO_2 NPs and CuO NPs on NOR activity of aerobic granular sludge and biofilm (Hou et al., 2015; Quan et al., 2015; Zheng et al., 2017a).

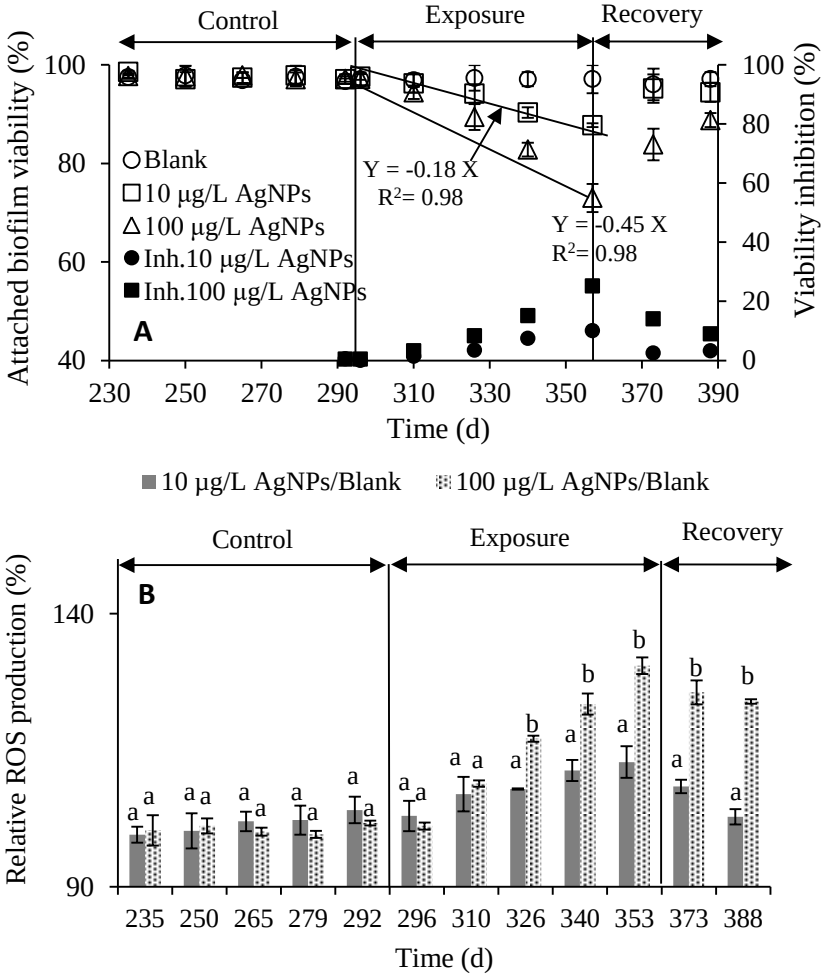

Figure 6.3: Long-term effect of PVP-AgNPs addition on (A) viability and (B) relative intracellular ROS generation of attached biofilm. Different superscript letters represent significant difference ($p < 0.05$) (error bars are only shown when larger than symbol size).

ROS is an important indicator of oxidative stress and has commonly been used to reveal the possible toxicological mechanisms of NPs to activated sludge and biofilm (Grün et al., 2018; Quan et al., 2015; Walden and Zhang, 2018; Wang et al., 2018; Zhang et al., 2016c; Zheng et al., 2017a). The H_2DCF-DA assay was used to detect the AgNP and/or Ag^+-mediated generation of intracellular ROS in nitrifying biofilm over the Exposure and Recovery periods (Figure 6.3 B).

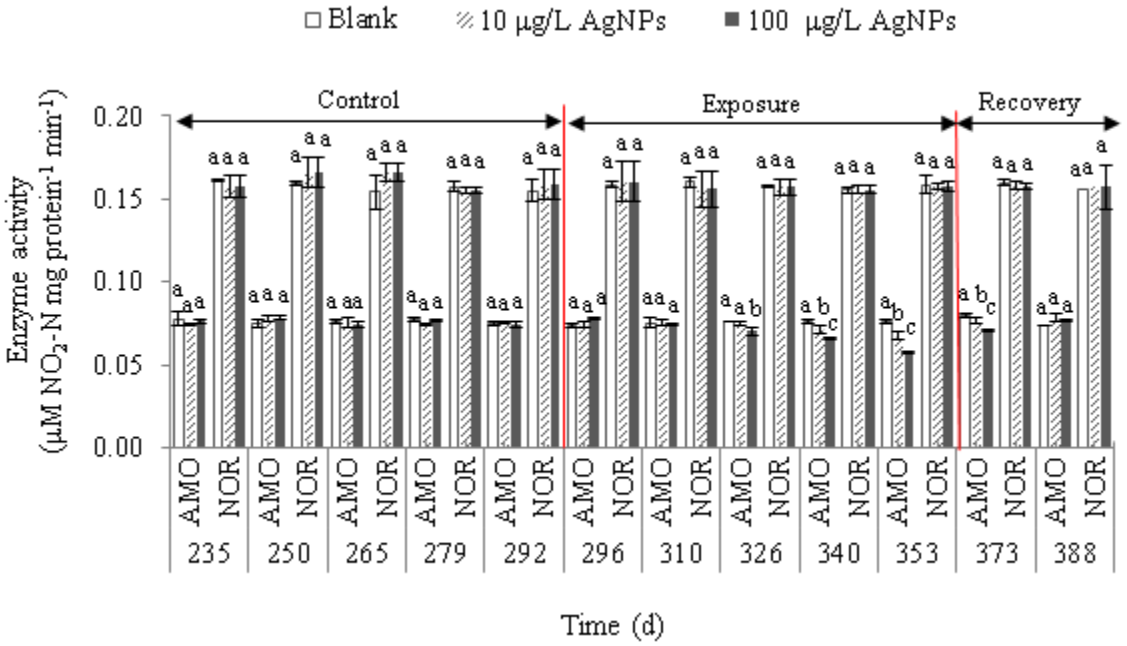

Figure 6.4: Long-term effect of PVP-AgNPs of on specific activity of ammonia monooxygenase (AMO) nitrite oxidoreductase (NOR). Different superscript letters represent significant difference ($p < 0.05$).

Intracellular ROS increased to 114 ± 0.97% and 130 ± 2% in $MBBR_2$ and $MBBR_3$, respectively, compared with the control (Figure 6.3 B). This is consistent with reported concentration-dependent ROS production in aerobic granular sludge and biofilm (Gu et al., 2014; Quan et al., 2015; Walden and Zhang, 2018). Significant ROS generation is reported for wastewater biofilm after 3 h exposure to 50 μg/L AgNPs (Walden and Zhang, 2018). Similarly, AgNP-induced ROS generation and subsequent oxidative damage is reported for nitrifying cells after 12 h exposure to 500 μg/L AgNPs with an observed up-regulation of transcripts encoding superoxide dismutase, peroxiredoxin, thiol peroxidase and cytochrome c peroxidase, involved in the detection and defence of the cell from oxidative damage (Zheng et al., 2017b). The nitrifying biofilm in $MBBR_2$ was able to regulate the oxidative stress over the first 15 days of the Recovery period (relative ROS production of 105 ± 1%). In $MBBR_3$, however, a relatively high relative ROS production (124 ± 0.5%) was still detected by the end of the Recovery period (Figure 6.3B).

6.3.4 Responses of nitrifying biofilm bacterial community to long-term AgNP exposure

Six major phyla *(Proteobacteria*, *Bacteroidetes*, *Nitrispirae*, *Chloroflexi*, *Planctomycetes*, *Acidobacteria*) were identified (relative abundance > 1%) over the six sampling points taken during the Acclimation, Control, Exposure and Recovery periods, in the control ($MBBR_1$) and AgNP-treated reactors ($MBBR_2$, $MBBR_3$) (Figure 6.5A), as previously reported in other studies on the microbial composition of wastewater nitrifying biofilm (Hoang et al., 2014; Young et al., 2016). The majority of sequences (40 to 70%) in all samples corresponded to the *Proteobacteria* phylum, mainly comprised of *Alphaproteobacteria* and *Gammaproteobacteria*. The nitrifying bacteria in biofilms belonged to *Nitrosomonadaceae* (AOB*, Proteobacteria) and Nitrospiraceae (*NOB*, Nitrospirae).* Various heterotrophic bacteria from the *Proteobacteria*, *Bacteroidetes*, *Chloroflexi* and *Acidobacteria* phyla were also detected in the three MBBRs in accordance with previous nitrifying biofilm systems treating wastewater (Abzazou et al., 2016; Young et al., 2016; Young et al., 2017). Species of the *Proteobacteria* phylum, contribute to the formation of initial dense biofilm layers close to the surface of the substratum, providing a growth matrix for nitrifiers (Hoang et al., 2014; Wagner and Loy, 2002). *Bacteroidetes* are known for consuming the EPS and by-products excreted by nitrifying bacteria (Ramirez-Vargas et al., 2015).

Nitrospirae, the phylum of major NOBs, was identified as the second major bacterial phylum (27% ± 2%) in the young biofilm over the Acclimation phase; however, the mature biofilm in the control phase consisted of lower abundance of *Nitrospirae* (8 to13%) (third major phylum), after *Bacteroidetes* (Figure 6.5A). Similar distribution of *Nitrospirae* in nitrifying MBBRs was reported previously over long-term operations (Hoang et al., 2014). *Nitrospirae* demonstrated higher abundancy (23 to 45%) by the end of the Recovery period, probably due to formation of new biofilm after major Ag-induced biofilm detachment and sloughing off. The control MBBR underwent a major shift in composition in parallel to Ag-treated MBBRs, consistent with a similar observed shift in control nitrifying SBR over long-term operations (Gwin et al., 2018; Ma et al., 2015). Changes in microbial composition likely help to stabilize and maintain the biofilm matrix (Flynn et al., 2016).

The principal coordinate analysis (PCoA) based on the Bray–Curtis distance matrix 50.6% of total variance on PCoA1 axis and 15.8% variance on PCoA3 indicated that the operational time (ADONIS R^2 = 0.82, p = 0.001) and AgNP addition (R^2 = 0.07, p = 0.001), respectively, influenced the biofilm microbial communality compositions in all MBBRs (Figure 6.5B). Although this analysis does not identify the OTUs responsible for community separation, it does indicate that the microbial ecology is affected by these factors (Young et al., 2017). The time and Ag stress are similarly reported as the major factors shaping the microbial community of activated sludge over long term exposure of AgNPs in SBRs (Sheng et al., 2018). Similarly, the higher impact of operational time on the variation of the initial microbial community structures across experiments is reported more than the AgNP-induced variation in nitrifying SBRs (Ma et al., 2015). The observed pattern at the phyla level (Figure 6.5A), indicated various responses among taxa, including a range from susceptibility towards silver (*e.g. Bacteroidetes* and *Chloroflexi)* to tolerance against this metal (*e.g. Proteopacteria),* as reported in previous studies (Grün et al., 2018; Gwin et al., 2018; Ma et al., 2015). *Chloroflexi* can participate in carbon oxidation and nitrification and their high sensitivity to AgNPs is related to the absence of a lipid outer membrane (Sutcliffe, 2011; Yang et al., 2014b). $MBBR_3$, receiving 121 μg/L Ag_{inf}, consisted of a significantly lower number of genera with smaller alpha diversity indices by the end of the Exposure period, as compared to other MBBRs (Table C.2). The Ag-induced detachment of biofilm and the decrease in biofilm thickness can have a profound effect on the biodiversity of biofilm, including both microbial richness and evenness. The high correlation of biofilm thickness with bacterial community diversity and evenness was previously reported in MBBR systems (Torresi et al., 2016). At the genus level in AOB and NOB communities, *Nitrosomonas* (*Proteobacteria* phylum) and *Nitrospira* (*Nitrospirae* phylum) were identified as the main AOB and NOB genera, respectively (Figure 6.6A). *Nitrosomonas* dominantly related to an unclassified *Nitrosomonas, Nitrosomonas sp*. Nm 84 and *Nitrosomonas sp*. AL212 (Figure $6.6B_1$) *Nitrospsira sp. was identified as the dominant species for the Nitrospira* genus (Figure $6.6B_2$). Long-term exposure to both [$AgNP_{inf}$] did not significantly impact the absolute abundance of AOB and NOB genera (Figure 6.6A), but their affiliated species demonstrated distinct susceptibility towards AgNPs (Figure 6.6B).

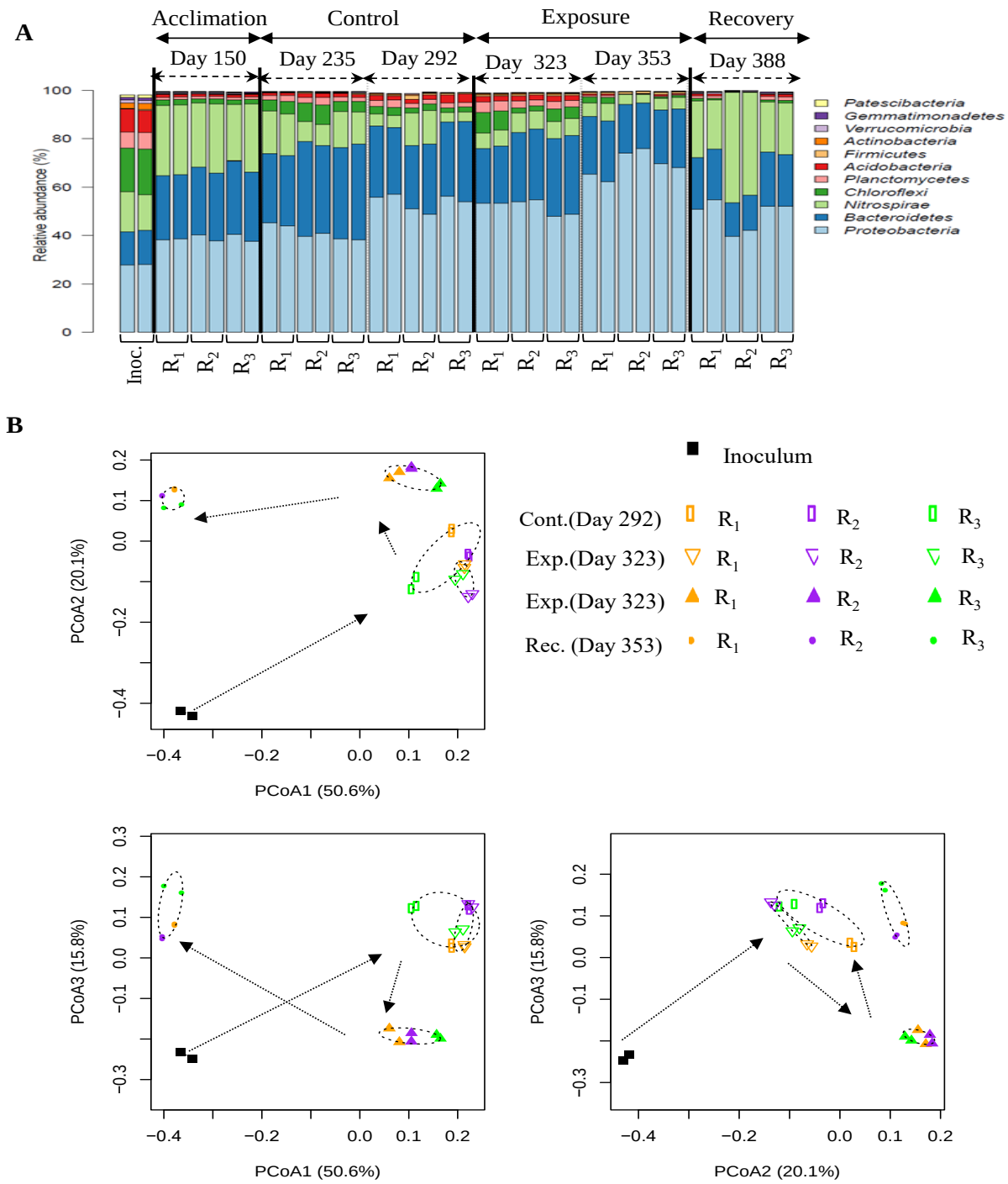

Figure 6.5: (A) Bacterial community composition of nitrifying $MBBR_1$ (R_1), $MBBR_2$ (R_2) and $MBBR_3$ (R_3) at different stages of operations (Acclimation, Control, AgNP Exposure, Recovery) at phylum level; (B) Principal coordinate's analysis (PCoA) based on Bray–Curtis distance in control (R_1) and Ag-treated reactors ($R_{2,3}$) in Control, Exposure and Recovery phases.

Contrary to the decrease in relative abundance of unclassified *Nitrosomonas*, *Nitrosomonas sp*. Nm 84 and *Nitrosomonas sp*. AL212 were significantly more abundant in both Ag-treated MBBRs at the end of the Exposure period (Figure 6.6B_1). *Nitrosomonas sp*. Nm 84 is related closely to *Nitrosomonas oligotropha* lineage (97%) and is involved in the production of significant amounts of EPS, especially under stress conditions (Stehr et al., 1995). Metaproteomic studies indicated that certain genes of *Nitrosomonas sp.* AL212 are involved in transcripts encoding of proteins involved in oxidative stress regulation (*e.g.* superoxide dismutase) and EPS protein synthesis (Purkhold et al., 2003; Sun et al., 2018). Therefore, the higher abundance of these species is likely correlated to the defence mechanisms of nitrifying biofilm by producing higher EPS and the superoxide dismutase enzyme to regulate oxidative stress. Similarly, the secretion of more EPS by bacteria is reported as a mechanism of defense in aerobic granular sludge upon AgNP exposure (Quan et al., 2015; Zhou and Xu, 2019). Different susceptibilities of *Nitrosomonas* and *Nitrospira* species, including both silver-sensitive and silver-tolerant species are reported, suggesting the broad diversity of biofilm bacterial responses to environmental stresses which preclude generalizations about the potential impacts of AgNPs on a given phenotype (e.g. AOB; Yang et al., 2014a). A minor decrease in relative abundance of *Nitrospira sp*. was observed in Ag-treated nitrifying biofilm. The relative abundance of NOB in both $MBBR_2$ and $MBBR_3$, however, was comparable with that in the control reactor by the end of the Exposure period.

The observed minimal long-term impact of environmental concentrations of AgNPs on the nitrifiers community structure and their abundance, was consistent with previously reported negligible implications of AgNPs for nitrifying bacterial communities in aerobic granular sludge, biofilm and activated sludge (Gwin et al., 2018; Jeong et al., 2012; Sheng et al., 2018; Yang et al., 2014b; Zhang et al., 2016c). The distribution of AOB and NOB species in the Recovery period were similar to that in the Acclimation period, likely due to the production of young biofilm in the post Ag-stress period. This was consistent with the observed recovery of treatment efficiency and key enzymatic activities in both Ag-treated MBBRs during this period.

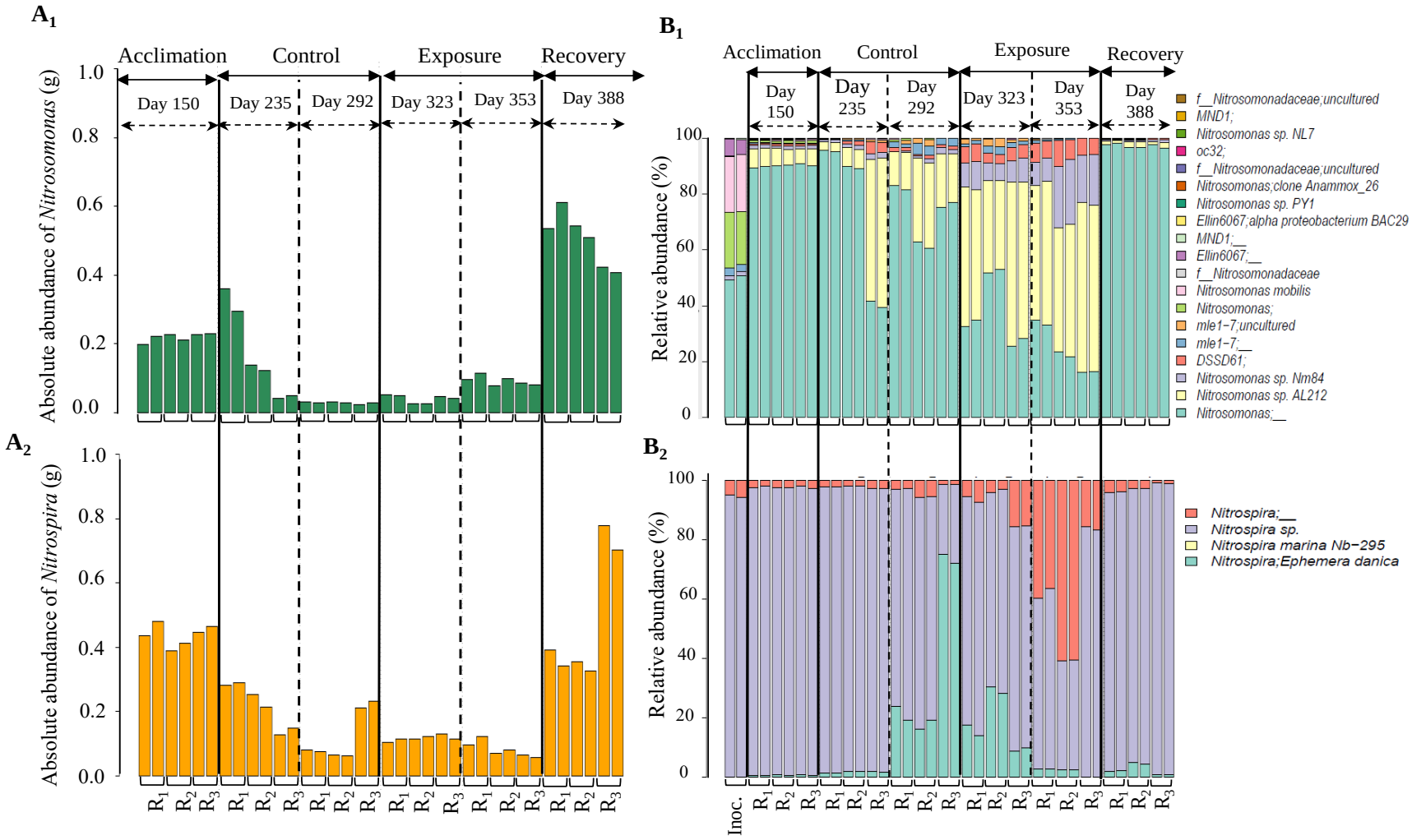

Figure 6.6: Absolute abundance of dominant (A_1) AOB and (A_2) NOB in nitrifying $MBBR_1$ (R_1), $MBBR_2$ (R_2) and $MBBR_3$ (R_3) at different stages of operation (Acclimation, Control, Exposure, Recovery), relative abundance of dominant species, affiliated to (B_1) *Nitrosomonas* and (B_2) *Nitrospira* genera. (Note: The absolute abundance of AOB and NOB are calculated using the DNA yield and biomass concentrations in MBBR at each sampling point.).

Recent studies have uncovered the potential for complete ammonia oxidation (comammox) to nitrate by the newly-identified species within the genus *Nitrospira* rather than by distinct AOB and NOB in biofilm-laden wastewater processes (Annavajhala et al., 2018; Sun et al., 2018). We did not detect any comammox-related species in this study. The next generation sequencing technology used in this study may not provide a high enough resolution to verify if a mix of conventional NOBs and Comammox, bacteria existed in the biofilm of the nitrifying reactors. Considering the minimal effect of AgNPs on taxa involved in nitrification, the higher sensitivity of other taxa likely contributed to the observed shift in the community composition as the members of the biofilm bacterial community are highly interactive. This is consistent with similar observed impact of AgNPs on the microbial composition of nitrifying sludge (Gwin et al., 2018).

6.4 Conclusion

Nitrifying MBBRs have demonstrated great potential as a cost-effective and compact technology to achieve nitrification even in cold climates but the effects and biological implications of ENPs are poorly understood in such attached-growth processes. The long-term continuous impact of AgNPs was evaluated for the first time at environmental concentrations (15 and 121 μg/L Ag) on the biological performance and microbial communities of nitrifying MBBRs and their post Ag-stress recovery capacity. NH_4-N removal efficiency was significantly affected with suppressed biofilm viability at both influent concentrations at 15 μg/L and 121 μg/L Ag in 60 days. Specific activities of intracellular AMO enzyme was significantly inhibited (12 to 24%) at both influent AgNP concentrations, with no significant effect on NOR activity. Sixty-day exposure to 121 μg/L Ag induced a significant increase of intracellular ROS concentration in attached biofilm. The attached biofilm in $MBBR_2$ (15 μg/L Ag_{inf}) and $MBBR_3$ (121 μg/L Ag_{inf}) were able to recover their original biological performances between 7 to 24 days in Recovery period. The abundance of AOB and NOB genera did not significantly change by long-term exposure to environmental relevant concentrations of AgNPs, but distinct susceptibility of their affiliated species was observed towards AgNPs. Quantitative AgNP analysis indicated the partial removal of AgNPs through the treatment process, with the risks associated with effluent released nanoparticles and AgNPs-rich biofilm and higher effluent ammonia. Our results imply significant risks posed by long-term exposure of AgNPs in nitrifying biofilm systems.

Acknowledgements

The authors thank the Natural Sciences and Engineering Research Council of Canada (Grant no. STPGP 430659–12), Environment and Climate Change Canada, PerkinElmer, Health Sciences Canada, the Fonds de Recherche du Québec Nature et Technologies (FRQNT), the Canadian Water Network (CWN), SNC Lavalin Environment, the City of Calgary and the City of Saint-Hyacinthe for their financial support. The authors thank Prof. Dominic Frigon for his help with experimental desing for bacterial community characterizations and contribution of analytical equipments and materials. The authors also thanks Mr.Arshath Abdul Rahim of McGill for assistance with spICP-MS analyses and data interpretation and Bing Guo for DNA extraction, bioinformatics analyses and data interpretation, Jean-Philippe Massé, Le Centre de Caractérisation Microscopique des Matériaux of Polytechnique Montreal for TEM/EDS analysis and the Terrebonne/Mascouche WRRF for assistance with wastewater sampling.

CHAPTER 7 GENERAL DISCUSSION

This chapter underlines the main findings from this project with respect to the initial research objectives and hypotheses. The main objective of this project was to determine the fate, transport and long-term impacts of environmental concentrations of AgNPs in attached-growth biological wastewater treatment processes. The specific objectives were to (1) determine the retention and distribution of AgNPs in aerobic biofilm-laden biological wastewater process and (2) determine the long-term impacts of AgNPs on primary biological functions and the microbial community of aerobic heterotrophic wastewater biofilms, achieving organic matter removal and aerobic autotrophic nitrifying wastewater biofilms, achieving ammonia removal. Based on these results and the current literature, the environmental implications of AgNPs in attached-growth biological processes, their long-term impacts on microbial communities of wastewater biofilm and fate of AgNPs in such processes are discussed below. Recommendations are covered as part of the Conclusions and Recommendations (Chapter 8).

7.1 Implications of AgNPs in attached-growth biological processes

Wastewater treatment process configurations govern biomass characteristics, microbial community stability and determine the bioavailability and transformation of AgNPs in the system, and their impact on biological treatment performance and effluent quality. AgNPs can negatively impact treatment processes and microbial composition of suspended growth processes at sufficiently high AgNP doses (>1 mg/L) (Wu et al., 2018; Xu et al., 2017a; Zhang et al., 2016c). Attached-growth biological processes, however, may respond differently to the presence of AgNPs as compared suspended growth processes, due to distinct process configuration with different oxygen demand, sludge retention time (SRT) and hydraulic retention time (HRT), unique structure of biofilm and its different phenotypes and genotypes.

Both mono-species based biofilms and wastewater biofilms are reported to have higher capacity, as compared to suspended-growth biomass, to mitigate the inhibitory effects of AgNPs, primarily due to the presence of extracellular polymeric substances (EPSs) and limited AgNP diffusion in biofilm matrix in simplified biological media over short term exposure conditions (Peulen and Wilkinson, 2011; Sheng and Liu, 2011; Walden and Zhang, 2018). The significantly higher SRT/HRT ratio and higher biomass surface area/volume ratio in biofilm-laden biological

processes, however, can result in a distinct interaction dynamics, bioavailability and biological implication of AgNPs in wastewater biofilm-laden process over long-term exposure scenarios.

Our primary objective was focused on assessing the vulnerability of attached-growth biological wastewater treatment processes, receiving continuous inflow of environmental relevant concentrations of AgNPs (10 to 600 μg/L AgNPs), using a high-rate COD-removal MBBR (HRT of 1 h). Our findings indicated a significant inhibition of soluble COD (S_{COD}) removal efficiency and biofilm viability at 100 μg/L Ag in 18 days and 600 μg/L Ag in 5 days, due to the accumulation of AgNPs in attached biomass and to the loss of active biofilm via detachment.

The long-term impacts of AgNPs were determined in a medium-rate COD removal MBBR (HRT of 3 h) and a nitrifying MBBR (HRT of 3 h), in two sequential experiments at influent AgNP concentrations of 10 and 100 μg/L. AgNPs significantly decreased S_{COD} and ammonia removal efficiencies after 64 days with observed biofilm membrane integrity damage, inhibition of both extracellular and intracellular key enzyme activities, concentration-dependent oxidative stress and a slight shift in microbial community composition. Considering the critical role of nitrification in biological nutrient removal and their reported higher sensitivity to AgNPs as compared to other processes (Arnaout and Gunsch, 2012; Choi and Hu, 2009), the recovery potential of the nitrifying biofilm was evaluated over a 35-day post-exposure recovery period. The ammonia removal efficiency, biofilm viability and key enzymatic activities were recovered in 7 days and 24 days in MBBRs, receiving an influent concentration of 10 and 100 μg/L AgNPs, respectively.

The inhibitory effect of AgNPs on treatment efficiency was highly correlated to the retained mass of total Ag in attached biofilm on the carriers. Higher biomass concentrations (with larger specific surface area) in smaller reactor volumes of MBBRs can enhance the deposition rate and the mass transport of AgNPs to attached biomass, leading to enhanced Ag retention per unit weight of biomass in the reactor. Thus, significant accumulation of AgNPs, over time, can extend the diffusion and associated mass transport of AgNP through the protective biofilm EPS into deeper layers of biofilm. Therefore, an extensive spatial distribution of AgNPs in the biofilm cells can deliver toxic Ag^{+} directly to adherent cells via interfacial dissolution of the surface-bound AgNPs and/or partly via direct uptake, leading to an enhanced time exposure and greater toxicity. Although previous studies suggested no lethal impact of certain nanoparticles (e.g.

CeO_2, TiO_2, CuO and AgNPs) on biofilm systems, our results indicated the adverse effect of PVP-AgNPs on structural and functional response of both heterotrophic and nitrifying biofilms in MBRRs, achieving organic matter and ammonia removal. The observed inhibitory effect of AgNPs in such processes were dependent on a combination of factors including the influent AgNP concentration, total mass loading and the exposure time. Our findings imply significant risks posed by long-term exposure at environmental-relevant concentrations of AgNPs in attached-growth biological processes which can affect the stability of such treatments systems and decrease the likelihood of achieving an effluent quality meeting the standards of the Canada-wide Strategy for the Management of Municipal Wastewater Effluent in terms of COD (< 25 mg/L), TSS (< 25 mg/L) and ammonia TSS (< 1.25 mg N/L), leading to adverse effects on downstream effluent receiving streams.

7.2 Impact of long-term exposure of AgNPs on microbial communities of wastewater biofilm

In addition to reactor configuration, microbial functional redundancy, microbial adaptability, and species-specific susceptibility to AgNPs are three important factors that affect the ecotoxicity of AgNPs. Multilayered structure with abundant EPS, inherent resistance, community-based resilience, and functional redundancy play critical roles in defense mechanisms of biofilm bacteria against NP toxicity (Tang et al., 2018). Biofilm thickness is another key driver for community composition and ecosystem function (Suarez et al., 2019; Torresi et al., 2016). Long-term exposure to influent concentrations of 10 and 100 μg/L AgNPs, resulted in a dose-dependent change in microbial communities' structure in both heterotrophic and nitrifying biofilms with various responses among taxa, including a range from susceptibility towards silver (e.g. *Bacteroidetes* and *Gemmatimonadetes)* to tolerance against silver (e.g. *Planctomycetes* and *Chloroflexi*). The bacterial community composition of heterotrophic biofilm slightly changed due to a decrease of silver-sensitive genera affiliated to three dominant orders in the *Bacteroidetes* phylum (*Sphingobacteriales*, *Flavobacteriales*, *Cytophagales*) known as the core members of microbial communities in WRRFs degrading complex organic materials, resulting in reduced abundance of *Bacteroidetes* and a correlated lower COD removal efficiency in MBBRs. The

richness and diversity of the bacterial community of heterotrophic biofilm, however, were minimally impacted.

The operational time and AgNP addition highly influenced the nitrifying biofilm microbial communality compositions. Long-term continuous exposure to both $[AgNP_{inf}]$ did not significantly impact the absolute abundance of nitrifiers, including the ammonia oxidizing bacteria (AOB) and nitrite oxidizing bacteria (NOB) genera in nitrifying MBBRs. The observed different susceptibility of *Nitrosomonas* and *Nitrospira* species, however, suggests the broad diversity of biofilm bacterial responses to environmental stresses and precludes generalizations about the potential impacts of AgNPs on a given phenotype (e.g. AOB). The distribution of AOB and NOB species during the Recovery period were similar to the Acclimation period, likely due to community resilience and production of young biofilm in post Ag-stress period. The observed minimal shift in both heterotrophic and nitrifying biofilm microbial community composition can still trigger a potential impairment of the biofilm biological functions pertaining to organic matter biodegradation and ammonia removal, enzymatic activities and biofilm structural properties.

Currently, limited information is available regarding the realistic temporal AgNP influent distribution profile in WRRFs due to analytical limitations for detection, quantification and characterization of AgNPs (Cervantes-Avilés et al., 2019). Thus, the majority of recent ecotoxicological studies used a constant influent AgNP inflow (Colman et al., 2018). Yet, the temporal variation in AgNP mass flow entering the WRRFs can influence their exposure concentrations, transformation, bioavailability and toxicological implications in biological wastewater processes (Cervantes-Avilés et al., 2019). The microbial community involved in biological wastewater treatment can tolerate fluctuations in influent AgNP concentration using different adaptation mechanisms including production of more EPS, microbial functional redundancy, community resilience via hormesis and the species-specific resistance within the microbial community (Tang et al., 2018; Zhang et al., 2016). Recent studies reported the capacity of wastewater microbial communities to recover from exposure to varying inflow of AgNP additions, periodic pulse and continuous inflow of 200 and 2000 μg/L AgNPs, depending on the AgNP concentration with an observed shift in community dynamic in 15 days (Alito and Gunsch, 2014; Gwin et al., 2018). More studies, however, are required to understand the potential impacts

of long-term exposure to varying inflow of environmental concentrations of AgNPs on wastewater treatment microbial communities and their genera specific effects.

Understanding the behavior of biofilm microbial communities, upon exposure to AgNPs are critical not only for wastewater treatment, but also for other relevant receptors that may be impacted by nanoparticles, to minimize possible consequences of nanoparticle exposures, particularly the antibiotic resistance proliferation, as reported recently in wastewater microbial communities (Gwin and Gunsch, 2018; Metch et al., 2018; Yuan et al., 2019). Long-term exposure to AgNPs in biofilm processes can lead to higher abundance of Ag-tolerant bacteria carrying silver resistance genes (Gwin and Gunsch, 2018). Limited data, however, are available regarding the prevalence of silver resistance genes in WRFFs and their downstream environments. Silver resistance genes are located in the plasmids and can be exchanged between different strains via horizontal gene transfer, increasing the microbial resistance to silver in wastewater microbial community (Li et al., 2015a). Antibiotic resistance genes (ARG) accompany these genes on the same plasmids, which can trigger an increase in the frequency of ARGs (Li et al., 2015a; Yuan et al., 2019). Thus, an increase in metal resistant species and the antibiotic resistance gene proliferation in WRRFs can negatively impact the capacity of the soil microbial communities leading to loss of soil fertility (McGee et al., 2017).

Molecular tchniques such as fluorescence in situ hybridization assay or denaturing gradient gel electrophoresis and 16S rRNA partial genes sequencing have been commonly used to determine the potential impact of different metal and metal oxide nanoparticles on microbial community of activated sludge, granular sludge and biofilm (Miao et al., 2017; Zheng et al., 2011). Polymerase chain reaction (PCR) based techniques such as quantitative PCR (qPCR) or reverse transcriptase qPCR are commonly used for the detection and quantification of the taxonomic and functional genes linked to specific bacteria such as nitrifying bacteria (Doolette et al., 2016; Kapoor et al., 2018). Yet such molecular techniques can underestimate species abundance or diversity and the functional gene abundance due to PCR bias and low-coverage sequencing data. Therefore, metagenomics analysis using direct sequencing of the genomic DNA can be used as comprehensive analysis of bacterial community diversity, functional genes such antibiotic resistance genes or metal resistance genes and metabolic pathways (Liu et al., 2019; Metch et al., 2018).

7.3 Fate and transport of AgNPs in attached-growth biofilm-laden processes

7.3.1 Behavior of AgNPs in MBBRs

Understanding the behavior of AgNPs in complex, organic matter-rich, environmental matrices such as wastewaters is the key component for their risk assessment, the design of better alternative treatment strategies and future regulations. Considering the current lack of systematic studies in this field, one of our specific objectives was to quantitatively characterize the retention, accumulation, aggregation and dissolution of AgNP in MBBRs, combined with the toxicological assessment of the potential risks of AgNPs in biofilm-laden biological wastewater processes. The quantitative characterization of nanoparticles in MBBRs, using spICP-MS, indicated distinct trends (Phases) for Ag concentration profiles in MBBRs. Both heterotrophic and nitrifying biofilms accumulated Ag in response to the AgNP addition and reached a relatively stable Ag retention efficiency (60% to 75% of [Ag_{inf}]) in the first 4 to 15 days of AgNP loading. A major fraction of the released total silver ([Ag_{eff}]) was associated with total suspended solids in effluent (TSS_{eff}) in MBBRs during this period. The attached biofilm ($Ag_{carrier}$) retained about 60% to 75% of cumulative mass of total Ag loading in the influent ($M_{Ag_{inf}}$) in MBBRs, indicating an initial high Ag biofilm retention capacity.

As the concentration of AgNPs increased inside the reactors afterwards, a second phase was observed in AgNP distribution file, with increase in effluent total Ag concentration over time, predominantly in NP form, and a periodic silver retention and release in biofilm and effluent biomass concentration increase. The saturation of the biofilm outer layers by local accumulation of the nanoparticles, the consequent decreased AgNPs deposition and their lower attachment efficiency onto the biofilm surface and biofilm sloughing off from the surface of the carriers resulted to a limited retention capacity of aerobic biofilm for AgNPs over a long term time exposure, compared to the commonly studied activated sludge systems.

The cumulative mass distribution of total Ag, in both organic matter removal and nitrifying MBBRs, suggest a lower retention capacity of nitrifying biofilm to retain Ag as compared to heterotrophic biofilm, likely due to their lower biomass concentration/volume ratio and limited

ability to produce EPSs (Barwal and Chaudhary, 2014). The Ag distribution profile corresponded with the AgNP inhibitory profile in MBBRs. An unperturbed phase comprised the time interval after injection of AgNPs, in which the biological activity of biofilm bacteria remained stable with no significant impact of AgNPs. Measured AgNP concentrations and their corresponding dissolved Ag in bioreactors, obtained from spICP-Ms analysis, were much lower than previously reported threshold concentrations for toxicity of AgNPs and dissolved Ag for both heterotrophic and nitrifying biofilms in this phase. As Ag concentration increased, a second phase corresponded to the period during which the biomass was significantly inhibited, corresponding to Ag distribution time profiles.

AgNP bioavailability can be highly influenced by their complexation/competition with wastewater components. Thus, the risk and toxicity of AgNPs in such environment could not solely be explained by their physical properties, such as size and surface activity, but also greatly depend on their chemical transformation (Zhang et al., 2018a). High concentrations of dissolved oxygen (6 to 8 mg O_2/L) and relevant pH (7.7) in aerobic biological wastewater treatment processes provide thermodynamically favorable conditions for oxidative dissolution of AgNPs, influencing their dynamics, especially at low NP concentrations (Azodi et al., 2016; Merrifield et al., 2017). Therefore, AgNPs and dissolved Ag usually coexist under oxygen-rich aqueous conditions, and they cooperate to produce hazardous effects in their corresponding environment, however, which fraction dominates toxicity appears inconclusive (Beer et al., 2012; Kawata et al., 2009; Navarro et al., 2008). The Ag^+-mediated toxicity of AgNPs is mostly reported in simple growth media, using silver nitrate ($AgNO_3$) as a source of bioavailable free Ag^+ ions at concentrations of 0.05 to 10 mg/L (Beer et al., 2012; Choi et al., 2018). The detected dissolved Ag in MBBRs, however, was likely partially or completely complexed via interaction with suspended biomass. Therefore, the measured dissolved Ag content in each reactor could not be fully attributed to the observed toxicity, and the presence of AgNP accounted for some toxicity of AgNPs, as reported in previous studies (Kawata et al., 2009; Navarro et al., 2008).

The concentration of dissolved Ag decreased over time in MBBRs which can be attributed to removal of Ag^+ by their interaction with functional groups of macromolecules such as cysteine and methioninein the biofilm EPS matrix and their organic ligands, such as thiols. Sulfidation and formation of partly sulfidated ($Ag(0)/Ag_2S$) particles, complexation of dissolved Ag with Cl^-

and formation of insoluble AgCl(s) species at low Cl/Ag concentrations and soluble chloro-silver complexes (i.e., $AgCl_2^-$ or $AgCl_3^{2-}$) at high Cl/Ag concentrations and potential reformation of the secondary NPs from dissolved Ag can also contribute the observed decrease in dissolved Ag in MBBR effluent over time (Azodi et al., 2016). We detected changes in chemistry of the particles (Ag_2S, AgCl) in the effluent of all MBBRs using TEM-EDS analysis. Despite the mitigation role of sulfidation and chlorination on the toxicity of AgNPs, the transformation products (Ag_2S and AgCl) inherit different morphologies or sizes and various toxicological responses compared to the initial AgNPs which can still remain bioavailable with inhibitory effects on microorganism (e.g. plants, soil, freshwater biofilm bacteria) (da Silva et al., 2011; Hassellöv et al., 2008; Wu et al., 2018). The findings of this research signify that short-term exposure tests may fail to incorporate the effect of Ag accumulation and extended mass transport into deeper layers of biofilm and the effect of interfacial dissolution of the surface-bound AgNPs, thus underestimating the potential toxicity of AgNPs in attached-growth biological process over long-term exposures.

Characterization (size, shape, composition) and quantification of both parent AgNPs and their corresponding transformed species at environmentally relevant conditions are critical for validating the toxicological data in environmental and eco-toxicological studies (Gondikas et al., 2018). Therefore, a multi-method approach is required to provide the required physical and chemical characteristics of AgNPs. Our data suggests that single particle inductively coupled plasma mass spectrometry (spICP-MS) combined with imaging techniques such as transmission electron microscopy (TEM) can be used as a baseline approach for detection, mass quantification and characterization of AgNPs in complex wastewater matrix. Time-of-flight secondary ion mass spectrometry (ToF-SIMS) and the synchrotron-based techniques such as X-ray photoelectron spectroscopy (XPS) can be used for identification and quantitative distribution of Ag chemical species in both wastewater and sludge samples (Azodi et al., 2016; Laborda et al., 2016; Potter et al., 2019)

7.3.2 Potential implications of released AgNPs for downstream treatments and terrestrial ecosystems

The observed AgNP-induced biofilm detachment in MBBRs not only can inversely affect the treatment efficiency, SRT of the reactors and the biomass specialization, but it can also increase the risk of environmental exposure of AgNPs via the release of retained AgNPs and Ag-rich biofilm in the treated effluent, with potential implications for downstream treatments and effluent receiving streams. Thus, the potential impact of AgNPs in the downstream receiving environments can still be a concern at environmentally relevant concentrations of AgNPs. Our results stress the need for strategies to control the release of such NPs from biofilm systems.

Disinfection processes, including chlorination, ultraviolet and ozonation, are used to enhance the quality of secondary effluent by eliminating organic micropollutants, pathogens and antibiotic resistance genes prior the effluent discharge (Giannakis et al., 2016; Zhang et al., 2015). Yet, the fate of AgNPs and their transformed species, such as partially sulfidized particle or chloro-silver complexes in such disinfection processes and their interaction with these oxidants is not well-understood. Oxidative dissolution of AgNPs was reported as the primary reaction upon their interaction with different types of disinfectant including ozone, ultraviolet or sodium hypochlorite (Telgmann et al., 2016; Thalmann et al., 2015; Yuan et al., 2013). The dissolution of nano-Ag_2S in wastewater effluent is also reported by ozone treatment with an observed transformation of Ag_2S to AgCl via an oxidative dissolution–reprecipitation pathway (Thalmann et al., 2015). The interaction of citrate-coated AgNPs with the oxidants in both chlorination and ultraviolet disinfection treatments of wastewater effluent was reported to enhance the disinfection by-products formation (e.g trihalomethane) (Metch et al., 2015). Therefore, more studies are required to evaluate the effect of such advanced oxidization processes on characteristics (size, morphology), chemical speciation and bioavailability of the effluent AgNPs in such processes.

The reuse of WRRFs effluent for irrigation and of biosolids for application in agricultural fields, are cost-effective and suitable strategies to recover water resources (Elgallal et al., 2016). Reclaiming AgNP-containing effluent and land application of AgNP-rich biosolids, however, are considered as main routes which AgNPs enter the terrestrial ecosystems through their wastewater–sludge–soil pathway, which can negatively impact the soil micro-ecosystem (Lead et

al., 2018; Liu et al., 2018; Wang et al., 2016). The estimated concentration of Ag in wastewater sludge was recently reported in the range of 2 to 860 mg/kg dry sludge by US EPA (Tang et al., 2014; Zhang et al., 2018a). Our TEM-EDS analyses indicated the association of effluent AgNPs with Cl and S and formation of partially sulfidized AgNPs or chloro-silver complexes in the effluent, which can attenuate the AgNP potential bioavailability and toxicity in soil environment or waste management processes such as composting. Partially sulfidized AgNPs, however, can continuously release bioavailable Ag^{+} (Zhang et al., 2018b).

The current understanding of AgNP transformations in actual field conditions with repeated biosolids applications is very limited. Our results show that long-term continuous exposure to AgNPs can result in a cumulative effect on NP-biomass interaction dynamics leading to NP-mediated susceptibility in attached-growth biological wastewater process. Therefore, the long-term behavior (bioavailability, accumulation) of AgNPs and their transformed species along the "wastewater–sludge–soil" pathway should be considered in eco-toxicological studies, evaluating the effect of land application of AgNP-rich biosolid in soil and sediment environments (Courtois et al., 2019). The long-term negative impact of sulfidized AgNPs on the soil ammonium oxidation process was reported over 140 days, indicating that the accumulation of Ag_2S in soils could potentially have adverse impacts on soil microbial communities (Kraas et al., 2017). Therefore, the fate and effects of AgNPs in biosolids are still of concern. The environmental risk assessment of NPs in such matrices is needed for their safer sustainable applications (e.g. biosolids valorisation onto agricultural lands) (Servin and White, 2016).

7.3.3 Environmetal implications of the present study

Combination of both toxicological methodologies and AgNPs characterization enabled us to demonstrate the distinct AgNP-biofilm interaction dynamics and inhibitory effect in biofilm-laden biologic wastewater processes over long-term exposure scenarios. Due to their technical and economic feasibility, lab and bench-scale experiments were used in this study to determine the fate and transport and the long-term impact of AgNPs in an aerobic attached-growth wastewater process. Rigorous physical and chemical characterization of AgNPs combined with biological and toxicological analyses in lab-scale MBBRs were used to determine the potential toxicity mechanisms of AgNP, the retention and transport of Ag (AgNPs, dissolved Ag and total

Ag) and their transformations. Modelling of obtained results, using the reaction rates, can be used for larger scale design processes. The statistical optimization analysis such as response surface methodology, using the lab-scale data such as temporal Ag distribution profile in MBBRs, can be used as an a systematic approach to find the optimal alternative treatment strategies for AgNP removal in full scale WRRFs (Vilela et al., 2018). This study contributes to a better understanding of the fate and behavior of AgNPs in biological wastewater processes, providing key information that can be used to predict the environmental risks of ENPs (transport, persistence and toxicity) in aquatic ecosystems.

Previous ecotoxicological studies have mainly focused on adverse effects of exposure to a single type of NPs, however, in realistic environmental scenarios, the NPs may interact with combination of different chemicals, including other NPs (Heys et al., 2016; Park et al., 2019). Titanium dioxide NPs (TiO_2), cerium dioxide NPs (CeO_2), zinc oxide NPs (ZnO), cupper oxide NPs and cerium dioxide NPs (CeO_2) are among the most commonly used metal oxide NPs in catalysis, cosmetics, paint and coatings, and chemical sensors (De la Calle et al., 2017; Tolaymat et al., 2017). Recent studies have been reported the different acute or chronic inhibitory effects of these NPs on COD and biological nitrogen and phosphorus removal, key enzyme activities and microbial community structures of activated sludge and biofilm systems, especially at high NP concentrations (Chen et al., 2014; Hou et al., 2015; Hu et al., 2017; Schug et al., 2014; Wang et al., 2018; Zhang et al., 2017; Zheng et al., 2011). The interactions of these nanoparticles can contribute to a different level of toxicity than the toxicity of each of the individual components, known as mixture toxicity, leading a synergistic or an antagonistic toxic effect (Lopes et al., 2016; Heys et al., 2016; Jośko et al., 2017; Park et al., 2019). The cytotoxic effect of CuNPs in HepG2 cells was enhanced by the ZnONPs, upon exposure to a mixture of both NPs (Li et al., 2015b). The dissolution of AgNPs and the interaction of released Ag^+ with other coexisting ZnONPs and TiO_2NPs provoked an adverse effect towards *D. magna*, induced by the synergistic action of Ag^+ (Lopes et al., 2016; Park et al., 2019).

Concentration addition and independent action models are commonly used to predict the mixture toxicity of chemicals in environmental risk assessment by the summation of the individual component toxicities (Heys et al., 2016). The mixture toxicity in these models, however, is predicted using the hypothesis that the components within a mixture will not interact or interfere

with each other. In the case of nanoparticles, mixture of NPs and components in environmental matrices influence their characteristics, transformation and potential toxicity which can result in the overall higher or lower toxicity than the individual components due to their interactions. Main approaches for the risk assessment of a mixture toxicity of compounds with mutual interactions includes (a) the whole mixture model which uses the toxicological data in the form of the biological response for an entire mixture and (b) a compound-based approach when toxicity data on each component is available in the mixture (Heys et al., 2016).

New approaches such as species sensitivity distribution (SSD) or adverse outcome pathways (AOP) have been used to integrate the multiple species responses into NP environmental risk assessments (ERA) (Chen et al., 2018; Garner et al., 2015; Gerloff et al., 2017). SSD uses a cumulative probability distribution to rank the species based on their sensitivity to a certain NPs, based on their toxicity measurements obtained from single-species bioassays of various species to determine the fraction of species in the total community which will experience the NP toxic effects (Garner et al., 2015). Predicted hazardous concentration at which no species are harmed (HC_0) and at which 5% of species are harmed (HC_5), known as the commonly used threshold concentrations for environmental risk assessment of chemicals, can be extracted from SSD for the different NPs, using limited set of laboratory based ecotoxicity data (Chen et al., 2018; Garner et al., 2015). AOP approach uses the molecular or biochemical endpoints for predicting the chemical impacts on individuals and populations by focusing on toxicity evaluation in terms of species and endpoint selection, creating a link between toxicity events at different levels in order to incorporate additional information required for chemical and site-specific risk assessment (Gerloff et al., 2017; Groh et al., 2015). The main outcomes of this research in combination with ERA approaches such as SSD or AOP can be helpful for environmental and agricultural product regulators, environmental risk assessment experts and municipalities to adequately address the safety and regulatory questions related to nanotechnology and adaptation of future regulations.

CHAPTER 8 CONCLUSIONS AND RECOMMENDATIONS

This research project sought to determine the fate, transport and long-term impact of environmental concentrations of AgNPs in attached-growth biological wastewater treatment processes. Three different moving bed biofilm reactors (MBBR) systems, representing the common MBBR configurations in WRRFs, achieving organic matter removal and nitrification were used. The fate and inhibitory effects of polyvinylpyrrolidone (PVP)-coated AgNPs (50 nm) at nominal concentrations (10, 100 and 600 μg/L) were investigated in a high-rate COD-removal MBBR with a very short hydraulic retention time (HRT of 1h) as compact secondary treatment for BOD removal. The long-term impact of continuous inflow of environmentally relevant influent concentrations of PVP-AgNPs (10-100 μg/L) on biological performance and microbial communities of aerobic heterotrophic wastewater biofilm was evaluated in a medium-rate COD removal MBBR (HRT of 3 h), as the pre-treatment of an activated sludge system or a BOD separation unit ahead of the biological N-removing step. Considering the critical role of nitrification, in biological nitrogen removal processes, the responses and recovery of nitrifying biofilm was upon long-term exposure to silver nanoparticles was evaluated in a nitrifying MBBR (HRT of 3 h), as a post carbon removal nitrifying biofilm system or a tertiary nitrification system, at environmentally relevant influent concentrations (10-100 μg/L AgNPs).

8.1 Conclusions

The following conclusions were drawn from this research for the following three topics:

(A) Fate and inhibitory effect of silver nanoparticles in high rate organic matter moving bed biofilm reactors (MBBRs)

- No inhibitory effect was observed at an average influent concentration of 10 μg/L Ag during 18 days. However, our results indicated an adverse effect of PVP-AgNPs on the structural and functional responses of the biofilm in MBRRs at influent AgNP concentrations of 100 μg/L in 18 days and of 600 μg/L in 5 days, respectively.
- A significant increase in effluent total suspended solids concentration, at influent AgNPs concentrations of 100 and 600 μg/L, indicated that significant biofilm detachment occurred.

- A significant proportion of Ag (38% to 75%) was released to the effluent, predominantly as NPs that were chemically transformed and potentially into less toxic forms of silver nanoparticles (Ag_2S, AgCl), over the Exposure period.
- SpICp-MS analyses indicated a concentration-dependent dissolution of AgNPs where the higher dissolution, in terms of the fraction of Ag dissolved relative to total Ag added, was observed at lower concentration of AgNPs in the effluent of reactors.

(B) Impacts of environmentally relevant concentrations of AgNPs (10 and 100 μg/L) on biological performance and microbial communities of aerobic heterotrophic wastewater biofilm in a medium rate organic matter removal continuous flow MBBR

- Soluble organic matter removal efficiency, biofilm viability and specific activities of intracellular dehydrogenase (DHA), and extracellular α-glucosidase (α-Glu) and protease (PRO) enzymes were significantly inhibited at both AgNP influent concentrations over a period of 64 days.
- With no change in intracellular ROS production at influent AgNP concentration of 10 μg/L, a 64-day exposure to 100 μg/L AgNPs induced an oxidative stress due to significant increase of intracellular ROS concentration in attached biofilm.
- Heterotrophic biofilm contributed to AgNPs removal efficiency at an initially high level (60% to 71%), similar to the observed retention capacity of biofilm in high-rate MBBRs (54% to 61%). Biofilm retention capacity gradually decreased afterwards, retaining only 25% of mass of Ag_{inf} by day 64, with an increase in total Ag release from the biofilm to the effluent over time, predominantly in an NP form. The observed pattern was due to the saturation of the biofilm outer layers by AgNPs, detachment of the biofilm outer layer, and release of easily detachable AgNPs from the effluent biomass.
- The concentration of effluent dissolved Ag_{eff} decreased over time in both MBBRs likely due to the removal of Ag^+ via their interaction with functional groups of macromolecules in the biofilm EPS and the formation of insoluble AgCl precipitates as confirmed by TEM-EDS analysis.
- The bacterial community composition was slightly changed due to a decrease or loss of silver-sensitive species in certain orders (e.g. *Burkholderiales* or *Gemmatimonadales*).

(C) Responses and recovery of nitrifying MBBRs upon long-term continuous exposure to environmentally relevant influent concentrations of AgNPs (10 and 100 μg/L)

- Ammonia removal efficiency, biofilm viability and specific ammonia monooxygenase (AMO) enzyme activity were significantly inhibited at both AgNP influent concentrations in 60 days. Nitrifying biofilms recovered their ammonia removal efficiency, biofilm viability and enzymatic activity by the end of a 35-day Recovery period.
- A 60-day exposure to 10 and 100 μg/L AgNPs induced a concentration-dependent ROS production in MBBR biofilms. A nitrifying biofilm at a low AgNP influent concentration was able to regulate the oxidative stress; however, a relatively high intracellular ROS production was still detected in MBBR with influent concentration of 100 μg/L AgNP by the end the recovery period.
- Operational time and AgNP concentration significantly influenced the biofilm microbial community composition.
- A 60-day exposure to 10 and 100 μg/L AgNPs did not significantly impact the abundance of ammonia oxidizing bacteria (AOB) and nitrite oxidizing bacteria (NOB) genera while some of their associated species demonstrated some susceptibility towards AgNPs.
- Nitrifying biofilms demonstrated an initial relatively stable Ag retention efficiency (about 72%), which decreased over time with an observed periodic Ag release and retention recovery, due to the saturation of the biofilm outer layers by AgNPs and/or biofilm sloughing off from the surface of the carriers.

8.2 Recommendations

Based on these findings, recommendations for further investigation are:

a) MBBR effluents contribute to a major release of AgNPs into downstream ecosystem. The majority of nano-toxicological studies documented the transformation processes and their impact on the stability and fate of AgNPs in wastewater. There remains a pressing need to better understand the bioavailability, accumulation and toxicity mechanisms of these transformed nanoparticles both in wastewater processes and effluent receiving ecosystems.

b) The interactions of AgNPs and biofilm EPSs play significant role in their fate and biological effects. Thus, characterization of the composition, element-specific and functional group speciation of EPSs are required to better understand the complex AgNP-EPS interactions in biofilm-laden biological processes and their effects on the fate and inhibition of AgNPs in such processes.

c) Most ecotoxicological studies were performed using only AgNPs, but AgNPs co-exist with other metal and metal oxide nanoparticles in WRRFs. Thus, more studies are required to evaluate the interactions of AgNPs and other nanoparticles, and their potential toxicological effects under environmentally relevant conditions.

d) The impacts of NPs on biological treatment systems and the related mechanisms are mainly evaluated in lab-scale process, representing only a specific part of the biological wastewater treatment system, resulting in contradictory results. Hence, there is a need to consider the whole liquid and solids treatment chains in real WRRFs.

e) Most of the current studies are focused on the potential adverse impacts of AgNPs on wastewater ecosystems and/or microbial community structure. NPs assessment in wastewater sludge and biosolids, despite their growing importance in ecotoxicity studies, is currently overlooked. Thus, long-term repeated AgNP-containing biosolid applications in different types of soil and quantitative characterization of AgNP transformation are required for better understanding of their fate and potential implications in the terrestrial ecosystems.

REFERENCES

Abad-Alvaro, I., Bolea, E., Laborda, F., & Castillo, J. R. (2017). An ICP-MS-based platform for release studies on silver-based nanomaterials. *Journal of Analytical Atomic Spectrometry, 32*(6), 1101-1108.

Abdal Dayem, A., Hossain, M. K., Lee, S. B., Kim, K., Saha, S. K., Yang, G.-M., Cho, S.-G. (2017). The role of reactive oxygen species (ROS) in the biological activities of metallic nanoparticles. *International Journal of Molecular Sciences, 18*(1), 120.

Abzazou, T., Araujo, R. M., Auset, M., & Salvadó, H. (2016). Tracking and quantification of nitrifying bacteria in biofilm and mixed liquor of a partial nitrification MBBR pilot plant using fluorescence in situ hybridization. *Science of the Total Environment, 541*, 1115-1123.

Ahlberg, S., Antonopulos, A., Diendorf, J., Dringen, R., Epple, M., Flöck, R., Helmlinger, J. (2014). PVP-coated, negatively charged silver nanoparticles: A multi-center study of their physicochemical characteristics, cell culture and in vivo experiments. *Beilstein Journal of Nanotechnology, 5*, 1944.

Ahmad, A., Wei, Y., Syed, F., Tahir, K., Rehman, A. U., Khan, A., Yuan, Q. (2017). The effects of bacteria-nanoparticles interface on the antibacterial activity of green synthesized silver nanoparticles. *Microbial Pathogenesis, 102*, 133-142.

Alexander, J. W. (2009). History of the medical use of silver. *Surgical Infections, 10*(3), 289-292.

Alito, C. L., & Gunsch, C. K. (2014). Assessing the effects of silver nanoparticles on biological nutrient removal in bench-scale activated sludge sequencing batch reactors. *Environmental Science & Technology, 48*(2), 970-976.

Alizadeh, S., Ghoshal, S., & Comeau, Y. (2019). Fate and inhibitory effect of silver nanoparticles in high rate moving bed biofilm reactors. *Science of the Total Environment, 647*, 1199-1210.

Annavajhala, M. K., Kapoor, V., Santo-Domingo, J., & Chandran, K. (2018). Comammox functionality identified in diverse engineered biological wastewater treatment systems. *Environmental Science & Technology Letters, 5*(2), 110-116.

APHA, AWWA, & WEF. (2012). Standard Methods for the Examination of Water and Wastewater, 22nd ed. American Public Health Association, American Water Works Association & Water Environment Federation:Washington, D.C.

Apprill, A., McNally, S., Parsons, R., & Weber, L. (2015). Minor revision to V4 region SSU rRNA 806R gene primer greatly increases detection of *SAR11 bacterioplankton*. *Aquatic Microbial Ecology, 75*(2), 129-137.

Arnaout, C. L., & Gunsch, C. K. (2012). Impacts of silver nanoparticle coating on the nitrification potential of *Nitrosomonas europaea*. *Environmental Science & Technology, 46*(10), 5387-5395.

Arnon, S., Dahan, O., Elhanany, S., Cohen, K., Pankratov, I., Gross, A., Shore, L. S. (2008). Transport of testosterone and estrogen from dairy-farm waste lagoons to groundwater. *Environmental Science & Technology*, 42(15), 5521-5526.

Asadishad, B., Chahal, S., Akbari, A., Cianciarelli, V., Azodi, M., Ghoshal, S., & Tufenkji, N. (2018). Amendment of agricultural soil with metal nanoparticles: Effects on soil enzyme activity and microbial community composition. *Environmental Science & Technology*. 52(4), 1908-1918

Aslam, M., McCarty, P. L., Shin, C., Bae, J., & Kim, J. (2017). Low energy single-staged anaerobic fluidized bed ceramic membrane bioreactor (AFCMBR) for wastewater treatment. *Bioresource Technology, 240*, 33-41.

Auffan, M., Bottero, J.-Y., Chaneac, C., & Rose, J. (2010). Inorganic manufactured nanoparticles: how their physicochemical properties influence their biological effects in aqueous environments. *Nanomedicine, 5*(6), 999-1007.

Auffan, M., Rose, J., Bottero, J.-Y., Lowry, G. V., Jolivet, J.-P., & Wiesner, M. R. (2009a). Towards a definition of inorganic nanoparticles from an environmental, health and safety perspective. *Nature Nanotechnology, 4*(10), 634.

Auffan, M., Rose, J., Wiesner, M. R., & Bottero, J.-Y. (2009b). Chemical stability of metallic nanoparticles: a parameter controlling their potential cellular toxicity in vitro. *Environmental Pollution, 157*(4), 1127-1133.

Auvinen, H., Kaegi, R., Rousseau, D. P., & Du Laing, G. (2017). Fate of silver nanoparticles in constructed wetlands—a microcosm study. *Water, Air, & Soil Pollution, 228*(3), 97.

Azimzada, A., Tufenkji, N., & Wilkinson, K. J. (2017). Transformations of silver nanoparticles in wastewater effluents: links to Ag bioavailability. *Environmental Science: Nano, 4*(6), 1339-1349.

Azodi, M., Sultan, Y., & Ghoshal, S. (2016). Dissolution behavior of silver nanoparticles and formation of secondary silver sanoparticles in municipal wastewater by single-particle ICP-MS. *Environmental Science & Technology, 50*(24), 13318-13327.

Badawy, A. M. E., Luxton, T. P., Silva, R. G., Scheckel, K. G., Suidan, M. T., & Tolaymat, T. M. (2010). Impact of environmental conditions (pH, ionic strength, and electrolyte type) on the surface charge and aggregation of silver nanoparticles suspensions. *Environmental Science & Technology, 44*(4), 1260-1266.

Bakar, S. N. H. A., Hasan, H. A., Mohammad, A. W., Abdullah, S. R. S., Haan, T. Y., Ngteni, R., & Yusof, K. M. M. (2018). A review of moving-bed biofilm reactor technology for palm oil mill effluent treatment. *Journal of Cleaner Production, 171*, 1532-1545.

Barker, L., Giska, J., Radniecki, T., & Semprini, L. (2018). Effects of short-and long-term exposure of silver nanoparticles and silver ions to *Nitrosomonas europaea* biofilms and planktonic cells. *Chemosphere, 206*, 606-614.

Barwal, A., & Chaudhary, R. (2014). To study the performance of biocarriers in moving bed biofilm reactor (MBBR) technology and kinetics of biofilm for retrofitting the existing

aerobic treatment systems: a review. *Reviews in Environmental Science and Bio/Technology, 13*(3), 285-299.

Beer, C., Foldbjerg, R., Hayashi, Y., Sutherland, D. S., & Autrup, H. (2012). Toxicity of silver nanoparticles—nanoparticle or silver ion? *Toxicology Letters, 208*(3), 286-292.

Behra, R., Sigg, L., Clift, M. J., Herzog, F., Minghetti, M., Johnston, B., Rothen-Rutishauser, B. (2013). Bioavailability of silver nanoparticles and ions: from a chemical and biochemical perspective. *Journal of the Royal Society Interface, 10*(87), 20130396.

Bertanza, G., Canato, M., & Laera, G. (2018). Towards energy self-sufficiency and integral material recovery in waste water treatment plants: Assessment of upgrading options. *Journal of Cleaner Production, 170*, 1206-1218.

Binh, C. T. T., Adams, E., Vigen, E., Tong, T., Alsina, M. A., Gaillard, J.-F., Kelly, J. J. (2016). Chronic addition of a common engineered nanomaterial alters biomass, activity and composition of stream biofilm communities. *Environmental Science: Nano, 3*(3), 619-630.

Birben, E., Sahiner, U. M., Sackesen, C., Erzurum, S., & Kalayci, O. (2012). Oxidative stress and antioxidant defense. *World Allergy Organization Journal, 5*(1), 9.

Biswas, K., Taylor, M. W., & Turner, S. J. (2014). Successional development of biofilms in moving bed biofilm reactor (MBBR) systems treating municipal wastewater. *Applied Microbiology and Biotechnology, 98*(3), 1429-1440.

Blaser, S. A., Scheringer, M., MacLeod, M., & Hungerbühler, K. (2008). Estimation of cumulative aquatic exposure and risk due to silver: contribution of nano-functionalized plastics and textiles. *Science of the Total Environment, 390*(2-3), 396-409.

Bondarenko, O., Juganson, K., Ivask, A., Kasemets, K., Mortimer, M., & Kahru, A. (2013). Toxicity of Ag, CuO and ZnO nanoparticles to selected environmentally relevant test organisms and mammalian cells in vitro: a critical review. *Archives of Toxicology, 87*(7), 1181-1200.

Borkar, R., Gulhane, M., & Kotangale, A. (2013). Moving bed biofilm reactor–a new perspective in wastewater treatment. *Journal of Environmental Science. Toxicology and Food Technology, 6*(6), 15-21.

Brar, S. K., Verma, M., Tyagi, R., & Surampalli, R. (2010). Engineered nanoparticles in wastewater and wastewater sludge–Evidence and impacts. *Waste Management, 30*(3), 504-520.

Brosseau, C., Émile, B., Labelle, M.-A., Laflamme, É., Dold, P. L., & Comeau, Y. (2016). Compact secondary treatment train combining a lab-scale moving bed biofilm reactor and enhanced flotation processes. *Water Research, 106*, 571-582.

Bundschuh, M., Filser, J., Lüderwald, S., McKee, M. S., Metreveli, G., Schaumann, G. E., Wagner, S. (2018). Nanoparticles in the environment: where do we come from, where do we go to? *Environmental Sciences Europe, 30*(1), 6.

Buonocore, E., Mellino, S., De Angelis, G., Liu, G., & Ulgiati, S. (2018). Life cycle assessment indicators of urban wastewater and sewage sludge treatment. *Ecological Indicators, 94*, 13-23.

Callahan, B. J., McMurdie, P. J., Rosen, M. J., Han, A. W., Johnson, A. J. A., & Holmes, S. P. (2016). DADA2: high-resolution sample inference from Illumina amplicon data. *Nature Methods, 13*(7), 581.

Cao, C., Huang, J., Yan, C., Liu, J., Hu, Q., & Guan, W. (2018). Shifts of system performance and microbial community structure in a constructed wetland after exposing silver nanoparticles. *Chemosphere, 199*, 661-669.

Caporaso, J. G., Kuczynski, J., Stombaugh, J., Bittinger, K., Bushman, F. D., Costello, E. K., Knight, R. (2010). QIIME allows analysis of high-throughput community sequencing data. *Nature Methods, 7*(5), 335-336. doi: 10.1038/nmeth.f.303

Cascio, C., Geiss, O., Franchini, F., Ojea-Jimenez, I., Rossi, F., Gilliland, D., & Calzolai, L. (2015). Detection, quantification and derivation of number size distribution of silver nanoparticles in antimicrobial consumer products. *Journal of Analytical Atomic Spectrometry, 30*(6), 1255-1265.

Cerqueira, M., & Pastrana, L. (2019). Does the future of food pass by using nanotechnologies? *Frontiers in Sustainable Food Systems, 3*, 16.

Cervantes-Avilés, P., Huang, Y., & Keller, A. A. (2019). Incidence and persistence of silver nanoparticles throughout the wastewater treatment process. *Water Research*, *156*,188-198.

Chacana, J., Alizadeh, S., Labelle, M.-A., Laporte, A., Hawari, J., Barbeau, B., & Comeau, Y. (2017). Effect of ozonation on anaerobic digestion sludge activity and viability. *Chemosphere*, 176, 405-411

Chaw, K., Manimaran, M., & Tay, F. E. (2005). Role of silver ions in destabilization of intermolecular adhesion forces measured by atomic force microscopy in *Staphylococcus epidermidis* biofilms. *Antimicrobial Agents and Chemotherapy, 49*(12), 4853-4859.

Chen, J., Tang, Y.-Q., Li, Y., Nie, Y., Hou, L., Li, X.-Q., & Wu, X.-L. (2014). Impacts of different nanoparticles on functional bacterial community in activated sludge. *Chemosphere, 104*, 141-148.

Chen, Y., Chen, H., Zheng, X., & Mu, H. (2012). The impacts of silver nanoparticles and silver ions on wastewater biological phosphorous removal and the mechanisms. *Journal of Hazardous Materials, 239*, 88-94.

Chen, Y., Zhao, Z., Peng, Y., Li, J., Xiao, L., & Yang, L. (2016). Performance of a full-scale modified anaerobic/anoxic/oxic process: high-throughput sequence analysis of its microbial structures and their community functions. *Bioresource Technology, 220*, 225-232.

Choi, O., Deng, K. K., Kim, N.-J., Ross, L., Surampalli, R. Y., & Hu, Z. (2008). The inhibitory effects of silver nanoparticles, silver ions, and silver chloride colloids on microbial growth. *Water Research, 42*(12), 3066-3074.

Choi, O., & Hu, Z. (2008). Size dependent and reactive oxygen species related nanosilver toxicity to nitrifying bacteria. *Environmental Science & Technology, 42*(12), 4583-4588.

Choi, O., & Hu, Z. (2009). Nitrification inhibition by silver nanoparticles. *Water Science and Technology, 59*(9), 1699-1702.

Choi, O., Yu, C.-P., Fernández, G. E., & Hu, Z. (2010). Interactions of nanosilver with *Escherichia coli* cells in planktonic and biofilm cultures. *Water Research, 44*(20), 6095-6103.

Choi, S., Johnston, M. V., Wang, G.-S., & Huang, C. (2017). Looking for engineered nanoparticles (ENPs) in wastewater treatment systems: qualification and quantification aspects. *Science of the Total Environment, 590*, 809-817.

Choi, Y., Kim, H.-A., Kim, K.-W., & Lee, B.-T. (2018). Comparative toxicity of silver nanoparticles and silver ions to *Escherichia coli*. *Journal of Environmental Sciences, 66*, 50-60

Claveau-Mallet, D., Wallace, S., & Comeau, Y. (2013). Removal of phosphorus, fluoride and metals from a gypsum mining leachate using steel slag filters. *Water Research, 47*(4), 1512-1520.

Colman, B. P., Baker, L. F., King, R. S., Matson, C. W., Unrine, J. M., Marinakos, S. M., Bernhardt, E. S. (2018). Dosing, not the dose: comparing chronic and pulsed silver nanoparticle exposures. *Environmental Science & Technology, 52*(17), 10048-10056.

Courtois, P., Rorat, A., Lemiere, S., Guyoneaud, R., Attard, E., Levard, C., & Vandenbulcke, F. (2019). Ecotoxicology of silver nanoparticles and their derivatives introduced in soil with or without sewage sludge: A review of effects on microorganisms, plants and animals. Environmental pollution.

da Silva, B. F., Pérez, S., Gardinalli, P., Singhal, R., Mozeto, A. A., & Barceló, D. (2011). Analytical chemistry of metallic nanoparticles in natural environments. *TrAC Trends in Analytical Chemistry, 30*(3), 528-540.

De la Calle, I., Menta, M., Klein, M., & Séby, F. (2017). Screening of TiO_2 and Au nanoparticles in cosmetics and determination of elemental impurities by multiple techniques (DLS, SP-ICP-MS, ICP-MS and ICP-OES). *Talanta, 171*, 291-306.

del Real, A. E. P., Castillo-Michel, H., Kaegi, R., Larue, C., de Nolf, W., Reyes-Herrera, J., Sarret, G. (2018). Searching for relevant criteria to distinguish natural vs. anthropogenic TiO_2 nanoparticles in soils. *Environmental Science: Nano, 5*(12), 2853-2863.

Demeter, M. A., Lemire, J. A., Mercer, S. M., & Turner, R. J. (2017). Screening selectively harnessed environmental microbial communities for biodegradation of polycyclic aromatic hydrocarbons in moving bed biofilm reactors. *Bioresource Technology, 228*, 116-124.

Di Trapani, D., Christensson, M., Torregrossa, M., Viviani, G., & Ødegaard, H. (2013). Performance of a hybrid activated sludge/biofilm process for wastewater treatment in a cold climate region: influence of operating conditions. *Biochemical Engineering Journal, 77*, 214-219.

Dobias, J., & Bernier-Latmani, R. (2013). Silver release from silver nanoparticles in natural waters. *Environmental Science & Technology, 47*(9), 4140-4146.

Donovan, A. R., Adams, C. D., Ma, Y., Stephan, C., Eichholz, T., & Shi, H. (2016). Single particle ICP-MS characterization of titanium dioxide, silver, and gold nanoparticles during drinking water treatment. *Chemosphere, 144*, 148-153.

Donovan, A. R., Adams, C. D., Ma, Y., Stephan, C., Eichholz, T., & Shi, H. (2018). Fate of nanoparticles during alum and ferric coagulation monitored using single particle ICP-MS. *Chemosphere, 195*, 531-541.

Doolette, C. L., Gupta, V. V., Lu, Y., Payne, J. L., Batstone, D. J., Kirby, J. K., McLaughlin, M. J. (2016). Quantifying the sensitivity of soil microbial communities to silver sulfide nanoparticles using metagenome sequencing. *PloS one*, 11(8), e0161979.

Doolette, C. L., McLaughlin, M. J., Kirby, J. K., Batstone, D. J., Harris, H. H., Ge, H., & Cornelis, G. (2013). Transformation of PVP coated silver nanoparticles in a simulated wastewater treatment process and the effect on microbial communities. *Chemistry Central Journal, 7*(1), 46.

Du, J., Tang, J., Xu, S., Ge, J., Dong, Y., Li, H., & Jin, M. (2018). A review on silver nanoparticles-induced ecotoxicity and the underlying toxicity mechanisms. *Regulatory Toxicology and Pharmacology*, 98, 231-239

Durán, N., Durán, M., de Jesus, M. B., Seabra, A. B., Fávaro, W. J., & Nakazato, G. (2016). Silver nanoparticles: A new view on mechanistic aspects on antimicrobial activity. *Nanomedicine: Nanotechnology, Biology and Medicine, 12*(3), 789-799.

Echegoyen, Y., & Nerín, C. (2013). Nanoparticle release from nano-silver antimicrobial food containers. *Food and Chemical Toxicology, 62*, 16-22.

El Badawy, A. M., Silva, R. G., Morris, B., Scheckel, K. G., Suidan, M. T., & Tolaymat, T. M. (2010). Surface charge-dependent toxicity of silver nanoparticles. *Environmental Science & Technology, 45*(1), 283-287.

Elgallal, M., Fletcher, L., & Evans, B. (2016). Assessment of potential risks associated with chemicals in wastewater used for irrigation in arid and semiarid zones: A review. *Agricultural Water Management, 177*, 419-431.

Ensign, S. A., Hyman, M. R., & Arp, D. J. (1993). In vitro activation of ammonia monooxygenase from *Nitrosomonas europaea* by copper. *Journal of Bacteriology, 175*(7), 1971-1980.

Fabrega, J., Luoma, S. N., Tyler, C. R., Galloway, T. S., & Lead, J. R. (2011a). Silver nanoparticles: behaviour and effects in the aquatic environment. *Environment International, 37*(2), 517-531.

Fabrega, J., Renshaw, J. C., & Lead, J. R. (2009). Interactions of silver nanoparticles with *Pseudomonas putida* biofilms. *Environmental Science & Technology, 43*(23), 9004-9009.

Fabrega, J., Zhang, R., Renshaw, J. C., Liu, W.-T., & Lead, J. R. (2011b). Impact of silver nanoparticles on natural marine biofilm bacteria. *Chemosphere, 85*(6), 961-966.

Falletti, L., & Conte, L. (2007). Upgrading of activated sludge wastewater treatment plants with hybrid moving-bed biofilm reactors. *Industrial & Engineering Chemistry Research, 46*(21), 6656-6660.

Farkas, J., Peter, H., Christian, P., Urrea, J. A. G., Hassellöv, M., Tuoriniemi, J., Thomas, K. V. (2011). Characterization of the effluent from a nanosilver producing washing machine. *Environment International, 37*(6), 1057-1062.

Flemming, H.-C., & Wingender, J. (2010). The biofilm matrix. *Nature Reviews. Microbiology, 8*(9), 623.

Flynn, K. M., Dowell, G., Johnson, T. M., Koestler, B. J., Waters, C. M., & Cooper, V. S. (2016). Evolution of ecological diversity in biofilms of *Pseudomonas aeruginosa* by altered cyclic diguanylate signaling. *Journal of Bacteriology, 198*(19), 2608-2618.

Foladori, P., Tamburini, S., & Bruni, L. (2010). Bacteria permeabilisation and disruption caused by sludge reduction technologies evaluated by flow cytometry. *Water Research, 44*(17), 4888-4899.

Folens, K., Huysman, S., Van Hulle, S., & Du Laing, G. (2017). Chemical and economic optimization of the coagulation-flocculation process for silver removal and recovery from industrial wastewater. *Separation and Purification Technology, 179*, 145-151.

Furtado, L. M., Bundschuh, M., & Metcalfe, C. D. (2016). Monitoring the fate and transformation of silver nanoparticles in natural waters. *Bulletin of Environmental Contamination and Toxicology, 97*(4), 449-455.

Garg, N. (2019). A Brief study on characteristics, properties, and applications of CdSe *Innovation in Materials Science and Engineering* (pp. 43-60): Springer.

Garner, K. L., Suh, S., Lenihan, H. S., & Keller, A. A. (2015). Species sensitivity distributions for engineered nanomaterials. *Environmental Science & Technology*, 49(9), 5753-5759.

Georgantzopoulou, A., Almeida Carvalho, P., Vogelsang, C., Tilahun, M., Ndungu, K., Booth, A. M., Macken, A. (2018). Ecotoxicological effects of transformed silver and titanium dioxide nanoparticles in the effluent from a lab-scale wastewater treatment system. *Environmental Science & Technology, 52*(16), 9431-9441.

Gerloff, K., Landesmann, B., Worth, A., Munn, S., Palosaari, T., & Whelan, M. (2017). The adverse outcome pathway approach in nanotoxicology. *Computational Toxicology*, 1, 3-11.

Giannakis, S., Voumard, M., Grandjean, D., Magnet, A., De Alencastro, L. F., & Pulgarin, C. (2016). Micropollutant degradation, bacterial inactivation and regrowth risk in wastewater effluents: Influence of the secondary (pre) treatment on the efficiency of advanced oxidation processes. *Water Research*, 102, 505-515.

Giebner, S., Ostermann, S., Straskraba, S., Oetken, M., Oehlmann, J., & Wagner, M. (2018). Effectivity of advanced wastewater treatment: reduction of *in vitro* endocrine activity and mutagenicity but not of *in vivo* reproductive toxicity. *Environmental Science and Pollution Research, 25*(5), 3965-3976.

Giese, B., Klaessig, F., Park, B., Kaegi, R., Steinfeldt, M., Wigger, H., Gottschalk, F. (2018). Risks, release and concentrations of engineered nanomaterial in the environment. *Scientific Reports, 8*(1), 1565.

Goel, R., Mino, T., Satoh, H., & Matsuo, T. (1998). Enzyme activities under anaerobic and aerobic conditions in activated sludge sequencing batch reactor. *Water Research, 32*(7), 2081-2088.

Gondikas, A. P., Morris, A., Reinsch, B. C., Marinakos, S. M., Lowry, G. V., & Hsu-Kim, H. (2012). Cysteine-induced modifications of zero-valent silver nanomaterials: implications for particle surface chemistry, aggregation, dissolution, and silver speciation. *Environmental Science & Technology, 46*(13), 7037-7045.

González-Fuenzalida, R., Sanjuan-Navarro, L., Moliner-Martínez, Y., & Campíns-Falcó, P. (2018). Quantitative study of the capture of silver nanoparticles by several kinds of soils. *Science of the Total Environment, 630*, 1226-1236.

Goswami, S., Sahareen, T., Singh, M., & Kumar, S. (2015). Role of biogenic silver nanoparticles in disruption of cell–cell adhesion in *Staphylococcus aureus* and *Escherichia coli* biofilm. *Journal of Industrial and Engineering Chemistry, 26*, 73-80.

Gottschalk, F., Sonderer, T., Scholz, R. W., & Nowack, B. (2009). Modeled environmental concentrations of engineered nanomaterials (TiO_2, ZnO, Ag, CNT, fullerenes) for different regions. *Environmental Science & Technology, 43*(24), 9216-9222.

Gottschalk, F., Sun, T., & Nowack, B. (2013). Environmental concentrations of engineered nanomaterials: review of modeling and analytical studies. *Environmental Pollution, 181*, 287-300.

Gray, E. P., Bruton, T. A., Higgins, C. P., Halden, R. U., Westerhoff, P., & Ranville, J. F. (2012). Analysis of gold nanoparticle mixtures: a comparison of hydrodynamic chromatography (HDC) and asymmetrical flow field-flow fractionation (AF4) coupled to ICP-MS. *Journal of Analytical Atomic Spectrometry, 27*(9), 1532-1539.

Groh, K. J., Carvalho, R. N., Chipman, J. K., Denslow, N. D., Halder, M., Murphy, C. A., Watanabe, K. H. (2015). Development and application of the adverse outcome pathway framework for understanding and predicting chronic toxicity: II. A focus on growth impairment in fish. *Chemosphere*, 120, 778-792.

Grün, A. Y., App, C. B., Breidenbach, A., Meier, J., Metreveli, G., Schaumann, G. E., & Manz, W. (2018). Effects of low dose silver nanoparticle treatment on the structure and community composition of bacterial freshwater biofilms. *PloS one, 13*(6), e0199132.

Grün, A. Y., Meier, J., Metreveli, G., Schaumann, G. E., & Manz, W. (2016). Sublethal concentrations of silver nanoparticles affect the mechanical stability of biofilms. *Environmental Science and Pollution Research, 23*(23), 24277-24288.

Gschwind, S., Hagendorfer, H., Frick, D. A., & Günther, D. (2013). Mass quantification of nanoparticles by single droplet calibration using inductively coupled plasma mass spectrometry. *Analytical Chemistry, 85*(12), 5875-5883.

Gu, L., Li, Q., Quan, X., Cen, Y., & Jiang, X. (2014). Comparison of nanosilver removal by flocculent and granular sludge and short-and long-term inhibition impacts. *Water Research, 58*, 62-70.

Gwin, C., & Gunsch, C. (2018a). Examining relationships between total silver concentration and Sil silver resistance genes in domestic wastewater treatment plants. *Journal of Applied Microbiology, 124*(6), 1638-1646.

Gwin, C. A., Lefevre, E., Alito, C. L., & Gunsch, C. K. (2018b). Microbial community response to silver nanoparticles and Ag^+ in nitrifying activated sludge revealed by ion semiconductor sequencing. *Science of the Total Environment, 616*, 1014-1021.

Hadioui, M., Leclerc, S., & Wilkinson, K. J. (2013). Multimethod quantification of Ag^+ release from nanosilver. *Talanta, 105*, 15-19.

Hadioui, M., Merdzan, V., & Wilkinson, K. J. (2015). Detection and characterization of ZnO nanoparticles in surface and waste waters using single particle ICPMS. *Environmental Science & Technology, 49*(10), 6141-6148.

Hasbullah, H., Sabri, N. S. M., Said, N., Rosid, S. M., Roslan, M. I., Ismail, A. F., Yusof, N. (2019). Nanoengineered materials for water and wastewater treatments. *Nanotechnology in Water and Wastewater Treatment* (pp. 303-335): Elsevier, Amsterdam, The Netherlands.

Hassard, F., Biddle, J., Cartmell, E., Jefferson, B., Tyrrel, S., & Stephenson, T. (2015). Rotating biological contactors for wastewater treatment–A review. *Process Safety and Environmental Protection, 94*, 285-306.

Hassard, F., Biddle, J., Harnett, R., & Stephenson, T. (2018). Microbial extracellular enzyme activity affects performance in a full-scale modified activated sludge process. *Science of the Total Environment*, 625, 1527-1534.

Hassellöv, M., Readman, J. W., Ranville, J. F., & Tiede, K. (2008). Nanoparticle analysis and characterization methodologies in environmental risk assessment of engineered nanoparticles. *Ecotoxicology, 17*(5), 344-361.

Hendren, C. O., Badireddy, A. R., Casman, E., & Wiesner, M. R. (2013). Modeling nanomaterial fate in wastewater treatment: Monte Carlo simulation of silver nanoparticles (nano-Ag). *Science of the Total Environment, 449*, 418-425.

Herrling, M. P., Lackner, S., Tatti, O., Guthausen, G., Delay, M., Franzreb, M., & Horn, H. (2016). Short and long term biosorption of silica-coated iron oxide nanoparticles in heterotrophic biofilms. *Science of the Total Environment, 544*, 722-729.

Heys, K. A., Shore, R. F., Pereira, M. G., Jones, K. C., & Martin, F. L. (2016). Risk assessment of environmental mixture effects. *RSC Advances*, 6(53), 47844-47857.

Ho, C. M., Yau, S. K. W., Lok, C. N., So, M. H., & Che, C. M. (2010). Oxidative dissolution of silver nanoparticles by biologically relevant oxidants: a kinetic and mechanistic study. *Chemistry–An Asian Journal, 5*(2), 285-293.

Hoang, V., Delatolla, R., Abujamel, T., Mottawea, W., Gadbois, A., Laflamme, E., & Stintzi, A. (2014). Nitrifying moving bed biofilm reactor (MBBR) biofilm and biomass response to long term exposure to 1 C. *Water Research, 49*, 215-224.

Hoque, M. E., Khosravi, K., Newman, K., & Metcalfe, C. D. (2012). Detection and characterization of silver nanoparticles in aqueous matrices using asymmetric-flow field flow fractionation with inductively coupled plasma mass spectrometry. *Journal of Chromatography A, 1233*, 109-115.

Hou, J., Miao, L., Wang, C., Wang, P., Ao, Y., & Lv, B. (2015a). Effect of CuO nanoparticles on the production and composition of extracellular polymeric substances and physicochemical stability of activated sludge flocs. *Bioresource Technology, 176*, 65-70.

Hou, J., You, G., Xu, Y., Wang, C., Wang, P., Miao, L., Lv, B. (2015b). Effects of CeO_2 nanoparticles on biological nitrogen removal in a sequencing batch biofilm reactor and mechanism of toxicity. *Bioresource Technology, 191*, 73-78.

Hou, L., Li, K., Ding, Y., Li, Y., Chen, J., Wu, X., & Li, X. (2012a). Removal of silver nanoparticles in simulated wastewater treatment processes and its impact on COD and NH_4 reduction. *Chemosphere, 87*(3), 248-252.

Hou, L., Li, K., Ding, Y., Li, Y., Chen, J., Wu, X., & Li, X. (2012b). Removal of silver nanoparticles in simulated wastewater treatment processes and its impact on COD and NH_4 reduction. *Chemosphere, 87*(3), 248-252.

Hsiao, I.-L., Hsieh, Y.-K., Wang, C.-F., Chen, I.-C., & Huang, Y.-J. (2015). Trojan-horse mechanism in the cellular uptake of silver nanoparticles verified by direct intra-and extracellular silver speciation analysis. *Environmental Science & Technology, 49*(6), 3813-3821.

Hu, Z., Lu, X., Sun, P., Hu, Z., Wang, R., Lou, C., & Han, J. (2017). Understanding the performance of microbial community induced by ZnO nanoparticles in enhanced biological phosphorus removal system and its recoverability. *Bioresource Technology*, 225, 279-285.

Huang, L., Zhao, S., Wang, Z., Wu, J., Wang, J., & Wang, S. (2016). In situ immobilization of silver nanoparticles for improving permeability, antifouling and anti-bacterial properties of ultrafiltration membrane. *Journal of Membrane Science, 499*, 269-281.

Huynh, K. A., & Chen, K. L. (2011). Aggregation kinetics of citrate and polyvinylpyrrolidone coated silver nanoparticles in monovalent and divalent electrolyte solutions. *Environmental Science & Technology, 45*(13), 5564-5571.

Ivask, A., Kurvet, I., Kasemets, K., Blinova, I., Aruoja, V., Suppi, S., Heinlaan, M. (2014). Size-dependent toxicity of silver nanoparticles to bacteria, yeast, algae, crustaceans and mammalian cells in vitro. *PloS one, 9*(7), e102108.

Oksanen, J., Blanchet, F. G., Kindt, R., Legendre, P., O'hara, R. B., Simpson, G. L., Wagner, H. (2010). Vegan: community ecology package. R package version 1.17-4.https://CRAN.R-project.org/package=vegan

Jeong, E., Chae, S., Kang, S., & Shin, H.-S. (2012). Effects of silver nanoparticles on biological nitrogen removal processes. *Water Science and Technology, 65*(7), 1298-1303.

Jeong, E., Im, W.-T., Kim, D.-H., Kim, M.-S., Kang, S., Shin, H.-S., & Chae, S.-R. (2014). Different susceptibilities of bacterial community to silver nanoparticles in wastewater treatment systems. *Journal of Environmental Science and Health, Part A, 49*(6), 685-693.

Jian-Zhou, H., Cheng-Cheng, L., Deng-Jun, W., & Zhou, D.-M. (2015). Biofilms and extracellular polymeric substances mediate the transport of graphene oxide nanoparticles in saturated porous media. *Journal of Hazardous Materials*, 300, 467-474.

Jiang, Q., Ngo, H. H., Nghiem, L. D., Hai, F. I., Price, W. E., Zhang, J., Guo, W. (2018). Effect of hydraulic retention time on the performance of a hybrid moving bed biofilm reactor-membrane bioreactor system for micropollutants removal from municipal wastewater. *Bioresource Technology, 247*, 1228-1232.

Jiménez-Lamana, J., & Slaveykova, V. I. (2016). Silver nanoparticle behaviour in lake water depends on their surface coating. *Science of the Total Environment, 573*, 946-953.

Johnson, A., Cisowska, I., Jurgens, M., Keller, V., Lawlor, A., & Williams, R. (2011). Exposure assessment for engineered silver nanoparticles throughout the rivers of England and Wales (CB0433). *Centre for Ecology and Hydrology, UK*.

Johnson, A. C., Jürgens, M. D., Lawlor, A. J., Cisowska, I., & Williams, R. J. (2014). Particulate and colloidal silver in sewage effluent and sludge discharged from British wastewater treatment plants. *Chemosphere, 112*, 49-55.

Jośko, I., Oleszczuk, P., & Skwarek, E. (2017). Toxicity of combined mixtures of nanoparticles to plants. *Journal of Hazardous Materials*, 331, 200-209.

Kaegi, R., Sinnet, B., Zuleeg, S., Hagendorfer, H., Mueller, E., Vonbank, R., Burkhardt, M. (2010). Release of silver nanoparticles from outdoor facades. *Environmental Pollution, 158*(9), 2900-2905.

Kaegi, R., Voegelin, A., Ort, C., Sinnet, B., Thalmann, B., Krismer, J., Mueller, E. (2013). Fate and transformation of silver nanoparticles in urban wastewater systems. *Water Research, 47*(12), 3866-3877.

Kalishwaralal, K., BarathManiKanth, S., Pandian, S. R. K., Deepak, V., & Gurunathan, S. (2010). Silver nanoparticles impede the biofilm formation by *Pseudomonas aeruginosa* and *Staphylococcus epidermidis*. *Colloids and Surfaces B: Biointerfaces, 79*(2), 340-344.

Kampe, S., Kaegi, R., Schlich, K., Wasmuth, C., Hollert, H., & Schlechtriem, C. (2018). Silver nanoparticles in sewage sludge: Bioavailability of sulfidized silver to the terrestrial isopod Porcellio scaber. *Environmental Toxicology and Chemistry, 37*(6), 1606-1613.

Kapoor, V., Phan, D., & Pasha, A. T. (2018). Effects of metal oxide nanoparticles on nitrification in wastewater treatment systems: A systematic review. *Journal of Environmental Science and Health, Part A*, 53(7), 659-668.

Kawata, K., Osawa, M., & Okabe, S. (2009). In vitro toxicity of silver nanoparticles at noncytotoxic doses to HepG2 human hepatoma cells. *Environmental Science & Technology, 43*(15), 6046-6051.

Kedia, A., & Kumar, P. S. (2012). Solvent-adaptable poly (vinylpyrrolidone) binding induced anisotropic shape control of gold nanostructures. *The Journal of Physical Chemistry C*, 116(44), 23721-23728.

Keller, A. A., Huang, Y., & Nelson, J. (2018). Detection of nanoparticles in edible plant tissues exposed to nano-copper using single-particle ICP-MS. *Journal of Nanoparticle Research, 20*(4), 101.

Keller, A. A., & Lazareva, A. (2013). Predicted releases of engineered nanomaterials: from global to regional to local. *Environmental Science & Technology Letters, 1*(1), 65-70.

Keller, A. A., McFerran, S., Lazareva, A., & Suh, S. (2013). Global life cycle releases of engineered nanomaterials. *Journal of Nanoparticle Research, 15*(6), 1692.

Kent, R. D., Oser, J. G., & Vikesland, P. J. (2014). Controlled evaluation of silver nanoparticle sulfidation in a full-scale wastewater treatment plant. *Environmental Science & Technology, 48*(15), 8564-8572.

Kermani, M., Bina, B., Movahedian, H., Amin, M., & Nikaein, M. (2008). Application of moving bed biofilm process for biological organics and nutrients removal from municipal wastewater. *American Journal of Environmental Sciences, 4*(6), 675.

Kim, B., Miller, J. H., Monsegue, N., Levard, C., Hong, Y., Hull, M. S., Knocke, W. R. (2016). Silver sulfidation in thermophilic anaerobic digesters and effects on antibiotic resistance genes. *Environmental Engineering Science, 33*(1), 1-10.

Kim, J. Y., Lee, C., Cho, M., & Yoon, J. (2008). Enhanced inactivation of *E. coli* and MS-2 phage by silver ions combined with UV-A and visible light irradiation. *Water Research, 42*(1), 356-362.

Kragelund, C., Tang, K., Ooi, G. T. H., Christensen, A., Kaarsholm, K. M. S., Sund, C.,. Andersen, J. (2018). *New innovative Moving Bed Biofilm Reactor (MBBR) concept removes pharmaceutical from municipal wastewater using only biological polishing.* Paper presented at the 12th Annual Water Research Meeting of Danish Water Forum.

Kroll, A., Behra, R., Kaegi, R., & Sigg, L. (2014). Extracellular polymeric substances (EPS) of freshwater biofilms stabilize and modify CeO_2 and Ag nanoparticles. *PLoS One, 9*(10), e110709.

Kubo, A.-L., Capjak, I., Vrček, I. V., Bondarenko, O. M., Kurvet, I., Vija, H., Kahru, A. (2018). Antimicrobial potency of differently coated 10 and 50 nm silver nanoparticles against clinically relevant bacteria *Escherichia coli* and *Staphylococcus aureus*. *Colloids and Surfaces B: Biointerfaces, 170*, 401-410.

Kumar, A., Vemula, P. K., Ajayan, P. M., & John, G. (2008). Silver-nanoparticle-embedded antimicrobial paints based on vegetable oil. *Nature Materials, 7*(3), 236.

Laborda, F., Bolea, E., Cepriá, G., Gómez, M. T., Jiménez, M. S., Pérez-Arantegui, J., & Castillo, J. R. (2016). Detection, characterization and quantification of inorganic engineered nanomaterials: a review of techniques and methodological approaches for the analysis of complex samples. *Analytica Chimica Acta, 904*, 10-32.

Lazareva, A., & Keller, A. A. (2014). Estimating potential life cycle releases of engineered nanomaterials from wastewater treatment plants. *ACS Sustainable Chemistry & Engineering, 2*(7), 1656-1665.

Lead, J. R., Batley, G. E., Alvarez, P. J., Croteau, M. N., Handy, R. D., McLaughlin, M. J., Schirmer, K. (2018). Nanomaterials in the environment: behavior, fate, bioavailability,

and effects—an updated review. *Environmental Toxicology and Chemistry, 37*(8), 2029-2063.

Levard, C., Reinsch, B. C., Michel, F. M., Oumahi, C., Lowry, G. V., & Brown Jr, G. E. (2011). Sulfidation processes of PVP-coated silver nanoparticles in aqueous solution: impact on dissolution rate. *Environmental Science & Technology, 45*(12), 5260-5266.

Levard, C.., Mitra, S., Yang, T., Jew, A. D., Badireddy, A. R., Lowry, G. V., & Brown Jr, G. E. (2013). Effect of chloride on the dissolution rate of silver nanoparticles and toxicity to *E. coli*. *Environmental Science & Ttechnology, 47*(11), 5738-5745.

Leyva-Díaz, J., Martín-Pascual, J., & Poyatos, J. (2017). Moving bed biofilm reactor to treat wastewater. *International Journal of Environmental Science and Technology, 14*(4), 881-910.

Li, L., Hartmann, G., Döblinger, M., & Schuster, M. (2013). Quantification of nanoscale silver particles removal and release from municipal wastewater treatment plants in Germany. *Environmental Science & Technology, 47*(13), 7317-7323.

Li, L., Leopold, K., & Schuster, M. (2012). Effective and selective extraction of noble metal nanoparticles from environmental water through a noncovalent reversible reaction on an ionic exchange resin. *Chemical Communications, 48*(73), 9165-9167.

Li, W.-R., Xie, X.-B., Shi, Q.-S., Zeng, H.-Y., You-Sheng, O.-Y., & Chen, Y.-B. (2010a). Antibacterial activity and mechanism of silver nanoparticles on *Escherichia coli*. *Applied Microbiology and Biotechnology, 85*(4), 1115-1122.

Li, X., & Lenhart, J. J. (2012). Aggregation and dissolution of silver nanoparticles in natural surface water. *Environmental Science & Technology, 46*(10), 5378-5386.

Li, X., Lenhart, J. J., & Walker, H. W. (2010b). Dissolution-accompanied aggregation kinetics of silver nanoparticles. *Langmuir, 26*(22), 16690-16698.

Li, X., Lenhart, J. J., & Walker, H. W. (2011). Aggregation kinetics and dissolution of coated silver nanoparticles. *Langmuir, 28*(2), 1095-1104.

Liang, Z., Das, A., & Hu, Z. (2010). Bacterial response to a shock load of nanosilver in an activated sludge treatment system. *Water Research, 44*(18), 5432-5438.

Lin, H., Ye, C., Lv, L., Zheng, C. R., Zhang, S., Zheng, L., Yu, X. (2014). Characterization of extracellular polymeric substances in the biofilms of typical bacteria by the sulfur K-edge XANES spectroscopy. *Journal of Environmental Sciences, 26*(8), 1763-1768.

Lin, S., Cheng, Y., Liu, J., & Wiesner, M. R. (2012). Polymeric coatings on silver nanoparticles hinder autoaggregation but enhance attachment to uncoated surfaces. *Langmuir, 28*(9), 4178-4186.

Liu, C., Leng, W., & Vikesland, P. J. (2018a). Controlled evaluation of the impacts of surface coatings on silver nanoparticle dissolution rates. *Environmental Science & Technology, 52*(5), 2726-2734.

Liu, J.-f., Chao, J.-b., Liu, R., Tan, Z.-q., Yin, Y.-g., Wu, Y., & Jiang, G.-b. (2009). Cloud point extraction as an advantageous preconcentration approach for analysis of trace silver nanoparticles in environmental waters. *Analytical Chemistry, 81*(15), 6496-6502.

Liu, J., & Hurt, R. H. (2010). Ion release kinetics and particle persistence in aqueous nano-silver colloids. *Environ. Sci. Technol, 44*(6), 2169-2175.

Liu, J., Pennell, K. G., & Hurt, R. H. (2011). Kinetics and mechanisms of nanosilver oxysulfidation. *Environmental Science & Technology, 45*(17), 7345-7353.

Liu, J., Wang, Z., Liu, F. D., Kane, A. B., & Hurt, R. H. (2012). Chemical transformations of nanosilver in biological environments. *ACS Nano, 6*(11), 9887-9899.

Liu, J., Williams, P. C., Geisler-Lee, J., Goodson, B. M., Fakharifar, M., Peiravi, M., Gemeinhardt, M. E. (2018b). Impact of wastewater effluent containing aged nanoparticles and other components on biological activities of the soil microbiome, Arabidopsis plants, and earthworms. *Environmental Research, 164*, 197-203.

Liu, X., Tang, B., Gu, Q., & Yu, X. (2014). Elimination of the formation of biofilm in industrial pipes using enzyme cleaning technique. *MethodsX, 1*, 130-136.

Liu, X., Yang, X., Hu, X., He, Q., Zhai, J., Chen, Y., Vymazal, J. (2019). Comprehensive metagenomic analysis reveals the effects of silver nanoparticles on nitrogen transformation in constructed wetlands. *Chemical Engineering Journal*, 358, 1552-1560.

Lopes, S., Pinheiro, C., Soares, A. M., & Loureiro, S. (2016). Joint toxicity prediction of nanoparticles and ionic counterparts: Simulating toxicity under a fate scenario. *Journal of Hazardous Materials*, 320, 1-9.

Lou, L., Yu, W., & Ramkumar, S. (2019). Wearable and smart responsive textiles. *High Performance Technical Textiles*, 439-473.

Loupasaki, E., & Diamadopoulos, E. (2013). Attached growth systems for wastewater treatment in small and rural communities: a review. *Journal of Chemical Technology & Biotechnology, 88*(2), 190-204.

Ma, Y., Metch, J. W., Vejerano, E. P., Miller, I. J., Leon, E. C., Marr, L. C., Pruden, A. (2015). Microbial community response of nitrifying sequencing batch reactors to silver, zero-valent iron, titanium dioxide and cerium dioxide nanomaterials. *Water Research, 68*, 87-97.

Mahdi, K. N., Peters, R. J., Klumpp, E., Bohme, S., Van der Ploeg, M., Ritsema, C., & Geissen, V. (2017). Silver nanoparticles in soil: aqueous extraction combined with single-particle ICP-MS for detection and characterization. *Environmental Nanotechnology, Monitoring & Management, 7*, 24-33.

Mallevre, F., Fernandes, T. F., & Aspray, T. J. (2016). *Pseudomonas putida* biofilm dynamics following a single pulse of silver nanoparticles. *Chemosphere, 153*, 356-364.

Maynard, A. D., Aitken, R. J., Butz, T., Colvin, V., Donaldson, K., Oberdörster, G., Stone, V. (2006). Safe handling of nanotechnology. *Nature, 444*(7117), 267.

McGee, C., Storey, S., Clipson, N., & Doyle, E. (2017). Soil microbial community responses to contamination with silver, aluminium oxide and silicon dioxide nanoparticles. *Ecotoxicology*, 26(3), 449-458.

McGillicuddy, E., Murray, I., Kavanagh, S., Morrison, L., Fogarty, A., Cormican, M., Morris, D. (2017). Silver nanoparticles in the environment: Sources, detection and ecotoxicology. *Science of the Total Environment, 575*, 231-246.

McQuarrie, J. P., & Boltz, J. P. (2011). Moving bed biofilm reactor technology: process applications, design, and performance. *Water Environment Research, 83*(6), 560-575.

Meier, C., Voegelin, A., Pradas del Real, A., Sarret, G., Mueller, C. R., & Kaegi, R. (2016). Transformation of silver nanoparticles in sewage sludge during incineration. *Environmental Science & Technology, 50*(7), 3503-3510.

Meincke, M., Bock, E., Kastrau, D., & Kroneck, P. M. (1992). Nitrite oxidoreductase from *Nitrobacter hamburgensis*: redox centers and their catalytic role. *Archives of Microbiology, 158*(2), 127-131.

Merrifield, R. C., Stephan, C., & Lead, J. (2017). Determining the concentration dependent transformations of Ag nanoparticles in complex media: Using SP-ICP-MS and Au@ Ag core–shell nanoparticles as tracers. *Environmental Science & Technology, 51*(6), 3206-3213.

Metcalf, & Eddy-AECOM. (2014). *Wastewater Engineering:Ttreatment and Resource Recovery. 5th ed.*,New York: McGraw-Hill

Metch, J. W., Burrows, N. D., Murphy, C. J., Pruden, A., & Vikesland, P. J. (2018). Metagenomic analysis of microbial communities yields insight into impacts of nanoparticle design. *Nature Nanotechnology*, 13(3), 253.

Metch, J. W., Ma, Y., Pruden, A., & Vikesland, P. J. (2015). Enhanced disinfection by-product formation due to nanoparticles in wastewater treatment plant effluents. *Environmental Science: Water Research & Technology*, 1(6), 823-831.

Miao, L., Wang, C., Hou, J., Wang, P., Ao, Y., Li, Y., You, G. (2017). Response of wastewater biofilm to CuO nanoparticle exposure in terms of extracellular polymeric substances and microbial community structure. *Science of the Total Environment, 579*, 588-597.

Mirzajani, F., Ghassempour, A., Aliahmadi, A., & Esmaeili, M. A. (2011). Antibacterial effect of silver nanoparticles on *Staphylococcus aureus*. *Research in Microbiology, 162*(5), 542-549.

Mitrano, D., Ranville, J., Bednar, A., Kazor, K., Hering, A., & Higgins, C. (2014). Tracking dissolution of silver nanoparticles at environmentally relevant concentrations in laboratory, natural, and processed waters using single particle ICP-MS (spICP-MS). *Environmental Science: Nano, 1*(3), 248-259.

Mitrano, D. M., Barber, A., Bednar, A., Westerhoff, P., Higgins, C. P., & Ranville, J. F. (2012). Silver nanoparticle characterization using single particle ICP-MS (SP-ICP-MS) and asymmetrical flow field flow fractionation ICP-MS (AF4-ICP-MS). *Journal of Analytical Atomic Spectrometry, 27*(7), 1131-1142.

Mitrano, D. M., Lesher, E. K., Bednar, A., Monserud, J., Higgins, C. P., & Ranville, J. F. (2012). Detecting nanoparticulate silver using single-particle inductively coupled plasma–mass spectrometry. *Environmental Toxicology and Chemistry, 31*(1), 115-121.

Mitzel, M. R., & Tufenkji, N. (2014). Transport of industrial PVP-stabilized silver nanoparticles in saturated quartz sand coated with *Pseudomonas aeruginosa* PAO1 biofilm of variable age. *Environmental Science & Technology, 48*(5), 2715-2723.

Mohanta, Y. K., Panda, S. K., Bastia, A. K., & Mohanta, T. K. (2017). Biosynthesis of silver nanoparticles from *Protium serratum* and investigation of their potential impacts on food safety and control. *Frontiers in Microbiology, 8*, 626.

Molleman, B., & Hiemstra, T. (2017). Time, pH, and size dependency of silver nanoparticle dissolution: the road to equilibrium. *Environmental Science: Nano*, 4(6), 1314-1327.

Morones, J. R., Elechiguerra, J. L., Camacho, A., Holt, K., Kouri, J. B., Ramírez, J. T., & Yacaman, M. J. (2005). The bactericidal effect of silver nanoparticles. *Nanotechnology, 16*(10), 2346.

Mu, H., & Chen, Y. (2011). Long-term effect of ZnO nanoparticles on waste activated sludge anaerobic digestion. *Water Research, 45*(17), 5612-5620.

Mueller, N. C., & Nowack, B. (2008). Exposure modeling of engineered nanoparticles in the environment. *Environmental Science & Technology, 42*(12), 4447-4453.

Nath, J., Dror, I., Landa, P., Vanek, T., Kaplan-Ashiri, I., & Berkowitz, B. (2018). Synthesis and characterization of isotopically-labeled silver, copper and zinc oxide nanoparticles for tracing studies in plants. *Environmental Pollution, 242*, 1827-1837.

Navarro, E., Piccapietra, F., Wagner, B., Marconi, F., Kaegi, R., Odzak, N., Behra, R. (2008). Toxicity of silver nanoparticles to Chlamydomonas reinhardtii. *Environmental Science & Technology, 42*(23), 8959-8964.

Navratilova, J., Praetorius, A., Gondikas, A., Fabienke, W., von der Kammer, F., & Hofmann, T. (2015). Detection of engineered copper nanoparticles in soil using single particle ICP-MS. *International Journal of Environmental Research and Public Health, 12*(12), 15756-15768.

Neale, P. A., Jämting, Å. K., Escher, B. I., & Herrmann, J. (2013). A review of the detection, fate and effects of engineered nanomaterials in wastewater treatment plants. *Water Science and Technology, 68*(7), 1440-1453.

Nogueira, R., Melo, L. s. F., Purkhold, U., Wuertz, S., & Wagner, M. (2002). Nitrifying and heterotrophic population dynamics in biofilm reactors: effects of hydraulic retention time and the presence of organic carbon. *Water Research, 36*(2), 469-481.

Nowack, B. (2017). Evaluation of environmental exposure models for engineered nanomaterials in a regulatory context. *NanoImpact, 8*, 38-47.

Nowack, B., Krug, H. F., & Height, M. (2011). 120 years of nanosilver history: implications for policy makers: ACS Publications, 1177-1183.

Ødegaard, H. (2000). Advanced compact wastewater treatment based on coagulation and moving bed biofilm processes. *Water Science and Technology, 42*(12), 33-48.

Ødegaard, H. (2006). Innovations in wastewater treatment:–the moving bed biofilm process. *Water Science and Technology, 53*(9), 17-33.

Ødegaard, H. (2016). A road-map for energy-neutral wastewater treatment plants of the future based on compact technologies (including MBBR). *Frontiers of Environmental Science & Engineering, 10*(4), 2.

OECD. (1976). Proposed method for the determination of the biodegradability of surfactants used in synthetic detergents. Organisation for Economic Co-operation and Development, Paris, France.

Ortega-Vinuesa, J., Martın-Rodrıguez, A., & Hidalgo-Alvarez, R. (1996). Colloidal stability of polymer colloids with different interfacial properties: mechanisms. *Journal of Colloid and Interface Science, 184*(1), 259-267.

Oyarzun, P., Alarcón, L., Calabriano, G., Bejarano, J., Nuñez, D., Ruiz-Tagle, N., & Urrutia, H. (2019). Trickling filter technology for biotreatment of nitrogenous compounds emitted in exhaust gases from fishmeal plants. *Journal of Environmental Management, 232*, 165-170.

Pace, H. E., Rogers, N. J., Jarolimek, C., Coleman, V. A., Gray, E. P., Higgins, C. P., & Ranville, J. F. (2012). Single particle inductively coupled plasma-mass spectrometry: a performance evaluation and method comparison in the determination of nanoparticle size. *Environmental Science & Technology, 46*(22), 12272-12280.

Parada, A. E., Needham, D. M., & Fuhrman, J. A. (2016). Every base matters: assessing small subunit rRNA primers for marine microbiomes with mock communities, time series and global field samples. *Environmental Microbiology, 18*(5), 1403-1414. doi: 10.1111/1462-2920.13023

Park, C.-B., Jung, J.-W., Baek, M., Sung, B., Park, J.-W., Seol, Y., Kim, Y. J. (2019). Mixture toxicity of metal oxide nanoparticles and silver ions on Daphnia magna. *Journal of Nanoparticle Research*, 21(8), 166.

Park, E.-J., Yi, J., Kim, Y., Choi, K., & Park, K. (2010). Silver nanoparticles induce cytotoxicity by a Trojan-horse type mechanism. *Toxicology in vitro*, 24(3), 872-878.

Park, H.-J., Kim, H. Y., Cha, S., Ahn, C. H., Roh, J., Park, S., Kim, Y. (2013a). Removal characteristics of engineered nanoparticles by activated sludge. *Chemosphere*, 92(5), 524-528.

Park, H.-J., Kim, J. Y., Kim, J., Lee, J.-H., Hahn, J.-S., Gu, M. B., & Yoon, J. (2009). Silver-ion-mediated reactive oxygen species generation affecting bactericidal activity. *Water Research*, 43(4), 1027-1032.

Park, H.-J., Park, S., Roh, J., Kim, S., Choi, K., Yi, J., Yoon, J. (2013b). Biofilm-inactivating activity of silver nanoparticles: a comparison with silver ions. *Journal of Industrial and Engineering Chemistry*, 19(2), 614-619.

Patlolla, A. K., Berry, A., May, L., & Tchounwou, P. B. (2012). Genotoxicity of silver nanoparticles in *Vicia faba*: a pilot study on the environmental monitoring of nanoparticles. *International Journal of Environmental Research and Public Health, 9*(5), 1649-1662.

Peulen, T.-O., & Wilkinson, K. J. (2011). Diffusion of nanoparticles in a biofilm. *Environmental Science & Technology, 45*(8), 3367-3373.

Pokhrel, L. R., Silva, T., Dubey, B., El Badawy, A. M., Tolaymat, T. M., & Scheuerman, P. R. (2012). Rapid screening of aquatic toxicity of several metal-based nanoparticles using the MetPLATE™ bioassay. *Science of the Total Environment, 426*, 414-422.

Potter, P. M., Navratilova, J., Rogers, K. R., & Al-Abed, S. R. (2019). Transformation of silver nanoparticle consumer products during simulated usage and disposal. *Environmental Science: Nano*, 6(2), 592-598.

Prabhu, S., & Poulose, E. K. (2012). Silver nanoparticles: mechanism of antimicrobial action, synthesis, medical applications, and toxicity effects. *International Nano Letters, 2*(1), 32.

Pulit-Prociak, J., & Banach, M. (2016). Silver nanoparticles–a material of the future? *Open Chemistry, 14*(1), 76-91.

Purkhold, U., Wagner, M., Timmermann, G., Pommerening-Röser, A., & Koops, H.-P. (2003). 16S rRNA and amoA-based phylogeny of 12 novel betaproteobacterial ammonia-oxidizing isolates: extension of the dataset and proposal of a new lineage within the nitrosomonads. *International Journal of Systematic and Evolutionary Microbiology, 53*(5), 1485-1494.

Qaderi, F., Sayahzadeh, A., & Azizi, M. (2018). Efficiency optimization of petroleum wastewater treatment by using of serial moving bed biofilm reactors. *Journal of Cleaner Production, 192*, 665-677.

Qiu, G., Wirianto, K., Sun, Y., & Ting, Y.-P. (2016). Effect of silver nanoparticles on system performance and microbial community dynamics in a sequencing batch reactor. *Journal of Cleaner Production, 130*, 137-142.

Quan, X., Cen, Y., Lu, F., Gu, L., & Ma, J. (2015). Response of aerobic granular sludge to the long-term presence to nanosilver in sequencing batch reactors: reactor performance, sludge property, microbial activity and community. *Science of the Total Environment, 506*, 226-233.

Quast, C., Pruesse, E., Yilmaz, P., Gerken, J., Schweer, T., Yarza, P., Glöckner, F. O. (2013). The SILVA ribosomal RNA gene database project: improved data processing and web-based tools. *Nucleic Acids Research, 41*(Database issue), D590-D596. doi: 10.1093/nar/gks1219

Radniecki, T. S., Stankus, D. P., Neigh, A., Nason, J. A., & Semprini, L. (2011). Influence of liberated silver from silver nanoparticles on nitrification inhibition of *Nitrosomonas europaea*. *Chemosphere, 85*(1), 43-49.

Reboleiro-Rivas, P., Martín-Pascual, J., Juárez-Jiménez, B., Poyatos, J., Hontoria, E., Rodelas, B., & González-López, J. (2013). Enzymatic activities in a moving bed membrane bioreactor for real urban wastewater treatment: effect of operational conditions. *Ecological Engineering, 61*, 23-33.

Reidy, B., Haase, A., Luch, A., Dawson, K., & Lynch, I. (2013). Mechanisms of silver nanoparticle release, transformation and toxicity: a critical review of current knowledge and recommendations for future studies and applications. *Materials, 6*(6), 2295-2350.

Revilla, M., Galán, B., & Viguri, J. R. (2016). An integrated mathematical model for chemical oxygen demand (COD) removal in moving bed biofilm reactors (MBBR) including predation and hydrolysis. *Water Research, 98*, 84-97.

Roco, M. C. (2011). The long view of nanotechnology development: the National Nanotechnology Initiative at 10 years: Springer.

Rujido-Santos, I., Naveiro-Seijo, L., Herbello-Hermelo, P., del Carmen Barciela-Alonso, M., Bermejo-Barrera, P., & Moreda-Piñeiro, A. (2019). Silver nanoparticles assessment in moisturizing creams by ultrasound assisted extraction followed by sp-ICP-MS. *Talanta, 197*, 530-538.

Rusten, B., Eikebrokk, B., Ulgenes, Y., & Lygren, E. (2006). Design and operations of the Kaldnes moving bed biofilm reactors. *Aquacultural Engineering, 34*(3), 322-331.

Safwat, S. M. (2018). Performance of moving bed biofilm reactor using effective microorganisms. *Journal of Cleaner Production, 185*, 723-731.

Schirmer, K. (2014). Mechanisms of nanotoxicity *Frontiers of Nanoscience* (Vol. 7, pp. 195-221): Elsevier.

Schug, H., Isaacson, C. W., Sigg, L., Ammann, A. A., & Schirmer, K. (2014). Effect of TiO_2 nanoparticles and UV radiation on extracellular enzyme activity of intact heterotrophic biofilms. *Environmental Science & Technology*, *48*(19), 11620-11628.

Schwertfeger, D., Velicogna, J. R., Jesmer, A. H., Saatcioglu, S., McShane, H., Scroggins, R. P., & Princz, J. I. (2017). Extracting metallic nanoparticles from soils for quantitative analysis: Method development using engineered silver nanoparticles and SP-ICP-MS. *Analytical Chemistry, 89*(4), 2505-2513.

Seitz, F., Rosenfeldt, R. R., Storm, K., Metreveli, G., Schaumann, G. E., Schulz, R., & Bundschuh, M. (2015). Effects of silver nanoparticle properties, media pH and dissolved organic matter on toxicity to *Daphnia magna*. *Ecotoxicology and Environmental Safety, 111*, 263-270.

Servin, A. D., & White, J. C. (2016). Nanotechnology in agriculture: next steps for understanding engineered nanoparticle exposure and risk. *NanoImpact*, 1, 9-12.

Shafer, M. M., Overdier, J. T., & Armstong, D. E. (1998). Removal, partitioning, and fate of silver and other metals in wastewater treatment plants and effluent-receiving streams. *Environmental Toxicology and Chemistry: An International Journal*, *17*(4), 630-641.

Sharma, V. K., Sayes, C. M., Guo, B., Pillai, S., Parsons, J. G., Wang, C., Ma, X. (2019). Interactions between silver nanoparticles and other metal nanoparticles under environmentally relevant conditions: A review. *Science of the Total Environment, 653*, 1042-1051.

Sheng, Z., & Liu, Y. (2011). Effects of silver nanoparticles on wastewater biofilms. *Water Research*, *45*(18), 6039-6050.

Sheng, Z., Van Nostrand, J. D., Zhou, J., & Liu, Y. (2015). The effects of silver nanoparticles on intact wastewater biofilms. *Frontiers in Microbiology*, 6, 680.

Sheng, Z., Van Nostrand, J. D., Zhou, J., & Liu, Y. (2018). Contradictory effects of silver nanoparticles on activated sludge wastewater treatment. *Journal of Hazardous Materials, 341*, 448-456.

Silva-Teira, A., Vázquez-Padín, J. R., Weiler, R., Fernández-González, R., Rogalla, F., & Garrido, J. M. (2018). Performance of a hybrid membrane bioreactor treating a low strength and alkalinity wastewater. *Process Biochemistry, 66*, 176-182.

Silva, T., Pokhrel, L. R., Dubey, B., Tolaymat, T. M., Maier, K. J., & Liu, X. (2014). Particle size, surface charge and concentration dependent ecotoxicity of three organo-coated silver nanoparticles: comparison between general linear model-predicted and observed toxicity. *Science of the Total Environment, 468*, 968-976.

Singh, A. K., Yadav, T. P., Pandey, B., Gupta, V., & Singh, S. P. (2019). Engineering nanomaterials for smart drug release: Recent advances and challenges. *Applications of Targeted Nano Drugs and Delivery Systems* (pp. 411-449): Elsevier.

Singla, R., Abidi, S. M., Dar, A. I., & Acharya, A. (2019). Nanomaterials as potential and versatile platform for next generation tissue engineering applications. *Journal of Biomedical Materials Research Part B: Applied Biomaterials*.

Song, J. E., Phenrat, T., Marinakos, S., Xiao, Y., Liu, J., Wiesner, M. R., Lowry, G. V. (2011). Hydrophobic interactions increase attachment of gum arabic-and PVP-coated Ag nanoparticles to hydrophobic surfaces. *Environmental Science & Technology, 45*(14), 5988-5995.

Song, R., Qin, Y., Suh, S., & Keller, A. A. (2017). Dynamic model for the stocks and release flows of engineered nanomaterials. *Environmental Science & Technology, 51*(21), 12424-12433.

Sonwani, R. K., Swain, G., Giri, B. S., Singh, R. S., & Rai, B. N. (2019). A novel comparative study of modified carriers in moving bed biofilm reactor for the treatment of wastewater: Process optimization and kinetic study. *Bioresource Technology*, *281*, 335-342.

Spieck, E., Ehrich, S., Aamand, J., & Bock, E. (1998). Isolation and immunocytochemical location of the nitrite-oxidizing system in *Nitrospira moscoviensis*. *Archives of Microbiology, 169*(3), 225-230.

Stehr, G., Zörner, S., Böttcher, B., & Koops, H. (1995). Exopolymers: an ecological characteristic of a floc-attached, ammonia-oxidizing bacterium. *Microbial Ecology, 30*(2), 115-126.

Stewart, P. S., & Franklin, M. J. (2008). Physiological heterogeneity in biofilms. *Nature Reviews Microbiology*, *6*(3), 199-210.

Su, H.-L., Lin, S.-H., Wei, J.-C., Pao, I.-C., Chiao, S.-H., Huang, C.-C., Lin, J.-J. (2011). Novel nanohybrids of silver particles on clay platelets for inhibiting silver-resistant bacteria. *PloS one, 6*(6), e21125.

Suarez, C., Piculell, M., Modin, O., Langenheder, S., Persson, F., & Hermansson, M. (2019). Thickness determines microbial community structure and function in nitrifying biofilms via deterministic assembly. *Scientific Reports, 9*(1), 5110.

Sun, Y., Guan, Y., Wang, D., Liang, K., & Wu, G. (2018). Potential roles of acyl homoserine lactone based quorum sensing in sequencing batch nitrifying biofilm reactors with or without the addition of organic carbon. *Bioresource technology, 259*, 136-145.

Sutcliffe, I. C. (2011). Cell envelope architecture in the *Chloroflexi*: a shifting frontline in a phylogenetic turf war. *Environmental Microbiology, 13*(2), 279-282.

Tan, C. H., Koh, K. S., Xie, C., Tay, M., Zhou, Y., Williams, R., Kjelleberg, S. (2014). The role of quorum sensing signalling in EPS production and the assembly of a sludge community into aerobic granules. *The ISME journal, 8*(6), 1186.

Tan, J.-M., Qiu, G., & Ting, Y.-P. (2015). Osmotic membrane bioreactor for municipal wastewater treatment and the effects of silver nanoparticles on system performance. *Journal of Cleaner Production, 88*, 146-151.

Tang, J., Wu, Y., Esquivel-Elizondo, S., Sørensen, S. J., & Rittmann, B. E. (2018). How microbial aggregates protect against nanoparticle toxicity. *Trends in Biotechnology*. *36*(11)1171-1182.

Tang, W.-W., Zeng, G.-M., Gong, J.-L., Liang, J., Xu, P., Zhang, C., & Huang, B.-B. (2014). Impact of humic/fulvic acid on the removal of heavy metals from aqueous solutions using nanomaterials: a review. *Science of the Total Environment*, 468, 1014-1027.

Tejamaya, M., Römer, I., Merrifield, R. C., & Lead, J. R. (2012). Stability of citrate, PVP, and PEG coated silver nanoparticles in ecotoxicology media. *Environmental Science & Technology*, 46(13), 7011-7017.

Telgmann, L., Nguyen, M. T. K., Shen, L., Yargeau, V., Hintelmann, H., & Metcalfe, C. D. (2016). Single particle ICP-MS as a tool for determining the stability of silver nanoparticles in aquatic matrixes under various environmental conditions, including treatment by ozonation. *Analytical and Bioanalytical Chemistry*, 408(19), 5169-5177.

Ter Haseborg, E., Zamora, T. M., Fröhlich, J., & Frimmel, F. H. (2010). Nitrifying microorganisms in fixed-bed biofilm reactors fed with different nitrite and ammonia concentrations. *Bioresource Technology, 101*(6), 1701-1706.

Thalmann, B., Voegelin, A., Von Gunten, U., Behra, R., Morgenroth, E., & Kaegi, R. (2015). Effect of ozone treatment on nano-sized silver sulfide in wastewater effluent. *Environmental Science & Technology*, 49(18), 10911-10919.

Théoret, T., & Wilkinson, K. J. (2017). Evaluation of enhanced darkfield microscopy and hyperspectral analysis to analyse the fate of silver nanoparticles in wastewaters. *Analytical Methods, 9*(26), 3920-3928.

Tiede, K., Boxall, A. B., Wang, X., Gore, D., Tiede, D., Baxter, M., Lewis, J. (2010). Application of hydrodynamic chromatography-ICP-MS to investigate the fate of silver nanoparticles in activated sludge. *Journal of Analytical Atomic Spectrometry, 25*(7), 1149-1154.

Tolaymat, T., El Badawy, A., Genaidy, A., Abdelraheem, W., & Sequeira, R. (2017). Analysis of metallic and metal oxide nanomaterial environmental emissions. *Journal of Cleaner Production, 143*, 401-412.

Tolaymat, T. M., El Badawy, A. M., Genaidy, A., Scheckel, K. G., Luxton, T. P., & Suidan, M. (2010). An evidence-based environmental perspective of manufactured silver nanoparticle in syntheses and applications: a systematic review and critical appraisal of peer-reviewed scientific papers. *Science of the Total Environment, 408*(5), 999-1006.

Toncelli, C., Mylona, K., Kalantzi, I., Tsiola, A., Pitta, P., Tsapakis, M., & Pergantis, S. A. (2017). Silver nanoparticles in seawater: A dynamic mass balance at part per trillion silver concentrations. *Science of the Total Environment, 601*, 15-21.

Torresi, E., Fowler, S. J., Polesel, F., Bester, K., Andersen, H. R., Smets, B. F., Christensson, M. (2016). Biofilm thickness influences biodiversity in nitrifying MBBRs: implications on micropollutant removal. *Environmental Science & Technology*, *50*(17), 9279-9288.

Tuoriniemi, J., Jürgens, M. D., Hassellöv, M., & Cornelis, G. (2017). Size dependence of silver nanoparticle removal in a wastewater treatment plant mesocosm measured by FAST single particle ICP-MS. *Environmental Science: Nano*, *4*(5), 1189-1197.

Unrine, J. M., Colman, B. P., Bone, A. J., Gondikas, A. P., & Matson, C. W. (2012). Biotic and abiotic interactions in aquatic microcosms determine fate and toxicity of Ag nanoparticles. Part 1. Aggregation and dissolution. *Environmental Science & Technology*, *46*(13), 6915-6924.

Van der Hoek, J. P., de Fooij, H., & Struker, A. (2016). Wastewater as a resource: Strategies to recover resources from Amsterdam's wastewater. *Resources, Conservation and Recycling*, *113*, 53-64.

Vance, M. E., Kuiken, T., Vejerano, E. P., McGinnis, S. P., Hochella Jr, M. F., Rejeski, D., & Hull, M. S. (2015). Nanotechnology in the real world: Redeveloping the nanomaterial consumer products inventory. *Beilstein Journal of Nanotechnology*, *6*, 1769.

Venkatesan, A. K., Rodríguez, B. T., Marcotte, A. R., Bi, X., Schoepf, J., Ranville, J. F., Westerhoff, P. (2018). Using single-particle ICP-MS for monitoring metal-containing particles in tap water. *Environmental Science: Water Research & Technology*, *4*(12), 1923-1932.

Vidmar, J., Oprčkal, P., Milačič, R., Mladenovič, A., & Ščančar, J. (2018). Investigation of the behaviour of zero-valent iron nanoparticles and their interactions with Cd^{2+} in wastewater by single particle ICP-MS. *Science of the Total Environment*, *634*, 1259-1268.

Von Mersi, W., & Schinner, F. (1991). An improved and accurate method for determining the dehydrogenase activity of soils with iodonitrotetrazolium chloride. *Biology and Fertility of Soils*, *11*(3), 216-220.

Wagner, M., & Loy, A. (2002). Bacterial community composition and function in sewage treatment systems. *Current Opinion in Biotechnology*, *13*(3), 218-227.

Walden, C., & Zhang, W. (2016). Biofilms versus activated sludge: considerations in metal and metal oxide nanoparticle removal from wastewater. *Environmental Science & Technology*, *50*(16), 8417-8431.

Walden, C., & Zhang, W. (2018). Bioaccumulation of silver nanoparticles in model wastewater biofilms. *Environmental Science: Water Research & Technology*, *4*(8), 1163-1171.

Wang, D., & Chen, Y. (2016). Critical review of the influences of nanoparticles on biological wastewater treatment and sludge digestion. *Critical Reviews in Biotechnology*, *36*(5), 816-828.

Wang, P., You, G., Hou, J., Wang, C., Xu, Y., Miao, L., Zhang, F. (2018). Responses of wastewater biofilms to chronic CeO_2 nanoparticles exposure: Structural, physicochemical and microbial properties and potential mechanism. *Water Research*, *133*, 208-217.

Wang, Y., Westerhoff, P., & Hristovski, K. D. (2012). Fate and biological effects of silver, titanium dioxide, and C_{60} (fullerene) nanomaterials during simulated wastewater treatment processes. *Journal of Hazardous Materials, 201*, 16-22.

Watkinson, A., Murby, E., & Costanzo, S. (2007). Removal of antibiotics in conventional and advanced wastewater treatment: implications for environmental discharge and wastewater recycling. *Water Research, 41*(18), 4164-4176.

Wen, L. S., Santschi, P. H., Gill, G. A., & Tang, D. (2002). Silver concentrations in Colorado, USA, watersheds using improved methodology. *Environmental Toxicology and Chemistry, 21*(10), 2040-2051.

Wiesner, M. R., Lowry, G. V., Alvarez, P., Dionysiou, D., & Biswas, P. (2006). Assessing the risks of manufactured nanomaterials: ACS Publications.

Wigginton, N. S., De Titta, A., Piccapietra, F., Dobias, J., Nesatyy, V., Suter, M. J., & Bernier-Latmani, R. (2010). Binding of silver nanoparticles to bacterial proteins depends on surface modifications and inhibits enzymatic activity. *Environmental Science and Technology, 44*(6), 2163-2168.

Wimmer, A., Ritsema, R., Schuster, M., & Krystek, P. (2019). Sampling and pre-treatment effects on the quantification of (nano) silver and selected trace elements in surface water-Application in a Dutch case study. *Science of the Total Environment, 663*, 154-161.

Wirth, S. M., Lowry, G. V., & Tilton, R. D. (2012). Natural organic matter alters biofilm tolerance to silver nanoparticles and dissolved silver. *Environmental Science & Technology, 46*(22), 12687-12696.

Wu, J., Zhu, G., & Yu, R. (2018). Fates and impacts of nanomaterial contaminants in biological wastewater treatment system: A review. *Water, Air, & Soil Pollution, 229*(1), 9.

Wu, Y.-L., Putcha, N., Ng, K. W., Leong, D. T., Lim, C. T., Loo, S. C. J., & Chen, X. (2012). Biophysical responses upon the interaction of nanomaterials with cellular interfaces. *Accounts of Chemical Research, 46*(3), 782-791.

Xu, Q., Li, S., Wan, Y., Wang, S., Ma, B., She, Z., Jin, C. (2017a). Impacts of silver nanoparticles on performance and microbial community and enzymatic activity of a sequencing batch reactor. *Journal of Environmental Management, 204*, 667-673.

Xu, Y., Wang, C., Hou, J., Wang, P., Miao, L., You, G., Zhang, F. (2017b). Long term effects of cerium dioxide nanoparticles on the nitrogen removal, micro-environment and community dynamics of a sequencing batch biofilm reactor. *Bioresource Technology, 245*, 573-580.

Yamashita, S., Yoshikuni, Y., Obayashi, H., Suzuki, T., Green, D., & Hirata, T. (2019). Simultaneous determination of size and position of silver and gold nanoparticles in onion cells using laser ablation-ICP-MS. *Analytical Chemistry*. *91* (7) 4544-4551.

Yang, Y., & Alvarez, P. J. (2015). Sublethal concentrations of silver nanoparticles stimulate biofilm development. *Environmental Science & Technology Letters, 2*(8), 221-226.

Yang, Y., Li, M., Michels, C., Moreira-Soares, H., & Alvarez, P. J. (2014a). Differential sensitivity of nitrifying bacteria to silver nanoparticles in activated sludge. *Environmental Toxicology and Chemistry, 33*(10), 2234-2239.

Yang, Y., Quensen, J., Mathieu, J., Wang, Q., Wang, J., Li, M., Alvarez, P. J. (2014b). Pyrosequencing reveals higher impact of silver nanoparticles than Ag^+ on the microbial community structure of activated sludge. *Water Research, 48*, 317-325.

Yang, Y., Wang, J., Xiu, Z., & Alvarez, P. J. (2013). Impacts of silver nanoparticles on cellular and transcriptional activity of nitrogen-cycling bacteria. *Environmental Toxicology and Chemistry, 32*(7), 1488-1494.

Yazdanbakhsh, A. R., Rafiee, M., Daraei, H., & Amoozegar, M. A. (2019). Responses of flocculated activated sludge to bimetallic Ag-Fe nanoparticles toxicity: Performance, activity enzymatic, and bacterial community shift. *Journal of Hazardous Materials, 366*, 114-123.

You, F., Tang, W., & Yung, L.-Y. L. (2018). Real-time monitoring of the Trojan-horse effect of silver nanoparticles by using a genetically encoded fluorescent cell sensor. *Nanoscale, 10*(16), 7726-7735.

Young, B., Banihashemi, B., Forrest, D., Kennedy, K., Stintzi, A., & Delatolla, R. (2016). Meso and micro-scale response of post carbon removal nitrifying MBBR biofilm across carrier type and loading. *Water Research, 91*, 235-243.

Young, B., Delatolla, R., Kennedy, K., Laflamme, E., & Stintzi, A. (2017). Low temperature MBBR nitrification: Microbiome analysis. *Water Research, 111*, 224-233.

Yuan, L., Li, Z.-H., Zhang, M.-Q., Shao, W., Fan, Y.-Y., & Sheng, G.-P. (2019). Mercury/silver resistance genes and their association with antibiotic resistance genes and microbial community in a municipal wastewater treatment plant. *Science of the Total Environment, 657*, 1014-1022.

Yuan, Z.-H., Yang, X., Hu, A., & Yu, C.-P. (2015). Long-term impacts of silver nanoparticles in an anaerobic–anoxic–oxic membrane bioreactor system. *Chemical Engineering Journal, 276*, 83-90.

Yuan, Z., Li, J., Cui, L., Xu, B., Zhang, H., & Yu, C.-P. (2013). Interaction of silver nanoparticles with pure nitrifying bacteria. *Chemosphere, 90*(4), 1404-1411.

Zhang, C., Hu, Z., Li, P., & Gajaraj, S. (2016a). Governing factors affecting the impacts of silver nanoparticles on wastewater treatment. *Science of the Total Environment, 572*, 852-873.

Zhang, C., Liang, Z., & Hu, Z. (2014). Bacterial response to a continuous long-term exposure of silver nanoparticles at sub-ppm silver concentrations in a membrane bioreactor activated sludge system. *Water Research, 50*, 350-358.

Zhang, W., Ke, S., Sun, C., Xu, X., Chen, J., & Yao, L. (2019). Fate and toxicity of silver nanoparticles in freshwater from laboratory to realistic environments: a review. *Environmental Science and Pollution Research, 26*(8), 7390-7404.

Zhang, W., Liu, X., Bao, S., Xiao, B., & Fang, T. (2016b). Evaluation of nano-specific toxicity of zinc oxide, copper oxide, and silver nanoparticles through toxic ratio. *Journal of Nanoparticle Research, 18*(12), 372.

Zhang, W., Xiao, B., & Fang, T. (2018a). Chemical transformation of silver nanoparticles in aquatic environments: mechanism, morphology and toxicity. *Chemosphere, 191*, 324-334.

Zhang, Z.-Z., Cheng, Y.-F., Bai, Y.-H., & Jin, R.-C. (2018b). Anammox granules show strong resistance to engineered silver nanoparticles during long-term exposure. *Bioresource Technology, 259*, 10-17.

Zhang, W., Ke, S., Sun, C., Xu, X., Chen, J., & Yao, L. (2019). Fate and toxicity of silver nanoparticles in freshwater from laboratory to realistic environments: a review. *Environmental Science and Pollution Research*, 1-15

Zhang, Y., Zhuang, Y., Geng, J., Ren, H., Zhang, Y., Ding, L., & Xu, K. (2015). Inactivation of antibiotic resistance genes in municipal wastewater effluent by chlorination and sequential UV/chlorination disinfection. *Science of the Total Environment*, 512, 125-132.

Zhang, Z.-Z., Cheng, Y.-F., Bai, Y.-H., & Jin, R.-C. (2018c). Anammox granules show strong resistance to engineered silver nanoparticles during long-term exposure. *Bioresource Technology*, 259, 10-17.

Zhang, Z., Gao, P., Li, M., Cheng, J., Liu, W., & Feng, Y. (2016c). Influence of silver nanoparticles on nutrient removal and microbial communities in SBR process after long-term exposure. *Science of the Total Environment, 569*, 234-243.

Zheng, X.-y., Lu, D., Chen, W., Gao, Y.-j., Zhou, G., Zhang, Y., Jin, M.-Q. (2017a). Response of aerobic granular sludge to the long-term presence of CuO NPs in A/O/A SBRs: nitrogen and phosphorus removal, enzymatic activity, and the microbial community. *Environmental Science & Technology, 51*(18), 10503-10510.

Zheng, X., Chen, Y., & Wu, R. (2011). Long-term effects of titanium dioxide nanoparticles on nitrogen and phosphorus removal from wastewater and bacterial community shift in activated sludge. *Environmental Science & Technology*, *45*(17), 7284-7290.

Zheng, Y., Hou, L., Liu, M., Newell, S. E., Yin, G., Yu, C., Gao, J. (2017b). Effects of silver nanoparticles on nitrification and associated nitrous oxide production in aquatic environments. *Science Advances, 3*(8), e1603229.

Zhou, H., & Xu, G. (2019). Effect of silver nanoparticles on an integrated fixed-film activated sludge–sequencing batch reactor: Performance and community structure. *Journal of Environmental Sciences, 80*, 229-239.

Ziaei-Azad, H., & Semagina, N. (2014). Bimetallic catalysts: Requirements for stabilizing PVP removal depend on the surface composition. *Applied Catalysis A: General*, 482, 327-335.

APPENDIX A SUPPLEMENTARY INFORMATION, ARTICLE 1

Journal: Science of the Total Environment

Title: Fate and inhibitory effect of silver nanoparticles in high rate moving bed biofilm reactors

Authors: Sanaz Alizadeh, Subhasis Ghoshal, Yves Comeau

Materials and Methods

A1. SpICP-MS: Instrumentation and Characterization

Transport efficiency (6.5% to 9.5%) was determined according to a previously published method (Paces et al., 2011) using a MBBR effluent spiked with National Institute of Standards and Technology (NIST) reference gold nanoparticle (60 nm) of 10.7×10^4 particles/mL. A calibration curve was prepared using standard dissolved Ag solution (PlasmaCAL), including one blank and five dissolved Ag solutions (0.05 to 5 μg/L) in 1% HNO_3 in both standard and single particle modes. Prior to each analysis, the collected samples from the lab-scale MBBR systems were diluted to reduce background interferences and dissolved Ag concentrations, to obtain reliable signals (counts per event) corresponding to NPs. The blanks and QC NPs (NIST) samples were also measured with MBBR samples to ensure the reliability of the measurements.

A2.Transmission electron microscopy

The AgNP suspension was added to Standard TEM grids (Electron Microscopy Sciences, Carbon film 200 mesh Cu grids), were kept in the dark and air-dried. Effluent AgNPs were imaged with a Jeol JEM-2100F transmission electron microscope (TEM) equipped with a Gatan Ultrascan US1000 camera, operated at an accelerating voltage of 200 kV and imaging resolution of 0.1 nm. Elemental analysis of the particles was performed with Energy Dispersive Spectroscopy (EDS) with Si(Li) detector (X-Max^{N}TSR, Oxford instruments, UK).

Table A.1: Characteristics of influent AgNP suspensions

Nominal $AgNP_{inf}$ conc.	**Mean size**	**$AgNP_{inf}$**	**Dissolved Ag_{inf}**	**Ag_{tot}**
μg/L	nm	μg/L	μg/L	μg/L
10	48 ± 3	8.1± 6	2.5 ± 0.6	10.8 ± 0.3
100	47 ± 2	75 ± 6	14.4 ± 6	131 ± 7
600	49 ± 1	442 ± 26	39 ± 19	631 ± 27

Table A. 2: Single particle ICP-MS instrumental parameter

Instrumentation	**Parameter**	**Description/Value**
Properties	Model	PerkinElmer NexION 300x ICP-MS
	Nebulizer	Meinhard Glass Concentric
	Spray chamber	Meinhard Glass Cyclonic
Instrument setting	Nebulizer gas flow rate	0.97 to 1.03 L/min
	Sample uptake rate	0.28 to 0.34 mL/min
	Plasma RF Power	1.6 kW
	Analyte	^{107}Ag
Analysis setting	Dwell time	100 μs
	Analysis time	100 to 150 s
	Transport efficiency	6.5% to 9.5%

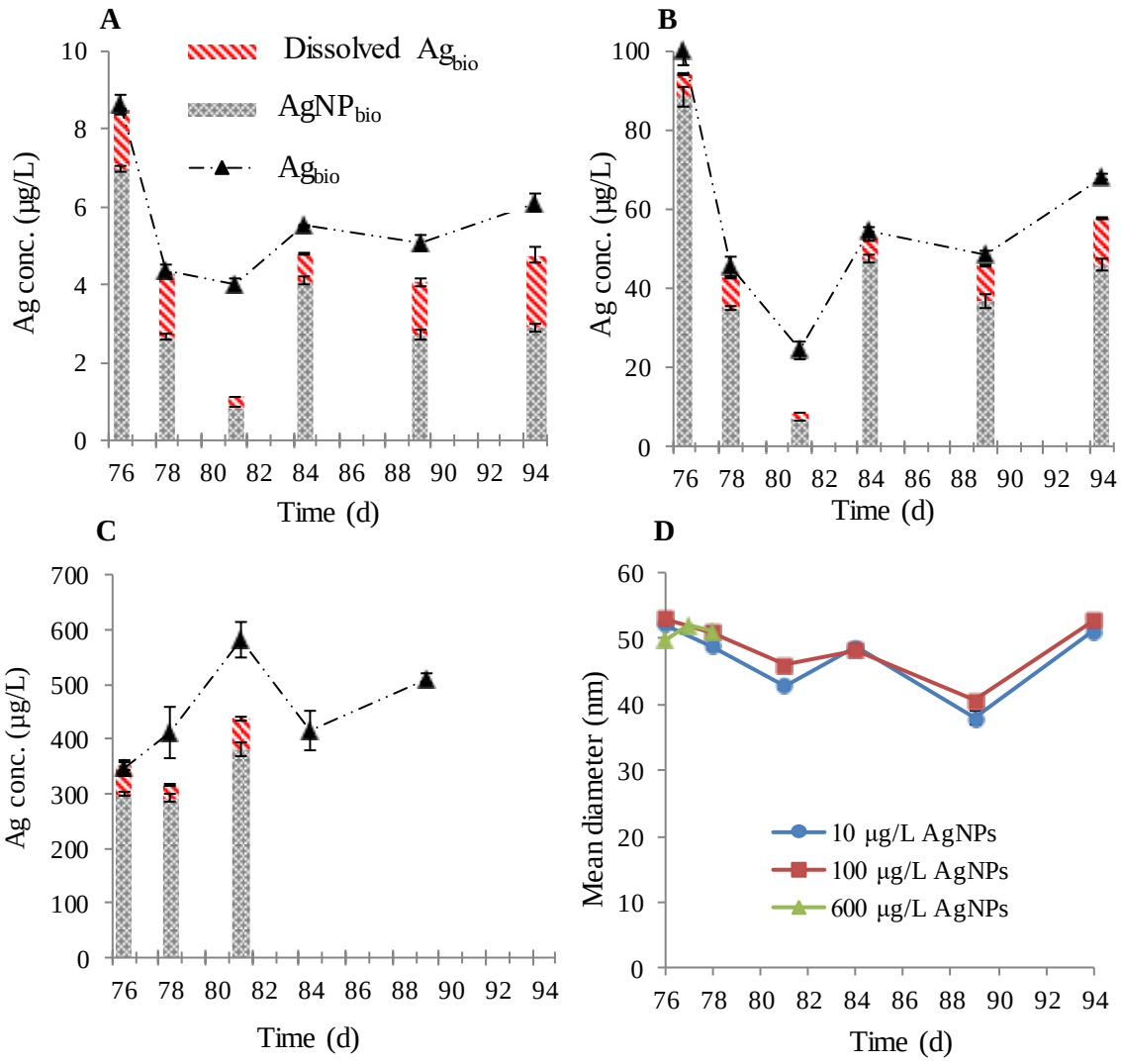

Figure A.1: Distribution of Ag in bioreactors receiving (A)10 μg/L,(B) 100 μg/L and (C) 600 μg/L AgNPs, (D) AgNPs mean diameter in effluent of MBBRs (error bars are only shown when larger than symbol size).

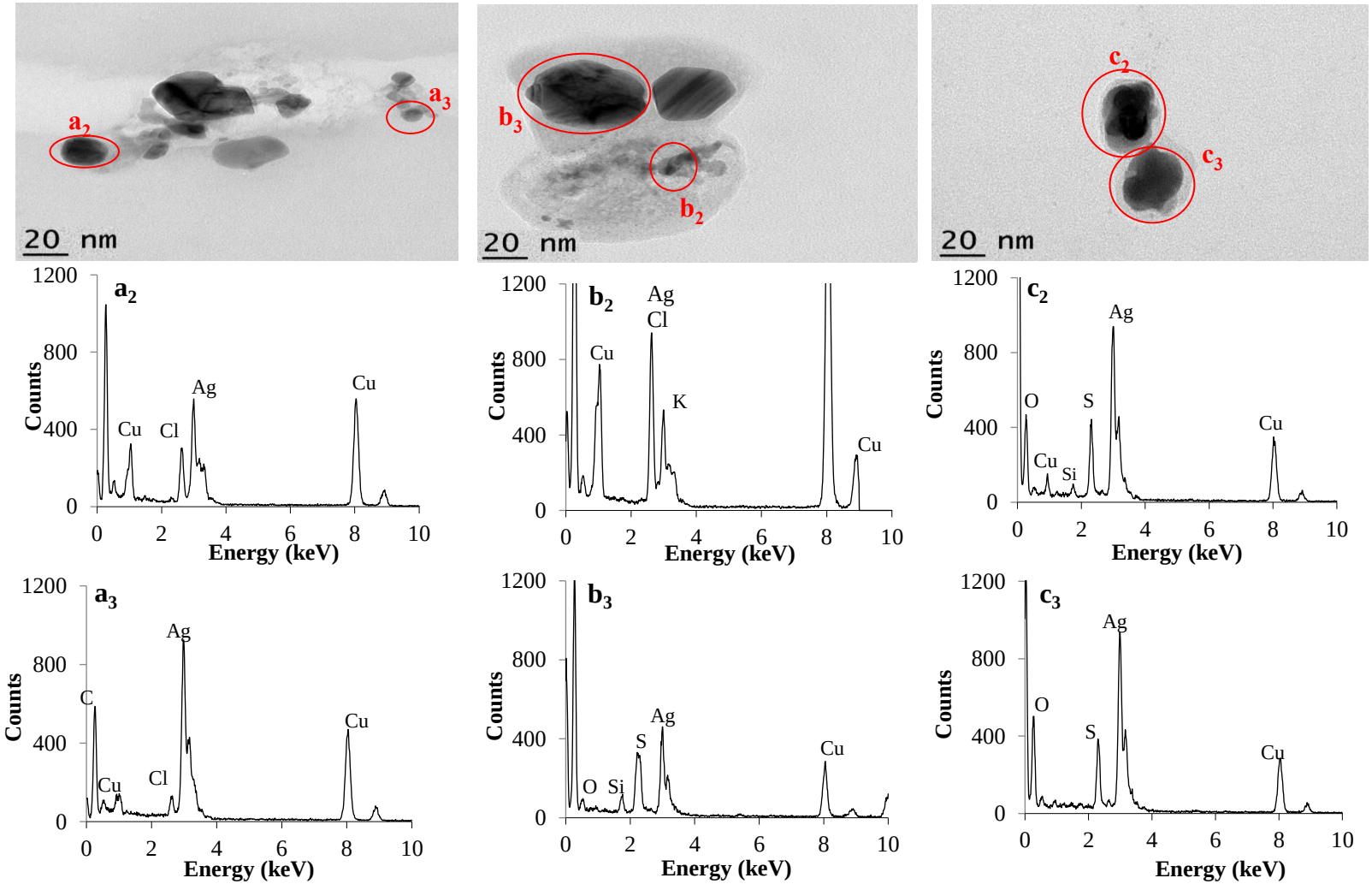

Figure A.2: TEM images of the AgNPs in effluent of MBBR receiving (A_1) 10 μg/L, (B_1) 100 μg/L and (C_1) 600 μg/L AgNPs and (a_2-c_3) EDS analysis of the AgNPs.

APPENDIX B SUPPLEMENTARY INFORMATION, ARTICLE 2

Journal: Environmental Science and Technology

Title: Impacts of continuous inflow of low concentrations of silver nanoparticles on biological performance and microbial communities of aerobic heterotrophic wastewater biofilm

Authors: Sanaz Alizadeh, Arshath Abdul Rahim, Bing Guo, Jalal Hawari, Subhasis Ghoshal, Yves Comeau

Materials and Methods

B1. Synthetic wastewater and reactor operational conditions

Sodium acetate, soy protein and peptone were used to mimic the readily-degradable carbonaceous content of wastewater. The concentrated solution (1.3 g S_{COD}/L) was prepared using an adopted recipe adapted from OECD (OECD, 1976) to obtain a typical C/N/P ratio of 100/12/2 for a medium to high strength domestic wastewater (Metcalf and Eddy AECOM, 2014)(Table B.1). Both reactors were inoculated with colonized K3 carriers, collected from the full-scale MBBR at the Mascouche Terrebonne WRRF (Quebec, Canada), for a period of seven days in the preliminary start-up phase, to favor biofilm growth with a representative microbial community of a WRRF. Subsequently, the K3 carriers were removed from the reactors.

In conventional activated sludge systems, sludge retention time (SRT) is an important design and operational parameters which is controlled by sludge wasting (Rusten et al., 2006). In MBBRs, the main design criteria are HRT, surface area loading rate and carrier filling ratio.The biomass develops on carriers which allow the operation of the process at shorter HRTs, higher surface loading rates and longer SRTs without sludge recycling, unlike in activated sludge systems (Rusten et al., 2006). In MBBRs, sludge wasting takes place by sloughing of attached biomass in MBBRs (Helness and Ødegaard, 2001; Ødegaard, 2006; Rusten et al., 2006).

B2. Characterization of biofilm biological responses

The attached biofilm was recovered from the surface of carriers according to a standardized procedure (Reboleiro-Rivas et al., 2013). Five carriers were chosen randomly at each sampling time. These carriers were cut and vortexed for 1 min and the resultant biofilm suspensions were collected by centrifuging for 5 min at 3000 × *g*. This process was repeated twice. The biofilm pellet obtained after the last centrifugation was resuspended in 5-8 mL of sterile saline water (0.5% NaCl). The biofilm suspensions were used for viability assessment and enzymatic activity assays. All enzymatic activity assays were performed in 2-mL micro-centrifuge tubes. All tests were conducted in triplicates, including the blank and positive control (70% propanol-treated inactivated biofilm), including five reads per replicate at the corresponding setting by microplate reader. All chemicals required for the enzymatic activity analyses were purchases from Sigma–Aldrich (St. Louis, MO, USA).

After each sampling, the removed carriers were replaced with carriers from the control MBBR, operated in parallel with tested MBBRs, to keep a constant number of the carriers in each MBBR (198 carrier) over the control period and the first 4 weeks of the exposure. The added K5 careers from control reactors were marked to differentiate them from the original ones in the tested MBBRs. Afterwards, they were replaced by new K5 carriers to keep the filling ratio constant. By the end of the sampling period, about 13% of carriers with active biofilm were removed from each reactor

B.2.1 Determination of key enzyme activities of biofilm

B2.1. 1 Intracellular dehydrogenase activity

Intracellular dehydrogenase activity was quantified using the protocol proposed by Von Mersi and Schinner (1991). The activity of the intracellular dehydrogenase enzyme was determined using 0.5% 2-(4-iodophenyl)-3-(4-nitrophenyl)-5-phenyl-2H-tetrazolium chloride (INT). The technique uses soluble and colorless INT reduction to the red insoluble iodonitrotetrazolium formazan (INF). Thus, one unit of the DHA activity was defined to produce 1 mg of INF in 60 min. Briefly, harvested biofilm (0.15 g) was spiked with 200 μL of TRIS buffer (1 M; pH 7.0) and 250 μL of 0.5% 2-(4-iodophenyl)-3-(4-nitrophenyl)-5-phenyl-2H-tetrazolium chloride (INT) solution (9.88 mM), slightly mixed using vortex for 30 seconds. After 2 hours incubation at

40 °C in the dark, the intercellular iodonitrotetrazolium formazan (INF) crystals were extracted with 1 mL ethanol/N,N-dimethylformamide solution (1/1 v/v). The INF extraction was preceded by 1 h incubation at 40 °C in dark, with shaking at 20 min intervals. The developed INF solution was collected by centrifuging the biomass suspension at 5000 × g for 5 min and filtration of the supernatant using 0.45 μm filters. The concentration of formazan was determined via absorbance measurements at 464 nm using a micro-plate reader (Synergy-HT, BioTek, USA). The extraction solution, ethanol/N,N-dimethylformamide solution (1/1 v/v) was used as reference blank and preparation of INF standard solution (100 mg/L). A 6-point standard calibration curve (0 to 1000 μg INF) was obtained for each analysis.

B.2.2.2 Extracellular enzymatic activity

Extracellular α-glucosidase and protease activities were determined according the proposed method by (Goel et al., 1998). The activity of the extracellular α-glucosidases enzyme was determined using 1% *p*-nitrophenyl α-D-glucopyranoside as substrate, which is converted by the enzyme to *p*-nitrophenol. The activity of the extracellular protease enzyme was determined using 0.5% azocasein, as a substrate for the reactions. Thus, one unit of extracellular α-glucosidases and protease activities were defined to produce 1 mmol *p*-nitrophenol or degrade 1 mg azocasein, respectively in 60 min at 37 °C. To measure the α-glucosidase activity, 500 μL Tris–HCl buffer (pH 7.6) and 250 μL 1% *p*-nitrophenyl α-d-glucopyranoside (substrate) were added to a 250 μL biofilm suspension. The tubes were incubated at 37 °C for 60 minutes. The enzyme activity was stopped by heating the tubes in boiling water bath for 5 min. The samples were centrifuged for 15 min at 3000 × *g* and the supernatant absorbance was measured at 410 nm using a micro-plate reader (Synergy-HT, BioTek, USA). A 5-point standard calibration curve (0 to 100 mM *p*-nitrophenol) was obtained for each analysis. For protease activity, 750 μL of biofilm suspension was mixed with 250 μL Tris–HCl buffer (pH 7.6) and 250 μL 0.5% azocasein (substrate) and incubated at 37 °C for 90 minutes. Protease activity was stopped using 500 μL of 10% trichloroacetic acid (TCA). The samples were centrifuged for 15 min at 3000 × *g* and the 500 μL of supernatant was collected. 2 M sodium hydroxide (500 μL) was added to samples and the absorbance was measured at 440 nm using a micro-plate reader (Synergy-HT, BioTek, USA).

The specific enzyme activities were calculated by dividing the enzyme activity units by biofilm VSS (dry weight) (Goel et al., 1998). Three replicates (0.75 to 1 mL) samples from the homogenized biofilm samples were filtered on 1.2 μm filters (Whatman® 934-AH™, GE Healthcare Life Sciences, USA) and the remaining solids were dried at 105 °C and 550 °C in ovens for measuring TSS and VSS, respectively. The weight of filter, filter and solid residue (dried at 105 °C for 1 hour) and residue (combusted at 550 °C for 20 min) were recorded and used for TSS and VSS calculations.The enzymatic activity inhibition (%) was calculated at each sampling date over the exposure period (day 125-189). The inhibition rate constant was obtained by plotting the inhibition (%) versus time (zero order rates constant). The half-life of each enzyme was calculated using the zero-order rate constant from its activity versus time profile.

B.3 Intracellular reactive oxygen species (ROS) production

The intracellular ROS production was determined using an established fluorescence assay (Gu et al., 2014). Briefly, 1 mL of biofilm suspension was rinsed three times with a 0.1 M phosphate buffer (pH 7.4) and the pellets were resuspended in 0.1 M phosphate buffer containing 50 μM dichlorodihydrofluorescein diacetate (H2DCF-DA, Molecular Probes, Invitrogen). The resulting mixture was incubated at 21 ± 1 °C in the dark for 30 min. Biofilm suspension was transferred into 96-well plates (Molecular Devices, USA) and the generated fluorescent fluorescein dichlorofluorescein (DCF) was measured at excitation/emission wavelengths of 495/525 nm.

B.4 SpICP-MS: instrumentation and characterization

National Institute of Standards and Technology (NIST) reference gold nanoparticle (60 nm) of 9.84 x 10^4 particle/mL, diluted in MBBR effluent, was used to determine the transport efficiency (5.5 to 9.5%). The calibration curve, including one blank and 5 dissolved Ag solutions (0.01 to 2 μg/L) in 1% HNO_3, was prepared using standard dissolved Ag solution (1000 mg/L, PlasmaCAL) prior to each analysis, in both standard and single particle modes. Prior to each analysis, the collected samples from the bench-scale MBBR systems were diluted to reduce background interferences and dissolved Ag concentrations, to obtain reliable signals (counts per event) corresponding to NPs. Each set of analysis included the blanks and QC NPs (NIST) to ensure the reliability of the measurement. The set of analyses also included spiked silver nanoparticles in

MBBR effluent (100 ng/L) and dissolved Ag (50 ng/L) as quality control for which 96% recovery was observed for both elements.

B.5 Cumulative total Ag mass distribution

The samples collected from suspended phase of MBBR (Ag_{susp}) and effluent samples contained suspended biomass but no K5 carriers. The samples were homogenized and allowed to settle for about 30 to 45 s and the aqueous supernatant was collected. AgNP and dissolved Ag concentrations were determined simultaneously using spICP-MS in the aqueous phase of the effluent ($AgNP_{eff}$, dissolved Ag_{eff}) and bioreactor suspension ($AgNP_{susp}$, dissolved Ag_{susp}). The total Ag concentration was determined in homogenized samples, including aqueous fraction and flocs in both effluent and bioreactor suspension, using ICP-MS in standard mode. The concentration of Ag associated with suspended floc (Ag_{floc}), for both the effluent and bioreactor suspension, was calculated using the aqueous phase Ag (*i.e.* AgNPs + dissolved Ag) obtained from spICP-MS analysis of the supernatant of the samples and Ag from the total metal analyses of the homogenized samples (Eq.1).

$$[Ag_{floc}]_{ti} = [Ag]_{ti} - ([AgNPs]+[\text{ dissolved Ag}])_{ti} \quad (1)$$

Where $[Ag]_{ti}$ represents $[Ag_{eff}]_{ti}$ for effluent and $[Ag_{susp}]_{ti}$ for the bioreactor. The mass of Ag in influent ($M_{Ag,inf}$) and effluent ($M_{Ag,eff}$) of each MBBR, for each time interval (Δt), were calculated using their corresponding total Ag concentrations, obtained from ICP-MS analysis and influent and effluent flow rates.

$$(M_{Ag,inf})_{ti} = (Q_{inf})_{ti} * [Ag_{inf}]_{ti} * (t_i - t_{i-1}) \quad (2)$$

$$(M_{Ag,eff})_{ti} = (Q_{eff})_{ti} * [Ag_{eff}]_{ti} * (t_i - t_{i-1}) \quad (3)$$

Where Q_{inf} (L/day), Q_{eff} (L/day) are the flow rate of influent and effluent, respectively.The mass of Ag in the suspended phase of the bioreactor($M_{Ag,susp}$), for each time interval (Δt), calculated using its corresponding total Ag concentration and the liquid volume (V_L) in the reactor, to considering the occupied volume by the carriers.

$$(M_{Ag,susp})_{ti} = V_L * [Ag_{susp}]_{ti} \quad (4)$$

$V_L = V_T$ * (1- carrier filling ratio* f_p) (5)

Where V_T is the total volume of the reactor. The actual volume of plastic, occupied at 100% filling ratio of K5 carrier were determined experimentally (f_p = 0.110 $L_{plastic}/L_{carrier}$). The mass of Ag in bioreactor consisted of the mass of Ag in the suspended phase of the bioreactor ($M_{Ag,susp}$) and the retained mass of Ag by attached biofilm on the carrier ($M_{Ag,carrier}$).

$$(M_{Ag,bio})_{ti} = (M_{Ag,inf})_{ti} - (M_{Ag,eff})_{ti} \quad (6)$$

In the final step, the retained mass of Ag by attached biofilm on the carrier ($M_{Ag,carrier}$) was estimated (Eq. 7).

$$(M_{Ag,carrier})_{ti} = (M_{Ag,bio})_{ti} - (M_{Ag,susp})_{ti} \quad (7)$$

The normalized mass of Ag per active surface area of carrier (mg $Ag/m^2_{active\ surface\ area}$) is calculated using the accumulated mass of Ag, obtained from mass balance calculation, total number of carriers in the reactor and the active surface area per media.

B6. Transmission electron microscopy

The AgNP suspension was added to Standard TEM grids (Electron Microscopy Sciences, Carbon film 200 mesh Cu grids), kept in the dark and air dried. For each MBBR, three replicates were prepared. Effluent AgNPs were imaged with a Jeol JEM-2100F transmission electron microscope (TEM) equipped with a Gatan Ultrascan US1000 camera, operated at an accelerating voltage of 200 kV and imaging resolution of 0.1 nm. Elemental analysis of the particles was performed with Energy Dispersive Spectroscopy (EDS) with Si(Li) detector (X-Max^{N}TSR, Oxford instruments, UK). Ten images per replicates were obtained for TEM and EDS analyses.

Table B.1: Concentrated feed composition for the synthetic wastewater.

Compound	**Chemical formula**	**Concentration**	
Sodium acetate trihydrate	$CH_3COONa \cdot 3H_2O$	467	mg COD/L
Sodium propionate	CH_3CH_2COONa	200	mg COD/L
Soy peptone	–	660	mg COD/L
Nutrient broth	–	153	mg COD/L
Dipotassium phosphate	K_2HPO_4	133	mg/L
Ammonium chloride	NH_4Cl	267	mg/L
Sodium chloride	NaCl	31	mg/L
Calcium chloride	$CaCl_2$	5	mg/L
Ferric chloride	$FeCl_3$	5	mg/L
Magnesium chloride	$MgCl_2$	4	mg/L

Table B.2 : Average characteristics of the MBBR synthetic influent after dilution with tap water.

Parameters	**Symbol**	**Units**	**Value**
Total COD	COD	mg/L	661 ± 9
Soluble COD	S_{COD}	mg/L	653 ± 5
Total carbonaceous BOD_5	$cBOD_5$	mg/L	320 ± 7
COD/BOD ratio	f_{COD_cBOD5}	g/g	2.07
Nitrogen fractionation			
Total Kjeldahl nitrogen	TKN	mg N/L	75.4 ± 3.5
Total ammonia ($NH_3 + NH_4^+$)	S_{NH4}	mg N/L	42.8 ± 2.1
Oxidized nitrogen (nitrite plus nitrate)	S_{NOx}	mg N/L	0.07 ± 0.01
S_{NH4}/TKN ratio	f_{SNH4_TKN}	g N/g N	0.56 ± 0.03
Phosphorus fractionation			
Total phosphorus	TP	mg P/L	19.4 ± 2.5
Soluble phosphate	S_{PO4}	mg P/L	12.1 ± 1.6
S_{PO4}/TP ratio	f_{SPO4_TP}	g P/g P	0.62 ± 0.03

Table B.3: Single particle ICP-MS instrumental parameter

Instrumentation	Parameter	Description/Value
Properties	Model	PerkinElmer NexION 300x ICP-MS
	Nebulizer	Meinhard Glass Concentric
	Spray chamber	Meinhard Glass Cyclonic
Instrument Setting	Nebulizer gas flow rate	0.97 - 1.03 L/min
	Sample uptake rate	0.28 - 0.34 mL/min
	Plasma RF Power	1.6 kW
	Analyte	^{107}Ag
Analysis setting	Dwell time	100 μs
	Analysis time	100s
	Transport efficiency	5.5 - 9.5%

Table B.4: Effect of AgNPs on the half-life and specific activity inhibition rate of heterotrophic biofilm enzymes. Note: different superscript letters represent significant difference ($p < 0.05$).

Parameter	**Half-life (d)**			**Inhibition rate (d^{-1})**		
Treatment	DHA	α-Glu	Protease	DHA	α-Glu	Protease
10 μg/L AgNPs	357 ± 30 ^{a}	210 ± 60 ^{b}	443 ± 30 ^{c}	0.14 ± 0.01^{g}	0.25 ± 0.08 ^{h}	0.11 ± 0.01 ^{k}
100μg/L AgNPs	116 ± 4 ^{d}	78 ± 2 ^{e}	186 ± 22 ^{f}	0.43 ± 0.02 ^{m}	0.64 ± 0.04 ^{n}	0.27 ± 0.03 ^{o}

Table B.5: Richness and diversity indices of bacterial communities of control biofilm ($MBBR_{10}^{124}$, $MBBR_{100}^{124}$) and AgNP-treated biofilm ($MBBR_{10}^{189}$, $MBBR_{100}^{189}$)

Treatment	Raw sequence (bp)	Effective sequence (bp)	OTUs	Coverage	Fait's phylogenetic diversity	Pielou's evenness index	Chao	Shannon	Simpson
$MBBR_1^{C}$	29935	25607	224	1	16.5	0.79	224	6.16	0.97
$MBBR_1^{64}$	28691	24555	215	1	17.1	0.78	215	6.03	0.96
$MBBR_2^{C}$	28359	24138	255	1	18.5	0.79	255	6.33	0.97
$MBBR_2^{64}$	27057	23062	262	1	19.7	0.83	262	6.64	0.98

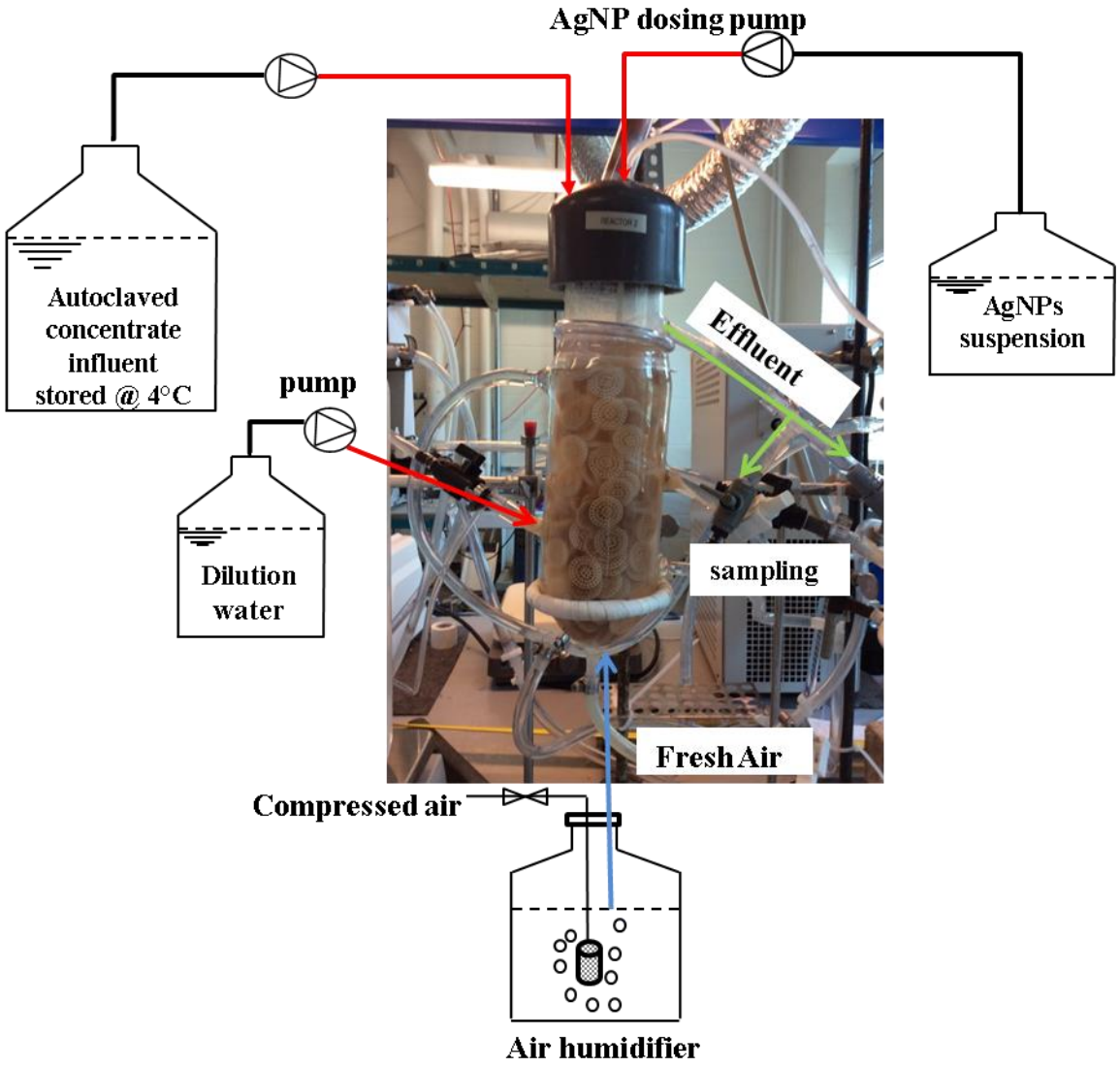

Figure B.1: Schematic of the experimental MBBR

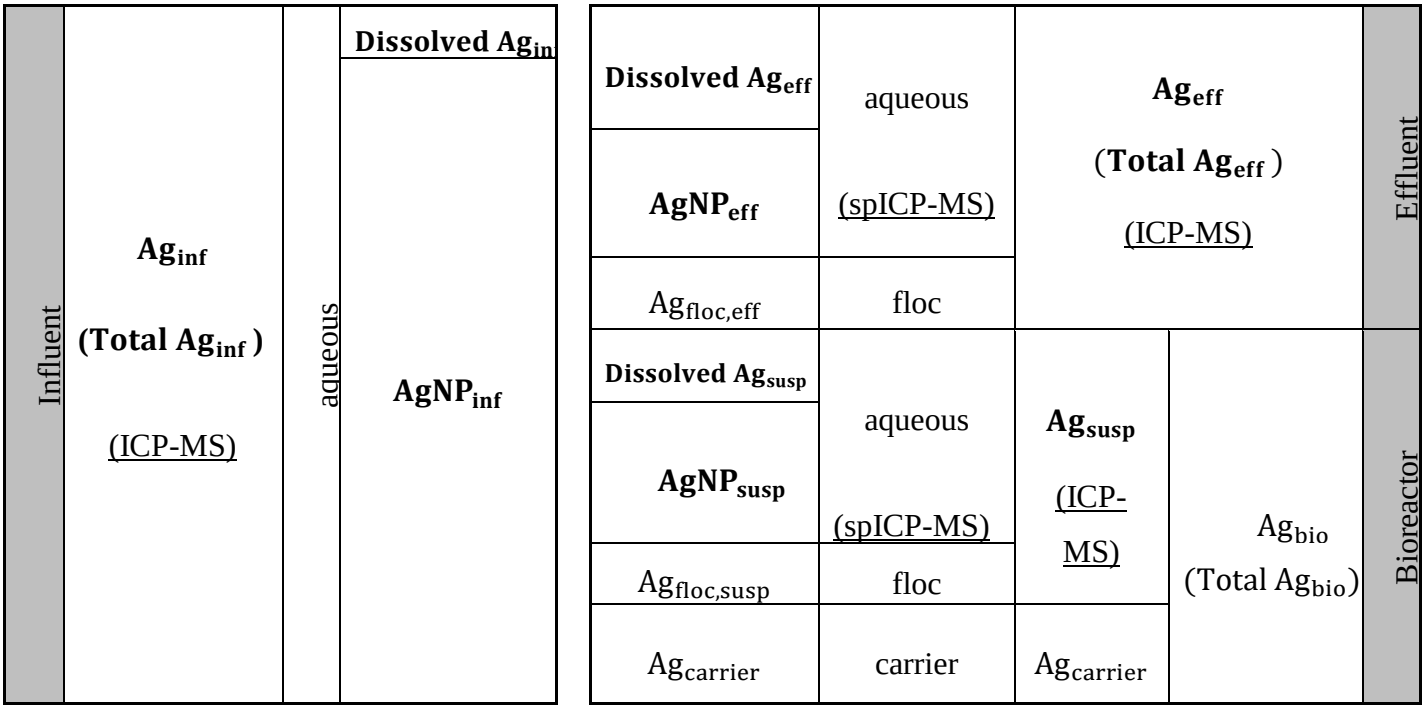

Figure B.2 : Fractionation of Ag in influent, bioreactor and effluent of MBBRs. (adapted from Alizadeh, et al.(2019)). Note: Bold characters refer to analytically determined parameters; susp: suspended phase in MBBR.

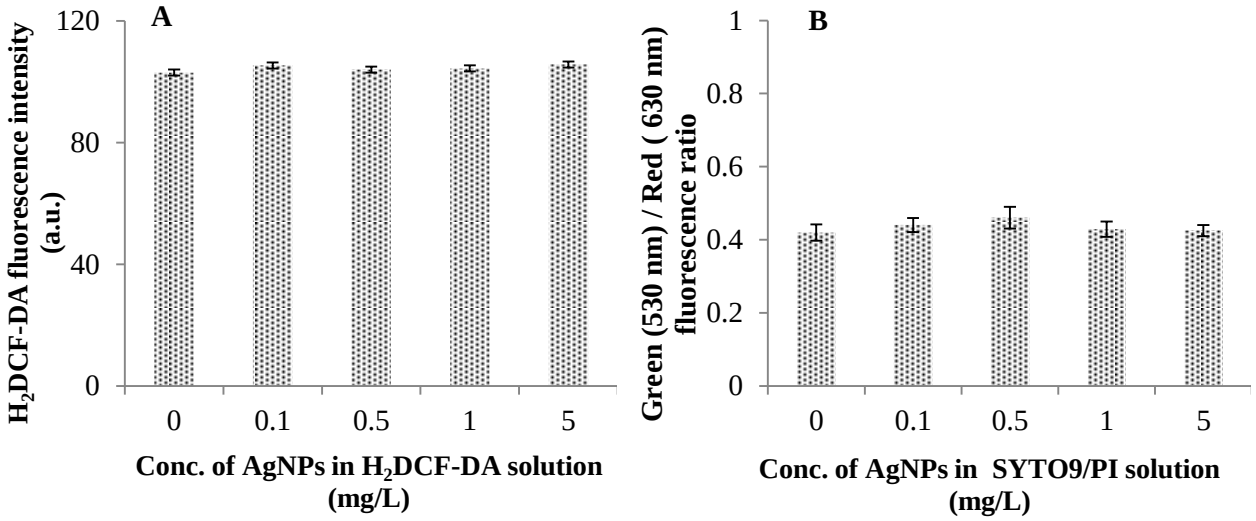

Figure B.3 : Quenching effect of AgNPs on fluorescence intensity of (A) H_2DCF-DA solution in ROS assay and (B) SYO9/PI solution in *Bac*light viability assay.

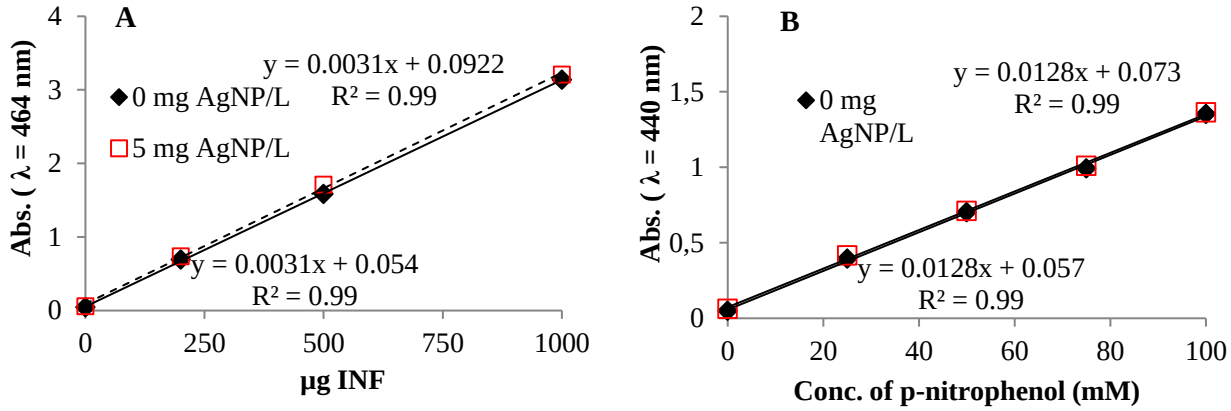

Figure B.4 : Calibration curves used in (A) intracellular DHA and (B) extracellular α-glucosidase activity assay at different Ag concentrations.

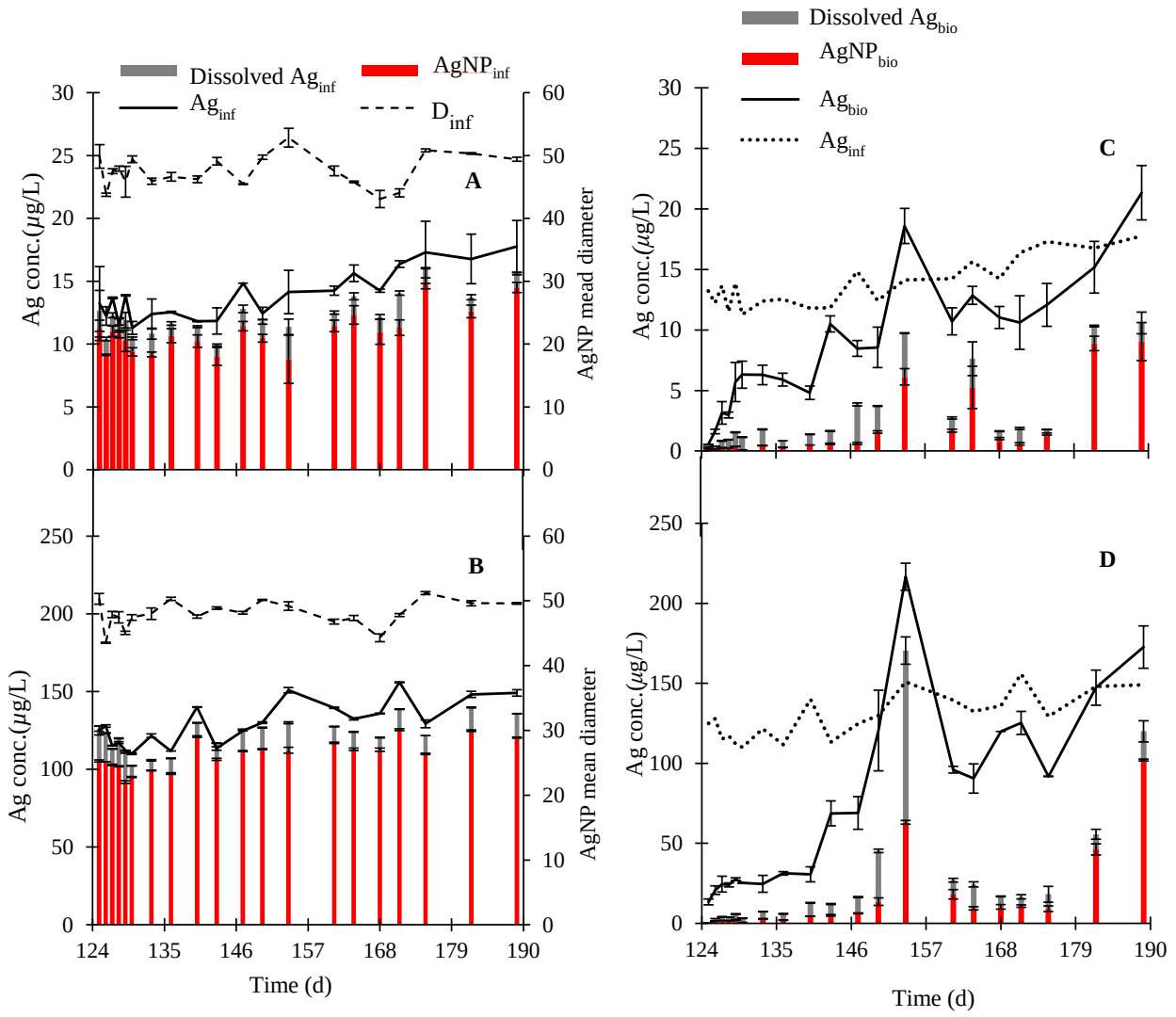

Figure B.5 : Distribution of Ag in influent (A-B) and bioreactor phases (C-D) of MBBRs receiving influent concetration of 10 μg/L AgNPs and 100 μg/L AgNPs, respectively (Error bars are only shown when larger than symbol size). Note: Ag_{inf} and Ag_{bio} represent the total Ag concentrations in the influent and suspended phase of MBBRs, respectively; D_{inf} corresponds to the mean diameter of the AgNPs in the influent. P.I-III refers to three observed phases in Ag distribution profile.

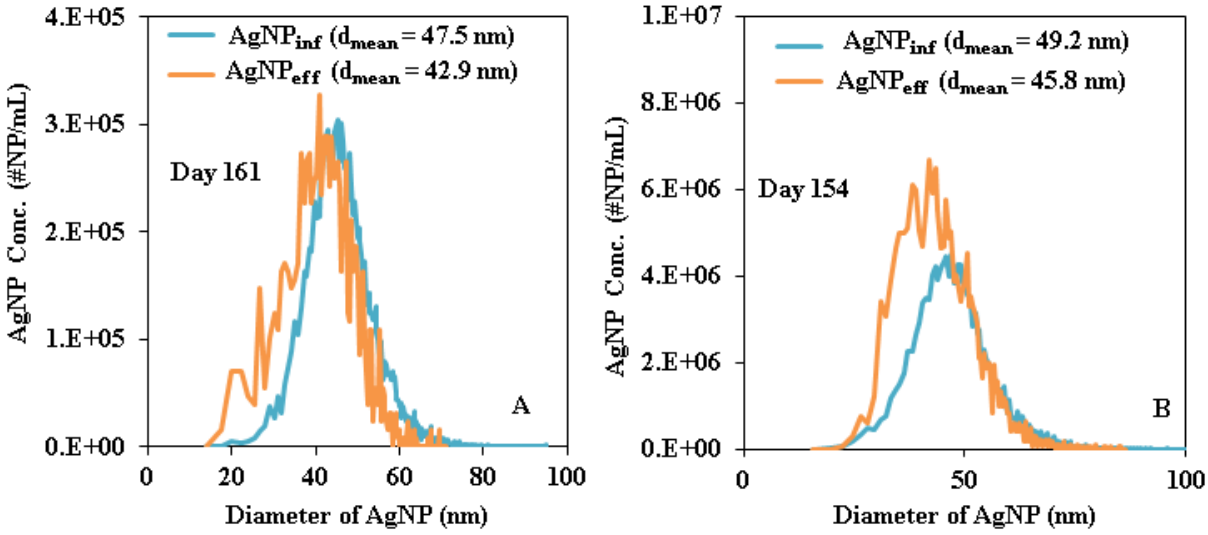

Figure B.6 : Particle size distribution of Ag NP in influent ($AgNP_{inf}$) and effluent ($AgNP_{eff}$) of (A) $MBBR_1$ on day 161 and (B) $MBBR_2$ on day 154 from spICP-MS showing reduction of AgNP mean diameter (d_{mean}) .

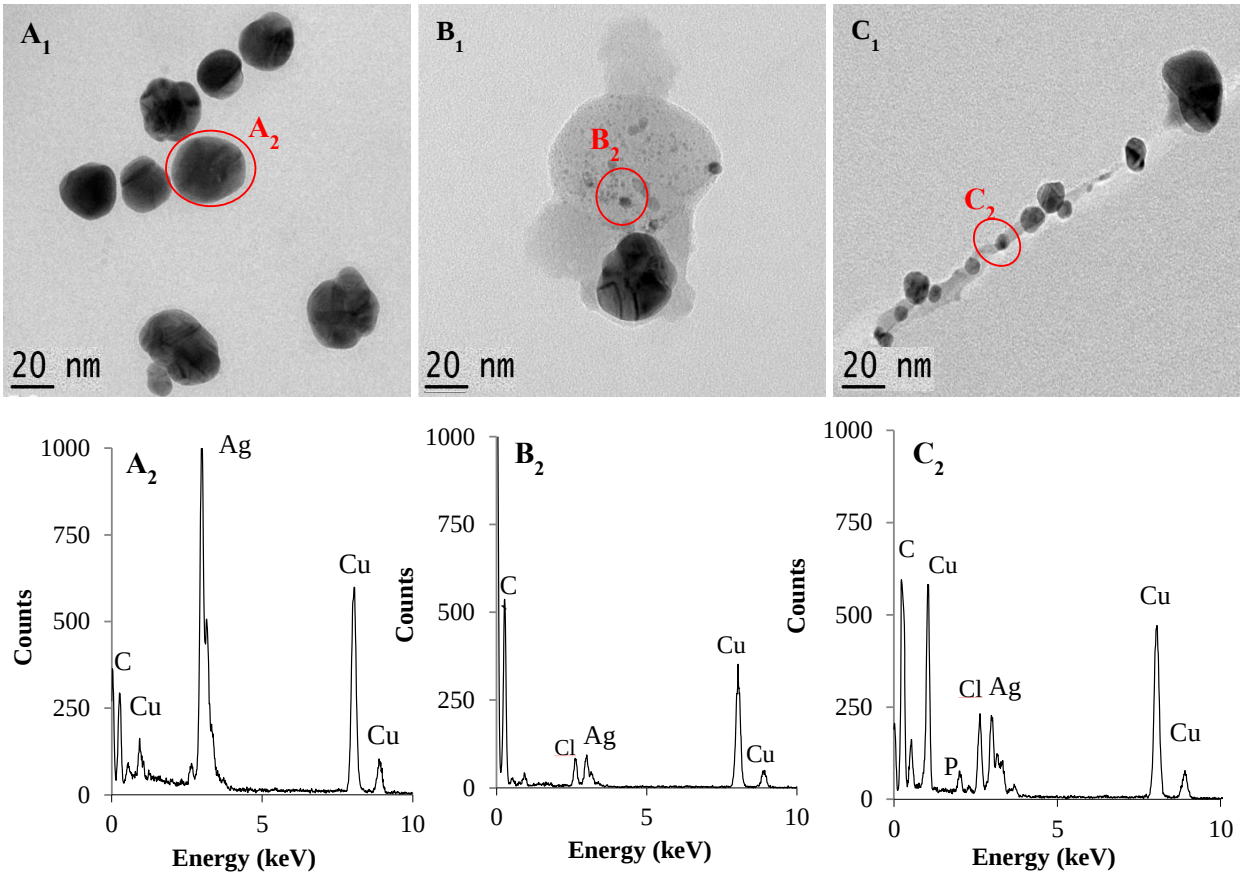

Figure B.7 : TEM images of the AgNPs in (A_1) influent and effluent of MBBR receiving (B_1) 10 μg/L (C_1) 100 μg/L AgNPs and (A_2-C_2) EDS analysis of the AgNPs.

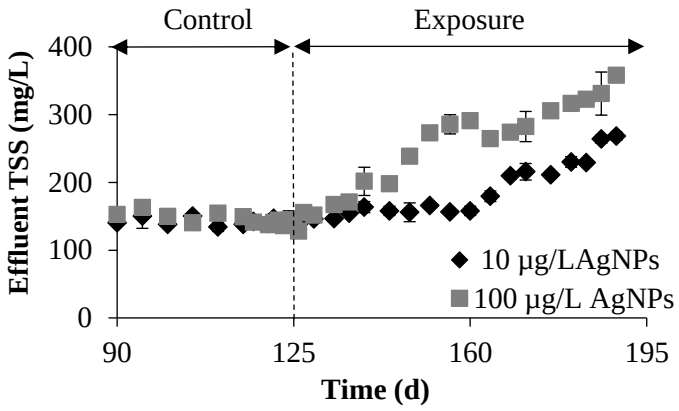

Figure B.8 : Effect of PVP-AgNPs on effluent TSS (mg/L) (Error bars are only shown when larger than symbol size).

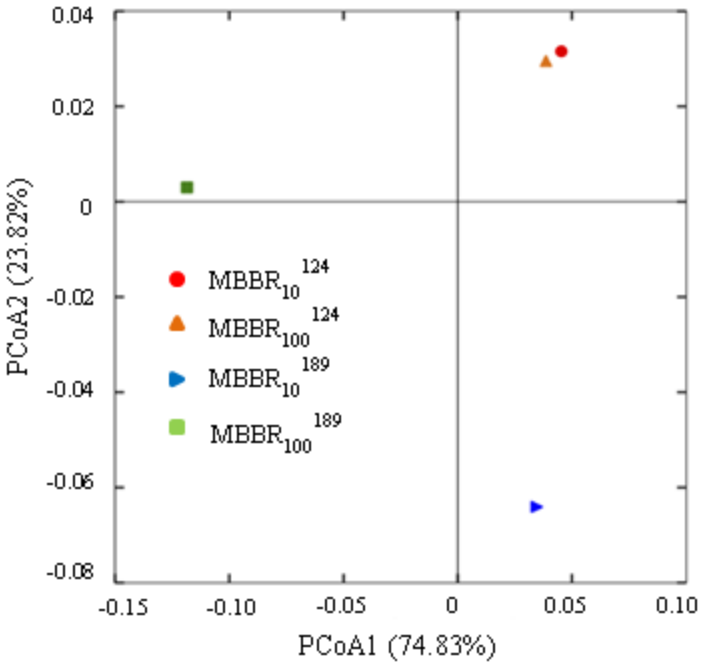

Figure B.9 : Principal coordinates analysis (PCoA) of weighted UniFrac distance based on 16S rDNA genes at different AgNP concentrations. Note: The characters 124 and 189 represents the biofilm collected in control period (day 124) and AgNP-treated biofilms at the end of the exposure period (day 189), respectively; $MBBR_{10}$ and $MBBR_{100}$ received nominal influent AgNP concentrations of 10 and 100 μg/L respectively over AgNP exposure period.

Microbial community analysis

Principal coordinate analysis (PCoA), based on the weighted UniFrac distance matrix with 75% of total variance on PCoA1 axis, indicated a similar microbial composition of control biofilms ($MBBR_{10}^{124}$, $MBBR_{100}^{124}$), prior to injection of AgNPs (Figure B.9). The pairwise Kruskal-Wallis test indicated no significant difference between the alpha diversity indices of control and Ag-treated biofilms.

APPENDIX C SUPPLEMENTARY INFORMATION, CHAPTER 6

Title: Responses and recovery of nitrifying MBBR biomass upon long-term continuous exposure to silver nanoparticles.

Table C.1: Single particle ICP-MS instrumental parameter

Instrumentation	Parameter	Description/Value
Properties	Model	PerkinElmer NexION 300x ICP-MS
	Nebulizer	Meinhard Glass Concentric
	Spray chamber	Meinhard Glass Cyclonic
Instrument Setting	Nebulizer gas flow rate	0.97-1.03 L/min
	Sample uptake rate	0.28-0.34 mL/min
	Plasma RF Power	1.6 kW
	Analyte	^{107}Ag
Analysis setting	Dwell time	100 μs
	Analysis time	100s
	Transport efficiency	5.5%-7.5%

Table C.2 : Biomass concertation, number of genera and the alpha diversity indices of microbial communities of control ($MBBR_1$) and Ag-treated reactors at influent 10 μg/L AgNPs ($MBBR_2$) and 100 μg/L AgNPs ($MBBR_3$) at different stages of operation (Acclimation, Control, AgNP Exposure, Recovery)

Period	Condition	Attached biofilm (g VSS/ $V_{reactor}$)	Number of Genera	Shannon	Evenness
Inoculation	Inoculum from WRRF	NA	489 ± 14	4.50 ± 0.05	0.719 ± 0.005
K_5 carries (n=5, Day 150)	$MBBR_1$	NA	307 ± 24	2.93 ± 0.04	0.511 ± 0.01
Acclimation (Day 150)	$MBBR_1$	1.48 ± 0.03	298 ± 38	2.90 ± 0.01	0.507 ± 0.01
	$MBBR_2$	1.50 ± 0.04	316 ± 9	2.91 ± 0.09	0.504 ± 0.012
	$MBBR_3$	1.53 ± 0.04	331 ± 15	2.87 ± 0.03	0.494 ± 0.008
Control (Day 235)	$MBBR_1$	1.68 ± 0.02	181 ± 20	2.85 ± 0.06	0.549 ± 0.001
	$MBBR_2$	1.65 ± 0.05	220 ± 12	3.08 ± 0.06	0.571 ± 0.004
	$MBBR_3$	1.67 ± 0.09	193 ± 20	3.18 ± 0.05	0.603 ± 0.003
Control (Day 292)	$MBBR_1$	1.67 ± 0.03	249 ± 29	3.46 ± 0.04	0.628 ± 0.007
	$MBBR_2$	1.68 ± 0.05	246 ± 23	3.29 ± 0.08	0.597 ± 0.004
	$MBBR_3$	1.71 ± 010	305 ± 47	3.40 ± 0.24	0.595 ± 0.03
Exposure (Day 323)	$MBBR_1$	1.68 ± 0.06	267 ± 5	3.48 ± 0.05	0.622 ± 0.007
	$MBBR_2$	1.62 ± 0.02	282 ± 4	3.25 ± 0.06	0.587 ± 0.001
	$MBBR_3$	1.56 ± 0.02	277 ± 38	3.30 ± 0.09	0.575 ± 0.002
Exposure (Day 353)	$MBBR_1$	1.71 ± 0.04	211 ± 2	3.06 ± 0.06	0.571 ± 0.012
	$MBBR_2$	1.59 ± 0.02	207 ±25	3.09 ± 0.044	0.581 ± 0.006
	$MBBR_3$	1.45 ± 0.02	183 ±12	2.85 ± 0.038	0.546 ± 0.005
Exposure (Day 388)	$MBBR_1$	1.67 ± 0.04	313 ± 7	2.53 ± 0.042	0.440 ± 0.006
	$MBBR_2$	1.65 ± 0.02	318 ± 24	2.56 ± 0.021	0.444 ± 0.009
	$MBBR_3$	1.57 ± 0.06	106 ± 20	1.89 ± 0.07	0.407 ± 0.033

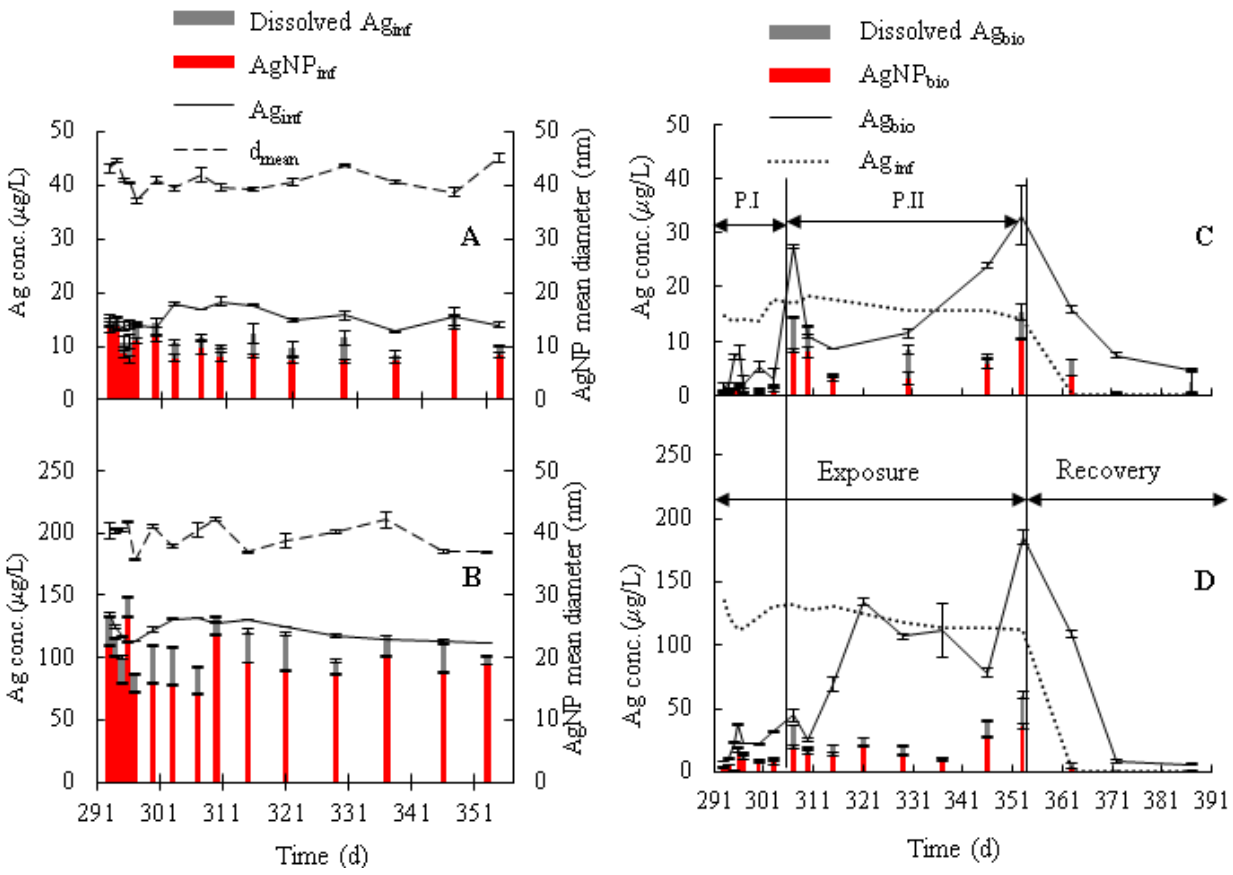

Figure C. 1: Distribution of Ag in influent (A-B) and bioreactor phases (C-D) of MBBRs receiving influent concetration of 10 μg/L ($MBBR_2$) and 100 μg/L AgNPs ($MBBR_3$), respectively (Error bars are only shown when larger than symbol size).

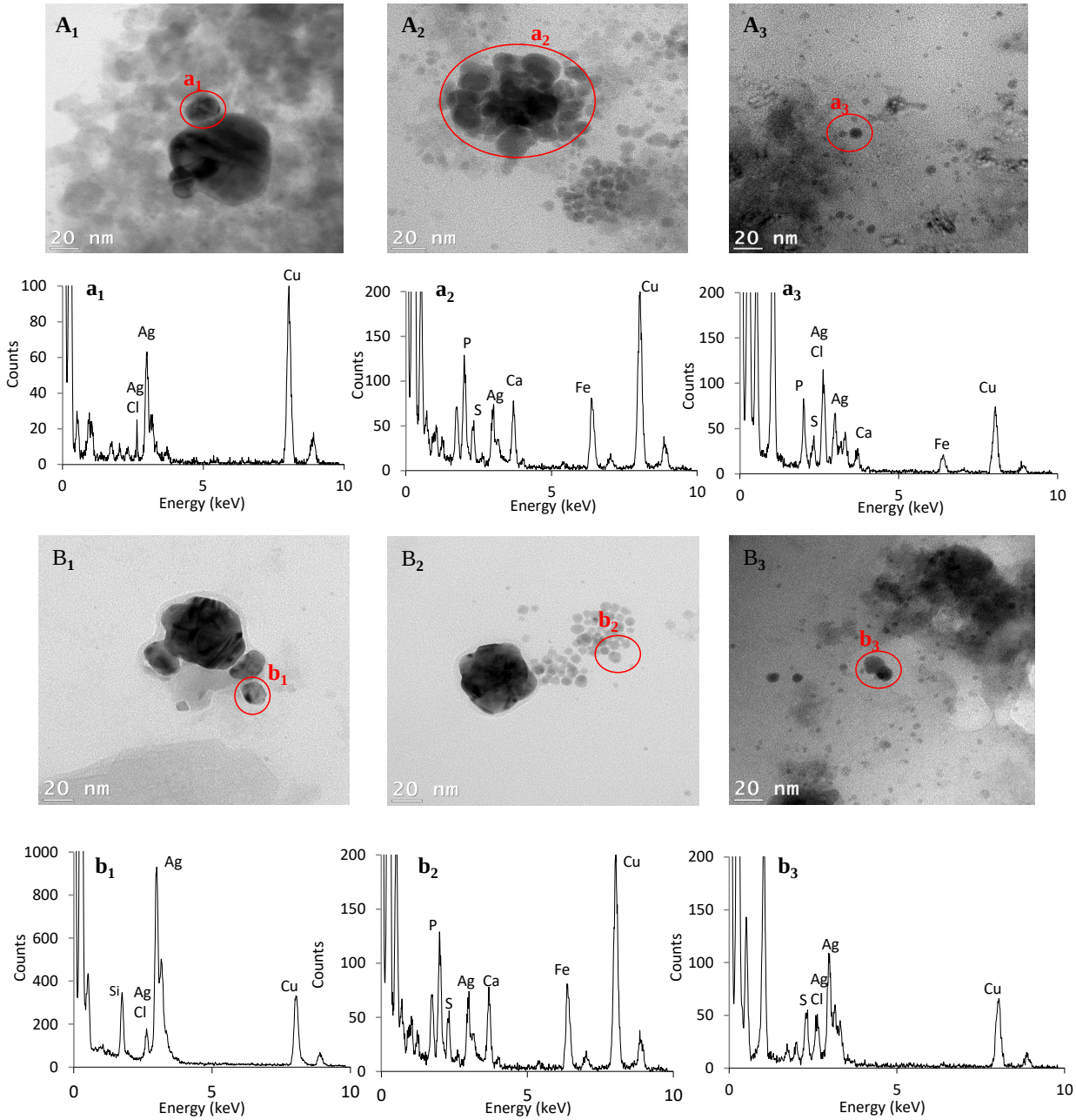

Figure C. 2: TEM images of the AgNPs in the effluent of MBBR receiving ($A_{1\text{-}3}$) 10 μg/L and ($B_{1\text{-}3}$) 100 μg/L AgNPs and (a_1-b_3) EDS analysis of the AgNPs.(Note: Subscripts 1 and 2 correspond to the end of the exposure period (day 353) and subscript 3 represent the end of the recovery phase (day 388)).